Cardiff University

School of Optometry and Vision Sciences

The Enhanced Generation of Corneal Epithelium from iPSCs using Chondroitin Sulphate as a Substrate

By

Sean Johnathan Charles Ashworth

This thesis is presented for the award of Doctor of Philosophy at Cardiff University.

August 2022

Summary

Proteoglycans are a type of extracellular matrix molecule consisting of a protein core with several covalently attached glycosaminoglycan chains (negatively charged polysaccharides). Certain glycosaminoglycan chains, for example chondroitin sulphate (CS) and dermatan sulphate (DS), can be sulphated in specific patterns that confer unique properties. These sulphation patterns and their distributions play an important role in the development and maintenance of stem cell niches in a wide range of tissues, including the cornea. Many tissue engineering approaches use native extracellular matrix cues extracted from the resident tissue to enhance generation and maintenance of therapeutic cells. However, there are few studies detailing specific glycosaminoglycan species in this process. This is especially true in the study of the generation of corneal epithelial cells from induced human pluripotent stem cells (hiPSCs). The aim of this thesis was to examine the effect of native glycosaminoglycan sulphation patterns on the generation of corneal epithelial cells from hiPSCs, using a defined differentiation method. The objectives of this thesis were to, firstly, identify specific CS and DS sulphation patterns present in the stem cell niche of the cornea and those associated with the corneal epithelium using CS/DS antibodies and immunohistochemistry. Following this, identified corneal epithelium-associated sulphation patterns were extracted from different tissue sources and enriched for sulphation patterns of interest using density centrifugation and anion exchange chromatography. Finally, these substrates were applied to hiPSCs and subsequently differentiated toward corneal epithelial cells and the gene expression was examined using RT-qPCR, along with morphological and immunohistochemical evaluation. From this study, it appeared a mixed substrate consisting of highly sulphated keratan sulphate, and CS/DS enriched in sulphation patterns recognised by the antibodies 5D4 and 7D4, yielded best potential enhancement of corneal epithelial differentiation as identified by the methods described herein. Other native sulphation patterns also revealed significant effects on gene expression.

Acknowledgements

I would like to thank my supervisors, Professor Andrew Quantock, Professor Clare Hughes and Dr Rob Young for their support, help and guidance.

I would also like to thank the members of the Biophysics Research Group for their encouragement, friendship and kindness as well as the rest of the staff and students in the School of Optometry and Vision Sciences.

Finally, I would like to thank my PhD sponsor, Fight for Sight (5069/5070), for funding my PhD as well as the BBSRC for project funds (BB/R0212441/1).

Abbreviations

BCA	Bicinchoninic acid
BSA	Bovine serum albumin
CLAL	Conjunctival limbal allograft
CLAU	Conjunctival limbal autograft
CLET	Cultivated limbal epithelial transplant
COMET	Cultivated oral mucosal epithelial sheet transplantation
CS	Chondroitin sulphate
DEA	Diethanolamine
DMMB	Dimethyl methylene blue
DS	Dermatan sulphate
ELISA	Enzyme-linked immunosorbent assay
ESCs	Embryonic stem cells
FACITs	Fibril-associated collagens with

	interrupted triple helices
HA	Hyaluronic acid or hyaluronan
hESCs	Human embryonic stem cells
hiPSCs	Human induced pluripotent stem cells
HS	Heparan sulphate
K14	Keratin-14
KLAL	Keratolimbal allograft
KS	Keratan sulphate
LSCD	Limbal stem cell deficiency
MMPs	Matrix metalloproteases
PSCs	Pluripotent stem cells
SEAMs	self-formed ectodermal autonomous multizones
SLET	Simple limbal epithelial transplant
SLRPs	Small leucine rich proteoglycan family
TSA	Tris/Saline/Azide

Table of Contents

1 Chapter 1: Introduction

The eye is one of the most uniquely structured organs in the body and enables us to perceive the world through vision. Each component of the eye is vital for clear vision and damage to any part can result in the lack thereof. This thesis centres primarily around the cornea which is located at the anterior surface of the eye and the use of pluripotent stem cells (PSCs) to generate the corneal surface cells, named corneal epithelium, with a focus on the effect of endogenous extracellular matrix molecules and how they can be applied to this technology.

1.1 The Cornea

The cornea is a curved, avascular tissue located in the anterior eye that serves as a clear, protective barrier. Despite its relatively simple tissue structure, the cornea is vital for protecting the eye from debris and infectious agents as well as being essential for vision by providing two thirds of the refractive power of the eye (DelMonte and Kim, 2011). The cornea is continuous with the sclera, with the limbus being the interface between the two structures. The average adult cornea is approximately 11-12 mm in diameter (Rüfer et al., 2005).

1.1.1 Structure

The adult human cornea is constituted of five layers. In order from the most anterior to the most posterior they are the epithelium, Bowman's layer, the stroma, Descemet's membrane and finally the corneal endothelium. These layers are important for the structure and function of the cornea an overview is shown in **Figure 1.1**.

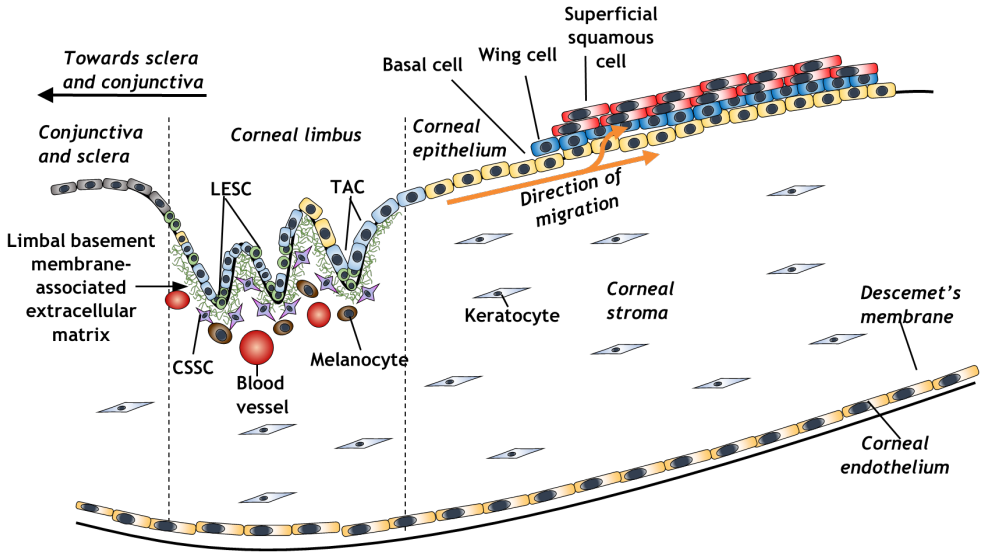

Figure 1.1 Schematic representation of the corneal limbal stem cell niche and some of its constituent elements (LESC, limbal epithelial stem cell; CSSC, corneal stromal stem cell; TAC, transient amplifying cell).

The most superficial layer, the epithelium – the primary focus of this study, is comprised of stratified, non-keratinised, squamous epithelium (approximately four to six cell layers or 40 to 50 µm) (DelMonte and Kim, 2011). The epithelial surface of the cornea is vital for protecting the sensitive structures within the eye from the two most common external insults, including pathogenic organisms and other environmental debris/stimuli (Bashir et al., 2017). The corneal epithelium is discussed in further detail in Section 1.1.2.

Bowman's layer is the interface between the epithelium and the corneal stroma and is usually described as an acellular condensation of the anterior stroma. Whilst useful histologically to differentiate between corneal epithelium and stroma, its biological function is unclear and incidental removal of Bowman's layer via photorefractive keratectomy shows little to no complication even after more than 10 years post-operation (Wilson and Hong, 2000).

Below Bowman's layer lies the corneal stroma which is responsible for most of the cornea's structural and physical characteristics and comprises approximately 80% of the corneal thickness. It mainly consists of collagen fibrils organised into layers named lamellae of which there are approximately 250 in the central cornea and 500 towards the periphery (Bergmanson et al., 2005; Radner et al., 1998). The corneal stroma is produced and maintained by a network of

keratocytes which are present throughout the stroma and whose morphology varies dependent on the location within the stroma (Poole et al., 1993). Keratocytes play an important role in the synthesis and remodelling of the extracellular matrix within the corneal stroma and produce collagen, glycosaminoglycans as well as matrix metalloproteases (MMPs) (DelMonte and Kim, 2011). The keratocyte population is highly heterogenous, with some cells in the peripheral corneal stroma have been identified with stem cell-like characteristics showing multipotent progenitor capacity, with the ability to differentiate towards mesenchymal and corneal epithelial phenotypes and shown as CSSCs in **Figure 1.1** (Du et al., 2005; Hashmani et al., 2013).

Finally, at the posterior stroma lies Descemet's membrane (DM) and the corneal endothelial cell layer. The endothelial layer is essential for maintaining the correct hydration of the corneal stroma (Bonanno, 2012) and corneal endothelial cells rely upon Descemet's membrane to maintain their phenotype and function (Chen et al., 2017). A sixth layer of the cornea has been reported located between Descemet's membrane and the posterior corneal stroma (Dua et al., 2013). However, some describe it as residual corneal stroma and not distinct enough from the stroma to be classified as a separate layer (McKee et al., 2011).

1.1.2 Corneal Epithelium

The corneal epithelium is vital for the integrity of the anterior eye and as such any damage to this layer can lead to severe consequences. The epithelium itself is widely accepted to be regenerated from the limbus at the edge of the cornea centripetally towards the centre of the cornea originating from limbal epithelial stem cells (Dorà et al., 2015). Limbal epithelial stem cells slowly differentiate as they migrate towards the central cornea, becoming transient amplifying cells where they multiply and differentiate before becoming a terminally differentiated stratified corneal epithelial cell. These transient amplifying cells also have some wound repair capability, being able to spontaneously increase the number of cell cycles to replace injured epithelial cells (Dua and Azuara-Blanco, 2000; Lehrer et al., 1998; Pellegrini et al., 1999).

1.1.3 Limbal Stem Cell Niche

Limbal epithelial stem cells are thought to reside in the basal layer of the limbal epithelium within the epithelial crypts which are arranged both circumferentially and occasionally slightly radially around the periphery of the cornea, a feature largely conserved across mammalian corneas (Chen et al., 2004; Cotsarelis et al., 1989; Grieve et al., 2015). They can be distinguished from adjacent cells by virtue of their smaller size and less columnar appearance (Romano et al., 2003).They can also be distinguished by expression of various proteins, including for example; ATP-binding cassette super-family G member 2 (ABCG2) – a transporter protein (Watanabe et al., 2004) and p63 and its various isoforms, namely ΔNp63 (Di Iorio et al., 2005; Kawakita et al., 2009). Another candidate marker for a limbal epithelial stem cell is ATP binding cassette, sub-family B, member 5 (ABCB5) (Ksander et al., 2014). Initially identified in cell fusion of progenitor cells and in the initiation of human melanoma (Frank et al., 2003; Schatton et al., 2008), it was found to be required not only for limbal epithelial stem cell maintenance and development but could also fully restore the cornea in limbal epithelial stem cell-deficient mice (Ksander et al., 2014). An empirical limbal epithelial stem cell marker remains to be determined and is complicated by the inherent heterogeneity of the limbal stem cell population (D.-Q. Li et al., 2021), but the three mentioned above are used most commonly and widely accepted.

1.1.4 Limbal Stem Cell Deficiency and Treatments

Further attempts to enrich or isolate limbal epithelial stem cell populations for use in studies and/or transplantation have been attempted and been successful, particularly in the treatment and study of limbal stem cell deficiency (LSCD), a disease characterised by loss of limbal epithelial stem cells with variable aetiology including genetic but primarily acquired through acute injury (Haagdorens et al., 2016). For example, one of the most successful procedures is cultivated limbal epithelial transplant (CLET), developed by Pellegrini *et al*, which involves taking a corneal limbal biopsy from the healthy donor eye, expanding limbal epithelial stem cells *in vitro* and transplanting them back into the original patient, with success being largely contingent upon the amount of ΔNp63+ limbal epithelial stem cells present in the biopsy (Pellegrini et al., 1997,

2016; Rama et al., 2010). An example of a successful CLET surgery is shown in **Figure 1.2**. Simpler versions of this technique have been developed, for example simple limbal epithelial transplant (SLET), whereby a small piece of limbal biopsy from a healthy donor is dissected and distributed over an amniotic membrane and placed on the cornea to regenerate the deficient cells on the injured eye without relying on cultured cells (Sangwan et al., 2012). Another slightly cruder technique is conjunctival limbal autograft (CLAU), in which 5 to 7 mm of limbus is harvested from a healthy eye and transplanted to the LSCD-afflicted eye (Kenyon and Tseng, 1989).

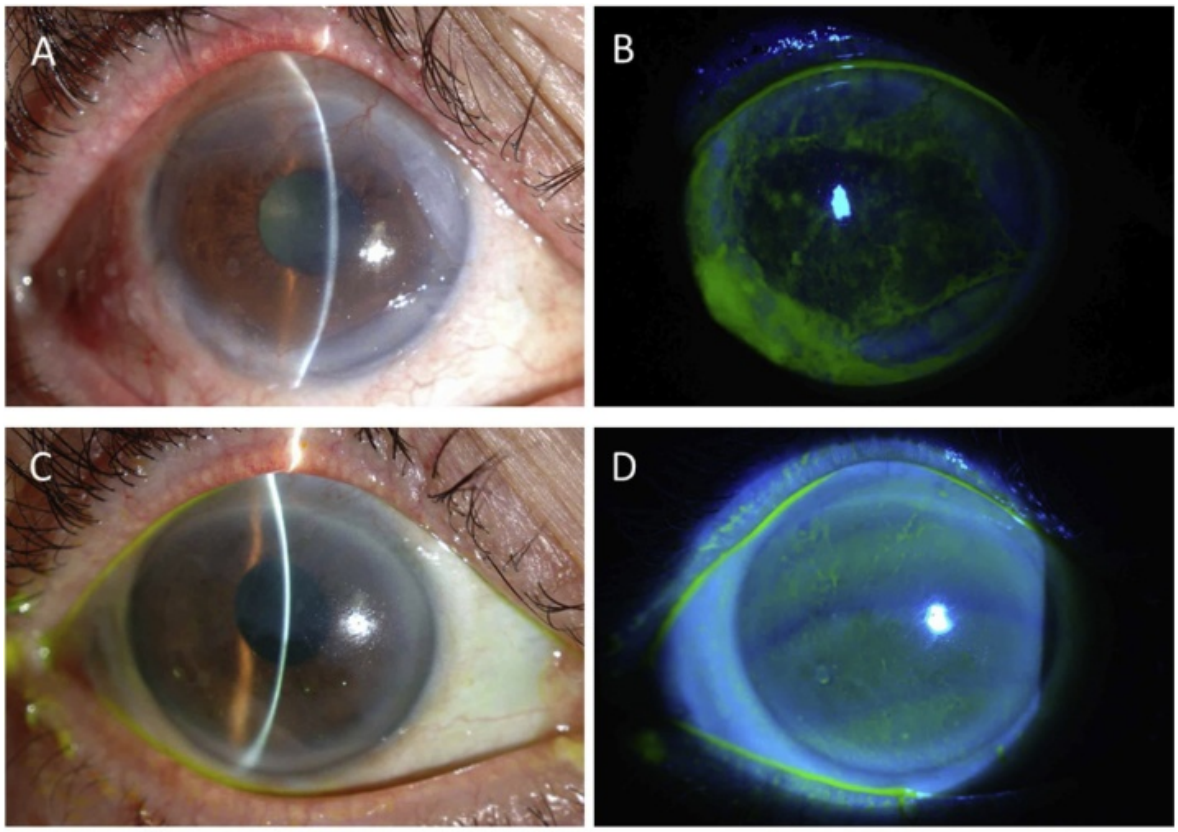

Figure 1.2 Treatment of limbal stem cell deficiency using cultivated limbal epithelial transplantation (CLET). (**A**) Stem cell deficient eye with ocular surface squamous neoplasia. (**B**) Image of the same eye showing an irregular and non-intact ocular surface with fluorescein staining. (**C**) The same patient's eye at 1 year post surgery, showing healthy corneal epithelial cells covering the cornea. (**D**) Fluorescein staining reveals a smooth and stable surface after CLET. Figure adapted from (Bains et al., 2019).

Whilst these techniques are effective in restoring the regenerative limbal epithelial stem cells to the corneal surface and, owing to their autologous nature, do not require immunosuppressant drugs, they are limited by the extent

of tissue damage requiring repair (Bains et al., 2019). This is particularly so for SLET which is not suitable for severe damage and is primarily only applicable for unilateral LSCD, owing to the reliance on having a healthy donor eye. This leads to another major drawback for both of these autologous techniques, in that they involve taking a limbal biopsy from a healthy eye, which could damage the healthy eye leading to bilateral LSCD and is especially damaging for the patient if the technique fails overall. This is unlikely, however, as the procedures are relatively safe (for CLET and SLET) and the success rate is relatively high, 76% for CLET, 78% for SLET and 90% (down to 60% where smaller grafts are used) for CLAU respectively at follow up (Baylis et al., 2011; Liang et al., 2009; Shanbhag et al., 2019).

Other techniques using allografts are available to treat bilateral LSCD for example cadaveric and living-relative conjunctival limbal allograft (CLAL) and keratolimbal allograft (KLAL) whereby donor tissue from living relatives or cadavers is used to restore the limbal region (Holland, 1996; Kwitko et al., 1995). These techniques typically feature slightly poorer outcomes and graft failure is common; they also require immunosuppressant drugs to be taken which result in further adverse effects (Atallah et al., 2016; Biber et al., 2011; Ilari and Daya, 2002). Owing to these issues further techniques were explored including cultivated oral mucosal epithelial sheet transplantation (COMET) whereby oral mucosal cells are transplanted onto the surface of the eye after being cultivated on amniotic membrane substrate and co-cultured with inactivated fibroblasts (Nakamura et al., 2004). An example of the results of the procedure is shown in **Figure 1.3**. Other approaches may use temperature responsive substrates rather than amniotic membrane to release the cultivated cell sheet (Nishida et al., 2004). The technique is relatively successful achieving a stable ocular surface in 70.8% of patients and is particularly suited to severe ocular surface disease for example Stephen-Johnsons syndrome. The main issue with the technique is neoangiogenesis peripherally on the cornea due to oral mucosal epithelium's requirement for a vascular bed, which may potentially affect visual improvement and few studies trace follow up more than 3 years (Nishida et al., 2004).

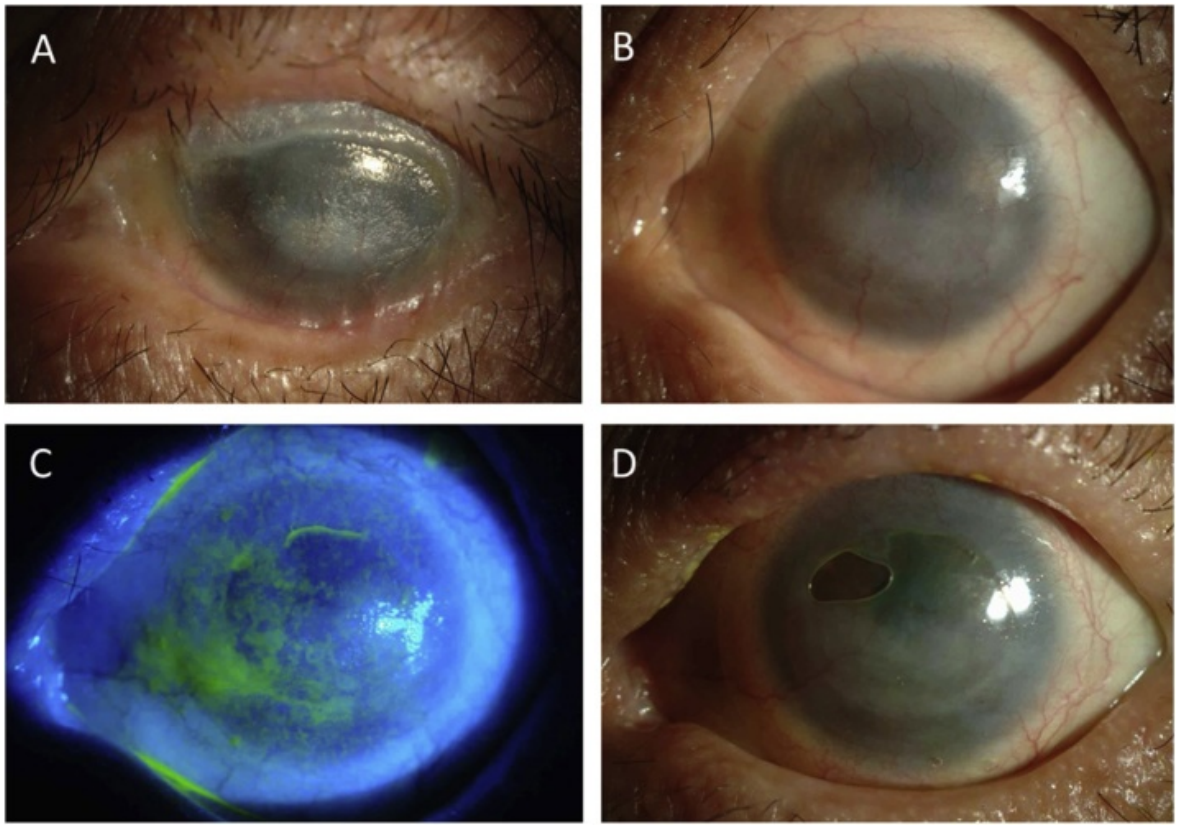

Figure 1.3 Clinical treatment of limbal stem cell deficiency using cultivated oral mucosal epithelial transplantation (COMET). (**A**) Limbal stem cell deficient eye showing keratinisation. (**B**) Non-keratinised epithelium derived from cultivated oral mucosal epithelial cell sheet covered the corneal surface at 3 years post operation. (**C**) Fluorescein staining of the same eye reveals no epithelial damage on the surface epithelium. (**D**) The repaired eye is able to be fitted with a contact lens that improved visual acuity substantially. Figure adapted from (Bains et al., 2019).

Newer approaches aim to solve the issues that have arisen from current therapies, especially for severe or bilateral LSCD. These issues are either the need for cadaveric or donor tissue and subsequent immunosuppressants, the need for multiple ocular surgeries in the case of SLET and CLET or the issues from using non-corneal epithelial cells in the case of COMET. To this end, many researchers have turned their attention to stem cell therapies, using a source of pluripotent stem cells, including both hiPSCs (Hayashi et al., 2016; Mikhailova et al., 2016; Susaimanickam et al., 2017) and human embryonic stem cells (hESCs) (Zhang et al., 2017) or other stem cells, e.g. mesenchymal stem cells or dental pulp cells (Calonge et al., 2019; Gomes et al., 2010).

Of these, iPSCs are arguably the most promising, as they can, in theory, be produced from a patient's somatic cells and eliminate the risk of allogeneic rejection due to using the patient's own cells. They are discussed in more detail in Section 1.4 along with prospective iPSC-based corneal cell therapies.

1.2 Extracellular Matrix in the Cornea

The extracellular matrix is a vital part of the cellular scaffold that maintains the shape and organisation of cells within the majority of tissues throughout the body. It is especially prevalent in connective tissue but plays an important role in cellular homeostasis in virtually all tissues. Extracellular matrix plays a key role in the function and structure of the cornea and confers the majority of the cornea's properties, for example corneal transparency, which arises from the careful balance of collagen and hydrated proteoglycans.

During development, the majority of the corneal extracellular matrix is synthesised by keratoblasts (primordial keratocytes that develop from neural crest cells below the epithelium) in the stroma and corneal epithelial or endothelial cells in their respective layer (Chen et al., 2015; Hay, 1980).

1.2.1 Collagen

Collagens are extracellular, structural proteins that are expressed ubiquitously throughout the body and are the most abundant proteins by weight in mammals. The common feature of these extracellular matrix molecules is the presence of a triple helix motif that can form most of their structure, in the case of collagen I or a small part, for example in collagen XII. Collagens represent a range of proteins of which there are 28 members in the collagen superfamily and healthy tissue function relies on the correct assembly and distribution of the various members of the collagen superfamily (Gordon and Hahn, 2010; Kadler et al., 2008; Ricard-Blum, 2011).

In the cornea, notable amounts of collagen are primarily observed in two of the layers of the cornea: in Bowman's layer and the corneal stroma. The cornea has been shown to be constituted primarily from collagen type I and type V within heteropolymeric fibrils with type V throughout these. These fibrils are uniform in diameter at approximately 31 nm and arranged in a pseudolattice of stacked

lamellae orthogonally rotated approximately 90˚from the previous layer (Ihanamäki et al., 2004; Leonard and Meek, 1997; Meek, 2009). Fibril-associated collagens (FACITs), for example collagen XII and collagen XIV are also important for the regulation of fibril association and interactions been adjacent layers of lamellae by modifying their interactive properties (Chen and Birk, 2013). Collagen VI is a nonfibrillar collagen present as a network throughout the stroma around other fibrils and close to corneal stromal cells, and is thought to possess both structural and regulatory roles (Doane et al., 1992).

Various collagen isoforms are also present in the corneal epithelium, particularly in the basement membrane as discussed below.

1.2.2 Basement Membrane Proteins

Basement membranes form a vital, functional component of most epithelial and endothelial tissues and the cornea is no exception. In the cornea various proteins are present across the entire ocular surface including the corneal epithelium and the conjunctival epithelium, including various collagens (type IV - α5 and α6 chains, VII, XV, XVII and XVIII), laminin-111, laminin 332, laminin chains α3, ß3,and γ2, fibronectin, matrilin-2 and -4 and perlecan. There are, however, differences between the different regions of the ocular surface and the limbal basement membrane, overall, more closely resembles that of the conjunctiva but there are some limbal-specific basmement membrane proteins, e.g. laminin α1, α2, ß1 chains, and agrin (Schlötzer-Schrehardt et al., 2007). Laminin plays a role in organogenesis of the eye and is expressed in a specific spatiotemporal manner throughout the development of the human eye (Byström et al., 2006).

1.2.3 Proteoglycans

Proteoglycans play a key role in the function and homeostasis of healthy cornea. See Section 1.3.3 for a more in-depth analysis of proteoglycans and their role in the cornea and specifically CS proteoglycans,which constitute a key focus of this thesis.

1.3 Proteoglycans and Glycosaminoglycans

Proteoglycans are an essential part of the extracellular matrix throughout the body and usually consist of glycosaminoglycans covalently attached to a specific

core protein. The six main subdivisions of glycosaminoglycans in the human body are hyaluronic acid or hyaluronan (HA), keratan sulphate (KS), chondroitin sulphate (CS), dermatan sulphate (DS), heparin and heparan sulphate (HS), each of which is typically bound to certain protein cores. The exception to this is HA which does not bind covalently to a core protein but interacts through protein-protein interactions, and heparin, which is also a free glycosaminoglycan chain. They are typically attached via an N or O link on an asparagine or serine amino acid residue respectively on the host protein (Nilsson et al., 1982). Some core proteins can have many attachment sites and contain different glycosaminoglycan species, for example aggrecan, which can contain multiple CS and KS attachment sites, which repeat between globular regions of protein (Rodriguez et al., 2006). These glycosaminoglycans consist of long, polysaccharide chains made up of different disaccharide units and have varying levels of sulphation (excluding HA) that further differentiates them (Prydz and Dalen, 2000).

1.3.1 Proteoglycan and glycosaminoglycan types and structure

Generally, proteoglycans are heterogeneous macromolecules that, dependent upon their location, can be extracellular, intracellular, pericellular and cell-surface associated (Karamanos et al., 2018). The protein core can vary in size, as can the amount of covalently attached glycosaminoglycan chains. For example decorin (36 kDa core protein) and biglycan (38 kDa core protein) can have one or two glycosaminoglycan chains respectively compared with aggrecan (208-220 kDa core protein) which can have over 100 glycosaminoglycan chains (Kiani et al., 2002; Varki et al., 2015).

Glycosaminoglycan structure can vary from molecule to molecule but largely follows a similar pattern. The typical disaccharide repeating unit consists of a hexosamine (almost always either glucosamine or galactosamine, and typically N-acetylated) and either a (hex)uronic acid (glucuronic or iduronic acid) or galactose (Caterson, 2012). Both of these components can be sulphated at various positions on the sugar molecules and their varying combinations give rise to the different subgroups of glycosaminoglycans which are outlined below in **Figure 1.4**.

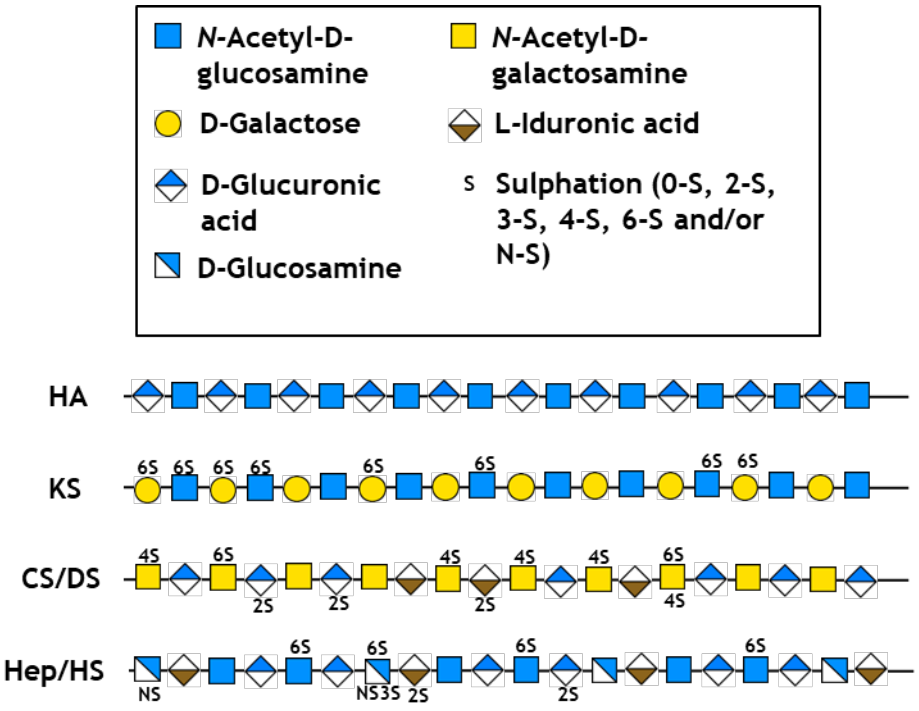

Figure 1.4 Chemical diversity of glycosaminoglycan chains. Hyaluronic acid (HA), keratan sulphate (KS), chrondroitin sulphate (CS)/DS (DS), heparin/heparan sulphate are shown with potential sulphation sites on the hexosamine, uronic acid and galactose sugars. Adapted from (Caterson, 2012).

The carboxyl groups of the hexuronic acids and sulphation on either of the disaccharide components confer a strong negative charge to the glycosaminoglycan chains, allowing them to bind to cationic molecules in cells and throughout the surrounding extracellular matrix as well as allowing a strong affinity for water (Caterson, 2012). The spacing and stereochemistry of these sulphate and carboxyl groups within small sections of glycosaminoglycan chains can allow for very specific conformations of the glycosaminoglycan allowing for different binding sites for extracellular matrix molecules, chemokines growth factors as well as morphogens conferring each individual glycosaminoglycan/proteoglycan molecule its biological properties and effects (Allen and Rapraeger, 2003; Cortes et al., 2009; Dyer et al., 2016; Purushothaman et al., 2012).

1.3.2 Proteoglycan/glycosaminoglycan synthesis

The synthesis of different proteoglycan combinations varies dependent upon the protein core and glycosaminoglycan chain(s) being attached. To summarise the process, initially the protein core is produced from mRNA by ribosomes and

subsequently translocated into the endoplasmic reticulum. This is then transported to the Golgi apparatus wherein the protein is glycosylated dependent upon the tissue and protein core. Finally, the proteoglycan is transported either to the extracellular surface where it either remains attached to the cell surface (e.g. the syndecan family of proteoglycans) or it is secreted into the extracellular matrix (e.g. aggrecan and decorin). Exceptions to this include serglycin, a HS/CS proteoglycan which is retained intracellularly in mast cell and other leukocytes and plays a role in inflammation, immune response and wound repair (Varki et al., 2015).

For CS, DS, Heparin and HS glycosaminoglycans, their synthesis begins in the Golgi apparatus, where a protein core typically has a serine hydroxyl group (followed by a glycine residue) which receives a xylose from xylosyltransferase (Xylt1/Xylt2). Two galactose molecules are then added by galactosyltransferases and the xylose residue is phosphorylated at the C-2 position This phosphorylation and subsequent dephosphorylation is important in the formation of the tetra saccharide linker region and the start of glycosaminoglycan synthesis (Koike et al., 2014; Wen et al., 2014). In CS the galactose residues can also be phosphorylated at positions on the residues which is thought to aid processing in the Golgi to become CS glycosaminoglycan chains (Prydz, 2015). The tetrasaccharide linker region is complete upon the addition of D-glucuronic acid by glucuronosyltransferase and the addition of the next residue determines whether the chain becomes CS/DS (N-acetylgalactosamine) or Heparin/HS (N-acetylglucosamine) (Karamanos et al., 2018; Varki et al., 2015).

For keratan sulphate (KS) chains, they are primarily poly-N-acetyllactosamine chains covalently linked to asparagine resides on the core protein in the case of KS I or serine/threonine residues on the core protein in the case of KS II with sulphations added variably along the polysaccharide chain (Varki et al., 2015).

1.3.3 Proteoglycan/glycosaminoglycan distribution in the cornea

Proteoglycans are essential for both the development and maintenance of the cornea. The primary group of proteoglycans present in the cornea are small leucine rich proteoglycan family (SLRPs) and are shown below in **Table 1.1**.

Table 1.1 SLRPs present in the cornea.

Proteoglycan	Core protein (kDa)	Glycosaminoglycan chains
Decorin	36	1 CS/DS
Biglycan	38	0-2 CS/DS
Lumican	37	3 – 4 KS I
Keratocan	37	3 – 4 KS I
Fibromodulin	59	2 – 4 KS I
Osteoglycin/Mimecan	25	2 – 3 KS I

All of these proteoglycans play an important role in collagen fibrillogenesis (and subsequent corneal transparency) as well as correct collagen spacing. They are also important for maintaining corneal hydration through their hydrophilic nature. KS proteoglycans are vital for normal corneal function, primarily keratocan and lumican especially in the organisation of collagen assembly into fibrils (Chakravarti et al., 1998). In the context of CS proteoglycans the interplay between biglycan and decorin have been shown in murine models to be implicated in collagen fibrillogenesis and are expressed widely throughout the corneal stroma, with biglycan levels decreasing towards maturity. Decorin and biglycan null mice have significantly disrupted collagen ultrastructure (Zhang et al., 2009), highlighting their role in regular collagen spacing through their glycosaminoglycan side chains (Iozzo, 1997). Similar effects are seen with biglycan/lumican null mice, which results in significant opacity but single proteoglycan knockouts alone do not have the same impact (Chen et al., 2014).

In terms of glycosaminoglycan distribution, the cornea is primarily constituted of KS glycosaminoglycan (both high and low sulphated), with DS and CS glycosaminoglycan are also present in slightly lower quantities, with CS located more preferentially towards the limbus and DS located more centrally (Ho et al.,

2014). Glycosaminoglycan distribution also may change with age and potentially be a factor in age-related corneal disease, with overall glycosaminoglycan and hyaluronic acid being higher in younger people and the proportion of sulphated glycosaminoglycans increasing with age and hyaluronic acid decreasing (Pacella et al., 2015).

1.3.4 CS interaction with growth factors and sulphation motifs

CS and DS are widely accepted to interact with growth factors and play a significant role in tissue development and maintenance as already mentioned. However, it is difficult to precisely identify what sulphation moieties are present within a tissue or decorating the surface of a cell, which dictate a significant proportion of a proteoglycan's stereochemistry and interactions. To address this, monoclonal antibodies have been developed that identify specific sulphation motifs on CS/DS (Sorrell et al., 1990) and KS (Caterson et al., 1983). The CS/DS specific antibodies are illustrated below in **Figure 1.5** based upon their location on the CS/DS chain after limited enzymatic digestions (Sorrell et al., 1993).

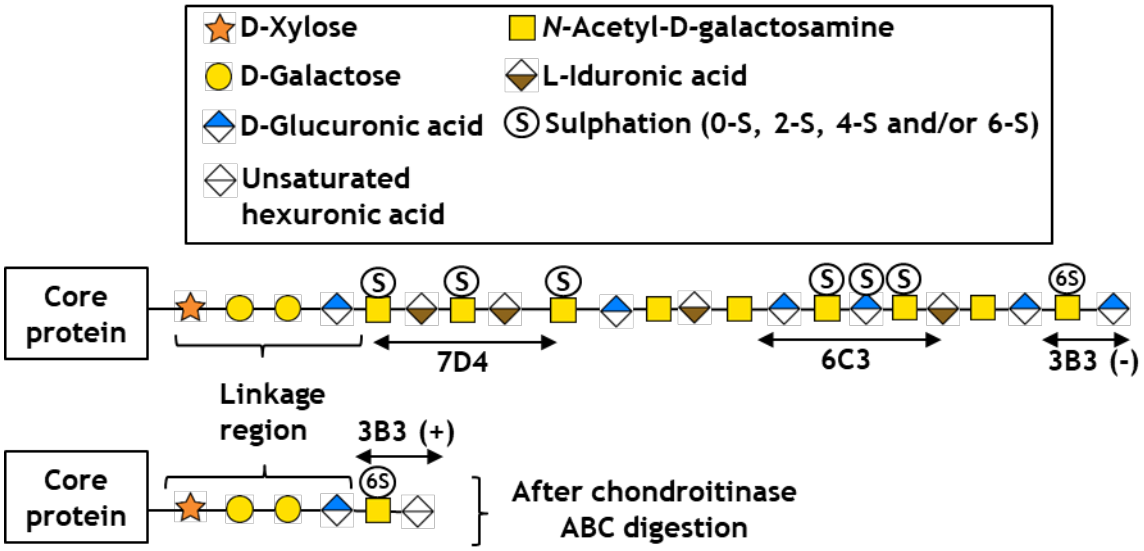

Figure 1.5 CS glycosaminoglycan chain showing the approximate binding location of various distinct sulphation motifs on the length of the glycosaminoglycan chain (sulphate groups not depicted). Adapted from (Caterson, 2012; Hayes et al., 2018).

Whilst the exact epitope of these monoclonal antibodies remains to be determined, they identify distinct sulphation motifs that are more structurally complex than standard 0-, 4- and 6-sulphated disaccharide CS chains which are

commonly used in cell scaffolds in any current corneal tissue engineering attempts (Lai, 2013; Lai et al., 2012; Osmond et al., 2017). These specific antibodies also immunolocalise to specific areas during development and in particular, stem cell niche sites and can also be used to isolate progenitor cells from articular cartilage (Hayes et al., 2016, 2008). Interestingly, one of the antibodies, 6C3, recognises a glycosaminoglycan epitope subjacent to basal stem cells in skin, a tissue very similar to corneal epithelium, also being derived from surface ectoderm (Sorrell et al., 1990). Biglycan (CS proteoglycan) and fibromodulin (KS proteoglycan) have also been shown to localise to stem cell niche sites in tendon tissue and subsequent knockouts resulted in significant impacts on the ability of tendon stem/progenitor cells to repair injury and disrupts the niche, furthering evidence for the role of CS proteoglycans in stem cell niche maintenance (Bi et al., 2007). In the cornea, biglycan knockouts have been carried out, however studies have only analysed stromal structural deficits and not epithelial changes or any associations with the limbus (which are morphologically distinct in murine tissue and so not wholly comparable to humans) (Chen et al., 2014; Zhang et al., 2009).

Whilst many associations with specific sulphation motifs and CS proteoglycans have been found to be implicated in stem cell niche maintenance and development *in vivo,* there is little study into the potential effects that these molecules could have on *in vitro* cell differentiation and maintenance, which will be explored in this thesis in the context of iPS cell differentiation towards corneal epithelial cells.

1.4 Pluripotent Stem Cells

Pluripotent stem cells (PSCs) have been a vital tool in the field of cell biology, not just by furthering the understanding of developmental pathways and pathological mechanisms, but they are also incredibly useful in the field of regenerative medicine as a potential source of cells for almost any tissue in the body. With the advent of the first pluripotent hESC lines being derived and characterised (Thomson et al., 1998), the field of stem cell biology has since expanded rapidly in the last two decades. Another breakthrough came from the discovery of iPSCs (Takahashi et al., 2007), allowing pluripotent stem cells to be

generated from adult somatic cells. These iPSCs were generated by viral transfection of four key pluripotency transcription factors: Oct3/4, Sox2, Klf4 and c-Myc. The discovery of these so called 'Yamanaka factors' has further increased the potential of the field and has reduced the restrictions of necessitating embryonic tissue and allowing the potential for autologous stem cell therapies and studies as well as patient-specific diseases modelling.

1.4.1 Anterior eye development

The development of the eye is a complex process that requires the interaction of different primordial cell types and germ layers. The optic vesicle forms as a bud from the neuroectoderm and subsequently becomes the optic cup after interaction with surface ectoderm and the resultant lens placode, which is also from surface ectoderm. The optic cup can then become neural retina or upon interaction with mesenchyme, pigment epithelium. The optic vesicle, prior to forming the optic cup, interacts with competent surface ectoderm as mentioned and this forms the lens placode. The lens placode then forms the lens vesicle which upon interaction with the neural retina matures into lens cells. The lens vesicle is also critical in the maturation of outer surface ectoderm to corneal epithelial cells through signalling interactions (Graw, 2010). After the formation of the primordial epithelium and lens, they separate, and the space between them is infiltrated by mesenchymal cells that will later form the corneal stroma and become keratocytes (Cvekl and Tamm, 2004)

This whole process is largely controlled by the master regulator of eye development, the transcription factor Pax6. Pax6 is constitutively expressed throughout the early stages of eye development in the surface and neuroectoderm and is essential for the differentiation and maturation of cornea, lens, ciliary body and retina, that allow for separation of lens and surface ectoderm and subsequent mesenchymal infiltration and corneal stromal development (Nishina et al., 1999).

PSC technologies to differentiate PSCs towards ocular cell phenotypes also provide a useful tool to interrogate the developmental pathways of ocular cell anlages and often mimic *in vivo* developmental studies, providing a tractable model system of developmental pathways.

1.4.2 Differentiation of PSCs towards ocular cell phenotypes

Due to the complexity of the eye and the fact it arises from different primordial cell lineages in development means that modelling specific cell types is challenging. For example, neuroectoderm gives rise to the retina via the optic vesicle, the iris and corneal stroma derives from neural crest origin and, finally, the corneal epithelium is derived from surface ectoderm. Generating cells of distinct origins using pluripotent stem cells towards ocular anlages is challenging however this is alleviated somewhat by the intrinsic self-organisation of pluripotent stem cells.

Various studies have shown optic cup-like structures and retinal development *in vitro* and that by using stepwise differentiation protocols, early eye field cells could be produced that matched development *in vivo* (Meyer et al., 2009). Further 3D studies demonstrated the self-organising potential of pluripotent stem cells and their ability to form both rods and cones *in vitro,* as well as retinal pigmented epithelium (Eiraku et al., 2011; Nakano et al., 2012). Further developments in differentiation procedures could more accurately represent spatiotemporal development of the visual field and produce functional, photosensitive photoreceptors and retinal pigment epithelium, allowing the development of potential cell therapies using PSC technology (Reichman et al., 2014; Zhong et al., 2014). The cellular self-organisation has also been interrogated using PSC technology showing the potential use in dissecting developmental pathways (Mellough et al., 2015). Some groups have also shown that photoreceptor precursors generated from PSC-derived optic vesicle structures can be isolated and transplanted in mice models, to become mature photoreceptors and restore vision (Lakowski et al., 2015). Similar selection panels have also been developed for human PSC-derived photoreceptor precursors further cementing their potential for use in therapeutic applications (Lakowski et al., 2018).

Whilst many studies focus on the neuro-retina (which PSCs generate more favourably), various studies have investigated the potential of PSCs to form corneal compartments and corneal epithelial cells *in vitro*. Initial attempts involved attempting to recreate the limbal niche using collagen IV and limbal

fibroblast-conditioned medium to differentiate PSCs towards a corneal epithelial phenotype, however generated cells were not very robust and differed from native corneal epithelium (Ahmad et al., 2007). Other studies have also shown to produce corneal epithelial-like cells that display corneal epithelial markers (K3/K12 and Pax6) from PSCs and have shown how the regulation of Pax6 is critical for differentiation (Brzeszczynska et al., 2014; Hayashi et al., 2012; Hongisto et al., 2017; Shalom-Feuerstein et al., 2012).

Whilst these studies are promising, they do not take into account the elaborate nature of whole eye development and solely focus on one cell type within the eye field. In development, signalling cues between distinct cell types are essential for differentiation of primordial cells into mature cellular phenotypes as in optic cup differentiation of PSCs. In addition, the resultant cells from these methods would require significant purification and optimisation to generate sufficient cells for transplantation. One promising method has generated 3D corneal organoid models that mimic the main three cell types of the cornea, namely stromal, epithelial and endothelial cells, however the scalability and generation of large amounts of corneal epithelial cells for transplant remains to be elucidated in this method (Foster et al., 2017). Recent work by our collaborators at Osaka University in Japan, has shown that hiPSCs can form self-formed ectodermal autonomous multizones (SEAMs) of ocular cells which present great promise as a tool for producing corneal epithelial cells from PSCs and can successfully generate transplantable cell sheets for the treatment of LSCD (Hayashi et al., 2016).

1.4.3 Self-formed ectodermal autonomous multizones (SEAMs)

SEAMs are an incredibly useful tool as they can mimic whole eye development to a certain extent in the more tractable 2D format and are so named as they spontaneously form different cell lineages from ectodermal anlages. They rely on the intrinsic self-organising capability of PSCs following prolonged culture and result in the formation of concentric rings of different cell types. Each zone within a SEAM is constituted of different cell types as shown in **Figure 1.6**.

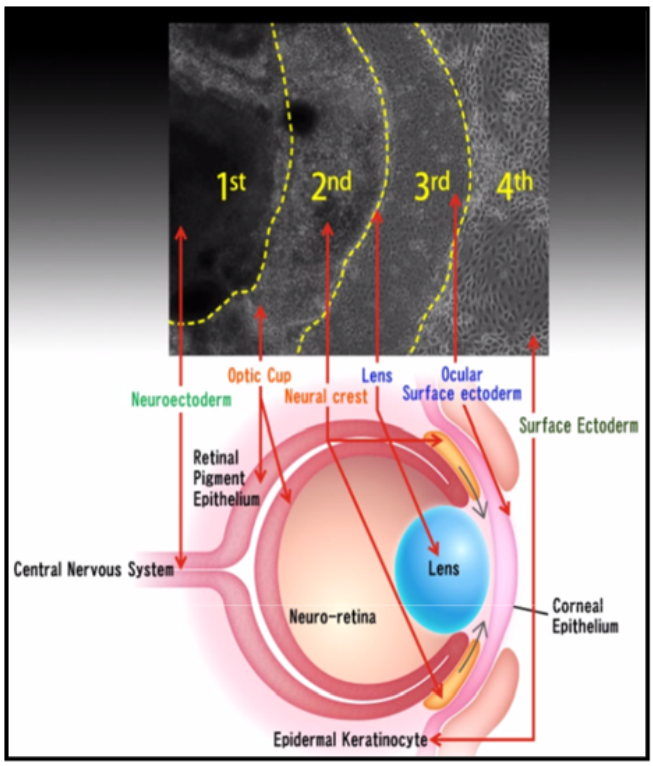

Figure 1.6 Human iPSCs form a primodium comprising four identifiable concentric zones, termed a self-formed ectodermal autonomous multi-zone (SEAM). Cell morphology in each zone is distinctive and partially mimics eye development. Adapted from (Hayashi et al., 2016).

Furthermore, cells isolated from SEAMs, in particular the zone 3 - ocular surface ectoderm-like cells have translational applications as they can be sorted and expanded to form corneal epithelium in an animal model of corneal blindness (Hayashi et al., 2016). Whilst a very promising technique, some issues with this protocol are the extended culture time of approximately 120 days (a large part of this being the 2 – 8 week corneal maturation stage), and the technical complexity of the procedure, requiring specialist facilities.

Further work by the group has shown that differing the sorting criteria for SEAM-generated epithelial progenitor cells can be improved by using CD200 as a negative sorting marker over TRA-1-60, as well as using cell-type specific adhesiveness to improve purification of corneal epithelial cells (Hayashi et al., 2018; Shibata et al., 2020). They have also shown how extracellular matrix molecules can greatly influence the differentiation propensity and cell morphology of these SEAM-derived corneal epithelial stem cells with different laminin isoform substrates and closely mirror those *in vivo* development.

LN332E8 was shown to promote the differentiation of corneal epithelial cells from iPSCs, a laminin isoform widely expressed in the basement membrane of the cornea (Schlötzer-Schrehardt et al., 2007; Shibata et al., 2018). Very recently the model has been shown to derive other eye cell types from the mixture of primordial cells, with 3D lacrimal gland organoids successfully being developed from SEAM cultures, showing its versatility and many possibilities (Hayashi et al., 2022). The presence of microglia-like cells has also been discovered, further demonstrating the complexity of this model (Shiraki et al., 2022)

These studies show the elegance and pliability of this method and that further interrogation of this method would be of great benefit, which leads towards the hypothesis of this study below, which is to investigate the effect of CS on the differentiation of these iPSC-derived corneal epithelial cells and other ocular cell types within SEAMs.

1.5 Hypothesis

The hypothesis of this study is that specific, isolated CS sulphation motifs from the extracellular matrix of the native corneal stem cell niche and engineered and native corneal epithelium can improve or alter the differentiation propensity of human corneal epithelial cells and other ocular cell lineages from SEAMs.

1.6 Experimental Aims

1.6.1 Aim for Chapter 2

The first aim of the project was to investigate the distribution of CS epitopes and CS proteoglycans in porcine cornea to inform the subsequent extraction and purification of CS isoforms from corneal tissue and identify corneal epithelial-associated CS sulphation motifs. This was to be conducted by analysing the presence of corneal epithelium in mature cornea, as well as the developing cornea using the SEAMs model and identify CS sulphation motifs associated with corneal epithelium. Initially porcine corneas were dissected from fresh whole globes and subsequently processed and analysed through immunohistochemistry to visualise the localisation of CS sulphation motifs as well as CS proteoglycans and identify any potential regulators of the stem cell niche or corneal epithelial-

associated CS species. The presence of sulphated glycosaminoglycans in the SEAM 2D model was also assessed to determine glycosaminoglycans present in the *in vitro* model.

1.6.2 Aim for Chapter 3

The next aim, following on from the preliminary microscopy studies, was to identify sources of glycosaminoglycans sulphation motifs of interest and perform extractions and enrich for these motifs of interest. Proteoglycans and glycosaminoglycans from porcine corneas were then extracted from both peripheral/limbal regions of the cornea as well as central corneal regions by guanidine hydrochloride chaotropic extraction. These extracted proteoglycans were then separated by isopycnic ultracentrifugation in the presence of caesium chloride and characterised to investigate their constituents. The proteoglycan and glycosaminoglycan composition of these preparations was assessed to identify the presence of glycosaminoglycan species of interest from the previous chapter. After characterisation and identification of enrichment targets, target CS proteoglycans and CS motifs were then enriched by ion-exchange chromatography and processed for use as a cell culture substrate upon which to grow and differentiate SEAMs.

1.6.3 Aim for Chapter 4

The final aim of the project was to culture SEAMs on the enriched glycosaminoglycan substrates, to investigate the effect of the glycosaminoglycans using an iPSC-based 2D eye model of the developing eye, specifically, the effect on the generation of SEAMs. As a result of the COVID-19 pandemic, this also involved establishing facilities for iPSC culture and SEAM generation in the UK, as this aim was due to be completed in specialist facilities in Osaka, Japan. Having successfully established facilities in Cardiff University, the generated SEAMs, grown upon specified glycosaminoglycan substrates, were analysed morphologically by light and immunofluorescence microscopy, as well as by qPCR for the expression of key corneal genes.

2 Chapter 2: Identification of stem cell niche associated CS epitopes

2.1 Introduction

The aim of this initial chapter was to identify potential candidate glycosaminoglycan and proteoglycan substrates, to inform their extraction and purification. They would then be used as a substrate upon which to differentiate corneal epithelial cells from iPSCs. The approach used here was to identify glycosaminoglycan sulphation patterns of interest, using specific CS/DS antibodies detailed in **Figure 1.5**. Key characteristics of CS/DS species of interest were those that were associated with either the corneal epithelium *in vivo* or *in vitro*. These include adult corneal epithelial cells from a mammalian tissue source or from stem cell-derived developing corneal epithelial-like cells. Also of particular interest, and investigated here, were glycosaminoglycan species of interest associated with the corneal epithelial stem cell niche, the corneal limbus.

Stem cell niches are key anatomical locations where normally quiescent multipotent stem cells can both proliferate and differentiate to maintain cellular homeostasis in their resident tissues as well as respond to illness or injury. They play a key role in the maintenance and repair of a wide range of structures throughout the body. Stem cell niches are not just the physical location within tissues but are comprised of various competing factors that will ultimately determine the cell fate of the resident stem cells. These components can include extracellular matrix molecules, adjacent cells, and cell-cell interactions. The nanotopography of the ambient surface and its physical properties can also play a role in the maintenance of the stem cell niche. Together, the conditions will ultimately provide stimuli for the stem cells to activate or repress certain genetic pathways and programmes thus determining their fate (Ferraro et al., 2010). Repurposing stem cell environmental cues and using them for the purposes of *in vitro* cell maintenance and differentiation is an established and useful tool and has been demonstrated in a variety of cell types. For example, in human mammary progenitor cells, substrate selection can be used to identify molecules that maintain the multipotency of the progenitor cells

in vitro as well as recognise signalling molecules that can keep the cells in a quiescent state (LaBarge et al., 2009). Another example is that of improving the *in vitro* maintenance of hematopoietic stem cells by presenting the cells with their native stem cell niche cues that are present *in vivo*, resulting in retainment of multipotency for a longer period compared to basal conditions (Roch et al., 2017).

There are some examples of this approach being used to recreate the limbal stem cell niche of the cornea, for example recreating the limbal epithelial crypts using collagen-based tissue equivalents (Levis and Daniels, 2016). Other interesting studies using this model include recreating the corneal stromal stem cell niche through the use of collagen gels as well as co-culturing supportive corneal stromal cells with limbal epithelial cells (Kureshi et al., 2015; Mukhey et al., 2018). Whilst effective at mimicking some aspects of the 3D physical environment, they do not capture the complete range of cell types and signalling molecules that are present in the corneal stem cell niche, which is a technically complex feat.

Many studies have explored the extracellular components of the limbal stem cell niche, focusing on both the cellular and acellular components. The general expression of various extracellular matrix molecules was established in a comprehensive study, which found various laminin isoforms (α1, α2 and ß2 chains) highlighted in the limbal niche along with other molecules, all located adjacent to ABCG2/p63/K19 positive epithelial stem cells. In the same study other molecules located in the limbus and the adjacent transition zone included CS and versican, a CS proteoglycan (Schlötzer-Schrehardt et al., 2007). The physical properties have also been explored with 3D imaging-derived models of the limbus detailing the interaction of limbal crypts and focal stromal projections being key to the highest concentration of stem cells expressing putative stem cell markers (Shortt et al., 2007). Whilst some of these factors have been used in attempts at engineering corneal epithelial cells, including using decellularized limbal scaffolds (Polisetti et al., 2021a, 2021b), much work is needed to understand the function and role of these components in the stem cell niche, and which components contribute to maintaining cells in their

multipotent state versus ensuring temporally and spatially correct differentiation.

This chapter focuses on identifying CS species present in the corneal limbus/corneal epithelium and in engineered corneal epithelial cells to inform and take cues from an aspect of native extracellular matrix deposition, similarly to the studies stated above. To investigate this, monoclonal antibodies recognising specific CS epitopes were utilised to identify potential candidate molecules, namely those associated with either the corneal limbus and epithelium *in vivo* or associated with engineered developing corneal epithelial cells *in vitro*. These antibodies and their binding are shown in **Figure 1.5**. Both the porcine corneal limbus and epithelium, representing mature adult limbus, as well as iPSC-derived corneal epithelial cells in SEAMs, representing a 2D model of the developing eye – including corneal epithelial-like cells, were investigated for potential molecular markers. Both models are well characterised, with the porcine limbus representing the most biochemically and anatomically similar animal model to human cornea (Hammond, 2021; Sharifi et al., 2019) and SEAMs representing an useful, tractable model of corneal development (Hayashi et al., 2016). Both analyses will be used to facilitate the further extraction of molecules of interest, namely CS molecules that have previously been identified as stem cell-associated or associated with the corneal epithelium.

Previously, these molecular markers, namely CS epitopes, have been investigated in the presumptive rabbit limbus and in human limbus, with the CS epitope recognised by the antibody 6C3 most notably being localised subjacent to the limbus in both rabbit and human limbus. Other epitopes present included those recognised by the 7D4, 4C3 and 3B3 anti-CS antibodies (detailed in **Figure 1.5**) (Yamada et al., 2015). Extracting sufficient glycosaminoglycan material enriched in these sulphation motifs for use in further studies would have been untenable to use a human source, due to the difficulty of obtaining sufficient tissue and subsequent ethical concerns. To this end, a commercial porcine source has been used, which could theoretically be a therapeutic source, as many medical products are still derived from high quality meat industrial byproducts, for example heparin derived from porcine intestinal mucosa is still

widely used in the USA and the UK, despite synthetic alternatives being available, this is typically due to synthetic heparin's much higher cost (Linhardt and Liu, 2012; van der Meer et al., 2017). Porcine tissue is also preferred over bovine as a reduced risk of bovine spongiform encephalopathy. Prior to attempting to extract proteoglycans and glycosaminoglycans from porcine tissue, it was necessary to determine the distribution in these tissues to inform their extraction and purification.

Detailed in this chapter are the results of immunohistochemical analyses of CS/DS epitopes in both porcine corneal tissue and developing SEAMs. Whilst similar studies have been done in other mammalian limbus studies for the former, the analysis here is novel in porcine corneal tissue and serves as a useful model of human cornea. For the SEAM analyses, this is the first documented analysis of distribution of sulphated CS glycosaminoglycan epitope mapping in the SEAM and also any PSC-derived corneal tissue or organoid. Various glycosaminoglycan species were identified that hold potential for further investigation and use as a substrate as detailed in this chapter. This subsequently enabled further attempts at extraction and purification for use as a substrate in the following chapters. These glycosaminoglycan species were the CS epitopes recognised by the antibodies 6C3, which was found to be strongly associated with the corneal limbus, and 7D4, which was found to be associated with the corneal epithelium *in vivo* and with developing iPSC-derived corneal epithelium *in vitro*.

2.2 Methods

2.2.1 Tissue Acquisition and Processing

Whole porcine globes were acquired from a local abattoir (Maddock Kembery Meats, Maesteg, Wales, UK), transported to the laboratory on ice (approximately 45 mins) and processed immediately after acquisition. Porcine tissue is used as a model system as the limbal crypts are relatively similar to human limbal morphology compared to other models e.g. murine limbus, and are also present on the entire circumference of the limbus, allowing for easier tissue processing and less wastage (Grieve et al., 2015).

The cornea was dissected from the rest of the globe using a scalpel and adherent iris and lens tissue were carefully removed. The cornea was then cut into quarters and pieces were trimmed as in **Figure 2.1**. These pieces were then immersed in a sequential sucrose gradient (10, 20 and 30% (w/v) sucrose in water) on a rotator for 20 minutes each at room temperature. The corneal pieces were then immersed in 50% (v/v) OCT (optimal cutting temperature compound)/50% (v/v) PBS on a rotator for 20 minutes before finally being transferred to OCT and rapidly frozen on liquid nitrogen cooled blocks and stored at -20°C prior to sectioning.

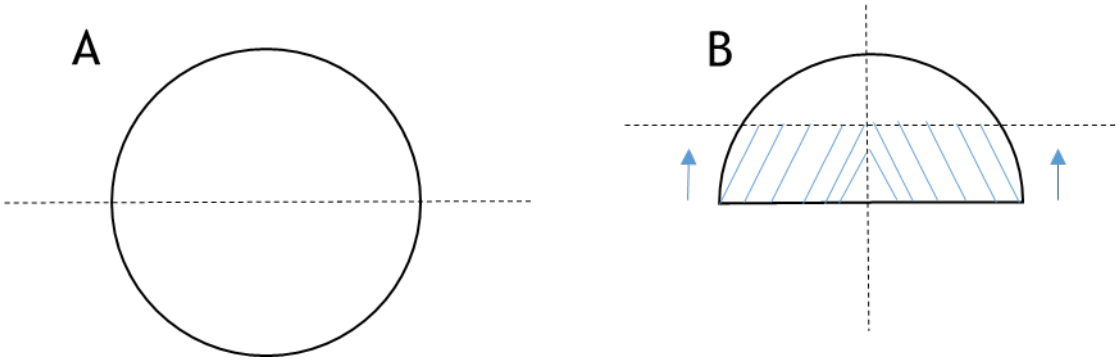

Figure 2.1 Dissection diagram for porcine cornea. (**A**) Whole cornea is bisected axially across the central cornea. (**B**) Each half corneal segment was bisected again and trimmed leaving the blue dashed segments for further processing with the blue arrows representing sectioning direction from the horizontal plane to the superior and dorsal edges of the cornea.

2.2.2 *Immunohistochemistry of porcine cornea*

All chemicals were from Merck, Gillinham, unless otherwise stated. Immunohistochemistry was performed as described previously with modifications as described (Yamada et al., 2015). Porcine cornea samples frozen in OCT were cryosectioned at 15 µm thick and adhered to Superfrost glass slides (Thermofisher, Loughborough) prior to staining. For chondroitinase ABC pre-treated sections (enzymatic digestion of CS chains and loss of epitopes/generation of neoepitopes), slides were rehydrated in PBS for 5 minutes and then incubated for 2 hours at 37°C in 0.1 U/ml chondroitinase ABC (Sigma-Aldrich, Gillingham) in 50mM Tris-HCl buffer with 60mM sodium acetate at pH 8.0 before processing as described below.

All sections were immersed in PBS for 5 minutes to rehydrate before being blocked in PBS with 1% (w/v) bovine serum albumin (BSA) and 0.05% (v/v) Tween 20 for 1 hour at room temperature. All primary and secondary antibodies were diluted in PBS with 1% (w/v) BSA and 0.05% (v/v) Tween 20. In-house primary monoclonal antibody concentrations were optimised and then applied as follows: 6C3 (1 in 10 dilution, mouse IgM), 7D4 (1 in 100 dilution, mouse IgM), 4C3 (1 in 100 dilution, mouse IgM) and decorin (1 in 100 dilution, mouse IgG) (Bidanset et al., 1992; Sorrell et al., 1990), all for approximately 16 hours at 4°C. Negative controls included primary antibody omission and a mouse non-specific IgM control. Sections were then washed before the application of the secondary antibody, goat anti-mouse antibody (IgM and IgG) or goat anti-rabbit (IgM and IgG) conjugated to Alex Fluor 488 (Thermofisher, Loughborough), diluted to 2 µg/ml for 30 minutes at room temperature. After the final wash, sections were mounted with Fluoroshield mounting medium with DAPI (Abcam, Cambridge) and imaged using an Olympus BX61 fluorescent microscope.

2.2.3 Immunohistochemistry of SEAMs

SEAMs were generated as described previously (Hayashi et al., 2017, 2016), and kindly provided for immunohistochemical analysis by Dr Jodie Harrington, Osaka University, and their generation is described as detailed in Chapter 4 Section 4.2.4. Cells were initially coated at three seeding densities in a 24 well plate format; 300, 600 and 900 cells in each well equating to approximately 937, 1913 and 2888 cells/cm^2 respectively. SEAMs after 4, 5 or 6 weeks of differentiation culture were fixed in 4% (wt/vol) PFA at room temperature for 20 minutes at room temperature. The SEAMs were then washed 3 times with TBS. SEAMs were then blocked in TBS containing 5% (vol/vol) normal donkey serum and 0.3% (wt/vol) Triton X-100 for 1 hour at room temperature. The SEAMs were then incubated with the following CS/DS and KS antibodies: 6C3 (1 in 10 dilution, mouse IgM), 7D4 (1 in 20 dilution, mouse IgM), 4C3 (1 in 20 dilution, mouse IgM) (Sorrell et al., 1990) and 5D4 (1 in 20 dilution, mouse IgM) (Caterson et al., 1983) overnight at 4 °C diluted in TBS containing 1% (vol/vol) normal donkey serum and 0.3% (wt/vol) Triton X-100. The SEAMs were then washed three times with TBS for 5 min. and subsequently incubated with the secondary antibody: 1:1000 dilution of Alexa Fluor® 488-conjugated goat anti-mouse IgG/IgA/IgM

secondary antibody (Invitrogen) for 1 hour at room temperature in the dark. The SEAMs were then washed three times with TBS for 5 min. Finally, the SEAMs were then incubated with Hoechst 33342 for 10 min at room temperature under protection from light, washed three times with TBS for 5 min and imaged under fluorescence microscopy using a Keyence BZ-x800 series Fluorescence Microscope. Negative controls were performed using primary antibody omission and shown in the appendix in **Figure 7.1** for 7D4 antibody staining in SEAMs and **Figure 7.2** for co-localisation studies performed in SEAMs.

2.3 Results

2.3.1 Identification of corneal epithelial and corneal limbus-associated CS sulphation motifs and CS proteoglycans in the porcine cornea

A panel of antibodies (7D4, 6C3 and 3B3) were used in this study to recognise native (non-digested) and chondroitinase digest-generated CS carbohydrate motifs as described in Chapter 1 of this thesis (Section 1.3.4). The CS/DS glycosaminoglycan-degrading enzyme chondroitinase ABC was used to digest CS and DS chains, as a control group for native sulfation epitopes recognised by 6C3 and 7D4. However, for the 3B3 antibody, enzymatic digestion is required to reveal the neoepitope, as it was originally generated against a chondroitinase digested proteoglycan. Chondroitinase ABC digestion is denoted by + (digested) or – (undigested native chains).

Of these three epitopes, the one recognised by 7D4 (-) (**Figure 2.2A**) was expressed throughout the central corneal stroma but not in the epithelium. There was also an area of increased signal density in the stromal region directly subjacent to the corneal epithelium. Whilst minimal staining was present in the limbal area. There was slightly increased positive signal in the area adjacent to the corneal limbus subjacent to the epithelium which corresponds with the location of transient amplifying cells.

Secondly, the epitope recognised by the antibody 6C3 (-) immunolocalised almost exclusively below the basement membrane of the corneal limbal crypt area (**Figure 2.2C)** and extended slightly into the basement membrane of the conjunctiva. The signal appeared to surround the cells directly below the

basement membrane of the limbal crypt but did not extend into the multipotent stem cell compartment in the basal layer of the limbus.

There was no positive staining for the epitope recognised by the antibody 3B3 (-) throughout the corneal stroma (**Figure 2.2E**) and its neoepitope was only revealed upon chondroitinase ABC treatment, with the 3B3 (+) antibody neoepitope showing an area of positive signal adjacent to the limbus, similar to but not identical to the 6C3 signal (**Figure 2.2F**).

All fluorescent staining is lost with chondroitinase ABC treatment for the 7D4 and 6C3 antibodies (**Figure 2.2B, D**). Negative controls conducted included an isotype (mouse IgM) control and showed no immunoreactivity detectable by immunofluorescence (**Figure 2.2G, H**). Other antibodies were also investigated, including CS/DS antibody 4C3, however staining results were either negative or non specific.

The abundant corneal CS/DS proteoglycan decorin was also probed using a monoclonal antibody to identify any associations with the corneal limbus or epithelium. The expression pattern appears to be diffuse throughout the corneal stroma, however an area of slightly higher signal intensity was observed in the peri-limbal area (**Figure 2.3A**).

Overall the CS/DS sulphation motifs recognised by the 7D4 and 6C3 antibodies are of interest owing to their association with the corneal epithelium, for the 7D4 antibody, and association with the basal layer of the corneal limbus, in the case of the 6C3 antibody.

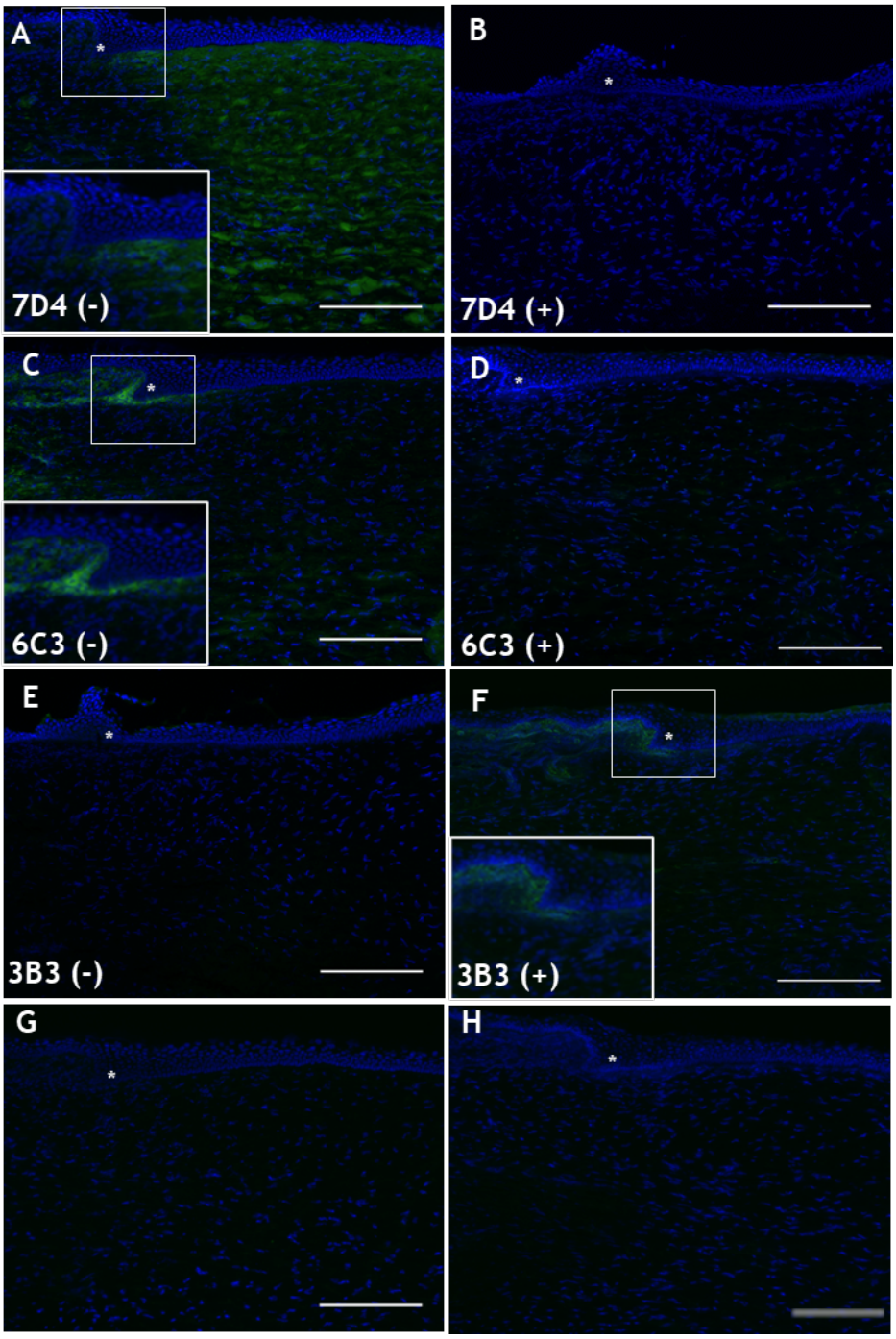

Figure 2.2 Immunolocalisation of 7D4, 6C3, and 3B3 monoclonal antibodies recognising distinct CS/DS sulphation motifs. (**A, C, E**) Images show epitope localisation without chondroitinase ABC pretreatment. Arrow in (**C**) represents high signal area adjacent to limbus where transient amplifying cells reside. (**B, D, F**) Images showing the same epitopes but with chondroitinase ABC treatment. (**G, H**) No primary antibody negative control image without and with chondroitinase ABC treatment respectively. The limbus is located towards the left in all images and identified with an asterisk and the central cornea is located to the right. The scale bar represents 200 µm. Magnified regions indicated by white boxes surrounding limbus are shown in (**A, C, F**).

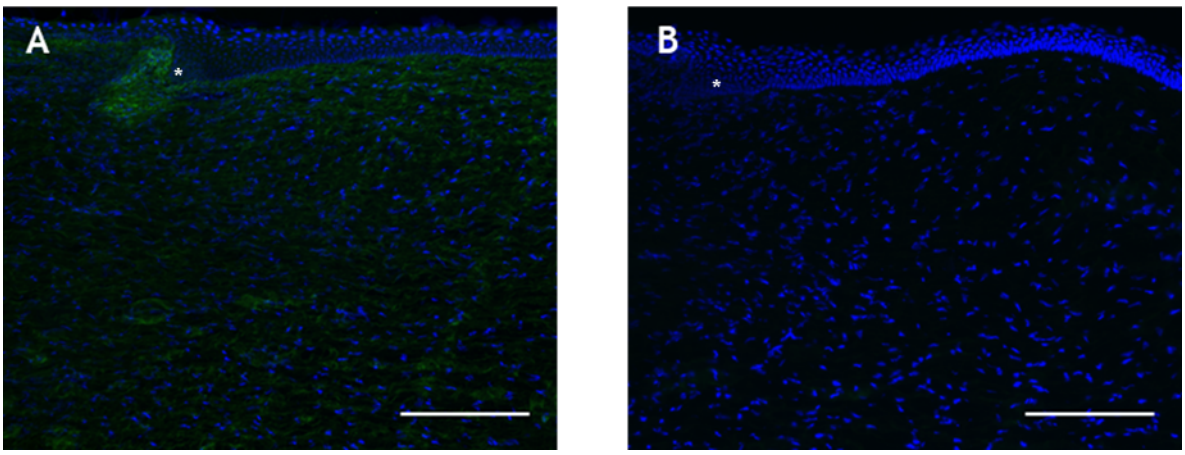

Figure 2.3 Immunolocalisation of decorin (core protein) proteoglycan in porcine corneal limbus. (**A**) Positive staining for decorin core protein with the limbal region indicated by the white asterisk. (**B**) Negative control in the same orientation. In both images sclera is towards the left and central cornea towards the right, with the limbus identified by an asterisk. Scale bars represent 200 μm.

2.3.2 Identification of CS/DS deposition in iPSC-derived corneal epithelial cells

Owing to the fact SEAMs are a useful model in mimicking whole eye development, various CS/DS sulphation epitopes could be present and may be of interest in accelerating or affecting differentiation. Various CS/DS markers were examined in developing SEAMs, including the epitopes recognised by the following antibodies: 4C3, 6C3 and 7D4, however preliminary results showed that the only CS/DS epitope present in developing SEAMs in zone 3 (wherein reside corneal epithelial cells), and indeed any other zones was 7D4 with the spatiotemporal labelling being very specific and highly interesting.

One important note in the observation of SEAMs and as a reminder, they typically possess a clear morphological pattern with three concentric zones followed by space between SEAMs as shown in **Figure 1.6** in Chapter 1. They are quite heterogenous and can also fuse together, whereby they typically still retain the zonal formation but lack the typical circular morphology. The first zone composes of a high optical density centre (zone 1) - representing neuronal cells. The second zone typically consists of a diffuse area of low then high optical density cells outside of the centre (zone 2) – representing neural crest, retina-like and lens-like cells. The third zone (zone 3), of particular interest in this study, lies outside of zone 2 and is typically of low optical density with tightly packed epithelial cells, which represent ocular surface ectoderm-like cells or early corneal epithelial-like cells. Lens cells are also sometimes present in this zone. Finally, the fourth zone (zone 4) lies outside of the edge of the zone 3 and cells are typically more dispersed, and this zone consists primarily of non-ocular surface epithelial-like cells.

Initial results of immunohistochemical labelling of the CS/DS epitope recognised by the antibody 7D4 are shown in **Figure 2.4**. SEAMs shown at weeks 4 (**Figure 2.4A**) and 6 (**Figure 2.4B**) show the increased size and differentiation of the zone 3 over the time course, which will later differentiate to represent mature corneal epithelial cells. Correspondingly, immunolocalization of the epitope recognised by the 7D4 CS/DS antibody shows widespread circumferential deposition of CS/DS in the transitional zone at the edge of zone 2 spreading into zone 3 at week 4 of SEAM differentiation (**Figure 2.4C, E**).

Two weeks further into differentiation at week 6, further CS/DS deposition can be seen in all zones, particularly increased amounts in zone 3, forming a mesh-like structure around clusters of cells (**Figure 2.4D, F**).

Further evidence can be witnessed in **Figure 2.5**, **Figure 2.6** and **Figure 2.7**, taken at weeks four, five and six of differentiation respectively, shown in higher detail and at varying seeding densities. Increasing the seeding density generally appeared to result in increased CS/DS deposition in addition to increasing across the time course, particularly in zones 3 and 4, which contain ocular surface and non-ocular surface epithelial-like cells, however this was not quantitatively confirmed. The positive signal spreads radially outward generally over the time course suggesting a role in either the development of corneal epithelial progenitors in the third zone of the SEAMs

At all timepoints, 7D4 antibody signal appears as an octagonal network surrounding clusters of cells in zone 3, however the extent of the signal throughout zone 3 and its distribution changes from four weeks to six weeks and varies slightly by seeding density. At week four, the signal generated by the 7D4 antibody primarily appears to locate close to the leading edge of cells located in zone 3 and does not extend greatly into other zones, as shown in **Figure 2.5B, D** and **F**. At week five, the signal generated by the 7D4 CS/DS antibody extends further into zone 3 and more widely throughout the zone, particularly at higher seeding densities as shown in **Figure 2.6D** and **F**. By week six, CS/DS deposition is present throughout zone 3 and extends into zone 4 and 2, with many cells present in octagonal clusters, particularly in regions closer to the centre of the SEAM as shown in **Figure 2.7C** and **F** and indicated with an asterisk in **F**.

Further markers were also investigated, including the CS/DS antibody 4C3 and the highly sulphated KS antibody, 5D4, however both revealed little to no specific staining at weeks 4, 5 and 6 of differentiation. 6C3 was present occasionally in zone 4, as shown in Section 2.3.4.

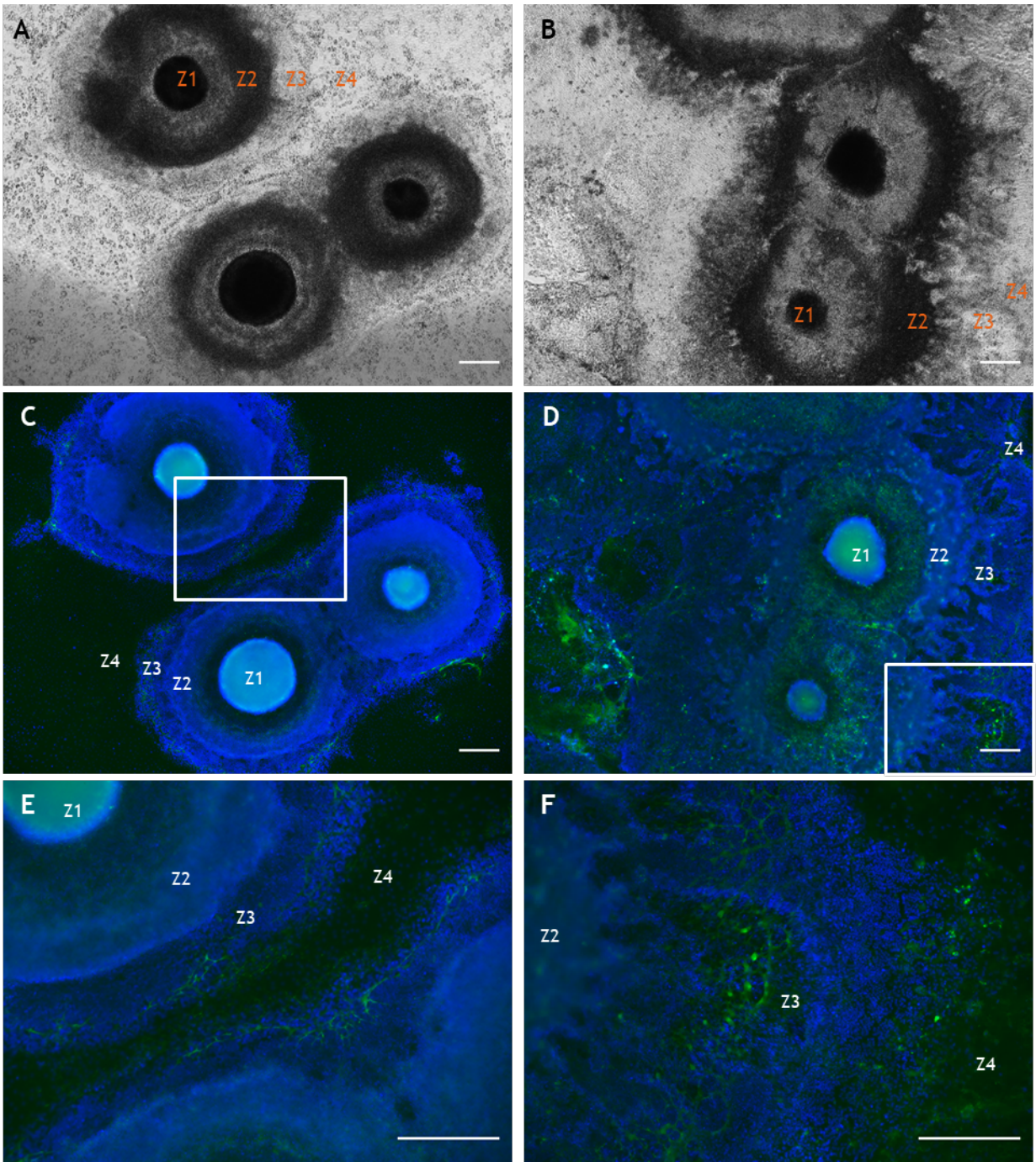

Figure 2.4 Comparison of CS/DS using antibody 7D4 within developing SEAM cultures at weeks 4 and 6 of differentiation with each zone (Z) indicated. **(A, B)** Wide-field phase contrast view of three SEAM colonies at week 4 (**A**) and 6 (**B**) of differentiation. (**C, D**) Immunofluorescence image of a SEAM at week 4 (**C**) and week 6 (**D**) of differentiation, 7D4 antibody signal is shown in green and nuclear Hoechst 334 staining in blue. (**E, F**) Higher magnification view of CS/DS immunolocalisation in selected regions in (**C**) and (**D**) respectively. Scale bars for all images represent 100 µm.

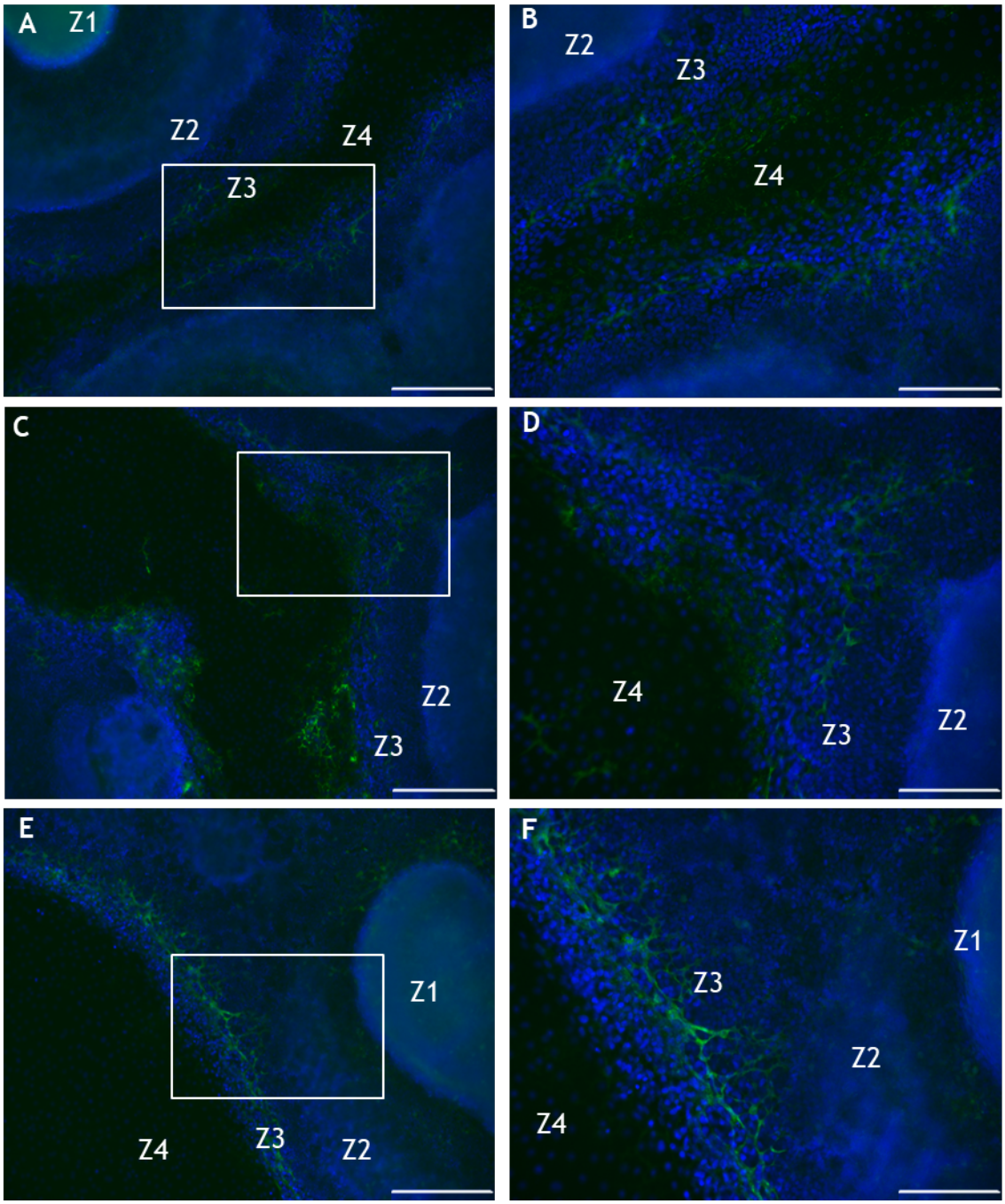

Figure 2.5 Immunolocalisation of 7D4 CS/DS antibody in a SEAM after 4 weeks of differentiation at different seeding densities with nuclei stained with Hoechst 334 in blue with each zone (Z) indicated. (**A**) Widefield-view of representative SEAMs at 300 seeding cell density. (**B**) Magnified view of area indicated by the white rectangle in (**A**). (**C**) Widefield-view of representative SEAMs at 600 seeding cell density. (**D**) Magnified view of area indicated by the white rectangle in (**C**). (**E**) Widefield-view of representative SEAMs at 900 seeding cell density. (**F**) Magnified view of area indicated by the white rectangle in (**E**). Scale bars represent 100 µm for (**A, C, E**) and 50 µm for (**B, D, E**).

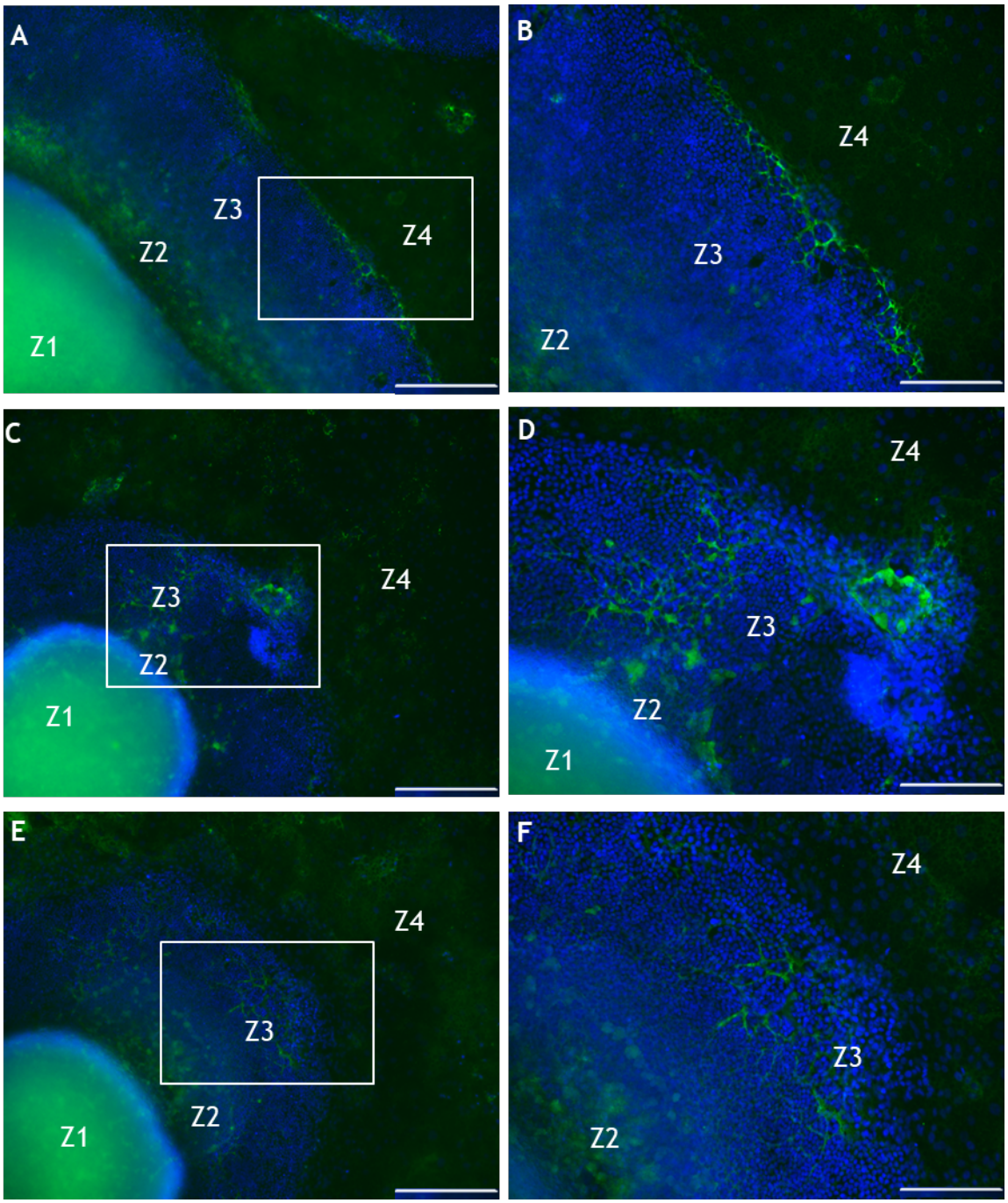

Figure 2.6 Immunolocalisation of 7D4 CS/DS antibody in a SEAM after 5 weeks of differentiation with each zone (Z) indicated with nuclei stained with Hoechst 334 in blue. (**A**) Widefield-view of representative SEAMs at 300 seeding cell density. (**B**) Magnified view of area indicated by the white rectangle in (**A**). (**C**) Widefield-view of representative SEAMs at 600 seeding cell density. (**D**) Magnified view of area indicated by the white rectangle in (**C**). (**E**) Widefield-view of representative SEAMs at 900 seeding cell density. (**F**) Magnified view of area indicated by the white rectangle in (**E**). Scale bars represent 100 µm for (**A, C, E**) and 50 µm for (**B, D, E**).

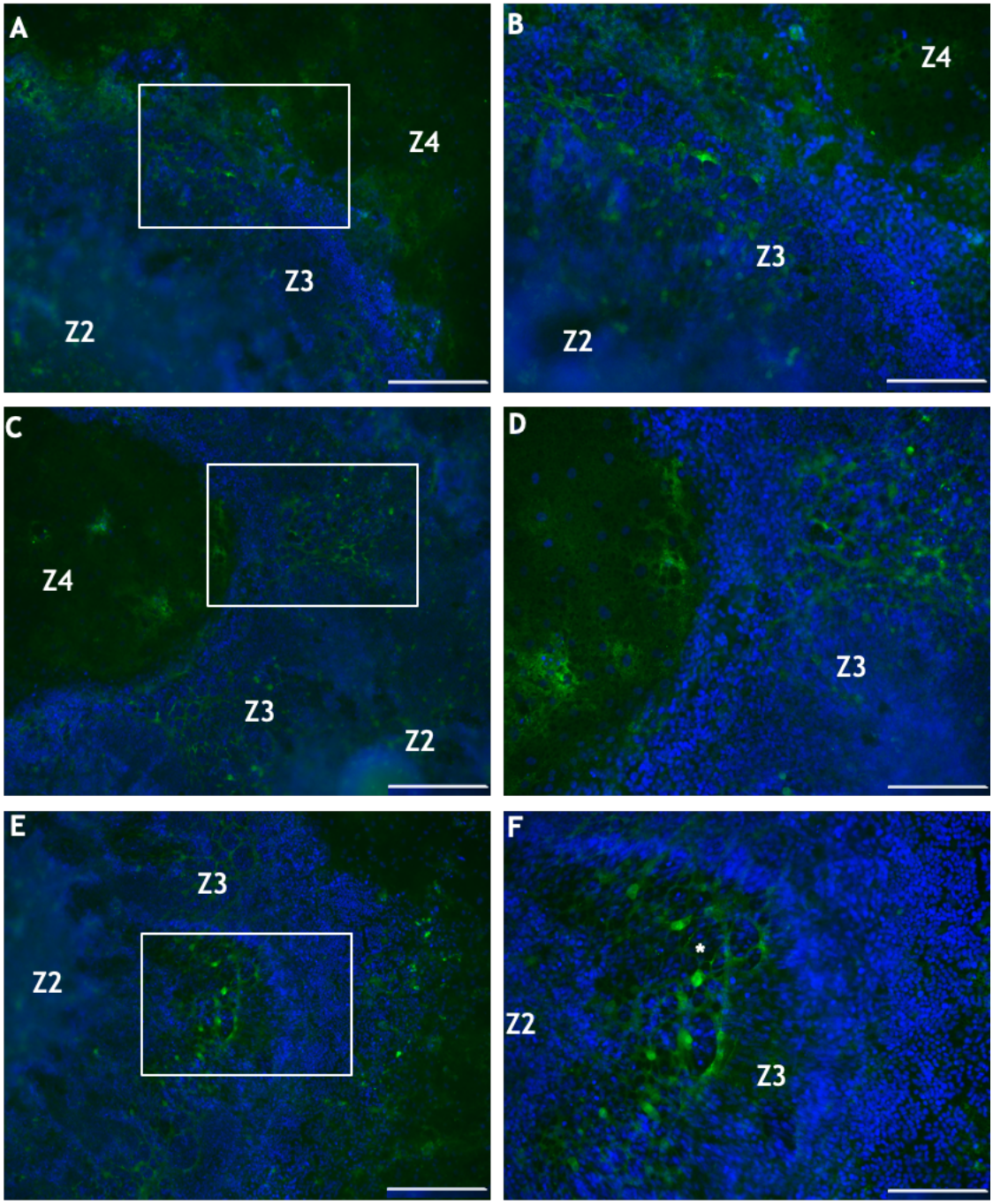

Figure 2.7 Immunolocalisation of 7D4 CS/DS antibody in a SEAM after 6 weeks of differentiation with nuclei stained with Hoechst 334 in blue with each zone (Z) indicated. (**A**) Widefield-view of representative SEAMs at 300 seeding cell density. (**B**) Magnified view of area indicated by the white rectangle in (**A**). (**C**) Widefield-view of representative SEAMs at 600 seeding cell density. (**D**) Magnified view of area indicated by the white rectangle in (**C**). (**E**) Widefield-view of representative SEAMs at 900 seeding cell density. (**F**) Magnified view of area indicated by the white rectangle in (**E**) with * showing octagonal cell clusters. Scale bars represent 100 µm for (**A, C, E**) and 50 µm for (**B, D, E**).

2.3.3 *Primordial corneal epithelial stem cells are located adjacent and beyond CS/DS deposits in the developing SEAM*

Finally, in order to ascertain whether the epitope recognised by the 7D4 antibody was associated with primordial corneal epithelial stem cells, as postulated above, a colocalization study was conducted at 4 weeks of SEAM differentiation with keratin-14 (K14), a primordial corneal epithelial marker. SEAMs of three different SEAM seeding densities (low, medium and high) were analysed to ascertain any interactions between the CS/DS epitope and primordial stem cells.

The K14 marker appeared to label selected cells located adjacent to and beyond the circumferential 7D4 staining in zone 3 where the immature corneal epithelial-like cells reside and extended into zone 4. K14-positive cells were located primarily on the outer edge of zone 3 and exterior of any 7D4 CS/DS signal, as seen in **Figure 2.8A**, **Figure 2.9A** and **Figure 2.10A**. The location and number of K14 positive cells did not appear to change much with seeding density. Concordant with observations in the previous section (2.3.2), CS/DS deposition also appears to increase with seeding density, as seen in **Figure 2.8B**, **Figure 2.9B** and **Figure 2.10B**.

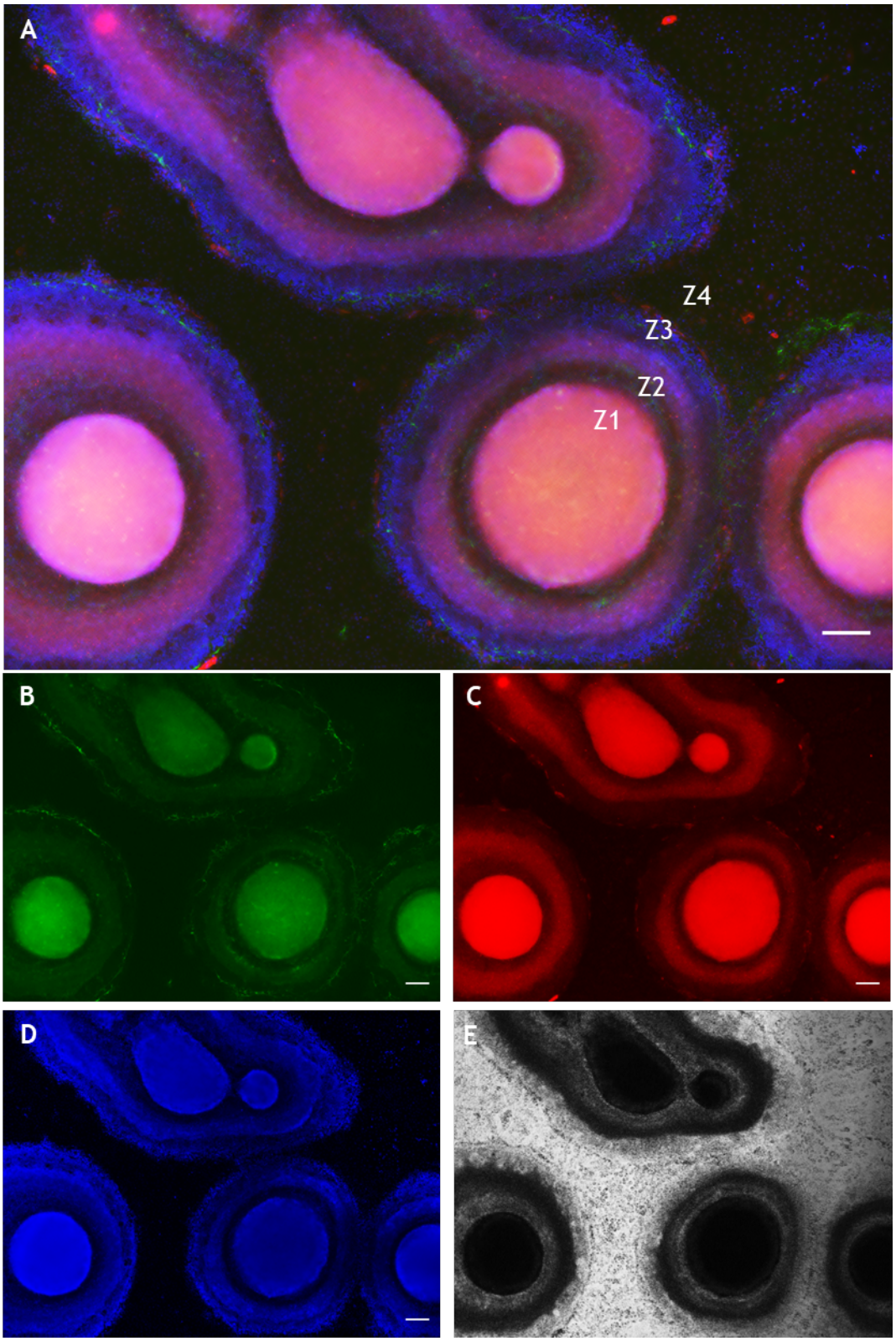

Figure 2.8 Immunolocalisation of CS/DS antibody 7D4 and keratin-14 in a SEAM after 4 weeks of differentiation at low seeding density (300 cells). (**A**) Fluorescence view of a representative SEAM. Keratin-14 (K14) is shown in red, 7D4 in green and Hoechst 334 nuclear stain in blue. (**B, C, D**) Show the single channel image of 7D4 (green), K14 (red) and Hoechst 334 (blue) respectively. (**E**) Brightfield view of the same regions. All scale bars represent 200 μm.

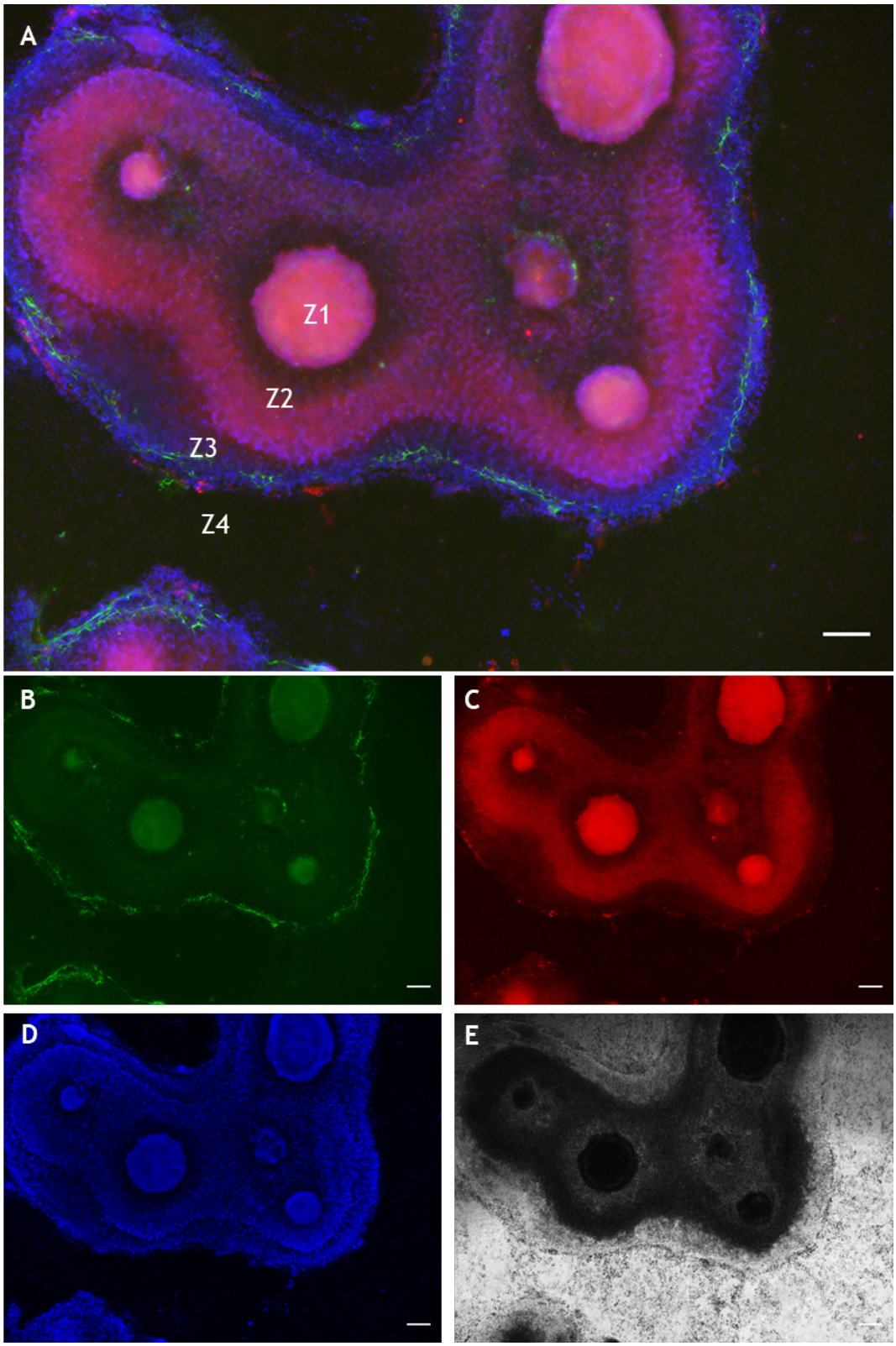

Figure 2.9 Immunolocalisation of CS/DS antibody 7D4 and keratin-14 in a SEAM after 4 weeks of differentiation at medium seeding density (600 cells). (**A**) Fluorescence view of a representative SEAM. Keratin-14 (K14) is shown in red, 7D4 in green and Hoechst 334 nuclear stain in blue. (**B, C, D**) Show the single channel image of 7D4 (green), K14 (red) and Hoechst 334 (blue) respectively. (**E**) Brightfield view of the same regions. All scale bars represent 200 μm.

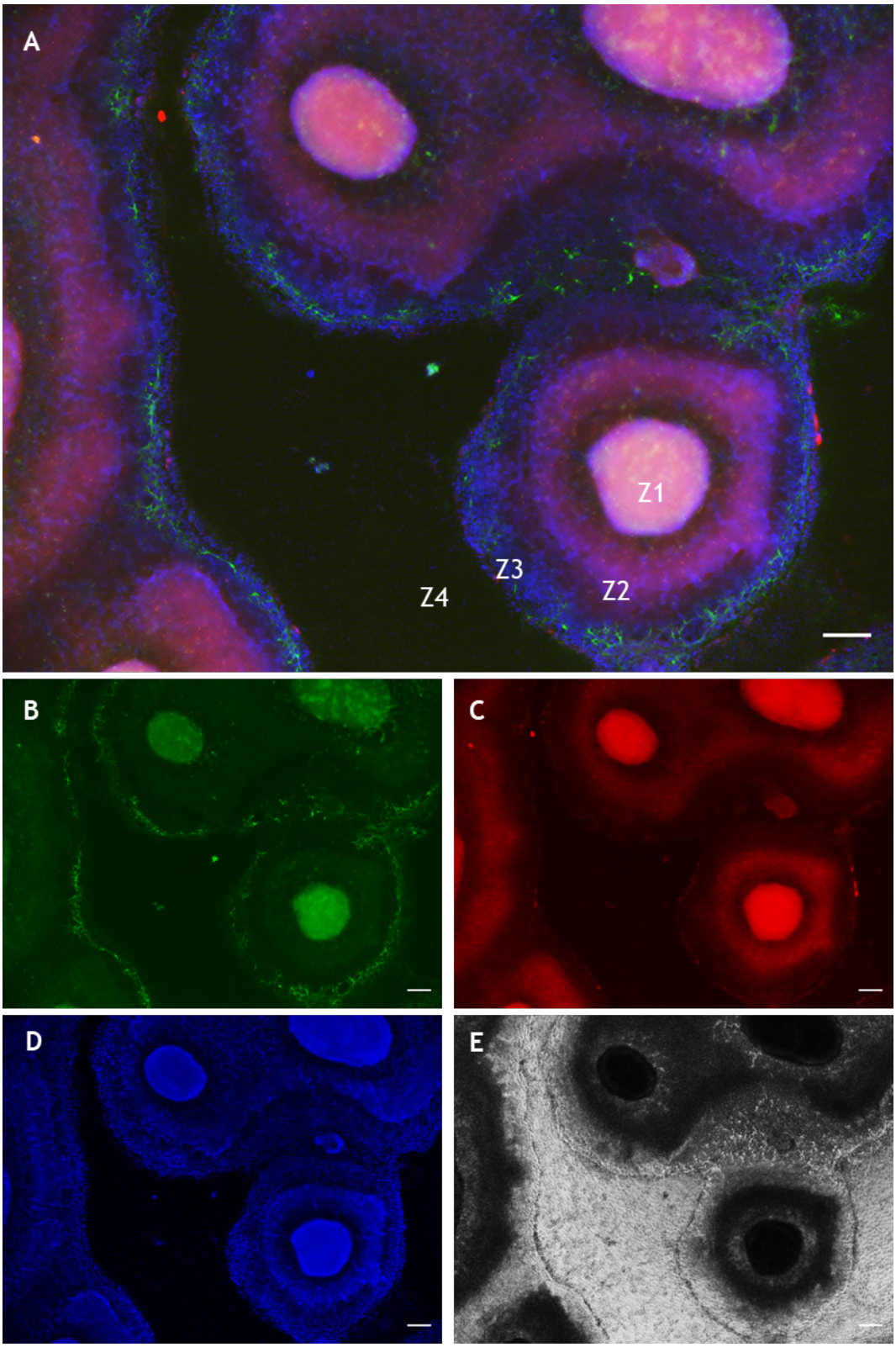

Figure 2.10 Immunolocalisation of CS/DS antibody 7D4 and keratin-14 in a SEAM after 4 weeks of differentiation at high seeding density (900 cells). (**A**) Fluorescence view of a representative SEAM. Keratin-14 (K14) is shown in red, 7D4 in green and Hoechst 334 nuclear stain in blue. (**B, C, D**) Show the single channel image of 7D4 (green), K14 (red) and Hoechst 334 (blue) respectively. (**E**) Brightfield view of the same regions. All scale bars represent 200 μm.

2.3.4 *The 6C3 CS/DS epitope is present in the outer zones of SEAMs*

An interesting incidental finding, was the presence of some small clusters of cells in zone 4 between SEAMs producing extracellular matrix rich in the 6C3 CS/DS epitope as shown in **Figure 2.11**. They were only seen in SEAMs seeded at the lowest seeding densities, where there is more space between and fewer SEAMs per cell culture well at weeks 4 and 5, suggesting they are a spontaneously differentiated cell type outside of the typically non-ocular surface epithelial cells found in zone 4.

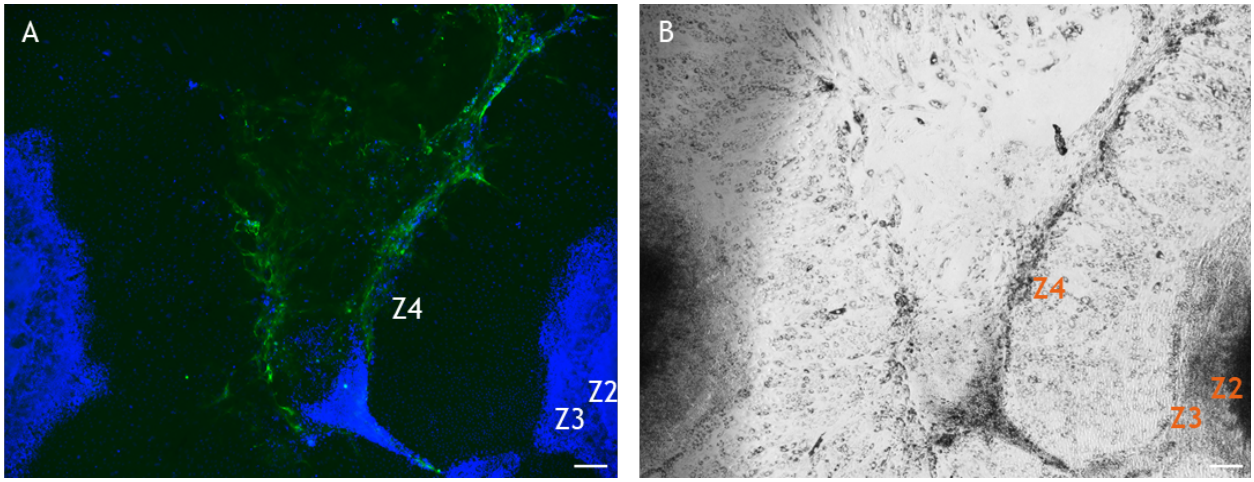

Figure 2.11 Immunolocalisation of CS/DS antibody 6C3 in zone 4 of a SEAM after 4 weeks of differentiation. (**A**) Fluorescence view of 6C3 antibody localisation at a seeding density of 300 cells in a region between two SEAMs (to the left and lower right of the image) with cell nuclei stained with Hoechst 334. (**B**) Brightfield image of the same area as in (**A**). Scale bars represent 200 µm.

2.4 Discussion

The antibodies employed in this study are specific to native CS/DS side chains and whilst the precise subtleties of these epitopes is not fully characterised, they are a useful tool in discovering distinct motifs and their distribution in tissues as they are structurally distinct from generic disaccharide repeats (Hayes et al., 2016, 2008; Sorrell et al., 1993, 1990). Here these sulphation motif antibodies were used to identify candidate molecules for extraction and use as cell culture substrate in order to later develop corneal epithelial cells and other ocular cell types from iPSCs. This was achieved through investigating the presence of specific sulphation patterns present within the adult corneal limbus and epithelium as well as investigating those present in SEAMs, which mimic human eye development.

The distribution of these motifs has been investigated in the presumptive corneal stem niche in the rabbit limbus (and to a certain extent human for which comparisons can be drawn from the rabbit tissue to porcine (Yamada et al., 2015), with porcine tissue bearing much more resemblance to human tissue (Grieve et al., 2015). Interestingly the antibody recognising the 6C3 epitope had very similar limbal basement membrane localisation to the presumptive limbus in the rabbit (and human as stated), further supporting the idea of the epitope recognised by the 6C3 antibody's role in maintenance of the stem cell niche in corneal tissue in addition to other connective tissues in which it was identified. In further collaborative, published work it has also been shown that 6C3 immunolocalisation is closely associated with the location of basal limbal stem cells identified by the stem cell markers ABCB5 and keratin 19 (Ashworth et al., 2021). The epitope recognised by the 7D4 antibody appears to have slightly higher signal in the limbal transition zone where it has been suggested transient amplifying cells reside (Gonzalez et al., 2018; Yoon et al., 2014), possibly suggesting a role of the epitope recognised by the 7D4 antibody plays a role in the maturation and differentiation of limbal stem cells towards the mature epithelial phenotype.

Initial results investigating the localisation of the protein cores of these glycosaminoglycan distributions suggest that decorin appears to have a higher

fluorescent signal in the limbal area. However, it is also widely present throughout the stroma, and appears not to interact with 6C3 staining for example and so performing co-localisation studies to rule out any interaction may not be of much benefit. Another issue is the lack of chondroitinase ABC in the decorin analysis, which may have helped further unmask the decorin antibody epitope leading to higher signal and perhaps unmasking further decorin deposition throughout the cornea. Further proteoglycan co-localisation studies would be particularly useful, for example biglycan, which has been shown to be present in other connective tissue stem cell niches throughout the body (Bi et al., 2007). However in preliminary studies conducted, staining was inconclusive and did not specifically highlight any region in the cornea and was expressed throughout the epithelium as has been identified previously (Funderburgh et al., 1998). Previous studies have also shown shown that distribution of decorin is relatively constant throughout developmental periods and across the cornea, whereas biglycan decreases throughout maturity (Zhang et al., 2009). The overabundance of these molecules in the cornea suggests that the protein cores are perhaps less important rather than the species of CS/DS glycosaminoglycan that reside on their chains throughout the corneal stroma and epithelial surface, hence the usefulness of looking at individual glycosaminoglycan isotopes recognisable by antibody. This is supported by biglycan upregulation in absence of decorin in mouse knockout models (Zhang et al., 2009). This compensatory effect may also explain the observation that decorin lacking DS chains appears to have no phenotype, as upregulation of biglycan may compensate for its effect (Moffatt et al., 2017). Regardless, the identity of these cores can also be elucidated by extraction and protein analysis as detailed in further chapters.

Secondly, investigations into the CS/DS deposition in SEAMs revealed interesting and novel insights into the proteoglycan/glycosaminoglycan deposition of iPSC-derived primordial corneal epithelial cells during their differentiation. The epitope recognised by the CS/DS 7D4 antibody clearly, and initially, at week four, localised on the border between zone 2 and 3 suggesting deposition of a specific matrix that potentially facilitates the formation of a barrier separating the two cell populations as described previously in developmental studies of connective tissue (Hayes et al., 2016). As the SEAM differentiated further in

weeks five and six, glycosaminoglycan-containing matrix deposition continued as cells deposit increasing amounts of matrix and further spread and divide in third zone. By week six, the epitope recognised by the 7D4 antibody was present on a network of extracellular matrix surrounding the corneal epithelial cells as well as at the leading edge of the dividing/migrating cells, suggesting two roles, both in maintenance as well as a barrier at the edge of the cells. Whatever its role, this is the first identification of specific CS/DS sulphation patterns being identified using this ocular organoid model in the context of corneal epithelial progenitor cells. Also of note, is that increasing seeding cell density appeared to result in more CS/DS deposition, which is interesting as higher seeding densities are also associated with increased propensity of iPSC-derived corneal epithelial cell generation (Hayashi et al., 2016). This was not quantitively assessed, however, which could be done by image analysis or extraction and biochemical analysis for full determination.

Interestingly, both the epitopes recognised by the 6C3 CS/DS antibody and the 5D4 KS antibody were not identified within the SEAMs zones themselves, with the exception of a few incidental 6C3 positive matrix enveloped cell clusters in zone 4. These small regions of cells depositing a matrix containing the epitope recognised by the 6C3 CS/DS antibody were identified in zone 4 at low seeding densities (300 cells per 24 well plate culture well). As the cells in this zone are the least well characterised, it is unclear what cell type they may represent, but they have been posited as being other epithelial cell types, for example skin and may be keratinocytes (Hayashi et al., 2016). This is further supported by the presence of the epitope recognised by the 6C3 antibody located directly subjacent to the stem cell/transient amplifying cell compartment in human skin (similar to the identification here using the 6C3 antibody in the porcine limbal stem cell niche) (Lavker and Sun, 2000; Sorrell et al., 1990).

Recently, it was discovered that microglia-like cells, which are resident immune cells of the central nervous system, were present in SEAMs, predominantly in zone 2 and zone 3 and thought to form a border between the two zones, very similarly to the signal generated by the 7D4 antibody. This could also be interpreted as either the CS/DS epitope being deposited by the microglia-like

cells or it is present as a cell surface CS/DS molecule (Shiraki et al., 2022). These immune cells may also offer an alternative explanation for the presence of the epitope recognised by the 6C3 antibody in zone 4, however due to the localisation within this non-ocular surface epithelial cell zone, this may be unlikely, but could be owing to another immune cell or potentially another surface ectoderm anlage.

Finally, in order to determine whether the CS/DS epitope of 7D4 was associated with developing corneal epithelial cells, a double stain was utilised investigating keratin-14 (K14) alongside the 7D4 antibody in 4 week SEAMs. K14 has been shown to be expressed by developing corneal epithelial cells and not the putative developing conjunctiva, however, in mature tissue, it is no longer expressed, except by a few basal cells (Kurpakus et al., 1994). It does appear that in some locations, there is very close interaction with K14+ cells with the 7D4 CS/DS antibody staining, however this is not universal and there was limited K14 expression at this timepoint, and due to time restraints more timepoints were not analysed.

Whilst useful to be able to identify candidate molecules for further extraction, the major limitation of this antibody-based approach is the lack of a defined sequence recognised by the epitope, only that a distinct structural motif in a CS/DS polysaccharide is present. Whilst many associations have been made with certain epitopes and stem cell niches, suggesting a unique function of certain epitopes this has yet to be fully elucidated and tested *in vitro*. The SEAM model is a good representation of human eye development, but of particular interest would have been investigating the presence of these markers on the developing embryonic human cornea to identify whether the presence of the epitope recognised by the 7D4 antibody was similarly mimicked *in vivo*.

Whilst interesting insights into the deposition of CS/DS were made in both the adult cornea as well as a model of a developing cornea, the primary aim of this chapter was to identify target CS/DS species for purification. To this end, both the sulphation epitopes recognised by the 7D4 and 6C3 antibodies were considered of interest. The epitope recognised by the 7D4 epitope was of particular interest, namely due its close association with the corneal epithelium

in vivo and also its presence in the developing zone of progenitor corneal epithelial cells *in vitro*. The epitope recognised by the 6C3 antibody, was, also, of particular interest. The 6C3 antibody localised almost exclusively to the corneal limbus basement membrane and the conjunctival basement membrane, suggesting an important role in the maintenance of stem cells in the limbal stem cell compartment. For these reasons, sources enriched in these epitopes were sought in the next chapter for extraction and purification for use as a substrate upon which to grow SEAMs.

2.5 Conclusions

Taken together these immunohistochemical observations provide a strong supportive argument for the potential benefits of using CS/DS sulphation motifs as a substrate in iPS cell culture to generate corneal epithelial cells. Their spatial and temporal expression both within SEAMs and the limbal crypt stem cell niche in the adult cornea suggests they play a role in maintaining the limbal stem cell niche, specifically in the case of the epitope recognised by the 6C3 antibody. CS sulphation patterns may also play a role in establishing basement membrane barriers, as seen with the epitope recognised by 7D4 in iPSC corneal epithelial differentiation, as well as an important role in supporting the corneal epithelium through close association from the corneal stroma. From these investigated CS motifs, the best identified targets for extraction and enrichment were the epitopes recognised by the 7D4 and 6C3 CS/DS antibodies due to their association with the stem cell niche in the case of 6C3 and associated with general corneal epithelial and stromal maintenance in the case of 7D4. In the next chapter, the aim was to locate sources rich in these epitopes and extract and purify them for use as a cell culture substrate.

3 Chapter 3: Isolation, purification, and characterisation of corneal epithelial-associated CS/DS epitopes

3.1 Introduction

In the previous chapter, corneal epithelial-associated glycosaminoglycan species of interest were successfully identified, namely the CS/DS sulphation epitopes recognised by the antibodies 6C3 and 7D4, in both porcine cornea and iPSC-derived developing corneal epithelial cells, for the latter. From these observations, the next goal of this thesis was to isolate these molecules and enrich them for use as a substrate, as described in Chapter 4. The overall aim of this chapter was to develop a purification and characterisation process for the extraction of suitable glycosaminoglycan substrates enriched in the sulphation epitope recognised by the antibodies 7D4 and 6C3, from both peripheral and central porcine cornea, using a combination of extraction and enrichment methods described in the literature for purification of proteoglycans and glycosaminoglycans. Initial results, from Chapter 2 of this thesis, however, revealed the abundance of the epitope recognised by the 6C3 antibody from porcine corneal extracts was very low and confirmed by direct ELISA, as described in this chapter. To this end, an alternative source using shark cartilage was also used, which is a rich source of CS/DS proteoglycans (Blanco et al., 2015; Vázquez et al., 2018), particularly the epitope recognised by the 6C3 antibody as shown here.

Separation and purification of proteoglycan extracts is well described, and various methods have been published over the years (Ly et al., 2010). The cornea, especially, is extremely rich in small leucine rich proteoglycans and their presence is essential in conferring the cornea's unique functional properties. The most well described of these properties is, namely, collagen fibril organisation (J. A. Rada et al., 1993; Takahashi et al., 1993) and also the maintenance of hydration (Bettelheim and Plessy, 1975). Proteoglycans also fulfil various other roles in the cornea, and have shown great importance in wound healing (Chakravarti, 2002; Saika et al., 2000) amongst many other functions, including a potential role in stem cell maintenance (Ashworth et al., 2021).

Due to the availability of large amounts of tissue, and similarity to the human cornea, porcine cornea lends itself as a good source to generate the most amount of product required for further studies described in this thesis. Indeed, many pharmaceutical preparations of proteoglycan and glycosaminoglycan products are still produced from food processing byproducts e.g. heparin from porcine as mentioned previously (van der Meer et al., 2017). The porcine cornea has also recently been identified as one of the best xenograft materials, owing to its similarity to the human cornea (Sharifi et al., 2019). Other studies are also investigating the use of porcine corneal extracts in bioengineering studies including the effect of porcine corneal stromal extract on keratocytes as well as using acellularized porcine corneal scaffolds (S. Li et al., 2021; Zhang et al., 2017). Non-human primates are largely avoided due to ethical concerns and scalability, as well as higher disease zoonotic disease risks, despite promising results in xenotransplantation (Hara and Cooper, 2011).

Corneal proteoglycan extraction typically consists of an initial extraction step using a chaotropic agent to solubilise the dense extracellular matrix and subsequent enrichment steps including density gradient centrifugation and anion exchange chromatography. Extractions have been previously well described in various species for example rabbit (Gregory et al., 1982), primate (Nakazawa et al., 1983), bovine tissue (Funderburgh et al., 1987), human (Wollensak and Buddecke, 1990) and finally porcine cornea, as in this study (Jody A. Rada et al., 1993). Bovine cornea yields more material due to their larger size, however porcine lends itself better to regenerative medicine as a result of increased compatibility as described above.

The objectives of this chapter were to, firstly, extract proteoglycans from both the peripheral and central cornea from a porcine source using guanidium hydrochloride, followed by caesium chloride density ultracentrifugation. The second objective was to use biochemical techniques to identify both the type of proteoglycan present, as well as the sulphation motifs present on the respective glycosaminoglycan side chain, namely those recognised by the antibodies 6C3 and 7D4. The final objective was to produce substrates enriched in CS/DS sulphation motifs of interest using ß-elimination and ion exchange

chromatography, free of impurities such as proteins and other contaminating glycosaminoglycans, for example KS and HS.

In summary, in this chapter a method to extract and enrich for the CS/DS epitope recognised by the antibody 7D4 from peripheral porcine cornea was successfully demonstrated. In addition, the production of a mixed substrate enriched in both the CS/DS epitope recognised by the antibody 7D4, and the KS sulphation motif recognised by the antibody 5D4 from central cornea was also achieved. Finally, a substrate enriched in the CS/DS epitope recognised by the 6C3 antibody was successfully produced from shark cartilage. All substrates were demonstrably free of contaminating proteins as well differing glycosaminoglycan species.

3.2 Methods

3.2.1 Overview

The overall strategy for extraction and enrichment of potential proteoglycan and glycosaminoglycan substrates is detailed in **Figure 3.1**. Initially crude extracts were obtained through the use of the chaotropic agent guanidine hydrochloride, after which caesium chloride isopycnic ultracentrifugation was used to separate proteoglycans and glycosylated proteins from other non-glycosylated native extracellular and pericellular matrix proteins. These crude extracts were either used immediately in anion exchange chromatography, or prior to this, the O' linked glycosaminoglycans (including CS/DS and some KS species) were selectively detached using alkaline ß-elimination, followed by precipitation using cetylpyridinium chloride (CPC), enabling the formation of a free glycosaminoglycan salt. Thereafter the samples were applied to an anion exchange column to elute glycosaminoglycan fractions enriched in specific epitopes of interest.

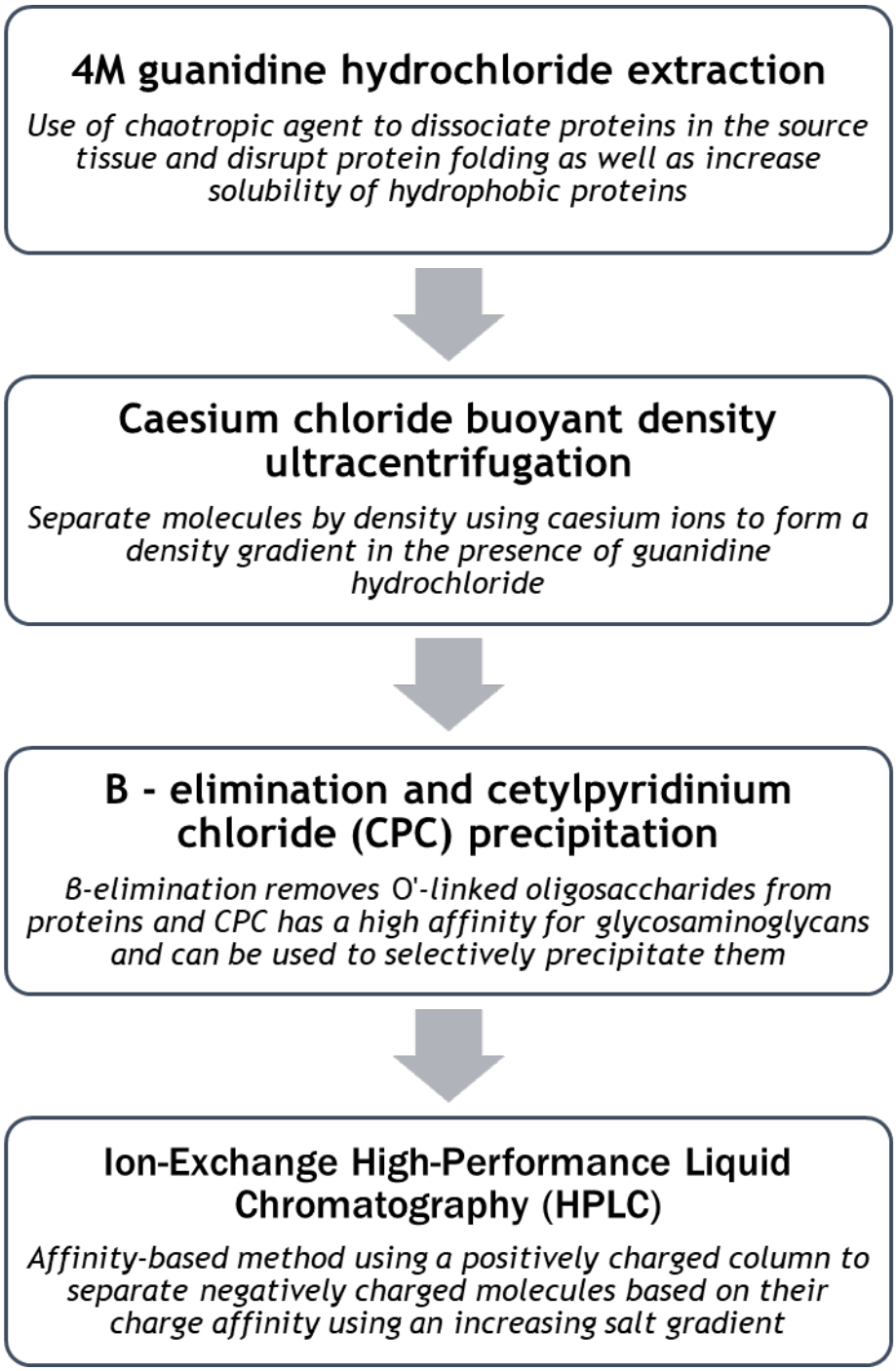

Figure 3.1 Flowchart of the proteoglycan and glycosaminoglycan extraction method described in this chapter.

3.2.2 Proteoglycan Extraction

The cornea was dissected from the whole porcine globe as described in Section 2.2.1 and further dissected into peripheral and central compartments as shown in **Figure 3.2**. The peripheral cornea compartment contains predominantly the limbal region and transitional zone cornea including sublimbal stroma as well as some conjunctival tissue. The central cornea compartment contains only transparent central cornea, consisting of a thin layer of epithelium along with corneal stroma and the endothelial layer. Pooled corneal samples from either peripheral and central cornea were weighed and 10 ml of 4 M guanidine hydrochloride at pH 5.8 was added per gram of tissue (wet weight) with 0.05 M sodium acetate, 10 mM sodium ethylene-diamine-tetraacetate (Na_2EDTA) and in the presence of the following protease inhibitors: 0.1 M 6-amino-caproic acid and 5 mM benzamidine hydrochloride. The tissue was incubated in extraction buffer for 48 hours at 4°C on a roller mixer. After incubation in 4 M guanidine hydrochloride, tissue was centrifuged at 3000 x g for ten minutes and the supernatant removed and passed through a 40 µm cell strainer (Thermofisher, Loughborough) to remove debris resulting in a crude extract from both central and peripheral cornea.

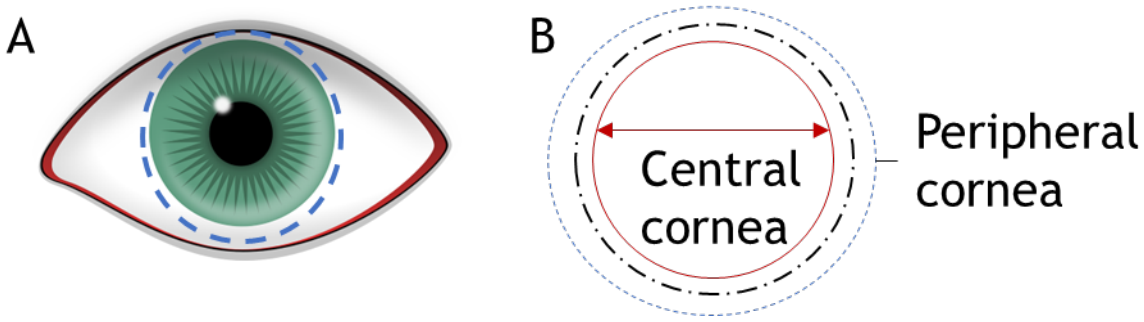

Figure 3.2 Corneal dissection diagram for proteoglycan extraction. (A) Diagram showing the region removed from whole porcine globe. (**B**) Representation of the central corneal compartment and the peripheral cornea, with the limbus represented as a black dashed line.

3.2.3 Density gradient centrifugation

Caesium chloride was added to the crude proteoglycan supernatant (from Section 3.2.2) to achieve a density of 1.5 g/ml (approximately 0.615 g/ml of caesium chloride added for peripheral cornea and 0.825 g/ml for central corneal

samples), after degassing using a vacuum pump and maintaining the guanidine hydrochloride molarity at 4 M for dissociative isopycnic ultracentrifugation.

Samples were subsequently ultracentrifuged at 100,000 x g for 48 hours separating the sample mixtures based on molecular density until equilibrium is reached. Density ultracentrifugation was performed using a Beckman Coulter L8-80MR Ultracentrifuge fitted with a 55.2 Ti rotor in 26.3 ml polycarbonate ultracentrifuge tubes (all from Beckman Coulter, High Wycombe, UK). Five dissociative fractions were generated from each compartment, from both peripheral and central samples, for further analysis. These fractions are termed D1 to D5 (D1 being the highest buoyant density and D5 being the lowest buoyant density, i.e. at the top of the density gradient) as shown in **Figure 3.3**. The gradient densities of each fraction were verified by weighing each fraction. Samples were then dialysed into distilled water following several water changes maintained at 4°C over 48 hours and used in further analysis or frozen at -20°C in aliquots for further use.

3.2.4 CS and DS glycosaminoglycans from shark tissue

Due to further sources of glycosaminoglycans being required to investigate all sulphation motifs identified in Chapter 2, namely the epitope recognised by the 6C3 antibody, a previously extracted sample of shark CS/DS was kindly provided by Professor Clare Hughes (Cardiff University). This extraction was performed on shark skeletal cartilage (species unknown) under associative conditions. The extraction was carried out as for dissociative conditions but with a reduced molarity of guanidine hydrochloride of 0.4 M to generate 3 fractions after density centrifugation, termed A1, 2 and 3. A1 was used for further studies due to being the highest glycosaminoglycan-containing fraction from this extraction.

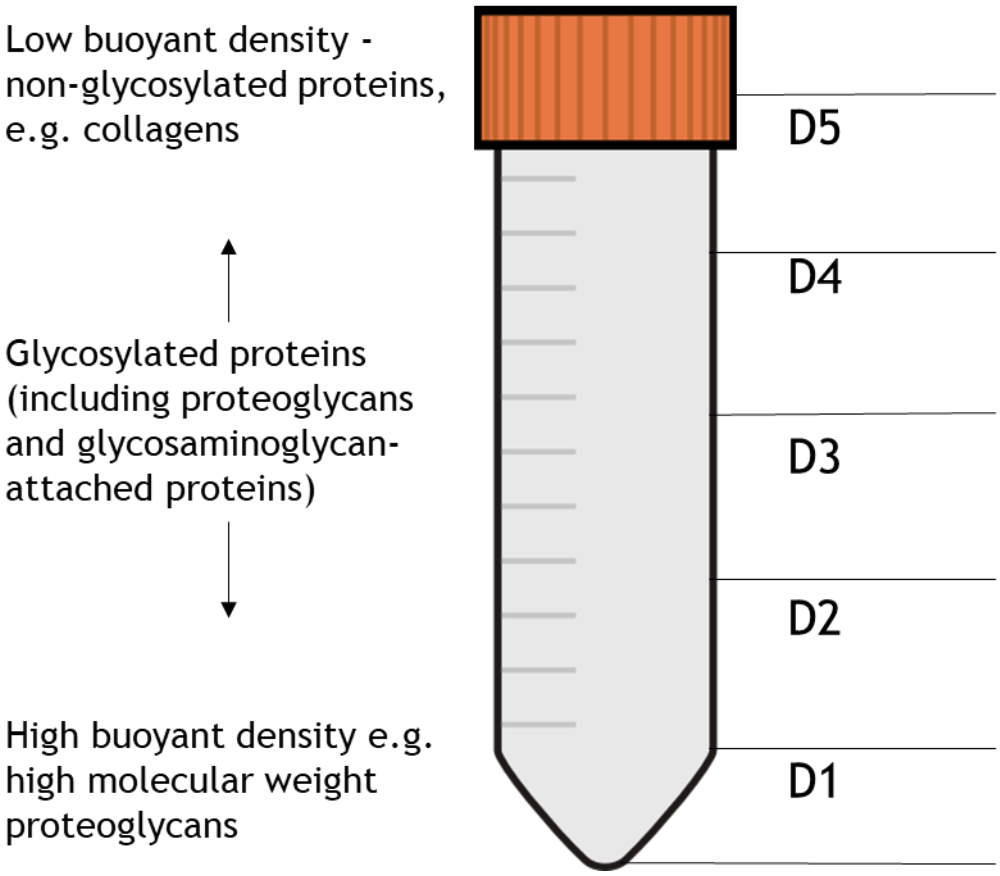

Figure 3.3 Representation of the different fractions generated and expected proteins after performing buoyant density (isopycnic) ultracentrifugation in the presence of caesium chloride under dissociative conditions.

3.2.5 *Quantification of protein using the BCA assay*

To calculate protein concentration of the samples a bicinchoninic acid (BCA) assay was performed. The BCA assay was performed using a Pierce BCA protein assay kit (Thermofisher, Loughborough) following the manufacturer's instructions. Briefly, a standard curve of varying concentrations of BSA and unknown samples are mixed with BCA and incubated at 37°C for 30 minutes to form a purple-coloured reaction product that is then read at 562 nm on a plate reader (Clariostar Plate Reader, BMG Labtech, Aylesbury, UK). Concentrations of unknowns were calculated using the linear regression of the standards.

3.2.6 *Quantification of glycosaminoglycans using the dimethylmethylene blue assay*

To calculate glycosaminoglycan concentration, a 1,9-dimethylmethylene blue (DMMB) assay was performed. For the DMMB assay, a standard curve of 0-40 µg/ml (the linear range of the assay) of purified CS glycosaminoglycans (Sigma-Aldrich, Gillingham) was performed. 40 µl of either the standard concentrations or appropriate dilutions of unknown samples were added to a micro well plate and 200 µl of DMMB (dimethyl methylene blue) solution (16 mg/L DMMB; 1% (v/v) ethanol; 2.05% (v/v) 1 M NaOH; 0.35% (v/v) of 98% formic acid in dH_2O) was added. The plates were then immediately read on a plate reader at 525 nm and concentrations calculated using the standard curve. The reaction product results in a purple colour after the induction of metachromasia of DMMB when bound to sulphated glycosaminoglycans in solution (Barbosa et al., 2003; Farndale et al., 1986, 1982).

3.2.7 *Direct ELISA for the detection of CS/DS and KS sulphation epitopes*

Dissociative fractions from central and peripheral cornea were used to coat Linbro 96 microwell plates (mpbio/Thermofisher, Loughborough) using 100 µl of 1 µg/ml glycosaminoglycan solution (as determined by DMMB assay, 100 ng of glycosaminoglycan per well total) diluted in Tris/saline/azide (TSA) coating buffer (50 mM Tris, 200 mM NaCl, 0.02% (v/v) NaN_3 without tween). The samples were covered and incubated at 4°C for 16 hours. After incubation, the plates were then washed twice with TSA wash buffer (as above but with 0.05% Tween). The plates were then blocked with 5% (w/v) BSA/TSA wash buffer for 1 hour at

37°C before addition of the primary antibodies. Primary antibodies, shown below in **Table 3.1**, were all diluted in 1% BSA/TSA wash buffer and applied to the plate undergoing incubation for 1 hour at 37°C. After the primary antibody incubation, microplates were washed, and the goat anti-mouse alkaline phosphatase conjugated secondary antibody (Thermofisher, Loughborough) was applied at a 1 in 5000 dilution in 1% BSA/TSA wash buffer as per manufacturer's instructions and incubated for 1 hour at 37°C. The plates were then thoroughly washed. Finally, samples were incubated with alkaline phosphatase substrate (4-nitrophenyl phosphate disodium salt hexahydrate) (Sigma-Aldrich, Gillingham) dissolved in diethanolamine (DEA) buffer (5 mg alkaline phosphatase substrate per 5 ml 0.1 M DEA buffer with 1 mM $MgCl_2$ at pH 9.8) for 1 hour at 37°C and the yellow reaction product absorbance was read at 405 nm on a CLARIOstar plate reader (BMG Labtech, Aylesbury, UK). All samples were processed in duplicate and the mean presented. A negative control of primary antibody omission was also included.

Direct ELISA was modified slightly for free glycosaminoglycans after further purification steps, including ion exchange chromatography, detailed in the following sections. After glycosaminoglycan content was determined using the DMMB assay as described in the previous section, anion exchange chromatography fractions, with a notable UV absorbance at 232 nm and detectable glycosaminoglycan content (from the DMMB assay), were coated onto Linbro 96 microwell ELISA plates (mpbio/Thermofisher, Loughborough). The plates were coated using 100 µl of 1 µg/ml glycosaminoglycan solution (as determined by DMMB assay) diluted in TSA coating buffer (50 mM Tris, 200 mM NaCl, 0.02% (w/v) NaN_3 without tween) for the crude extract samples, but not for free glycosaminoglycans after ß-elimination and ion exchange chromatography. The free glycosaminoglycans were coated as above but using 80% saturated ammonium sulphate (4.1 M) as the coating buffer, which has previously been used for optimal immobilisation of free glycosaminoglycan chains of CS/DS (Hof et al., 2019). The samples were then covered and incubated at 4°C for 16 hours and the ELISA was performed as described above. All samples were performed in duplicate and included a negative control of primary antibody omission.

For contamination detection, the substrates generated of interest were also investigated for HS using the 10E4 HS primary antibody (1:100, Amsbio, Abingdon, UK) using the above ELISA protocol.

Table 3.1 Antibodies used in direct ELISA and Western Blot (WB) for the identification of glycosaminoglycan sulphation motifs and proteoglycans in porcine corneal extracts. * 6C3 antibody in was used neat for porcine corneal extract, 1:5 for shark extract

Antibody	Epitope	Dilution for ELISA	Dilution for WB	Source
6C3	Unique CS/DS sulphation motif	1:5	Neat/1:5*	Mouse monoclonal IgM (Sorrell et al., 1990)
7D4	Unique CS/DS sulphation motif	1:5	1:5	Mouse monoclonal IgM (Sorrell et al., 1990)
5D4	Highly sulfate KS sulphation motif	1:100	1:1000	Mouse monoclonal IgG (Caterson et al., 1983)
Decorin (28.4)	Decorin core protein	N/A	1:5	Rabbit polyclonal IgG (Bidanset et al., 1992)
Biglycan	Biglycan core protein	N/A	1:5	Rabbit polyclonal IgG (Roughley et al., 1993)
Keratocan (KER-1)	Keratocan core protein	N/A	1:5	Mouse monoclonal IgM (Gealy et al., 2007)
Lumican (LUM-1)	Lumican core protein	N/A	1:5	Mouse monoclonal IgM (Kerr, 2005; Melrose et al., 2008)

3.2.8 Western blot

Proteoglycan samples for Western blot were analysed using 5 µg (10 µg for detection of the epitope recognised by the 6C3 antibody in cornea) of protein (or 10 µg of glycosaminoglycan from DMMB assay for shark extracts) as determined by the BCA Protein Assay Kit ((Thermofisher, Loughborough) according to manufacturers instructions as described in Section 3.2.5. For enzyme digests, prior to electrophoresis, 5 µg of protein of each sample were incubated with one of the following enzymes. For chondroitinase ABC digest,

samples were reconstituted with 0.1 U/ml chondroitinase ABC (Sigma-Aldrich, Gillingham) in 50mM Tris-HCl buffer with 60mM sodium acetate at pH 8.0 for 1 hour at 37°C. For Peptide-N-glycosidase F (PNGase F, Sigma-Aldrich, Gillingham), enzyme digests were carried out in 50 mM Tris-HCl at pH 7.5 in the presence of 1% sodium dodecyl sulphate (SDS) and 0.5% Triton X100 with at an enzyme concentration of 16 units/ml overnight at 37°C. Samples were made up with Novex™ Tricine SDS Sample Buffer (2X) (Thermofisher, Loughborough) and 10% (v/v) 2-mercaptoethanol and heated to 100°C for 5 minutes to reduce disulphide bonds. Samples were then loaded and run on NuPAGE™ 4 to 12% gradient, Bis-Tris polyacrylamide gel electrophoresis (PAGE) protein gel (Thermofisher, Loughborough) and electrophoresed for approximately 40 minutes at 150 V. The resultant gel was then transferred using the iBlot system (7 minute transfer) onto nitrocellulose as per manufacturer's instructions (Thermofisher, Loughborough).

3.2.9 Immunolabelling of proteoglycan blots

After transfer, the nitrocellulose membranes were immersed in 5% (w/v) BSA/TSA blocking buffer for 1 hour and left to dry overnight for downstream processing. Subsequently, the blots were immersed in the primary antibody solutions shown in **Table 3.1** diluted in 1% (w/v) BSA/TSA overnight at 4°C on a rolling mixer. They were then washed 3 times for five minutes each in TSA. Blots were then incubated with anti-mouse or rabbit alkaline phosphatase conjugated secondary antibody (Thermofisher, Loughborough) applied at 1 in 5000 dilution in 1% (w/v) BSA/TSA for 1 hour at room temperature on a roller mixer. Finally, after four more five minute washes, blots were then incubated in BCIP/NBT substrate mixed in alkaline phosphatase buffer (100 mM Tris-HCl pH 9.0, 150 mM NaCl, 1 mM $MgCl_2$) (Promega, Chilworth) for 15-30 minutes until colour development. Immunoblots were then imaged using Canon LIDE 200 flatbed scanner (Canon (UK), Uxbridge, UK).

3.2.10 Extract preparations and sample selection for anion exchange chromatography

Unless otherwise stated, 500 µg (as measured by DMMB for sulphated glycosaminoglycan content) of proteoglycan fractions from density

centrifugation were freeze dried and reconstituted in either 1 ml of anion exchange chromatography starting buffer (0.1 M NaCl in 10 mM Tris-HCl at pH 7.4) for crude extracts or 1 ml of distilled water for alkaline ß-elimination samples.

3.2.11 Alkaline ß-elimination

Alkaline ß-elimination is well described, and releases O' linked glycans from proteins in solution through an elimination reaction (Lee et al., 1977) and can be performed in the presence of sodium borohydride or without (Coulson-Thomas et al., 2015). Initially, an equal volume of 1 M NaOH was added to the prepared sample fractions in distilled water, yielding a 0.5 M solution of NaOH that was incubated overnight at room temperature. An equal volume of 1 M acetic acid was then added to neutralise the solution and the sample was then dialysed extensively against distilled water as described in the Section 3.2.3. Samples were then freeze dried and reconstituted in 0.5 ml of 50 mM sodium sulphate.

3.2.12 CPC precipitation

CPC has a high affinity for glycosaminoglycans, and can be used to selectively precipitate them, so is a suitable molecule for a washing step prior to anion exchange chromatography (Buzzega et al., 2010). After ß-elimination, to samples in 50 mM sodium sulphate, room temperature 10% (w/v) CPC solution was then added dropwise, until a dense, cloudy precipitate formed, which was the resultant CPC salt. The samples were then centrifuged at room temperature for 5 minutes at 2000 x g and the supernatant discarded. The pellet was then washed twice in 0.05% (w/v) CPC to remove further contaminants. After the wash step, 0.5ml of 80% (v/v) propan-1-ol in distilled water was added, in which the CPC precipitate dissolves, with the resultant jelly-like product mixed to form a solution. To this solution, 100 µl of saturated sodium acetate solution was then added along with a drop of acetic acid to decrease the pH of the solution. This resulted in the formation of a glycosaminoglycan sodium salt. Finally, 3ml of cold ethanol was added to precipitate the sodium salt of the glycosaminoglycan chains as a dense white precipitate, which was achieved overnight at 4°C on a roller mixer. Samples were then centrifuged, again at 2000 x g, the supernatant discarded, and precipitate was air-dried before being reconstituted to 1 ml in

anion exchange starting buffer (0.1 M NaCl in 10 mM Tris-HCl at pH 7.4) and applied to an anion exchange column described below.

3.2.13 Anion exchange chromatography

In this study 500 µg of either crude extracts (glycosaminoglycan content as measured by the DMMB assay) or the reaction product from the ß-elimination and CPC washing of free O' linked glycosaminoglycan side chain mixtures were applied to a 5 ml HiTrap Q Fast Flow column (Cytiva Life Sciences, Sheffield, UK), attached to an ÄKTA explorer P-900 anion exchange chromatography system (GE Healthcare, Amersham, UK). The run conditions were as follows and have been previously described (Santos et al., 2017). Samples were run at a flow rate of 2 ml/minute on a linear buffer gradient from 0.1 M NaCl to 3 M NaCl in 10 mM Tris-HCl at pH 7.4 (after filtering buffer using a 0.22 µm filter) for eight column volumes (40 ml total). The column was equilibrated with 5 column volumes of starting buffer before application of the proteoglycan or glycosaminoglycan sample. Overall, 16 fractions were collected of 2.5 ml each. UV absorbance at 232 nm was monitored for detection of glycosaminoglycans . Fractions that eluted during peak 232 nm UV absorbance were deemed of interest and these resultant fractions were dialysed into distilled water and measured for glycosaminoglycan content and protein as described in previous sections using the DMMB assay and the BCA assay.

3.2.14 Silver Stain

In order to detect any small amounts of protein contaminants remaining in the anion exchange chromatography free glycosaminoglycan fractions, a silver stain was employed. The BCA assay (described above) did not reveal any detectable protein, which is limited to a 20 µg/ml detection limit, according to the manufacturer's protocol. Essentially, proteins separated by SDS-PAGE are fixed to the gel and a solution containing silver ions is applied which produces visible staining upon light exposure (Merril et al., 1984). In this study, anion exchange chromatography fractions from free glycosaminoglycans with enriched substrates were applied to the same gel and SDS-PAGE was performed as described in Section 3.2.8 using 1 µg of glycosaminoglycan as determined by the DMMB assay and 0.5 and 1 ng of BSA as a standard. Buffer was used as a negative control.

Subsequently, the Pierce Silver Stain Kit (Thermofisher, Loughborough, UK) was used for protein detection following the manufacturer's instructions before imaging.

3.2.15 Barium acetate gel electrophoresis and alcian blue staining for the detection of ß-eliminated glycosaminoglycans

Free glycosaminoglycan chains, generated following alkaline ß-elimination and anion exchange chromatography, were separated using barium acetate gel electrophoresis, followed by wet transfer to a CPC derivatised nitrocellulose membrane, as described previously (Maccari and Volpi, 2002; Volpi and Maccari, 2015).

Briefly, the barium acetate gels were prepared using a 0.5% (w/v) agarose (for molecular biology, Merck, Gillingham, UK) solution dissolved in 40 mM barium acetate buffer at pH 5.8 (buffered with 1 M acetic acid). The solution was heated to dissolve the agarose, cooled for 30 minutes and poured into a horizontal gel electrophoresis apparatus (7 x 10 cm gel, 5mm thick) containing a 10-well loading comb. 10 µg of glycosaminoglycans, as measured by the DMMB assay, from a set of standard samples, comprising of HS (Sigma-Aldrich, Gillingham), CS (Sigma-Aldrich, Gillingham) and KS, were added to wells either individually or as a mixture. The KS standard used was from ß-eliminated central D1 fraction, which had no detectable 6C3 or 7D4 CS/DS epitope present. For substrate samples, 5 µg of glycosaminoglycan of purified samples from either cornea or shark preparations were added to appropriate wells. For mixed standards, equal amounts of glycosaminoglycans were loaded, totalling 10 µg. All samples were prepared in distilled water with 20% (v/v) added cresol red solution. The cresol red solution was prepared at 0.1 mg/ml with 30% (v/v) glycerol. The electrophoretic run was then performed in 50 mM 1,2-diaminopropane (PDA) buffer, buffered at pH 9 with glacial acetic acid, for 150 min at 50 mA.

After electrophoresis, gels were then capillary blotted onto a CPC derivatised nitrocellulose membrane. Briefly, membranes were immersed in freshly prepared 1% (w/v) CPC in 30% (v/v) 2-propanol in distilled water for 5 minutes and washed for 15 minutes with 150 mM NaCl, with vigorous shaking. The

membrane was then rinsed several times in the 150 mM NaCl solution and left to equilibrate in the final rinse until blotting was performed. The capillary blot was assembled as in **Figure 3.4**. The blotting stack was prepared by first immersing both ends of a long piece 3MM Whatman paper suspended over a buffer reservoir of 100 mM Tris-acetate pH 7.3. The agarose gel was then placed on the 3 MM paper with the wells parallel to the two buffer reservoirs as shown in **Figure 3.4**. The CPC derivatised NC membrane was then placed on top of the gel and any air bubbles removed. Three further pre-wet filter papers, two pre-wet sponges, and 5 cm of absorbent paper tissue were then placed on top of the NC membrane, with air bubbles being removed with the addition of each layer of the stack. A 500 g weight was placed on top of the stack and the capillary blotting was then performed overnight at room temperature with sufficient buffer to enable complete transfer (approximately 1 L).

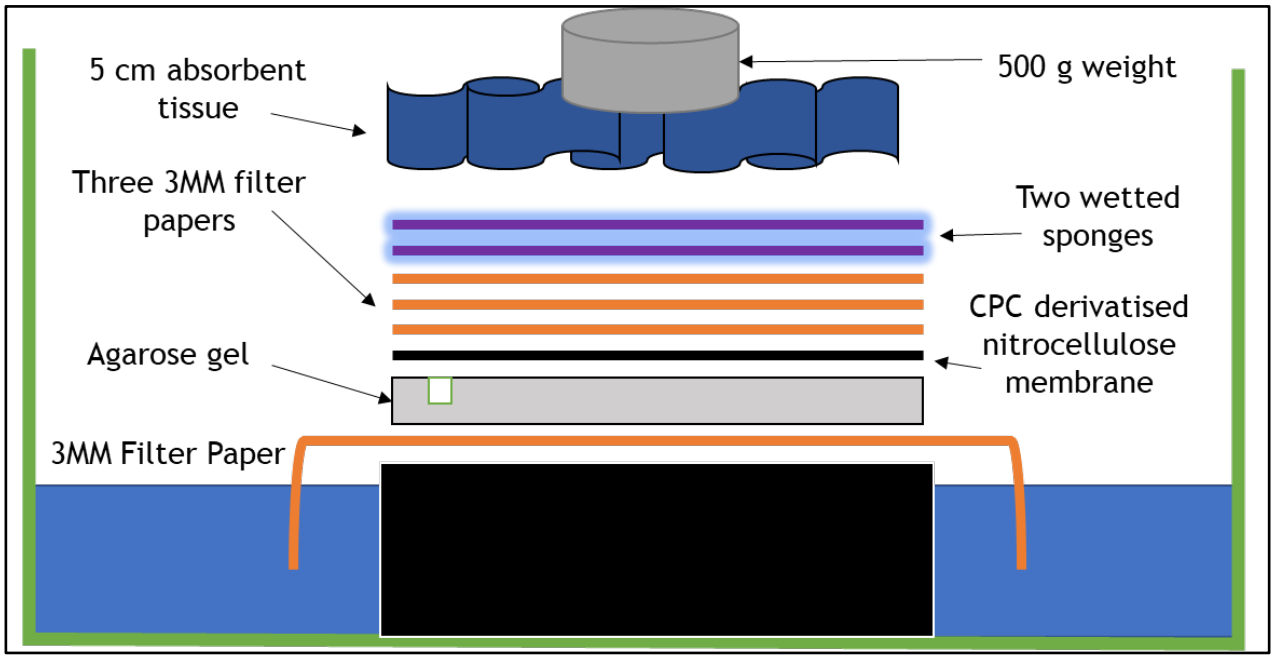

Figure 3.4 Diagram depicting the assembly of capillary blotting stack to enable glycosaminoglycan transfer to a cetyl pyridinium chloride (CPC) derivatised nitrocellulose membrane.

After blotting onto nitrocellulose, glycosaminoglycans were detected using alcian blue staining. The alcian blue solution was prepared immediately prior to use. 50 mg of dye was dissolved in 20 ml of a 1:19 ratio solution of 8 M guanidine hydrochloride and 18 mM sulphuric acid containing 0.25% (v/v) Triton X-100. The

transferred membrane was incubated in the alcian blue solution for approximately 2 hours until visible bands were clear. Background staining was removed by several washes in 150 mM NaCl before the blots were imaged using Canon LIDE 200 flatbed scanner (Canon (UK), Uxbridge, UK).

3.3 Results

3.3.1 Glycosaminoglycan and protein quantification of porcine corneal extracts reveals a rich source of proteoglycans and glycosaminoglycans

A total of four extractions were performed in this study and used in further downstream experiments. A total of 20 porcine corneas were utilised for each extraction with a mean wet weight of 4.86 (±1.02 SD) g from peripheral cornea and a mean net weight of 4.45 (±1.14 SD) g from central cornea as summarised in **Table 3.2**.

Both protein and glycosaminoglycan concentrations were measured using the BCA and DMMB assays respectively for the various fractions of equal volume generated from buoyant density gradient ultracentrifugation and summarised in **Table 3.3**. The mean concentration distributions for both proteins and glycosaminoglycans are shown in **Figure 3.5** and **Figure 3.6**, respectively.

As is to be expected with caesium chloride density gradient centrifugation, the majority of protein was detected in the low density D5 fraction containing a visibly significant amount of insoluble proteins with, presumptively, a large amount of these proteins being insoluble collagen. Smaller, but considerable amounts of protein were detected in the higher density gradient fractions (D1-D4), with decreasing amounts from D4 to D1. Conversely, D5 fractions contained lesser amounts of glycosaminoglycan than D1 to D4 fractions. The majority of glycosaminoglycan-containing proteins, i.e. proteoglycans, were predominantly found across fractions D4 to D1, with the peak concentration for both peripheral and central cornea detected in D3 fraction.

Table 3.2 Summary of wet weights of corneal samples from both the peripheral and central cornea in each corneal proteoglycan preparation showing mean ± standard deviation (SD).

Preparation	Peripheral Cornea Weight (g)	Central Cornea Weight (g)
#1	3.90	3.47
#2	5.42	4.80
#3	4.11	3.62
#4	6.01	5.90
Mean (±SD)	4.86 (±1.02)	4.45 (±1.14)

Table 3.3 Summary of average protein and glycosaminoglycan concentration from porcine corneal fractions showing mean ± standard deviation (SD).

Corneal Region	Fraction	Protein Concentration µg/ml (± SD)	GAG Concentration µg/ml (± SD)
Peripheral	D1	60.95 (±42.7)	90.87 (±43.09)
	D2	86.74 (±42.82)	161.81 (±127.84)
	D3	175.13 (±55.75)	175.10 (±37.95)
	D4	292.33 (±54.38)	151.99 (±32.94)
	D5	1077.75 (±453.12)	77.78 (±67.24)
Central	D1	60.50 (±20.56)	125.68 (±29.20)
	D2	134.31 (±58.05)	184.94 (±48.30)
	D3	224.48 (±67.23)	291.92 (±56.60)
	D4	346.51 (±96.56)	253.21 (±68.19)
	D5	897.26 (±280.29)	58.40 (±55.54)

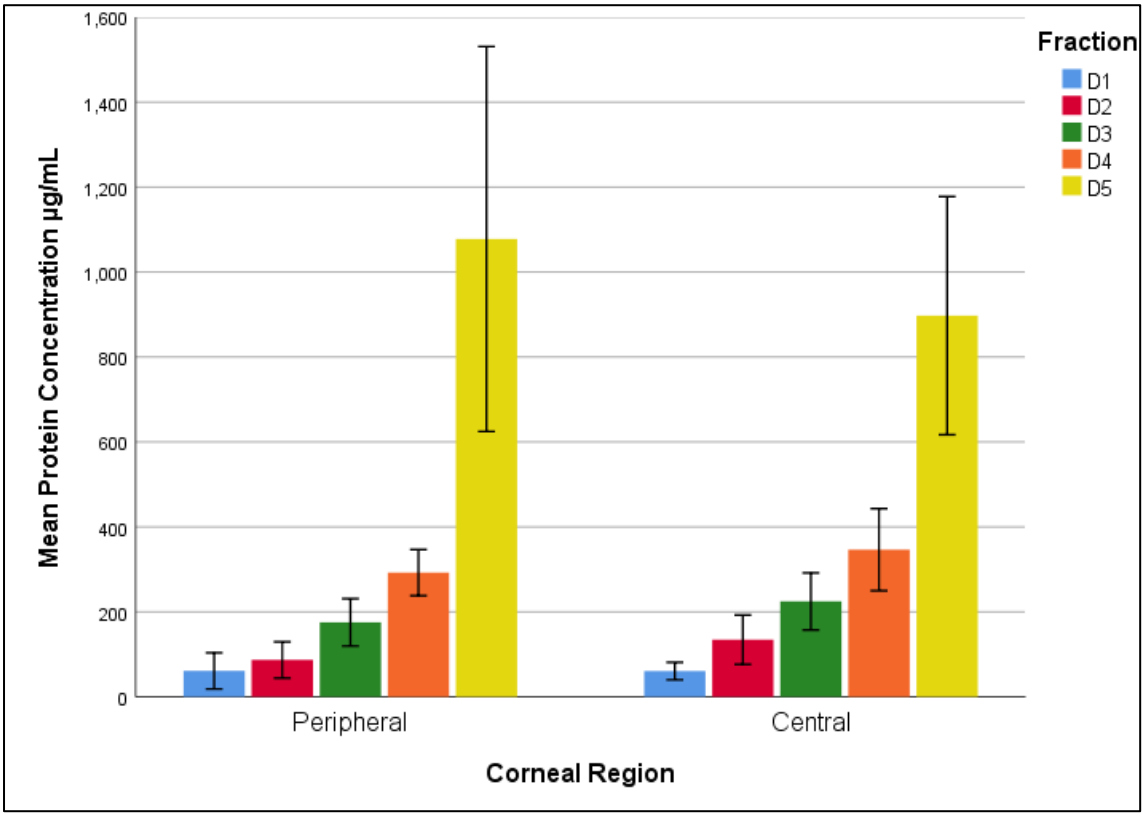

Figure 3.5 Overview of protein concentrations detected in each fraction of porcine cornea from both the periphery and center using BCA assay. Error bars represent one standard deviation (n = 4).

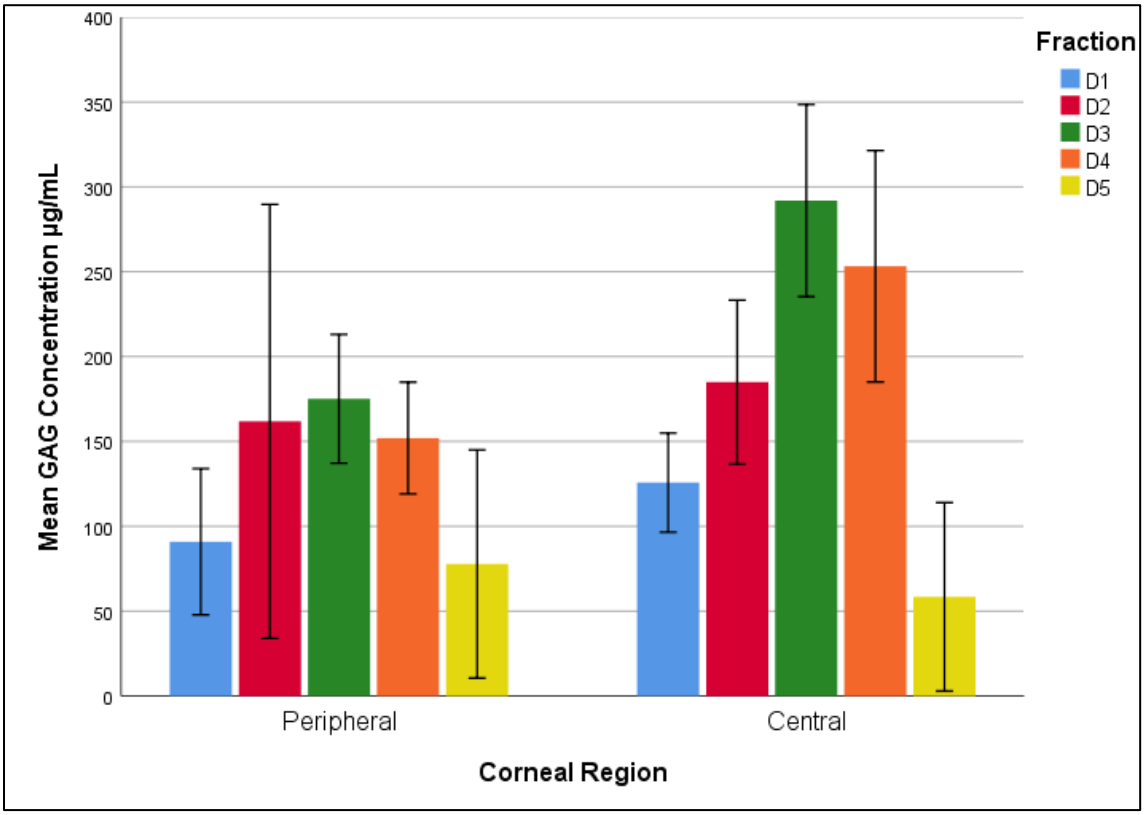

Figure 3.6 Summary of sulphated glycosaminoglycan (GAG) concrentation distributions throughout buoyant density fractions from both peripheral and central porcine cornea as detected by the dimethylmethylene blue assay. Error bars represent one standard deviation (n = 4).

3.3.2 Characterisation of sulphation patterns present in porcine corneal density gradient fractions reveals those enriched in the CS/DS epitope recognised by the 7D4 antibody

To investigate the distribution and confirm immunohistochemical observations, direct ELISA was performed on corneal samples for the glycosaminoglycan antibodies 6C3 and 7D4, which were identified in Chapter 2 and described in Section 1.3.4. Glycosaminoglycan sulphation motifs of interest were analysed using ELISA for antibodies 6C3 and 7D4, to recognise distinct CS/DS epitopes, as well as the 5D4, which recognises highly sulphated KS, a key component of the corneal extracellular matrix. Their mean distributions (n = 4) as a measure of absorbance are shown in **Figure 3.7**. The highly sulphated KS epitope recognised by the antibody 5D4 was widely detected throughout all fractions with reduced signal in fraction D5, whilst the epitope recognised by the 7D4 CS/DS antibody was primarily only detected across fractions D2-D4, with slightly higher signal and an even distribution in central cornea but a more noticeable peak in the peripheral D3 fraction but lower than central cornea overall. The epitope recognised by the 6C3 antibody, identified in the previous chapter associated with the limbus, was undetectable by ELISA.

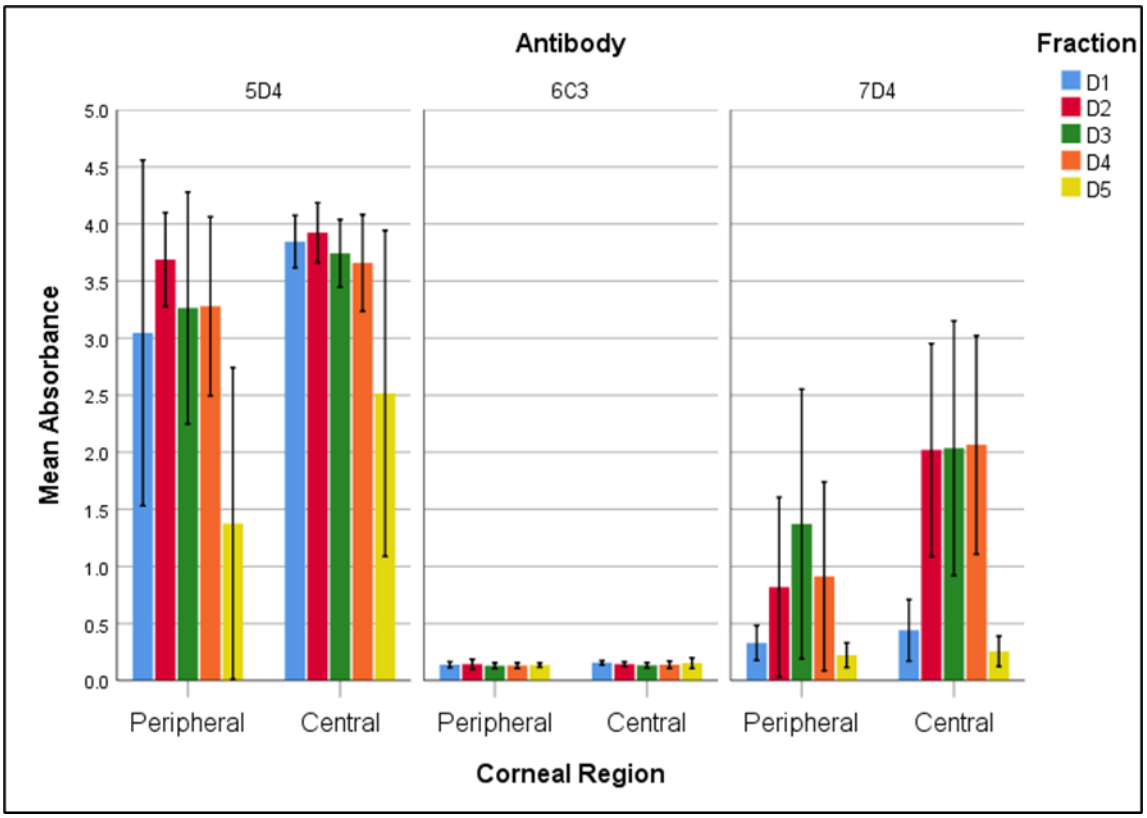

Figure 3.7 Summary of the presence of various glycosaminoglycan distinct sulphation patterns in the different corneal ultracentrifugation fractions as detected by enzyme-linked immunosorbent assay. Antibodies used include the heavily sulphated KS antibody 5D4 and two distinct CS/DS antibodies, 6C3 and 7D4. Error bars represent one standard deviation (n = 4).

3.3.3 *Western blot analysis of glycosaminoglycan sulphation motifs in corneal density gradient centrifugation fractions reveals the presence of the CS/DS epitopes recognised by 6C3 and 7D4 antibodies*

Following identification of glycosaminoglycan sulphation epitopes using direct ELISA, further investigation was carried out to investigate the molecular size range of these sulphated molecules and assess any differences between peripheral and central cornea using Western blot of each fraction. Representative images are shown from corneal proteoglycan preparations. Initially, the KS sulphation epitope, recognised by the antibody 5D4, and the CS/DS epitopes, recognised by the antibodies 7D4 and 6C3, were examined to identify their size and presence in each corneal fraction.

The KS epitope recognised by the 5D4 antibody was present across all fractions and staining patterns revealed bands of increased molecular weight and heterogeneity from the low buoyant density D4 fraction to the high buoyant density D1 fraction as shown in **Figure 3.8A**. Of note is the difference between the low density fraction D4 between peripheral and central cornea. To identify further differences between KS proteoglycans and the type of KS linkage present (either O' or N' linked), the N-glycosidase enzyme was used. N-glycosidase selectively cleaves N-linked glycans, including N-linked KS, but not O' linked KS or CS/DS, which is attached through an O' linkage. In the peripheral cornea, only an approximately 100 kDa broad band was seen in **Figure 3.8A** which was lost upon N-glycosidase treatment as shown in **Figure 3.8B**, suggesting the presence of only N' linked KS species in this density gradient fraction. Otherwise, little difference was seen between other fractions after N-glycosidase treatment, with reduced signal overall and distinct bands noticeable at approximately 75, 60, 45 and 37 kDA in **Figure 3.8B**. These may be O' linked KS proteoglycans or as a result of insufficient enzyme, possibly indicative of core protein sizes.

The CS/DS epitope recognised by the 7D4 antibody appeared to be present across all fractions, with visibly reduced signal in the peripheral D4 fraction as shown in **Figure 3.9A**. The band detected was of high molecular weight (100-150 kDa) and appeared less heterogenous than that of the KS epitope staining.

In contrast to ELISA findings, 6C3 antibody also yielded slight signal in an immunoblot, however required high concentrations of both protein (10 µg of protein, compared to 5 µg for other antibodies) and antibody (undiluted) suggesting it is a very low abundance. The signal localised to a high molecular weight, high buoyant density protein that had highest signal in the D1 fraction at approximately 300 kDa in peripheral cornea and 250 kDa in central cornea as shown in **Figure 3.9B**. There also appeared to be another, lower weight band present in central cornea at approximately 100 kDa, which was not seen in peripheral corneal extracts.

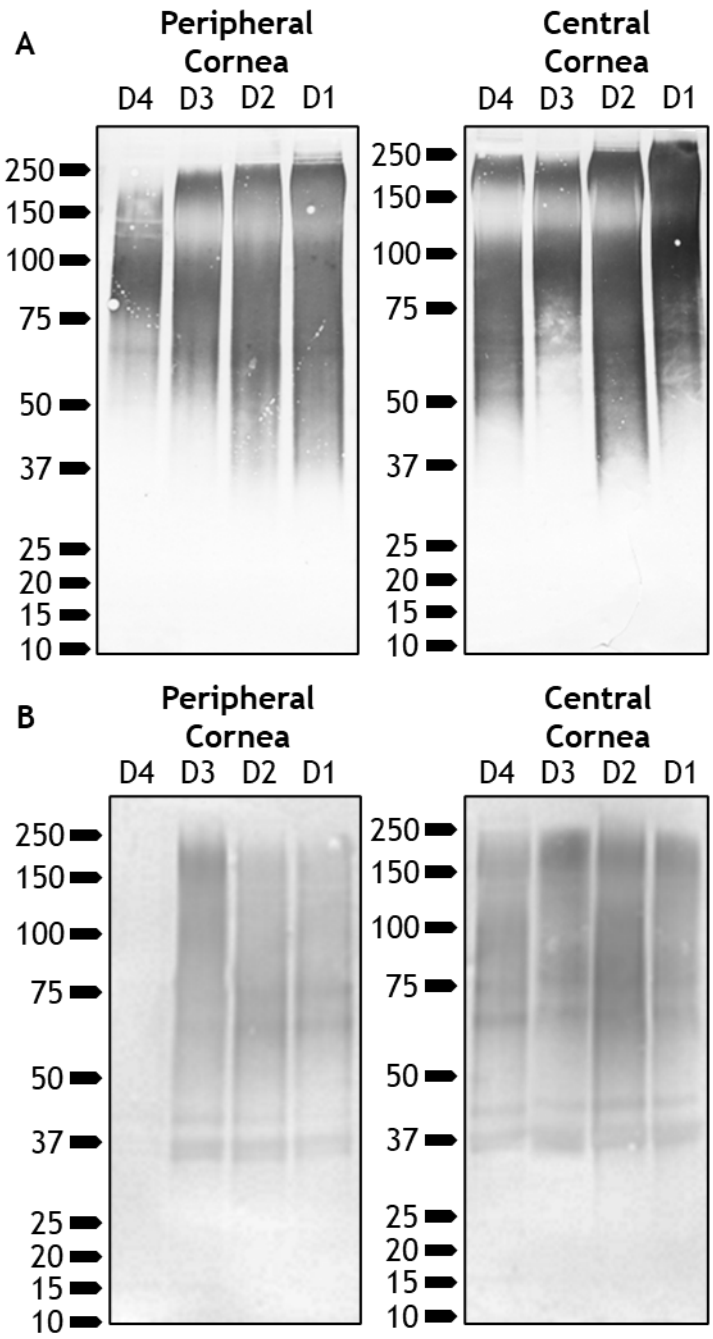

Figure 3.8 Western blot analysis of density gradient fractions from corneal extracts with molecular weight marker in kDa shown showing the antibody 5D4, which recognises highly sulphated KS. (**A**) Immunoblot of native 5D4 antibody signal. (**B**) Immunoblot of the same sulphation epitope after treatment with peptide-N-glycosidase F enzyme.

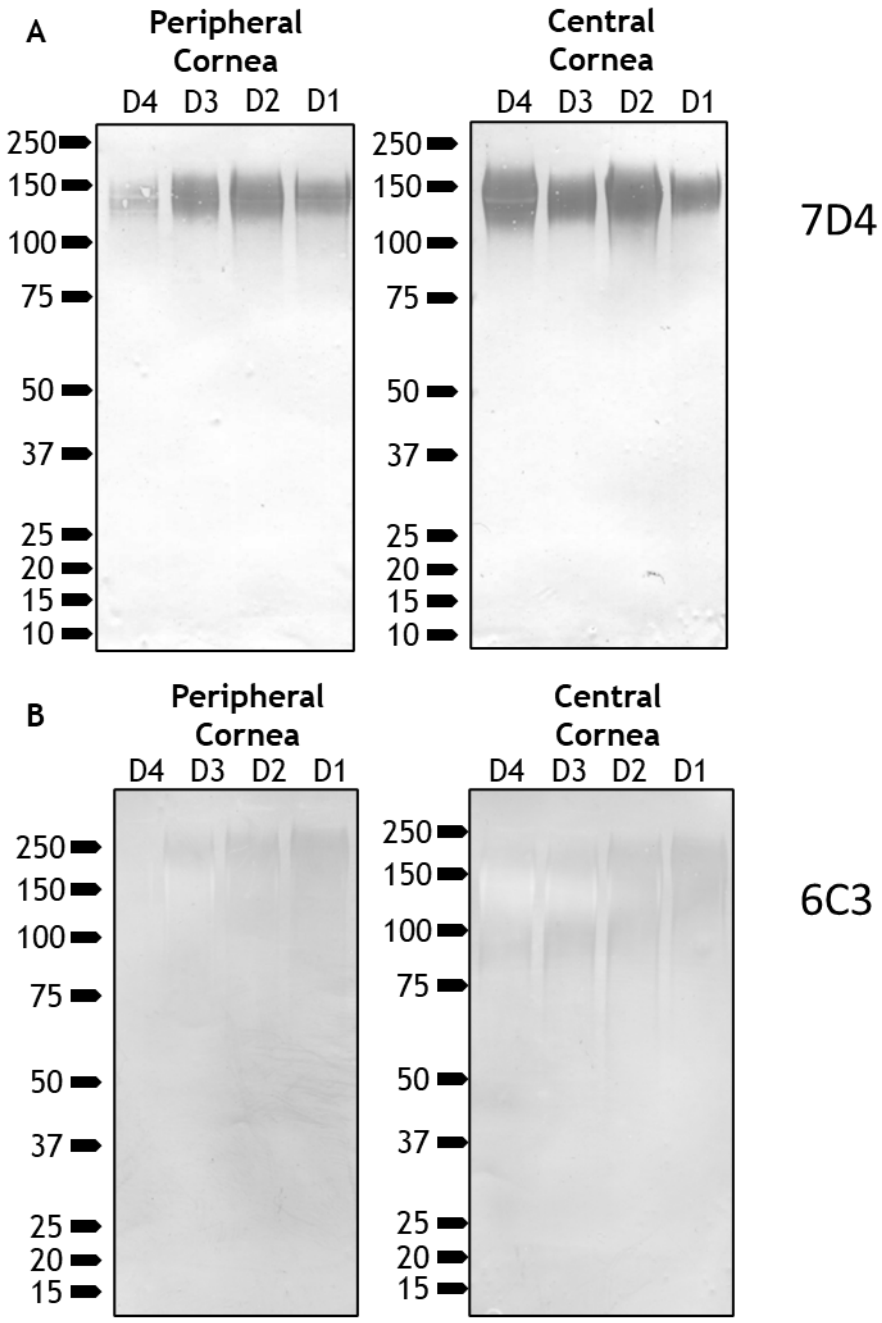

Figure 3.9 Western blot analysis of density gradient fractions from corneal extracts with molecular weight marker in kDa shown of two distinct CS/DS antibodies. (**A**) Immunoblot showing the distinct CS/DS epitope revealed by the 7D4 antibody. (**B**) Immunoblot of the distinct CS/DS epitope revealed by the 6C3 antibody.

3.3.5 Western blot analysis of a subset of small leucine-rich proteoglycans present in corneal density centrifugation fractions

Four abundant corneal proteoglycans were also investigated in this study, including the two CS/DS proteoglycans decorin and biglycan as well as two KS proteoglycans, keratocan and lumican.

Faint immunostaining for biglycan was present in all fractions except peripheral D1 fraction, as shown in **Figure 3.10A**, staining was stronger following partial chondroitinase ABC digestion as shown in **Figure 3.10B**. There was a broad band at approximately 130 kDa that had higher signal in the peripheral cornea and decreased signal in central cornea in **Figure 3.10A.** After partial chondroitinase ABC treatment, the protein core was revealed at approximately 37 kDa as shown in **Figure 3.10B**.

Decorin was present in all fractions, but reduced staining was seen in D1 in the peripheral cornea as seen in **Figure 3.11**. Before chondroitinase digestion it presented as a diffuse, broad band at approximately 130 kDa as shown in **Figure 3.11A**. After partial digestion, the core protein antibody epitope was revealed further and showed the same higher molecular weight broad band as well as revealing a discrete band of approximately 41 kDa, of the protein core, as shown in **Figure 3.11B**. Other bands are present at approximately 75 kDa, in the peripheral D4 and D3 fractions, which are indicative of either partially digesting decorin or potentially associated with other extracellular matrix proteins

For the two KS proteoglycans investigated in this study, keratocan and lumican, antibody signal for both proteins were more clearly revealed after enzyme digestion using PNGase F. Keratocan had little signal prior to enzyme digestion as shown **Figure 3.12A**. Two bands were revealed after enzyme treatment, one at 25 kDA and another fainter band at approximately 37 kDa present in all fractions in central cornea, but with reduced signal in D4 and D1 in peripheral fractions in **Figure 3.12B**.

Lumican signal was present in all fractions before PNGase treatment as a broad band that increased in molecular weight towards the highest buoyant density fraction, D1 as shown in **Figure 3.13A**. After PNGase treatment, two bands were visible at both approximately 37 kDa and 75 kDa, with the larger band absent in peripheral D4 fraction, as in **Figure 3.13B**. There were also slight differences in band intensity, with more signal in D2 and D1 in central cornea and the highest signal seen in D3 and D2 in peripheral cornea.

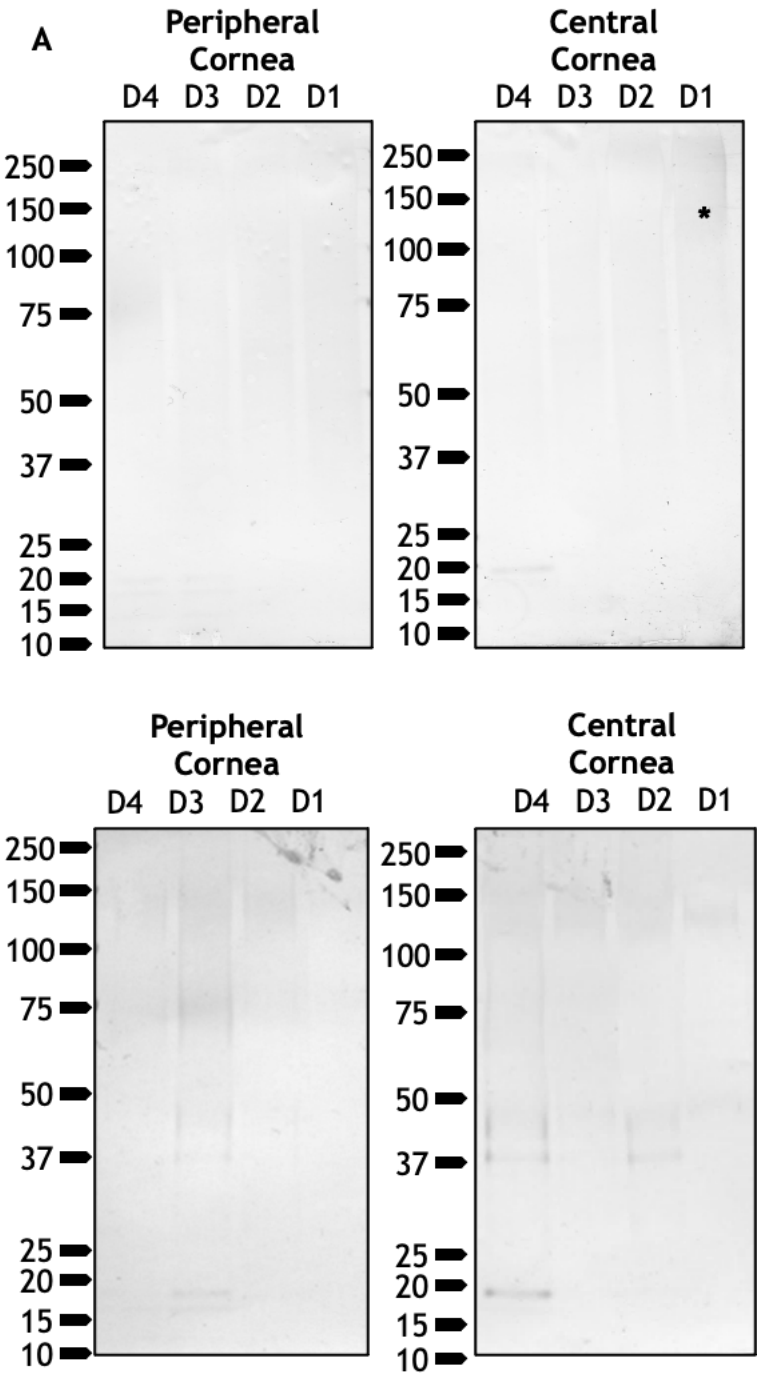

Figure 3.10 Western blot analysis of density gradient fractions from corneal extracts with molecular weight marker in kDa shown of the small CS/DS proteoglycan, biglycan (100-150 kDa, 42 kDa for the core protein). (**A**) Immunoblot showing the small leucine-rich repeat proteoglycan biglycan, with faint band indicated by *. (**B**) Immunoblot of biglycan after partial chondroitinase ABC digestion.

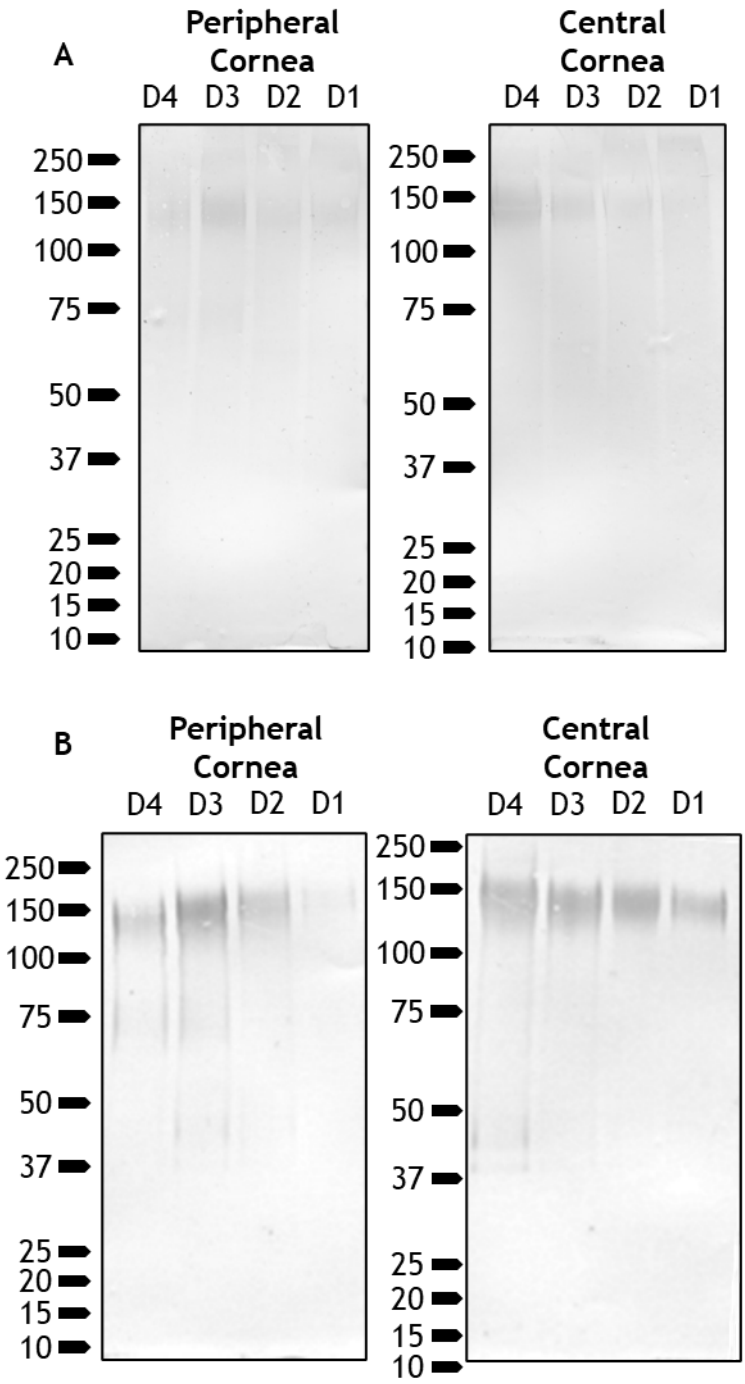

Figure 3.11 Western blot analysis of density gradient fractions from corneal extracts with molecular weight marker in kDa shown of the small CS/DS proteoglycan, decorin (100-150 kDa, 42 kDa for the core protein). (**A**) Immunoblot showing the small leucine-rich repeat proteoglycan decorin. (**B**) Immunoblot of decorin after partial chondroitinase ABC digestion

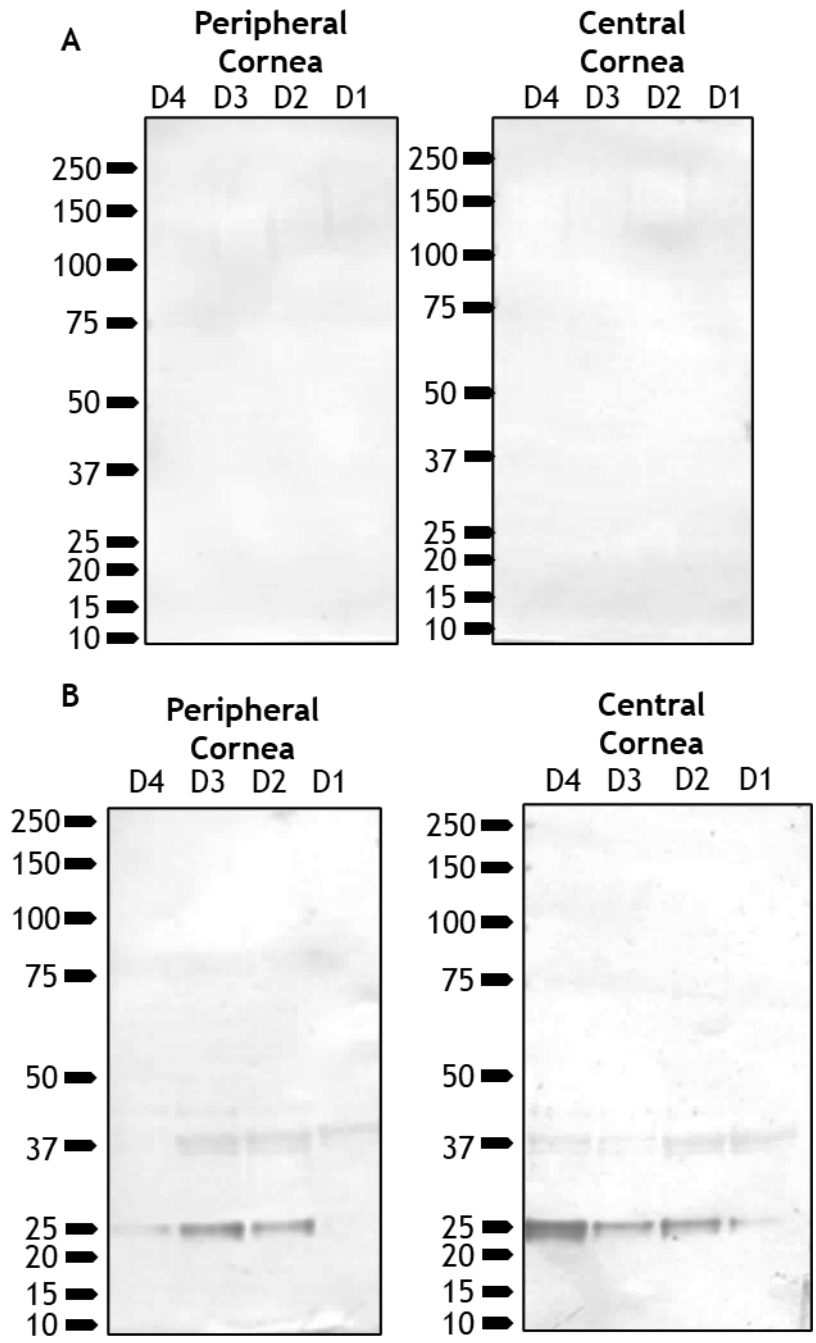

Figure 3.12 Western blot analysis of density gradient fractions from corneal extracts with molecular weight marker in kDa shown of the KS proteoglycan keratocan. (**A**) Immunoblot of the native proteoglycan which is undetectable before enzymatic digestion. (**B**) Immunoblot of the same proteoglycan after treatment with peptide-N-glycosidase F enzyme.

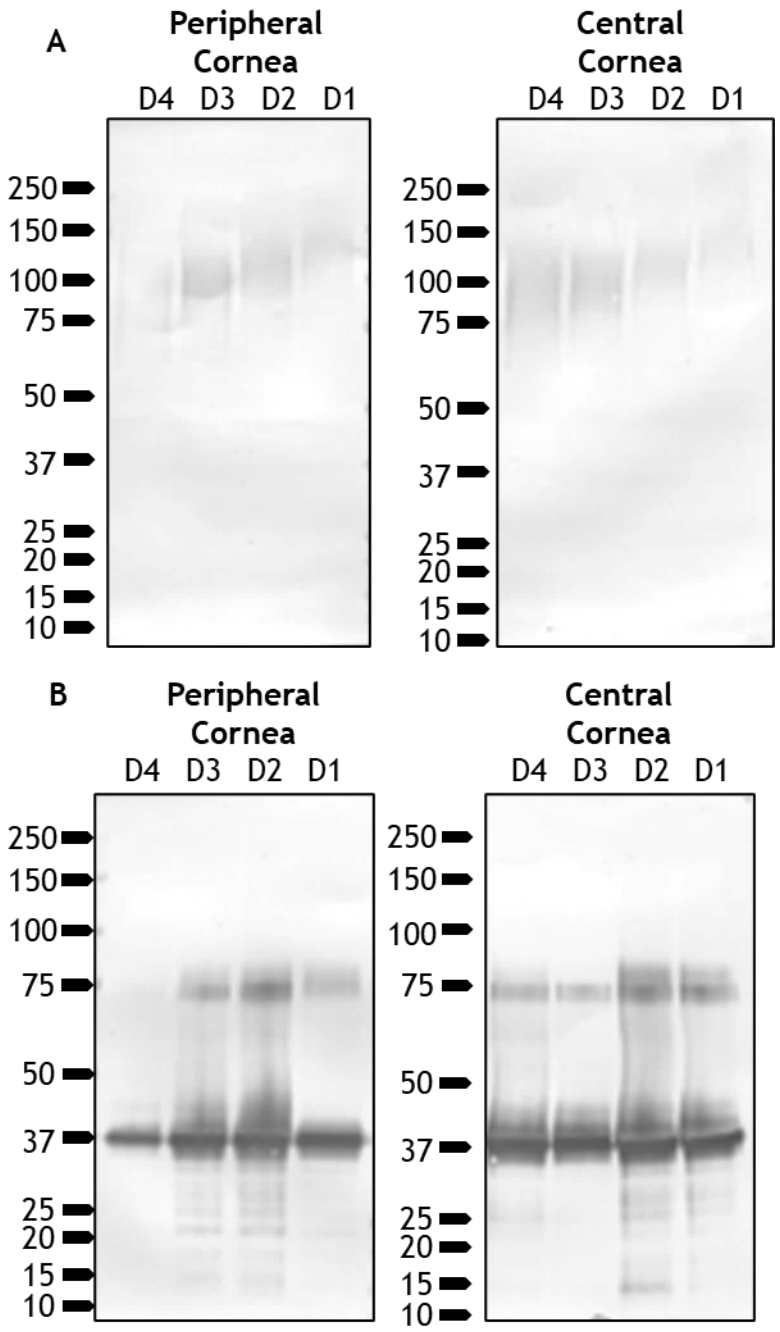

Figure 3.13 Western blot analysis of density gradient fractions from corneal extracts with molecular weight marker in kDa shown of the KS proteoglycan lumican. (**A**) Immunoblot of the native proteoglycan. (**B**) Immunoblot of the same proteoglycan after treatment with peptide-N-glycosidase F enzyme.

3.3.6 *Shark cartilage provides a rich source of the CS/DS epitope recognised by the 6C3 antibody*

Owing to low abundance of the CS/DS epitope recognised by the 6C3 in the cornea, it was necessary to find another source. In order to determine another source of glycosaminoglycans rich in the sulphation motif recognised by the 6C3 antibody, shark cartilage was used as it is a rich source of chondroitin/DS. The glycosaminoglycan epitopes, recognised by the 6C3 and 5D4 antibodies were both present on a very high molecular weight molecules resulting in a large broad band for both epitopes as shown in **Figure 3.14A**. Performing ELISA on the extracted sample also showed high signal of both 6C3 and 5D4 antibodies and little to no 7D4 signal as shown in **Figure 3.14B**.

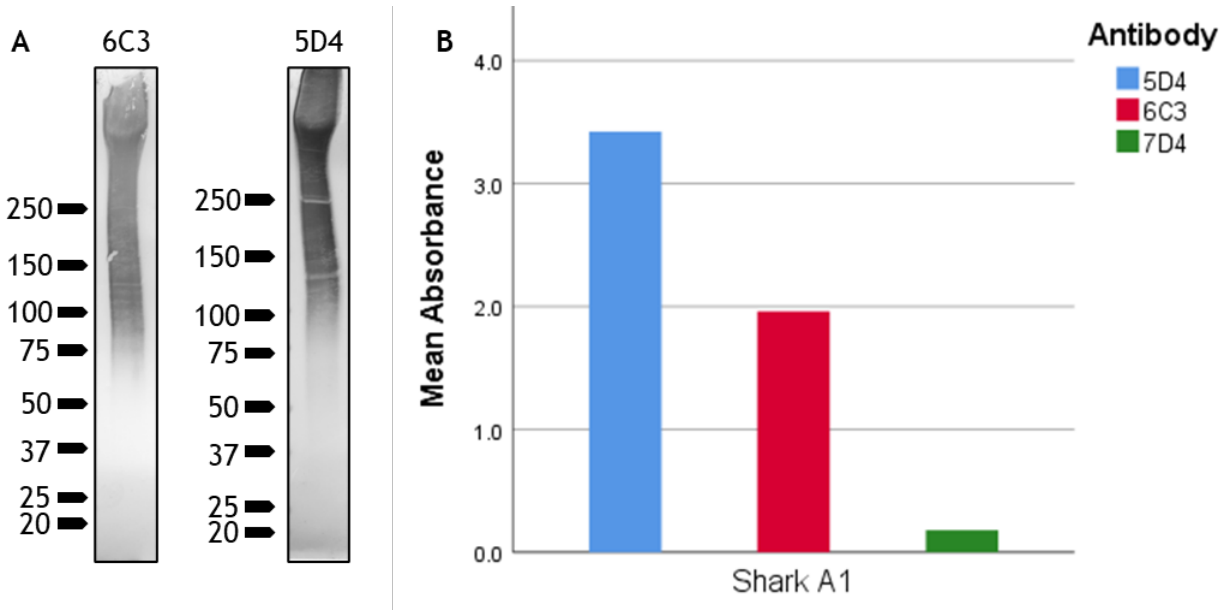

Figure 3.14 Proteoglycan extraction from shark skeletal cartilage. (**A**) Immunoblot showing signal from the 6C3 CS/DS antibody and 5D4 highly sulphated KS antibody. (**B**) ELISA showing the three main sulphation epitopes of interest, recognised by the antibodies 5D4, 6C3 and 7D4.

3.3.7 *Ion exchange chromatography and 232 nm profile of free glycosaminoglycans from buoyant density fractions PD3 and CD3*

The samples chosen for further purification from those identified in the previous sections were, initially, the central and peripheral D3 fractions due to their high presence of the epitope recognised by the 7D4 antibody in both corneal compartments. They also had the highest glycosaminoglycan concentration enabling the highest potential product yield. The peripheral D4 fraction was also included as detailed further in the chapter. The samples chosen from both peripheral and central cornea will now be referred to as PD4/PD3 and CD3 from herein, referring to the peripheral or corneal density gradient fraction selected respectively.

The initial pilot run of anion exchange chromatography was performed on free glycosaminoglycan chains from fractions CD3 and PD3 to maintain parity and determine differences between the same dissociative fractions from different corneal compartments. They were also chosen due to having the highest glycosaminoglycan content and high signal for the CS/DS sulphation epitope recognised by the 7D4 antibody, as mentioned, as well as high signal for the 5D4 antibody, which recognises a highly sulphated KS epitope.

There were clear differences between the two corneal compartment samples during anion exchange chromatography, and also between different fractions from the same corneal compartment, e.g. PD3 and PD4 as detailed in Section 3.3.10. Initially the CD3 fraction appears to have two glycosaminoglycan peaks as detected by absorbance at 232 nm, one at approximately 1.2 M NaCl and another at approximately 1.75 M NaCl as shown in **Figure 3.15A**, however this initial peak was void of glycosaminoglycan content and most likely an artefact. The PD3 fraction appeared to have two peaks at 1.75 M NaCl and 2.2 M NaCl respectively as shown in **Figure 3.15B**.

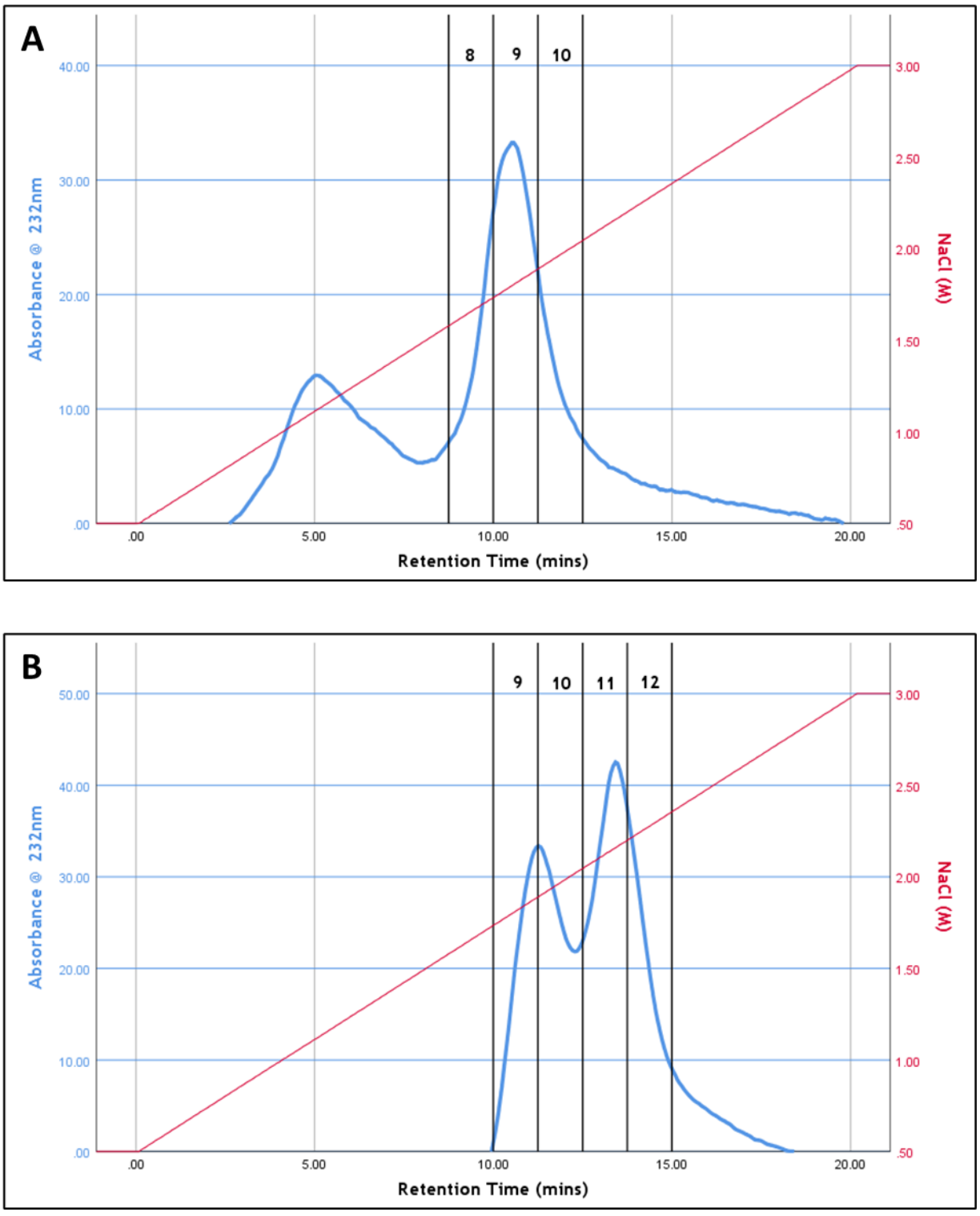

Figure 3.15 Anion exchange chromatography analysis of free glycosaminoglycan chains after extraction and alkaline β-elimination from porcine cornea showing glycosaminoglycan absorbance at 232 nm and the NaCl molarity over the ion gradient. (**A**) Representative anion exchange chromatography absorbance trace from CD3 glycosaminoglycan corneal fraction. (**B**) Representative anion exchange chromatography absorbance trace from PD3 glycosaminoglycan corneal fraction.

3.3.8 Glycosaminoglycan analysis of free glycosaminoglycans from buoyant density fractions PD3 and CD3 following ion exchange chromatography

A summary of the glycosaminoglycan content of the fractions before and after anion exchange chromatography are given below in **Table 3.4**, as determined by the DMMB assay. The overall glycosaminoglycan content was quite low, and recovery was poor after anion exchange chromatography, and lower for the peripheral fractions from anion exchange chromatography as identified in **Table 3.4**.

Table 3.4 Summary of glycosaminoglycan content, by weight, of different fractions before and after ß-elimination, CPC precipitation and anion exchange chromatography (IEX) in the third preparation CD3 and PD3 samples. The total percentage recovery was also noted from the original starting amount of 500 µg of glycosaminoglycan.

Sample	IEX Fraction	Glycosaminoglycan Amount (µg)	Recovery (%)
CD3 Density Gradient Fraction		500.0	-
PD3 Density Gradient Fraction		500.0	-
CD3 Free Glycosaminoglycans	8	15.3	12.6
	9	46.5	
	10	1.2	
PD3 Free Glycosaminoglycans	9	1.4	6.9
	10	30.1	
	11	3.2	

3.3.9 ELISA analysis of glycosaminoglycan sulphation motifs in the fractions generated from anion-exchange chromatography on CD3 and PD3

Having separated these samples using ion exchange, these enriched fractions were subsequently assessed for the presence of individual glycosaminoglycan species, namely the epitope recognised by 7D4.

Prior to purification, both the PD3 and CD3 density gradient fractions had a relatively large amount of both the sulphation epitopes of interest present, as recognised by the 7D4 CS/DS antibody and 5D4 KS antibody, as shown in **Figure 3.16A**. After anion exchange chromatography, the relative signal for both epitopes was lower than as for the unprocessed samples, shown in **Figure 3.16B** but was highest during the peak fraction (identified by 232 nm peak) for both epitopes (fraction 9 for CD3 and fraction 10 for PD3). All PD3 anion exchange fractions contained some KS signal as detected by the 5D4 antibody. All CD3 anion exchange fractions contained both CS/DS and KS as detected by antibody signal, with the exception of fraction 10 in this trial, which only contained KS signal as detectable by ELISA.

As a result of not being able to selectively enrich a CS/DS substrate from these density centrifugation fractions, due to the presence of contaminating KS, further fractions were investigated, namely the D4 fraction from peripheral cornea (PD4), as detailed in Section 3.3.10 below.

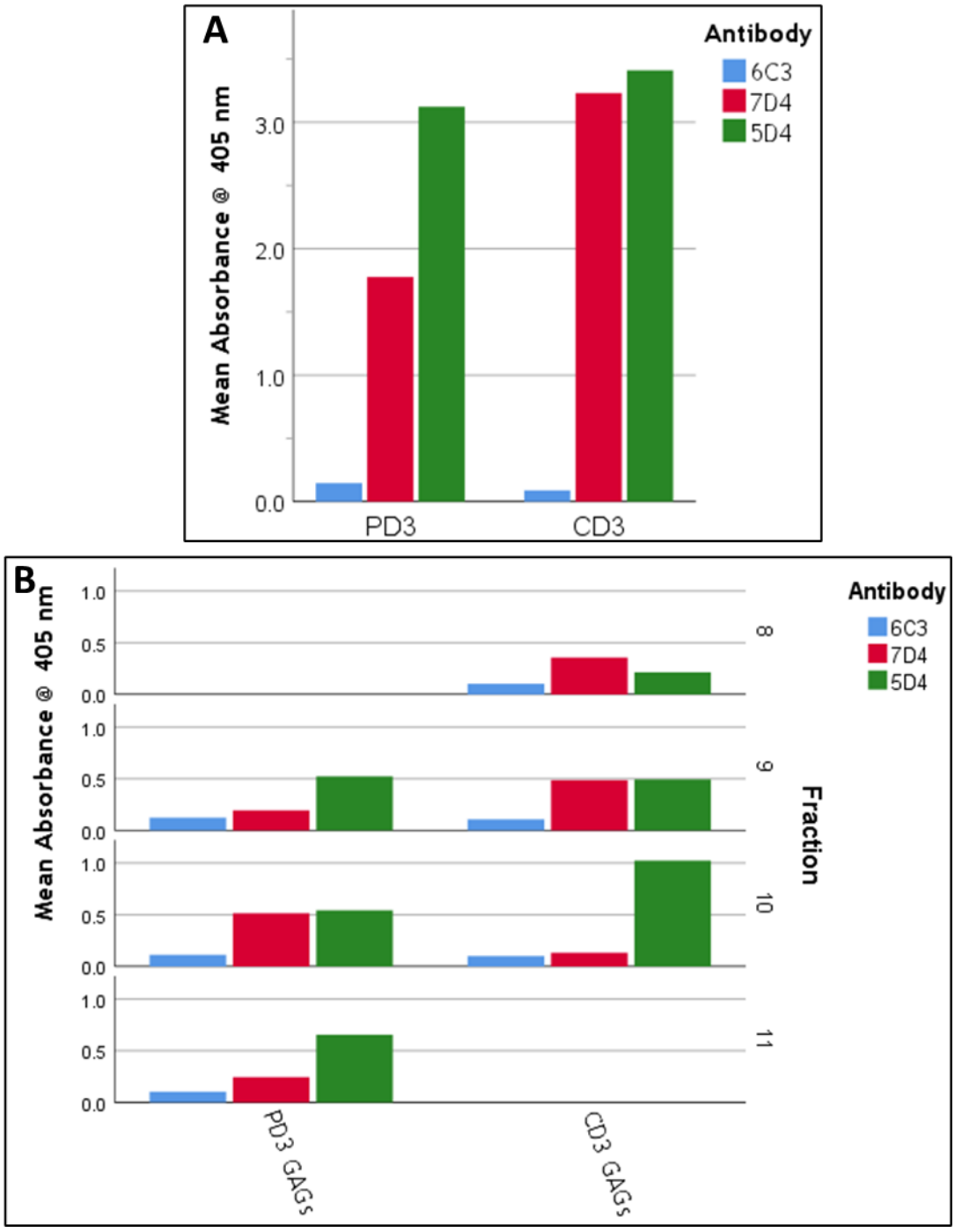

Figure 3.16 ELISA analysis of dissociative fractions PD3 and CD3 from the third corneal proteoglycan extraction for the CS/DS antibodies, 6C3 and 7D4, and KS antibody, 5D4. (**A**) Analysis of PD3 and CD3 fractions before ß-elimination, CPC precipitation and anion exchange chromatography. (**B**) Analysis of PD3 and CD3 fractions after ß-elimination, CPC precipitation and anion exchange chromatography showing free glycosaminoglycan (GAG)-containing anion exchange chromatography fractions.

3.3.10 Ion exchange chromatography and 232 nm profile of proteoglycans and free glycosaminoglycans from buoyant density fractions PD4 and CD3

After the initial trial, further attempts at enrichment using the fourth preparation of corneal proteoglycans, which had slightly higher signal for the sulphation epitopes of interest as shown in **Figure 3.19A**. The PD4 density gradient fraction was also used due to the observation in the previous chapter that O' linked KS glycosaminoglycans appeared to be absent in this fraction, reducing the likelihood of co-elution with the O' linked CS/DS glycosaminoglycans. Also investigated here was whether the PD4 fraction could yield separation of KS and CS/DS glycosaminoglycans without the need for ß-elimination prior to anion exchange chromatography and performed post hoc, using the method described in this chapter. Accordingly, anion exchange chromatography was used to separate both proteoglycans from PD4 and CD3 fractions as well as free glycosaminoglycans produced from ß-elimination and CPC precipitation from this preparation.

Initially, the free glycosaminoglycans from PD4 and CD3 were each applied to the ion exchange column and shown in **Figure 3.17**. For CD3, the absorbance pattern was largely similar to CD3 from the previous preparation, but eluted very slightly later, with an absorbance peak in fraction 9 at approximately 1.75 M NaCl as demonstrated in **Figure 3.17A.** PD4, however was markedly different from PD3 described in Section 3.3.7. Whilst two peaks were also present for this sample, they appeared much earlier at approximately 1.2 and 1.4 M NaCl respectively in **Figure 3.17B** in anion exchange fractions 5, 6 and 7.

For whole proteoglycans used in anion exchange chromatography, the absorbance peaks were very distinct from the above. In the case of whole proteoglycans from CD3, the absorbance peak was at approximately 2.2 M NaCl in **Figure 3.18A**, whereas for the PD4 proteoglycans, unlike for the free glycosaminoglycan chains, there was only a singular peak at approximately 1.6 M NaCl as shown in **Figure 3.18B**.

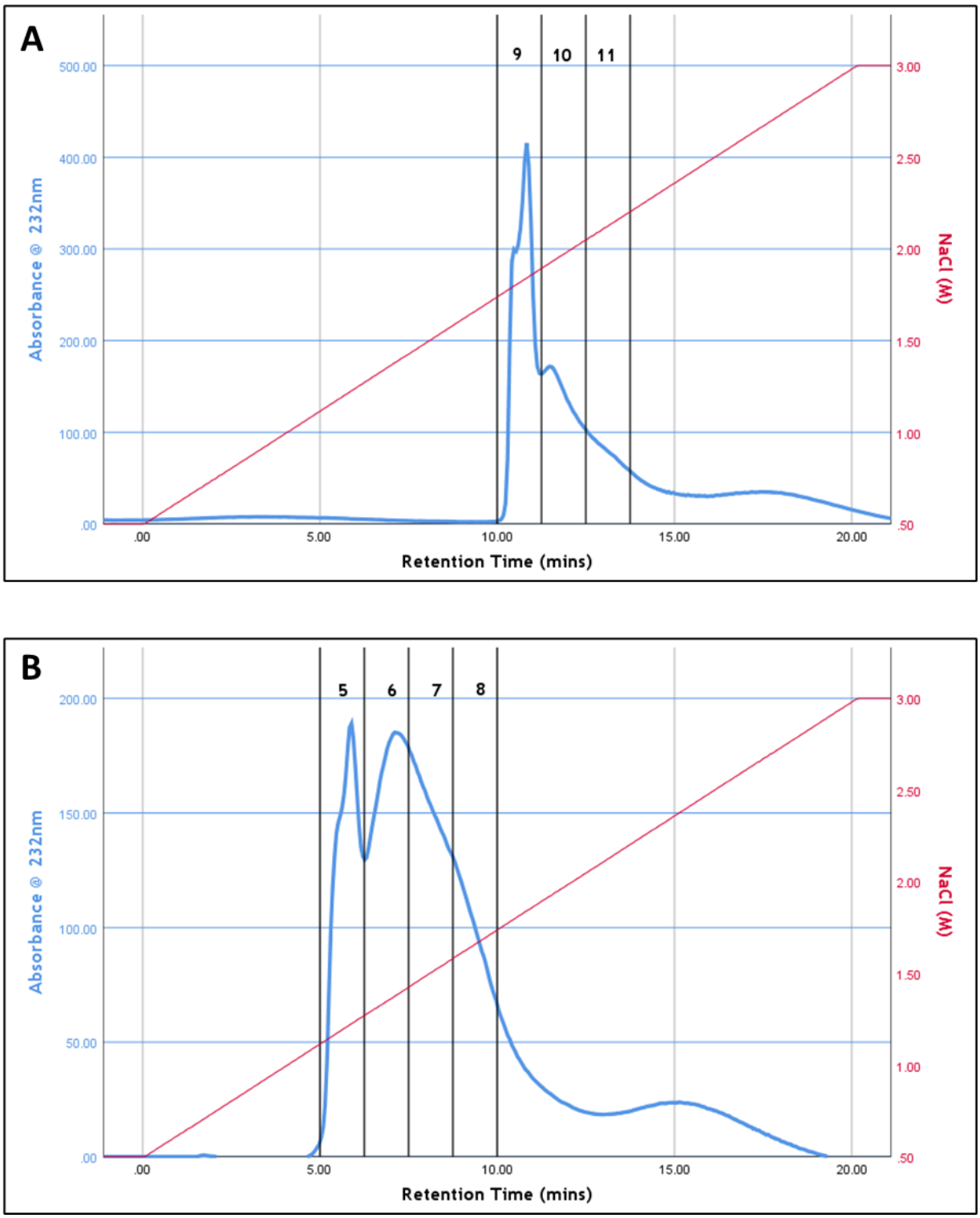

Figure 3.17 Anion exchange chromatography analysis of free glycosaminoglycan chains after extraction and alkaline ß-elimination from porcine cornea showing glycosaminoglycan absorbance at 232 nm and the NaCl molarity over the ion gradient. (**A**) Representative anion exchange chromatography absorbance trace from CD3 glycosaminoglycan corneal fraction. (**B**) Representative anion exchange chromatography absorbance trace from PD4 glycosaminoglycan corneal fraction.

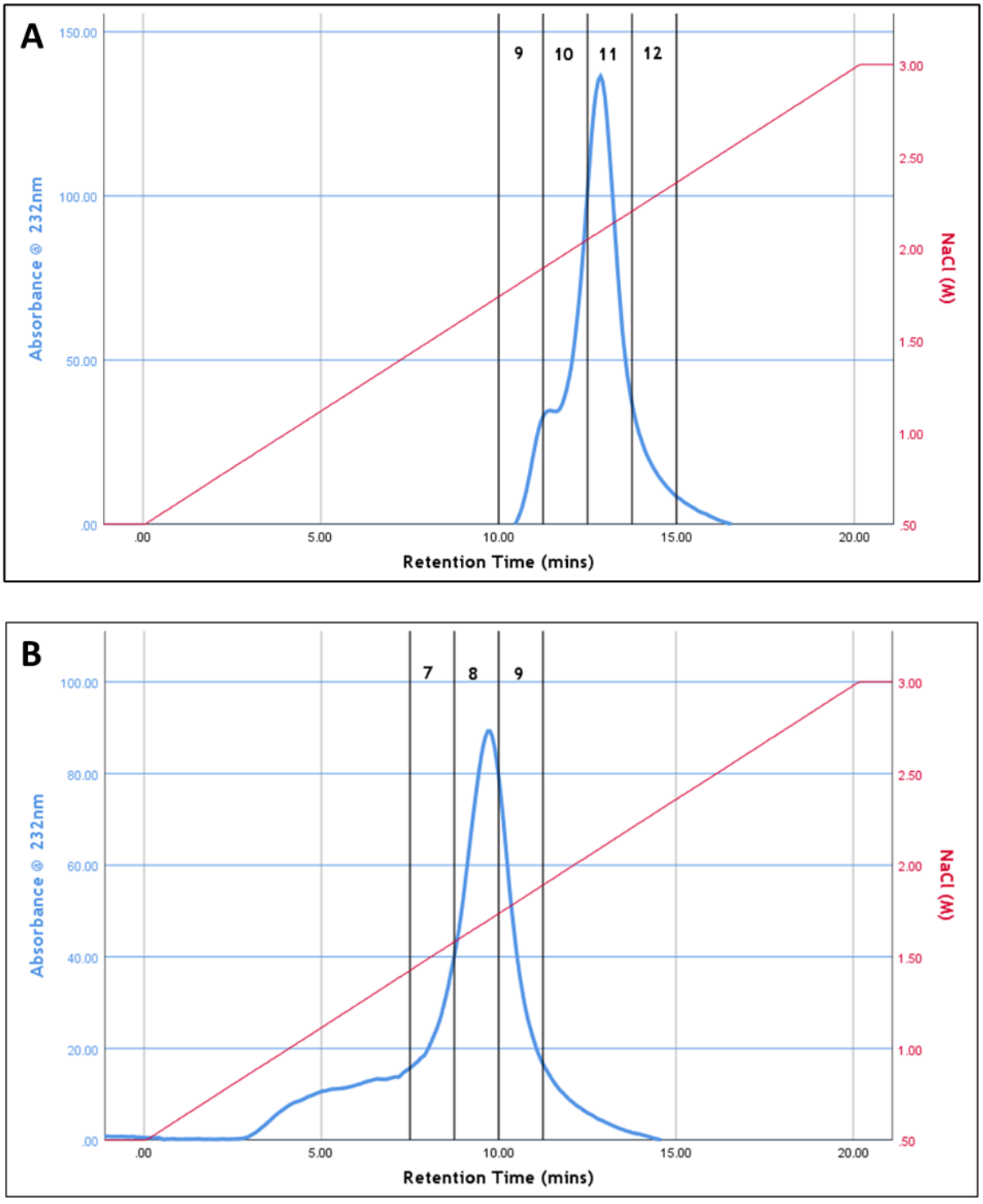

Figure 3.18 Anion exchange chromatography analysis of crude proteoglycan extractions from porcine cornea showing glycosaminoglycan absorbance at 232 nm and the NaCl molarity over the ion gradient. (**A**) Representative anion exchange chromatography absorbance trace from CD3 corneal fraction. (**B**) Representative anion exchange chromatography absorbance trace from PD4 corneal fraction.

3.3.11 Glycosaminoglycan analysis of free glycosaminoglycans and proteoglycans from buoyant density fractions PD4 and CD3 following ion exchange chromatography

After anion exchange chromatography, fractions were determined of interest identified by peaks of UV absorbance at 232 nm and the summary of glycosaminoglycan contents are shown in **Table 3.5**.

In terms of glycosaminoglycan content, the whole proteoglycans applied directly to the anion exchange column had a slightly lower recovery rate than for their free glycosaminoglycan counterparts and slightly lower amounts overall, with the peak glycosaminoglycan content contained within anion exchange chromatography fraction 11 for CD3 and 8 for PD4 as seen in **Table 3.5**.

For free glycosaminoglycans from the CD3 density gradient fraction, the majority was found in anion exchange fraction 10, similar to as was seen in Section 3.3.8, but slightly delayed elution, which may be inherent variation in the samples from different preparations. For the PD4 density gradient fraction, the majority of the glycosaminoglycan was present in fractions 6 and 7 as shown in **Table 3.5**, eluting much earlier than those seen in glycosaminoglycans from the PD3 density centrifugation fraction. Overall yield and percentage recovery was slightly higher than for the previous preparation, and sufficient glycosaminoglycan was produced to be used for cell culture for various fractions of interest.

Table 3.5 Summary of glycosaminoglycan content, by weight, of different fractions before and after ß-elimination, CPC precipitation and anion exchange chromatography (IEX), as well as solely after anion exchange chromatography in the fourth preparation CD3 and PD4 samples. The total percentage recovery was also noted from the original starting amount of 500 µg of glycosaminoglycan.

Sample	IEX Fraction	Glycosaminoglycan Amount (µg)	Recovery (%)
CD3 Density Gradient Fraction		500.0	-
PD4 Density Gradient Fraction		500.0	-
CD3 Free Glycosaminoglycans	9	26.6	34.5
	10	105.3	
	11	40.6	
PD4 Free Glycosaminoglycans	5	0.2	14.9
	6	39.2	
	7	35.3	
CD3 Proteoglycans	10	64.1	32.8
	11	84.4	
	12	15.5	
PD4 Proteoglycans	7	10.0	8.0
	8	22.0	
	9	7.9	

3.3.12 *ELISA analysis of glycosaminoglycan sulphation motifs in the fractions generated from anion-exchange chromatography of CD3 and PD4 reveals free glycosaminoglycan substrates enriched in sulphation motifs of interest*

The anion exchange eluates for PD4 and CD3, including both free glycosaminoglycans and whole proteoglycans, with detectable sulphated glycosaminoglycan content, were analysed by ELISA for the presence of sulphation epitopes detailed previously, recognised by the antibodies 6C3, 7D4 and 5D4 as shown in **Figure 3.19**.

The absorbance detected for each of the CS/DS and KS antibodies in PD4 and CD3 density gradient fractions prior to anion exchange chromatography is shown in **Figure 3.19A**. The glycosaminoglycan epitopes recognised by the 7D4 and 5D4 epitopes were abundant in both preparations. Following separation by direct anion exchange chromatography of CD3 and PD4 density gradient fractions (whole proteoglycans), the distribution of glycosaminoglycans recognised by the 7D4 and 5D4 antibodies was assessed by ELISA. Glycosaminoglycan epitopes were seen in anion exchange fractions 7-12 as shown in **Figure 3.19B**. Peak absorbance for 5D4 was seen in PD4 eluates in fractions 7-9 and for CD3, fractions 10-12. Similarly, a smaller amount of signal from the epitope recognised by the 7D4 antibody was detected in fractions 7-9 of the PD4, with a peak in fraction 9 and detected in fractions 10-12 for the CD3 density gradient fraction after anion exchange. The absorbance reading recorded in the anion exchange fractions were reduced compared to the direct ELISA carried out on the density gradient fractions PD4 and CD3, prior to anion exchange chromatography using the same coating concentrations. Anion exchange chromatography did not yield further separation of CS/DS, recognised by the 7D4 antibody, and KS, recognised by the 5D4 antibody, from these density gradient fractions.

In contrast, ß-elimination, followed by CPC precipitation of PD4 and CD3 density gradient fractions with subsequent anion exchange chromatography showed a different profile of separation to that of PD4 and CD3 applied directly to an anion exchange column as seen in **Figure 3.19B**. Reduced signal generated by

the KS antibody, 5D4, was observed in the CD3 free glycosaminoglycan fractions, and a relative increase of signal generated by the CS/DS antibody, 7D4 was witnessed, similarly as in Section 3.3.9, but the two species were not separated, as before. Interestingly, the PD4 free glycosaminoglycans eluted much earlier than as for the CD3 free glycosaminoglycans, and PD3 free glycosaminoglycans, as seen in Section 3.3.9 and were detectable in fractions 5-7 from anion exchange. Of particular note, was the lack of KS detected by the 5D4 antibody in all anion exchange fractions, and a peak of the CS/DS antibody signal, 7D4, enriched in fraction 7 after anion exchange chromatography.

Two substrates of interest were identified from these fractions detailed here, namely, the first of these was the free glycosaminoglycans from PD4 in fraction 7 of anion exchange chromatography, which was enriched in the CS/DS epitope recognised by the antibody 7D4 (with no KS detected). The second, was the free glycosaminoglycans from CD3 in fraction 10 after anion exchange chromatography, which was enriched in both the CS/DS epitope recognised by 7D4, and KS, as recognised by the 5D4 antibody. Henceforth this 7D4 containing sample from PD4 free glycosaminoglycans will be referred to as ‘7D4’ substrate and the ‘5D4/7D4’ mixed substrate from CD3 free glycosaminoglycans will also be referred to as such for simplification.

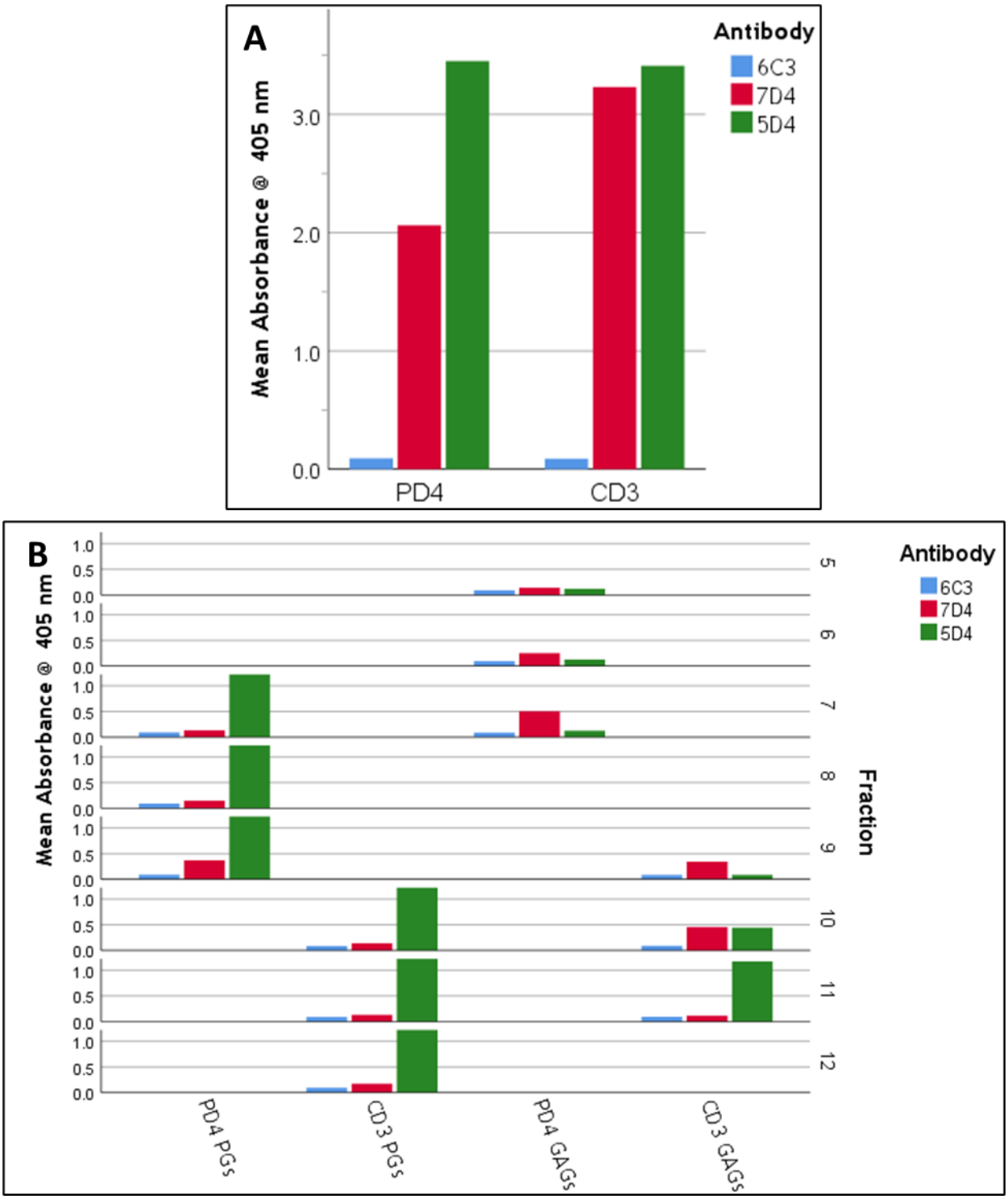

Figure 3.19 ELISA analysis of dissociative fractions PD4 and CD3 from the fourth corneal proteoglycan extraction for the CS/DS antibodies, 6C3 and 7D4, and KS antibody, 5D4. (**A**) Analysis of the same fractions before ß-elimination, CPC precipitation and anion exchange chromatography. (**B**) Analysis of the same fractions after ß-elimination, CPC precipitation and anion exchange chromatography (GAGs - Free Glycosaminoglycans) or just anion exchange chromatography (PGs - Proteoglycans) showing glycosaminoglycan-containing fractions after anion exchange chromatography.

3.3.13 Anion exchange separation of free glycosaminoglycans from shark and generation of a substrate enriched in 6C3

Finally, anion exchange chromatography was conducted on free glycosaminoglycans, following ß-elimination and CPC precipitation, from shark skeletal cartilage as detailed in **Figure 3.20**. Absorbance at 232 nm peaked at 1.75 M and slowly decreased after this point. The starting glycosaminoglycan content in both the starting sample and eluted fractions after processing is detailed below in **Table 3.6**, with the highest yield detected in fraction 11.

Table 3.6 Summary of glycosaminoglycan content, by weight, of different fractions before and after ß-elimination, CPC precipitation and anion exchange chromatography (IEX) of shark proteoglycan extract from skeletal cartilage. The total percentage recovery was also noted from the original starting amount of 500 µg of glycosaminoglycan

Sample	IEX Fraction	Glycosaminoglycan Amount (µg)	Recovery (%)
Shark Density Gradient Fraction		500.0	-
Shark Free Glycosaminoglycans	9	0.6	26.2
	10	42.8	
	11	87.4	

Following anion exchange chromatography, ELISA analysis for the detection of sulphation epitopes was performed as before, revealing two fractions enriched in the 6C3 CS/DS sulphation epitope, with very low but detectable 7D4 CS/DS sulphation epitope signal as shown in **Figure 3.21B**. All of the 5D4 signal present in the original sample in **Figure 3.21A** was lost upon enrichment. Fraction 11 after anion exchange chromatography will from now on be referred to as the 6C3 substrate in further work.

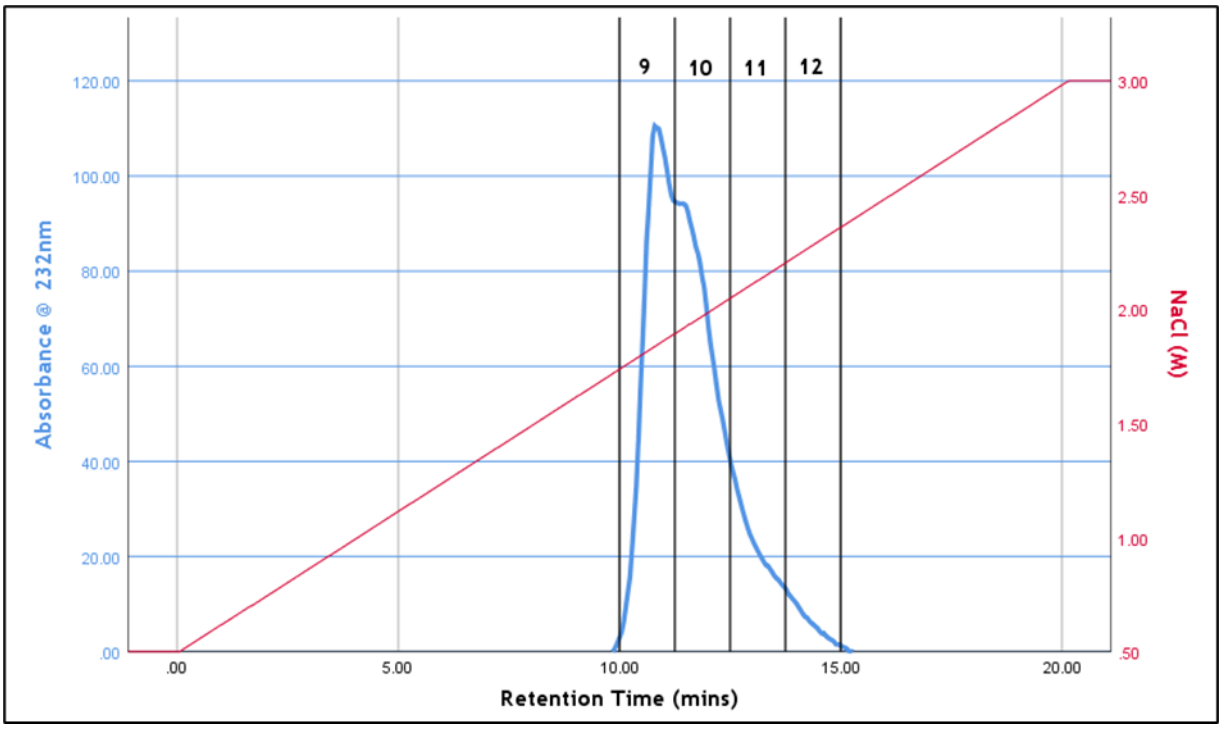

Figure 3.20 Anion exchange chromatography analysis of free glycosaminoglycan chains after extraction and alkaline ß-elimination from shark skeletal cartilage showing glycosaminoglycan absorbance at 232 nm and the NaCl molarity over the ion gradient.

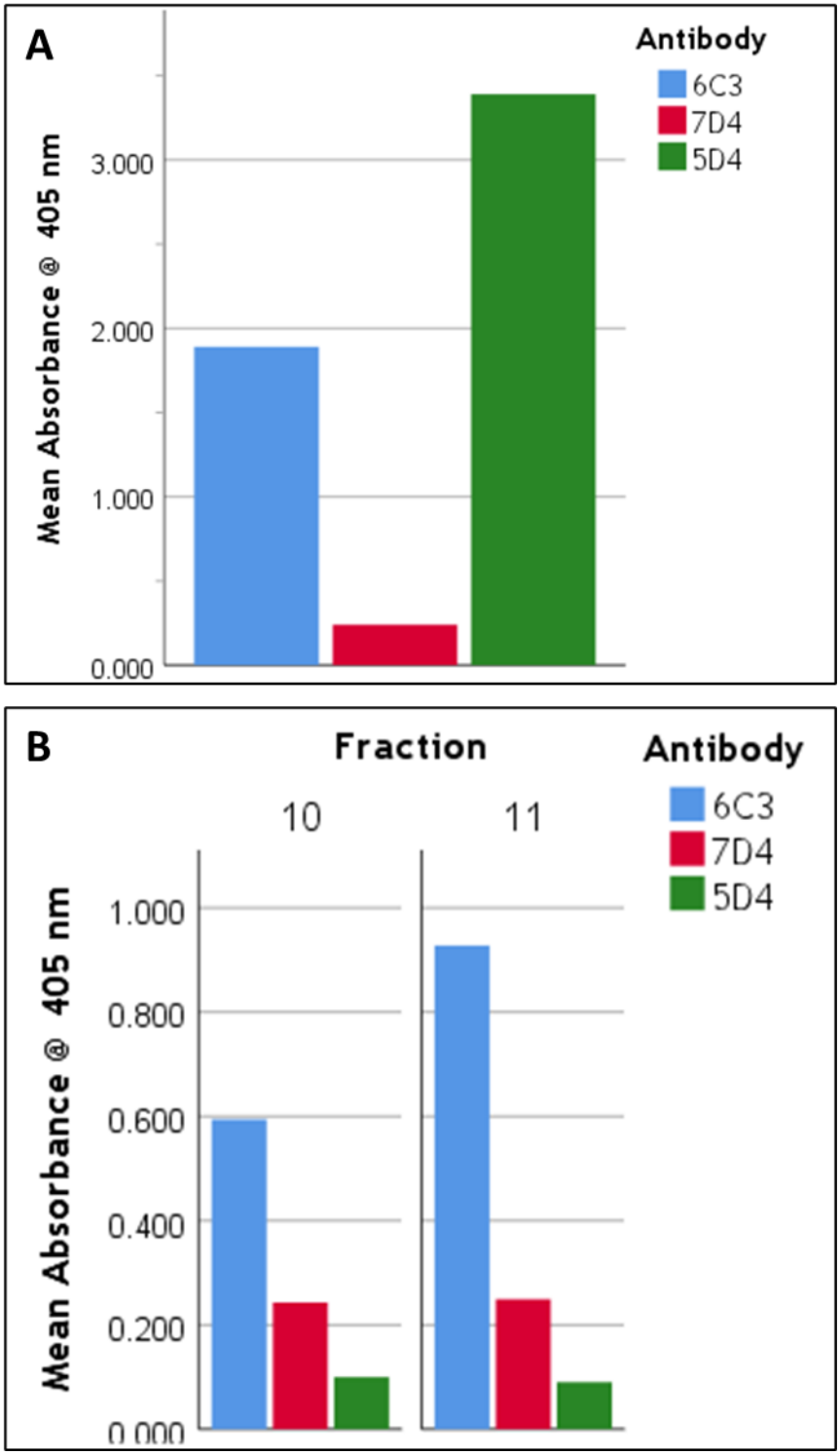

Figure 3.21 ELISA analysis of proteoglycan extraction from shark skeletal cartilage for the CS/DS antibodies, 6C3 and 7D4, and KS antibody, 5D4. (**A**) Analysis of shark skeletal cartilage before ß-elimination, CPC precipitation and anion exchange chromatography. (**B**) Analysis of the same sample but after ß-elimination, CPC precipitation and anion exchange chromatography showing glycosaminoglycan-containing fractions after anion exchange chromatography.

3.3.14 Analysis of glycosaminoglycan substrates of interest for contaminants

In order to examine the presence of potential contaminants remaining in the enriched glycosaminoglycan fractions, two methods were employed. Initially a silver stain was used, which is sensitive enough to detect nanogram levels of protein present in a sample after SDS-PAGE. In this study, no protein was detected as shown in **Figure 3.22A**, the detection range being limited to 1 ng, as 0.5 ng was undetectable using a BSA standard at 66.5 kDa, meaning there is less than 1 ng of protein per 1 µg of glycosaminoglycan present in the sample.

Barium acetate gel electrophoresis and free glycosaminoglycan chain blotting was employed to detect the glycosaminoglycans present in the sample. CS, KS and HS standards and mixtures of these were employed to identify whether these different glycosaminoglycan species would be separated and detectable using this method. When electrophoresed in isolation, it was possible to clearly detect a large difference between HS and CS, with KS being located between the two in **Figure 3.22B**. When all three standards were run together, it was difficult to determine HS from the KS band. In spite of this in **Figure 3.22B**, both 6C3 and 7D4 substrates appeared to have no HS or KS present, with the 5D4/7D4 substrate having a definite band present where CS/DS would be expected, and a faint broad band in line with KS, but it cannot be ruled out that HS is present from this assay. As a result of this, an ELISA using the HS antibody 10E4 was also performed, but no signal was detected for any fractions identified in this chapter.

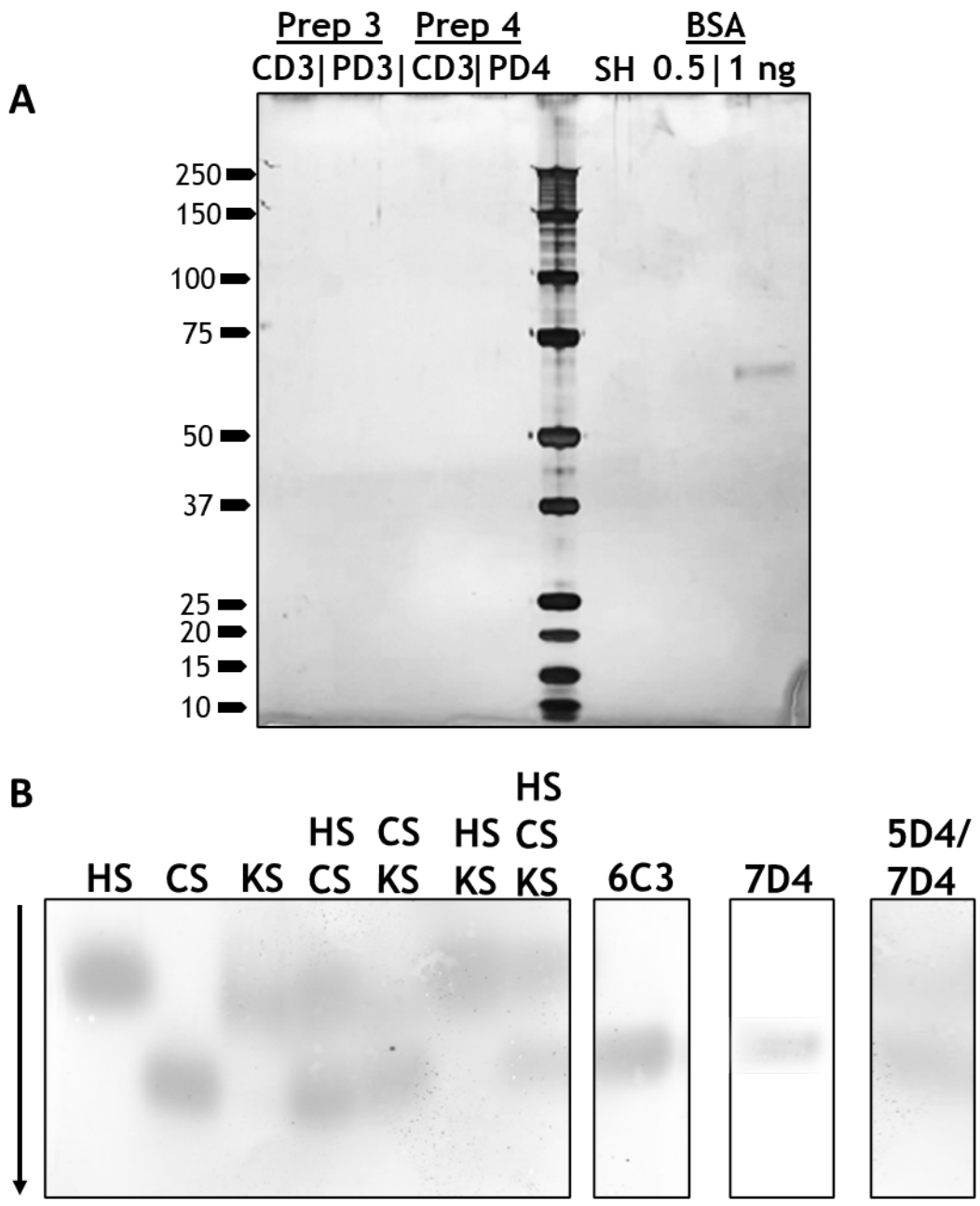

Figure 3.22 Investigating potential contaminants in the anion exchange chromatography-generated fractions to be used for cell culture substrates. (**A**) Silver Stain image showing free glycosaminoglycan chains from the following anion exchange chromatography fractions: preparation 3 (Prep 3) CD3 fraction 9 and PD3 fraction 10; preparation 4 (Prep 4) PD4 fraction 7 and CD3 fraction 10 and finally fraction 11 from shark skeletal cartilage (SH). (**B**) Glycosaminoglycan blot image after barium acetate agarose gel electrophoresis, stained with alcian blue, showing various glycosaminoglycan standards and mixtures along with enriched glycosaminoglycan fractions. 6C3 represents fraction 11 from shark skeletal cartilage, 7D4 represents fraction 7 from PD4 from preparation 4 and finally 5D4/7D4 represents fraction 10 from CD3 from preparation 4 also. The arrow on the left indicates the direction of travel from the well origin.

3.4 Discussion

The overall aim of this chapter proteoglycan extraction was successful in its attempt to identify and extract CS/DS proteoglycans and relevant sulphation epitopes of interest from porcine cornea. Enriched substrates, compatible with cell culture and void of mixed glycosaminoglycan species and detectable contaminants, were produced for the CS/DS epitopes recognised by the antibodies 6C3, from shark, and 7D4, from peripheral corneal. A mixture of the epitopes recognised by the KS antibody 5D4 and the CS/DS antibody 7D4 was also generated from the central and peripheral cornea.

3.4.1 Density centrifugation and direct ELISA to identify CS/DS epitopes of interest

From the five fractions generated after isopycnic ultracentrifugation, many proteins were separated out and a relatively large amount of glycosaminoglycan was detected in each fraction in the typical glycosaminoglycan containing fractions D4 to D1. ELISA analysis showed the presence of varying signal of both the 5D4 KS and 7D4 CS/DS sulphation epitope antibodies. This was the first such examination of CS/DS sulphation epitopes extracted from both peripheral and central cornea, with KS having been described previously as relatively even across the cornea, as was seen here (Ho et al., 2014).

Unfortunately, despite the promising association of the epitope recognised by the CS/DS antibody 6C3 with the limbal stem cell niche, it was unable to be detected by ELISA but only detected with very weak signal by Western blot as discussed below. Whilst promising, owing to the lack of detection by ELISA, it would have been difficult to rapidly detect the epitope recognised by 6C3 in downstream purification steps from porcine cornea and would have been difficult to generate sufficient quantities of biologically relevant substrate. To this end, an alternative source was investigated from shark cartilage. Of course, this source is not optimal or as well adapted for mammalian studies as porcine cornea, however, many studies use CS or DS salts extracted from shark and often these contain impurities, so further purification is often required, whereas here the purification was performed in-house (da Cunha et al., 2015; Santos et al., 2017). Here shark extract was shown to be a rich source of CS/DS particularly in

the epitope recognised by the 6C3 antibody but had a notable amount of KS as detected by ELISA and Western Blot as shown in **Figure 3.14**, but these glycosaminoglycan species were readily separated.

3.4.2 Western blot analysis of CS/DS sulphation motifs and corneal proteoglycans

In the Western blot analysis, the glycosaminoglycan sulphation motifs as well as a set of the primary corneal small leucine-rich repeat proteoglycans were analysed with the exception of osteoglycin (mimecan) and fibromodulin which are less well characterised and less abundantly expressed in the cornea as the other proteoglycans identified in the case of osteoglycin (García et al., 2016).

Initially the presence of the abundant KS found in the cornea was detected with the KS 5D4 antibody, which recognises a highly sulphated epitope. KS was present across a broad range of molecular weights and in all buoyant density fractions, reflecting the diverse range of KS proteoglycans present in the cornea and their different glycosaminoglycan attachments (Caterson and Melrose, 2018). High molecular weight 5D4 signal was detected in all fractions except the peripheral D4 fraction and was completely lost upon N-glycosidase treatment as shown in **Figure 3.8B**. In terms of KS proteoglycans to which this sulphation epitope is attached, it is likely present on both lumican and keratocan as discussed here.

Lumican presented at an expected broad band between 75 and 150 kDa and after N-glycosidase treatment presented as an a band at 75kDa or 37 kDa as shown in **Figure 3.13**, with the former representing lumican that has retained KS through O' linkage (Dunlevy and Rada, 2004) and the latter the lumican protein core with no further KS attachments (Funderburgh and Conrad, 1990). Interestingly, in the lowest molecular density fraction D4 in peripheral cornea, only N-linked KS lumican proteoglycan was present as shown by the singular band after digestion.

Keratocan, another important corneal KS proteoglycan, was also detected as shown in **Figure 3.12**, however a limitation was the antibody used, KER-1 (Gealy et al., 2007), as a high signal is only generated after N-glycosidase treatment

and so native molecular weight was not observed and compared with 5D4, but it typically presents as a broad band ranging from 50 kDa to approximately 200 kDa, similarly to lumican (Corpuz et al., 1996). After N-glycosidase treatment, the protein core was revealed at 25 kDa and 37 kDa as has previously been described (Funderburgh et al., 1993).

Owing to the molecular weight and abundance of the sulphation motif recognised by the 7D4 antibody and decorin in **Figure 3.9A** and **Figure 3.11** respectively, it is highly likely that it is present on this protein core, possibly with a small amount situated on biglycan. This also correlates with the widespread distribution of 7D4 signal throughout the corneal stroma corresponding to decorin's presence throughout the stroma and biglycan only predominantly being present on the epithelial surface and after injury/corneal damage. The increased signal of biglycan in the sclera and corneal limbus, identified in this study by peripheral corneal density gradient fractions in **Figure 3.10** is also consistent with the same study investigating decorin and biglycan extracts from adult cornea (Funderburgh et al., 1998).

Finally the epitope recognised by the 6C3 antibody was detected at very low levels in both the peripheral and central corneal extracts in Western blot at a slightly higher molecular weight in peripheral cornea as mentioned above and shown in **Figure 3.9B**. It is difficult to determine the protein core to which this epitope is attached, but taking together the results from the immunohistochemistry in Chapter 2 and knowledge from previous localisation studies analysing the expression of a range of extracellular matrix molecules (Schlötzer-Schrehardt et al., 2007), it is most likely versican, especially in the case of the peripheral cornea, owing to its large molecular weight and the fact that versican is an important regulator of apoptosis and cell proliferation, a key factor in the stem cell niche (Sheng et al., 2005; Wight et al., 2020). This also aligns with the fact that the epitope recognised by 6C3 antibody and specific versican isoforms have very similar immunohistochemical staining patterns in human skin, subjacent to basal keratinocytes, in addition to the corneal limbus(Sorrell et al., 1990; Zimmermann et al., 1994). It would have been useful to repeat the immunoblot using a lower percentage gel to achieve better

resolution in the gel for higher molecular weight proteins to determine the versican isoform, but this was outside the scope of this chapter, which was to identify proteoglycans and glycosaminoglycans of interest that were abundant for extraction.

Owing to the low abundance of the epitope recognised by 6C3 in the corneal extracts, an alternative richer source was identified in shark skeletal cartilage as shown in **Figure 3.14**. Both the 6C3 CS/DS antibody and 5D4 KS antibody were present with their signal showing very large molecular weight proteoglycans, but notably, the epitope recognised by the 6C3 antibody had a very strong detectable signal in both Western blot and ELISA, providing a tractable source of glycosaminoglycans containing the epitope recognised by the 6C3 antibody for use in further enrichment and cell culture studies.

3.4.3 Anion exchange chromatography and contamination evaluation

In this study, anion exchange chromatography was performed for the enrichment of glycosaminoglycans chains after detachment of the glycosaminoglycan side chains, in order to attempt to either separate individual glycosaminoglycans and proteoglycans or enrich for certain sulphation epitopes in sufficient quantities for use as a cell culture substrate.

One notable alternative to anion exchange chromatography is immunoprecipitation, using antibodies to capture and purify target proteins through antibody affinity interactions and is a highly specific and effective method, however it is primarily optimised for the use of the antibody binding proteins A and G, which do not bind the IgM CS sulphation epitope antibodies used in this study but instead bind IgG class antibodies from most mammalian species (Erntell et al., 1983; Sorrell et al., 1990). Immunoprecipitation methods exist for IgM class antibodies, one such example is protein L immunoprecipitation, which is a ligand for the kappa light chain of IgM (Björck, 1988; Myhre and Erntell, 1985) but it is considered inefficient for immunoprecipitation due the pentameric structure of IgM and can lead to low yields (Teye et al., 2017). As a result of this they can be converted to IgG class antibodies, but again this also yields a new set of technical challenges (Dang et al., 2013; Filpula, 2007). Taken together, immunoprecipitation was considered

out of the scope of this study due to the increased technical expertise required and concerns of low yields that would be insufficient for biological effect. Notwithstanding, immunoprecipitation could be of extreme interest in further studies, but for the purposes of this thesis, anion exchange chromatography coupled with the methods described here were sufficient to extract enriched glycosaminoglycan species for use as a substrate.

Separation of the CS/DS epitope recognised by 7D4 from KS was achieved as in the case of the PD4 density gradient fraction, and despite a low yield, sufficient glycosaminoglycan was present to use in cell culture as shown in **Figure 3.19B** and **Table 3.5**. In these defined conditions, a separation of the CS/DS and KS epitopes recognised by the antibodies 7D4 and 5D4 was achieved in the central fraction, in CD3 fraction 9 as in **Figure 3.19B**. However this fraction had a relatively low 7D4 profile and a low product yield. A glycosaminoglycan-rich fraction containing both KS and CS/DS was generated with a high glycosaminoglycan concentration, which may be of potential use. The difference between the two corneal compartments, in the ability to separate KS and CS/DS may be explained partly due to the significantly different ratios sulphation patterns of the KS chains between central and peripheral cornea, with the ratio of lesser sulphated KS increasing dramatically towards the peripheral cornea, which may explain why it is possible to separate KS from CS/DS in the PD4 fraction, in addition with the differential deglycosylation of lumican in this fraction as identified in Western blot analysis. The ratio of CS to DS also changes across the cornea, with DS being located more centrally and CS more peripherally (Ho et al., 2014), which again, may be an explanation for the large differences in fractionation seen between peripheral and central samples. They may also have different chain lengths as well as interactions with other molecules during anion exchange chromatography, which may have further contributed to the complexity seen.

Of further interest, also, would have been to investigate the different ion exchange traces for all samples, including the higher molecular weight fractions D2 and D1 from both peripheral and central cornea, as there may have been further differences between the glycosaminoglycans present as well as

proportion of KS to CS/DS. The difference between CS/DS could also be explored further using the methods described here, as well as inclusion of DS standards in the glycosaminoglycan blotting as shown in **Figure 3.22B** and repeated for various other samples. However, this was slightly outside the scope of this chapter, in which the primary goal was to obtain samples enriched in specific glycosaminoglycan epitopes for use in cell culture and this was achieved in the limited timeframe.

Further verification of the constituents of each generated fraction would, of course, be beneficial. For example, after barium acetate gel electrophoresis or SDS-PAGE also performing immunoblotting for each of the antibodies would have been of benefit, for example 6C3, 5D4, 7D4, amongst others, including the less sulphated KS antibody 1B4 (Mehmet et al., 1986) or other CS antibodies. In the case of the KS antibody 1B4, however, 5D4 was found to be virtually universally present wherever 1B4 was detected and highly sensitive (Mehmet et al., 1986), most likely as both of these epitopes are present on most keratan sulphate chains. In the cornea, the KS epitope recognised by 5D4 is present consistently across all corneal zones, unlike the epitope recognised by 1B4, which decreases towards central cornea as mentioned above, so the 5D4 antibody was the best candidate for KS contamination detection across both compartments available in this study (Ho et al., 2014). Due to the limited amount of substrate product generated and the large amount used by these detection methods, however, the presence was detected by ELISA which only requires a very small amount of glycosaminoglycan for detection. Other analytical methods would have also been advantageous also to further confirm the contents and chemical composition of the enriched glycosaminoglycan fractions, for example disaccharide analysis, which typically involves a combination of enzymatic digestion followed by chromatography and subsequent mass spectrometry. This method enables the characterisation and location determination of sulphation or acetylation modifications as well as uronic acid epimerisation, but needs a significant amount of substrate (Gill et al., 2013; Yang et al., 2012). This would enable further characterisation of the glycosaminoglycan species present, but through the methods described in this chapter, the substrates were deemed satisfactory to proceed to the next stage of research. These three substrates are those

enriched in the epitopes recognised by 6C3, 7D4 and 5D4/7D4 and are investigated as substrates for iPSC differentiation in the following chapter.

3.5 Conclusions

The overall aim of this chapter was achieved in that proteoglycan and glycosaminoglycan-containing fractions were extracted from porcine cornea and shark cartilage enriched in sulphation epitopes of interest and free of contaminants. Several substrates enriched in the CS/DS epitopes recognised by the antibodies 7D4 and 6C3, as well as the KS and CS/DS epitopes, recognised by the 5D4/7D4 antibodies were generated. This subsequently allowed for the subsequent effect on pluripotent stem cells to be investigated, and their role, if any, in the differentiation of corneal epithelial cells and other ocular cell types to be explored in the next chapter.

4 Chapter 4: Cultivation of iPS cells on glycosaminoglycan substrates and their differentiation towards corneal epithelial cells

4.1 Introduction

Having successfully identified and purified enriched glycosaminoglycan substrates, the final stage of this project was to examine their effect on differentiation of corneal epithelial cells and other ocular cell lineages from iPS cells, using the SEAM development model (Hayashi et al., 2017, 2016). The SEAM consists of four zones of different cell types derived from the ectodermal lineage as explained in Chapter 1. As a reminder, these zones are as follows. The first zone (zone 1) represents neuronal cells. The second zone typically represents neural crest, retina-like and lens-like cells. The third zone (zone 3), of particular interest in this study, lies outside of zone 2 and typically represents ocular surface ectoderm-like cells or early corneal epithelial-like cells. Lens cells are also sometimes present in this zone. Finally, the fourth zone (zone 4) lies outside of the edge of the zone 3 consists primarily of non-ocular surface epithelial-like cells.

The extracellular matrix is a useful tool for iPS cell maintenance and can be used to maintain their pluripotency. It has, for example, enabled iPS cell culture without a feeder system, which was a significant step in facilitation and access to iPS cell culture (Miyazaki et al., 2012). The substrate upon which iPS cells are maintained can also have a significant effect on the ability to differentiate towards different cell lineages. The extracellular matrix substrate, laminin, has been shown to influence the development and differentiation of SEAMs, particularly the laminin isoform used can have a significant impact on the SEAM morphology and differentiation (Shibata et al., 2018). Further work has also shown how cell type-specific adhesion to defined substrates can be used to isolate preferential cells to use in further downstream experiments or therapeutic approaches (Shibata et al., 2020). Only a small subset of extracellular matrix molecules has been investigated using this incredibly tractable model system, with the effect of other abundant corneal matrix

molecules, for example, collagens, proteoglycans and glycosaminoglycans, remaining largely unknown. The SEAM model, particularly, serves as a useful resource to investigate the effect of these molecules on the developing cornea and the subsequent formation of mature corneal epithelial cells.

The above observations lead to the aim of this chapter, which was to investigate native glycosaminoglycan motifs present in the cornea on developing SEAMs. The objectives of this chapter were to, firstly, investigate whether glycosaminoglycans could be immobilised onto cell culture surfaces in the presence of laminin, which is required for cell adhesion, and then, perform the assessment of different coating protocols on glycosaminoglycan availability. Having established a substrate coating protocol that enables cell adhesion to laminin with detectable glycosaminoglycan, the next steps were to establish the facilities to culture iPSCs and generate SEAM cultures. This was due to the unavailability of specialist facilities as a result of the coronavirus pandemic and inability to travel to Osaka University, Japan as planned. The final objective of this chapter was to assess the effect of glycosaminoglycans on naïve iPSCs and their subsequent differentiation into SEAMs, using gene expression and immunohistochemical methods. In this chapter, I describe a successful method of combining glycosaminoglycans with the iPSC feeder-free substrate, laminin for the adhesion of iPSCs in the presence of the polysaccharide substrates, whilst retaining their pluripotency. Immunohistochemical, morphological and gene expression analysis also reveal significant impacts on SEAM formation and gene expression in the presence of glycosaminoglycan substrates derived from cornea.

4.2 Methods

4.2.1 Direct ELISA and glycosaminoglycan substrate coating

In order to determine whether glycosaminoglycan substrates could be immobilised onto the cell culture surface in the presence of laminin (LN511 E8 fragment, Takara Bio, Paris, France), which is required for iPS cell attachment, substrates identified in the previous chapter were investigated to ascertain the optimal sequence of application and concentration of coating for both substrates. Hence, plates were coated with laminin, followed by glycosaminoglycan preparations, or vice versa. Enriched glycosaminoglycan

substrates of the CS/DS sulphation epitopes, recognised by the antibodies 6C3 (derived from shark cartilage) and 7D4 (derived from peripheral cornea), as well as a mixed substrate (derived from central cornea) consisting of epitopes recognised by 7D4 antibody and the KS sulphation epitope recognised by the 5D4 antibody, were used to coat Nunclon Delta 96-well cell culture plates (Thermofisher, Loughborough). They were coated at concentrations of 0.05, 0.1, 0.25 and 0.5 μg/cm^2 glycosaminoglycan (as determined by DMMB assay) dissolved in 80% saturated ammonium sulphate. Plates were coated overnight at 4°C in the ammonium sulphate solution as has been described previously (Hof et al., 2019). Laminin dissolved in phosphate-buffered saline (PBS) without calcium or magnesium (Merck, Gillingham, UK) was applied either before or after overnight glycosaminoglycan coating at a concentration of 0.5 μg/cm^2 of laminin for 1 hour at 37°C. In between coating with either laminin or glycosaminoglycan preparations, several washes were carried out gently with PBS solution. The cell culture plate was then gently washed several more times before being processed for direct ELISA as described in Chapter 3 (Section 3.2.7).

4.2.2 iPSC culture and maintenance

The iPS cell line used was the 201B7 line, originally produced from adult human fibroblasts using traditional iPSC generation, using transduction of Oct3/4, Sox2, Klf4 and c-Myc (Takahashi et al., 2007). This cell line has been used in the majority of papers reporting SEAM formation by Hayashi and colleagues (Hayashi et al., 2017, 2016). The cells were obtained from ATCC (LGC, Oxford, UK). The iPSCs were maintained and differentiated as previously described by Hayashi *et al*. with little to no modification (Hayashi et al., 2017, 2016) and detailed below. All cells used were below 40 passages, as recommended previously (Hayashi et al., 2017).

Prior to seeding, cell culture treated six-well plates (Nunclon Delta plates, Thermofisher, Loughborough) in which the cells were maintained and expanded, were coated with LN511E8 at 0.5 μg/cm^2 in 1.5ml PBS without calcium and magnesium for the six-well plates, and incubated at 37°C for 2 hours or 4°C overnight. After coating, 0.25 ml (24 well plate) or 0.75 ml (6 well plate) cell culture media, namely StemFit Medium 04 or Stemfit Medium 02 (discontinued)

(Amsbio Biotechnology, Abingdon, UK) with 50 units/mL of penicillin and 50 µg/mL of streptomycin (Thermofisher, Loughborough, UK), was added to the laminin solution and removed with a small remainder left to prevent drying of the cell culture plate. The media and coating solution mixture was then quickly replaced with 0.5 ml or 1.5 ml (24 well plate or 6 well plate respectively) of media containing 10 µM of the Rho-associated protein kinase (ROCK) small molecule inhibitor, Y-27632 (STEMCELL Technologies, Cambridge, UK), and incubated at 37°C to equilibrate to temperature, immediately prior to cell seeding. ROCK inhibitor is commonly added for the first 24 hours after cell seeding in feeder-free cultures to promote survival and pluripotency (Miyazaki et al., 2012; Vernardis et al., 2017). A vial of 2 x 10^5 frozen iPS cells stored in 0.2 ml of STEM-CELLBANKER (Amsbio Biotechnology Abingdon, UK) was then rapidly defrosted at 37°C and added to a 15 ml conical tube containing 5 ml of StemFit media before centrifugation at 200 x g for 5 minutes at room temperature. After centrifugation, the supernatant was removed, 1 ml of ROCK inhibitor-containing media was added to the cell pellet which was resuspended to a single cell suspension by gentle pipetting. Cells were then counted using a haemocytometer and Trypan blue exclusion (Thermofisher, Loughborough, UK). Defrosted cells were then added to the precoated six-well plates at a density of 65,000 cells per well (approximately 6800 cells/cm^2) and mixed gently to ensure the cells were evenly spread after seeding. After approximately 24 hours, the medium was replaced with fresh StemFit medium without ROCK inhibitor and incubated at 37°C in 5% CO_2 for 7 ± 1 days until approximately 70-80% confluence. The medium was changed every 2 days until day six, after which it was changed every day until regular passaging as described below.

For cell passaging, a six well plate was coated as described above on the day of passage and incubated at 37°C until cells were ready to be added. The media was removed from cells ready for passage, after 7 ± 1 days of culture, and the cells were washed with 2 ml of PBS, after which 500 µl of pre-warmed dissociation solution was added (a mixture of 50% (vol/vol) TrypLE Select (Thermofisher, Loughborough, UK) and 50% (vol/vol) 0.5 mM EDTA solution (Merck, Gillingham, UK)). The cells were incubated in the dissociation solution for 4 to 5 minutes at 37°C, the solution was removed, and the cells were then

washed gently with 2 ml of PBS before the addition of 1 ml StemFit medium containing 10 µM ROCK inhibitor to each well. The cells were then detached from the culture plates using a cell scraper (Thermofisher, Loughborough, UK), pipetted 10 times using a 1000 µl pipette tip before being transferred to a collection tube. The cells were then counted using Trypan blue exclusion and a haemocytometer. After the cell number was verified, 13,000 cells per well were added to the new 6-well plate for continuation of cell culture or used in further experiments, for example immunohistochemistry or initiation of SEAM culture. As before, after approximately 24 hours, the medium was replaced with fresh StemFit medium without ROCK inhibitor and incubated at 37°C in 5% CO_2 for 7 ± 1 days until approximately 70-80% confluence. The medium was changed every 2 days until day six, after which it is changed every day. Upon receipt of the 201B7 cell line, cells were passaged 3 times to adapt to the laminin 511E8 substrate before use in experiments or frozen and stored in STEM-CELLBANKER, as described below.

For cryostocks, surplus cells from passaging above were centrifuged at 200 x g at room temperature, the supernatant removed and the cells resuspended in freezing media with 2 x 10^5 cells in each 0.2 ml. 0.2 ml of cell suspension was added to each cryovial for storage, and they were then frozen at -80°C in isopropanol before storage in liquid nitrogen until required.

4.2.3 Assessment of pluripotency markers of iPSCs with and without glycosaminoglycan substrates

Pluripotency is vital for the ability of iPSCs to differentiate and so in order to examine the pluripotency of iPSCs on different substrates and during their maintenance, two pluripotency markers were used, SSEA-4 and TRA-1-60 (Natunen et al., 2011; Wright and Andrews, 2009). Verifying pluripotency is essential to ensure the iPSCs have not differentiated and will be able to differentiate normally and these markers are recommended to verify pluripotency (Hayashi et al., 2017).

Using twenty-four well plates, wells were coated with either laminin alone, as described in the previous section, using 0.5 ml of 0.5 µg/cm LN511E8 PBS and incubated at 37°C for 2 hours, or using the dual coating method of adding

glycosaminoglycan prior to laminin coating, as in the ELISA protocol in Section 4.2.1 detailed above. For the dual coat, briefly, glycosaminoglycans were dissolved in filter-sterilised 80% saturated ammonium sulphate solution, before 0.5 ml of solution was applied to the 24 well plates at a concentration of 0.5 $\mu g/cm^2$ (as was determined to yield the highest glycosaminoglycan signal). Plates were then incubated at 4°C overnight. After incubation, plates were washed several times with PBS before the addition of laminin solution and incubated for 2 hours as above. The laminin solution was then removed and replaced with 0.5 ml of ROCK inhibitor-containing media prior to cell seeding. For this pluripotency assay, cells were seeded at 3000 cells per well, using cells from passaging described above.

The cells were then grown normally until day 5, when visible iPSCs colonies had formed before being washed in PBS and fixed in 4% PFA (wt/vol) dissolved in PBS for 10 minutes at room temperature. The cells were then washed 3 times with PBS and were then blocked in PBS containing 5% BSA for 1 hour at room temperature. The antibodies were then applied, using either FITC-conjugated anti-SSEA-4 or Alexa Fluor 647-conjugated anti-TRA-1-60 (both 1:100 dilution, Biolegend UK Ltd, London, UK), for 1 hour at room temperature, both dissolved in 1% BSA in PBS. Finally, cells were washed 3 times and then incubated with DAPI for 10 min at room temperature under protection from light, washed three times with TBS for 5 min and imaged under fluorescence microscopy using an Olympus IX71 microscope.

4.2.4 Experimental protocol for four week SEAM differentiation in the presence and absence of glycosaminoglycans

The SEAM differentiation timeline and protocol is summarised in **Figure 4.1** and detailed below. Twenty-four well cell culture plates were coated and prepared as described above, either using laminin alone or the dual coating method of both laminin and the free glycosaminoglycan substrates of 6C3 (from shark), 7D4 (from peripheral cornea) or 5D4/7D4 (central cornea), see Sections 3.3.10 and 3.3.11. Harvested cells, from passaging described in Section 4.2.2, were then added to wells of each 24-well plate using ROCK inhibitor media at the highest seeding density (as recommended in (Hayashi et al., 2017)) of 900 cells per well

(approximately 2900 cells/cm^2). The ROCK inhibitor media was replaced with normal StemFit media without ROCK inhibitor after 24 hours and the media was replaced every 2 days until day 7, after which it was replaced every day until day 10.

At day 10 (day 0 of differentiation), StemFit media was replaced with differentiation media (DM). DM consisted of Glasgow's modified Eagle's medium (GMEM) with 10% Knockout serum replacement (KSR), 1 mM sodium pyruvate, 0.1 mM nonessential amino acids, 2 mM L-glutamine, 50 units/mL of penicillin, 50 µg/mL of streptomycin and 55 µM 2-mercaptoethanol (all from Thermofisher, Loughborough, UK). The DM was subsequently changed every two to three days and the developing SEAMs were monitored daily for four weeks. At four weeks, multiple SEAMs were either harvested using 500 µl of TRIzol per SEAM well (Thermofisher, Loughborough, UK) and stored at -80°C for further RNA extraction (Section 4.2.6), following manufacturer's instructions. Two SEAM wells were pooled for each experimental sample for gene expression analysis, each well consisting of between approximately 3-8 SEAMs. Two samples (pooled from two wells – approximately 6-16 SEAMs) from two independent experiments for each substrate were taken for gene expression analysis (n = 4 total). Or SEAMs were fixed in 4% PFA in PBS for 20 minutes, washed several times and stored in PBS until they were immunolabelled for immunohistochemical analysis as described in Section 4.2.5. Immunohistochemistry was performed on multiple SEAMs in two independent experiments on each substrate.

4.2.5 Experimental protocol for eight week SEAM differentiation in the presence and absence of glycosaminoglycans

For the normal SEAMs (those differentiated exactly as described by Hayashi *et al.*, 2017), and those grown on 7D4 and 5D4/7D4 substrates (not 6C3 substrate), SEAMs were differentiated further after the above 4 week differentiation. At the 4 week timepoint, developing SEAMs were switched to corneal differentiation medium (CDM) for four further weeks, which selectively encourages the differentiation and growth of corneal epithelial cells. CDM consists of a 1:1 mixture of DM and CnT-PR media (without EGF and FGF2) (Caltag Medsystems, Buckingham, UK), supplemented with 20 ng/ml keratinocyte growth factor (KGF)

(STEMCELL Technologies, Cambridge, UK) and 10 μM ROCK inhibitor. Again, the media was changed every two to three days. After the four weeks of further differentiation, SEAMs were either harvested using TRIzol or fixed in 4% PFA as described above.

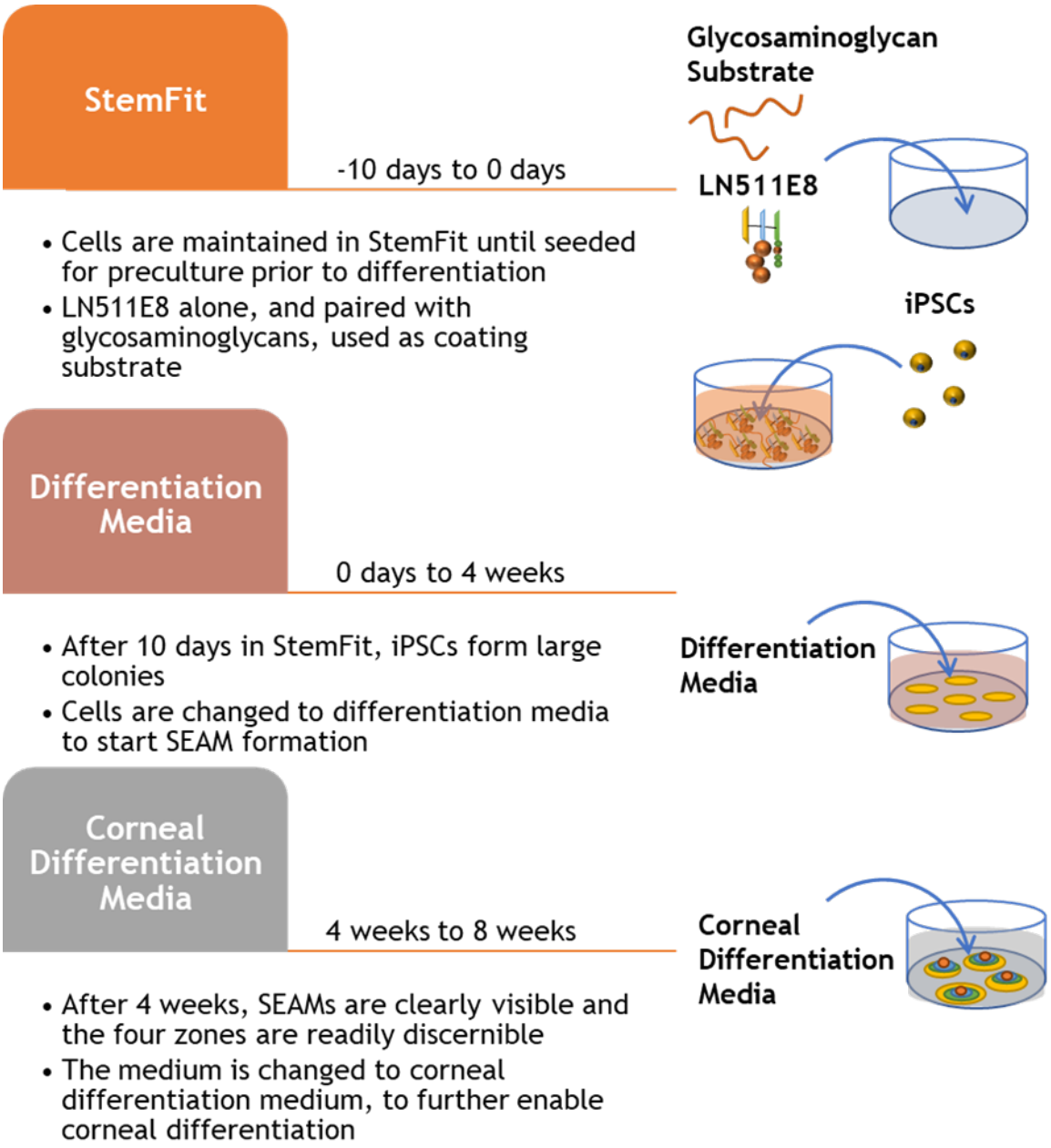

Figure 4.1 Timeline and schematic of SEAM differentiation by defined factors. The first 4 weeks relies on the inherent self-organisation of iPSCs to form SEAMs using Differentiation Media. After this, cells are selectively differentiated to encourage the further growth and differentiation of corneal epithelial cells, through the use of an epithelial proliferation medium, named Corneal Differentiation Media, and addition specific corneal epithelial growth factors, namely keratinocyte growth factor.

4.2.6 SEAM imaging and immunohistochemistry

Immunohistochemistry performed on SEAMs was similar to that described in Chapter 2 Section 2.2.3, but with slight modifications as detailed below. Fixed SEAMs, from the four week timepoint, were blocked in TBS containing 5% (vol/vol) normal donkey serum and 0.3% (wt/vol) Triton X-100 for 1 hour at room temperature. The cells were then incubated with the following antibodies, mouse anti-p63 (4A4, Abcam, Cambridge, UK), rabbit anti-TUBB3 (T2200, Merck, Gillingham, UK) and PAX6 (PRB-278p, Biolegend UK Ltd, London, UK). Co-localisation was carried out for p63 (1:200)/TUBB3 (1:500) and p63 (1:200)/PAX6 (1:300) to investigate the presence of neuronal/epithelial and corneal epithelial cells respectively (Hayashi et al., 2017). The antibody incubation was performed overnight at 4 °C, with antibodies diluted in TBS containing 1% (vol/vol) normal donkey serum and 0.3% (wt/vol) Triton X-100. The cells were then washed three times with TBS for 5 min and subsequently incubated with the secondary antibody: 1:200 dilution of Alexa Fluor® 488-conjugated donkey anti-mouse IgG and IgM and Alexa Fluor 594 Donkey anti-rabbit IgG/IgM (Thermofisher, Loughborough, UK) secondary antibodies for 1 hour at room temperature in the dark. Cells were then washed three times with TBS for 5 min. Finally, cells were washed 3 times and then incubated with DAPI for 10 min at room temperature under protection from light, washed three times with TBS for 5 min and imaged under fluorescence microscopy using an Olympus IX71 microscope. Negative controls with primary antibody omission were performed and shown in the appendix in **Figure 7.3**.

4.2.7 Reverse transcription and quantitative polymerase chain reaction (RT-qPCR)

SEAM extracts frozen in TRIzol were defrosted and processed according to manufacturer's instructions for RNA extraction. Briefly, to the 1 ml of TRIzol extracted RNA, 0.2 ml 1-bromo-3-chloropropane (Merck, Poole, UK) was added and incubated for 3 minutes. Samples were then inverted several times and centrifuged for 15 minutes at 12,000 × g at 4°C.The upper, aqueous phase was transferred to a new tube and to this, 0.5 ml of isopropanol (Merck, Poole, UK) was added and incubated for 10 minutes before being centrifuged at 12,000 x g at 4°C. The supernatant was discarded and the RNA pellet resuspended in 1 ml

of 75% ethanol. The RNA samples were then vortexed briefly and centrifuged for 5 minutes at 7500 x g at 4°C. The supernatant was discarded and the RNA pellet air dried for 20 minutes. The generated total RNA pellet was resuspended in 50 µl of distilled water and heated at 55°C for 15 minutes. The RNA yield was determined using a NanoDrop Lite (Thermofisher, Loughborough, UK) and the absorbances at 260 and 280 nm and calculated ratio ($A_{260/280}$) were used to establish the RNA purity. Only RNA with an $A_{260/280} > 1.8$ was used for further analysis. RNA was either used immediately for reverse transcription or stored at -80°C until further use.

Reverse transcription of RNA was performed using the High-Capacity RNA-to-cDNA Kit as per manufacturer's instructions (Thermofisher, Loughborough, UK), using 800 ng of calculated RNA for each sample. Resultant cDNA was used immediately for qPCR or stored at -20°C until further use.

After cDNA generation, qPCR was performed using the TaqMan minor groove binder (MGB) probe system following manufacturer's instructions and as described in (Hayashi et al., 2016). TaqMan MBG probes used are shown below in **Table 4.1**. Equal amounts of cDNA was loaded into each reaction (16 ng), as determined by RNA yield prior to reverse transcription. All experimental samples were analysed in triplicate for each sample. The qPCR was performed using an Agilent AriaMx Real-time PCR system (Agilent Technologies LDA UK Ltd, Stockport, UK) using thermocycler conditions of an initial cycle of 95°C for 10 minutes, followed by 40 cycles at 95°C for 15 s and 60°C for 60 s and cycle threshold (Ct) was calculated using AriaMx software. No cDNA template and no reverse transcriptase controls were also performed and generated no signal.

Table 4.1 List of TaqMan MGB qPCR probes used, their ID and general function or role, as adapted from (Hayashi et al., 2016).

Gene	ID	Function
CDH1	Hs01023894_m1	Epithelial cell marker
PAX6	Hs00240871_m1	Ocular lineage specification marker
SOX2	Hs01053049_s1	Neural cell-specific marker
NGFR (P75)	Hs00182120_m1	Neural crest marker
TUBB3	Hs00801390_s1	Neural cell-specific marker
SOX10	Hs00366918_m1	Neural crest marker
GAPDH	Hs99999905_m1	Housekeeping gene
TP63	Hs00978339_m1	Epithelial cell marker

The relative gene expressions was calculated using the $2^{-\Delta\Delta Ct}$ method (Livak and Schmittgen, 2001). A summary of the calculations is shown below.

$$\Delta Ct = Ct\ (gene\ of\ interest) - Average\ Ct(GAPDH)$$

$$\Delta\Delta Ct = \Delta Ct\ (SEAM\ on\ substrate) - Average\ \Delta Ct\ (normal\ SEAM)$$

$$Relative\ Gene\ Expression = 2^{-(\Delta\Delta Ct)}$$

4.2.8 Statistical analysis

For the qPCR data, the relative gene expression values for each gene were converted to log forms to reduce the skewness of the data and subsequently tested for normality with the Shapiro-Wilk test. For each gene, normally distributed genes were tested for significant differences using one-way ANOVA followed by Tukey's posthoc test to determine differences between normal SEAMs and each substrate group. For non-normally distributed groups, a Kruskal-Wallis test followed by Dunn's posthoc test with Bonferroni significance correction was performed. Any significant differences were represented graphically (*, ** and *** represent $p < 0.05$, 0.01, 0.001 respectively).

4.3 Results

4.3.1 Optimisation of coating conditions using glycosaminoglycan substrates

In order to ascertain whether the free glycosaminoglycan substrates were able to bind to and immobilise onto cell culture surfaces used for iPS cell culture, direct

ELISA was performed. The antibody signal generated for each substrate was assessed at different concentrations and in different orders of addition before or after laminin-511E8 coating, which is required for iPS cell adhesion. It was also necessary to identify which order of substrate application provided the highest substrate signal for optimal presentation of glycosaminoglycan substrates to cells and interacting molecules.

The results are shown in **Figure 4.2**. There was little difference between the order of the substrate application overall. However, applying glycosaminoglycan substrate before the laminin substrate, which is required for cell adhesion, resulted in slightly higher signal, particularly for the KS epitope recognised by the antibody 5D4. The signal appeared to be the same as coating in the absence of laminin for all substrates as seen in **Figures 3.19** and **3.21**, with the exception of the 5D4/7D4 substrate, which, interestingly, appeared to increase in the presence of laminin.

For the 7D4 substrate, only the 7D4 antibody gave signal over background signal, compared to no signal for the 6C3 and 5D4 antibodies. The signal generated by the 7D4 antibody appeared to increase slightly with increasing coating concentration, but only in the sample where glycosaminoglycans were applied first, but overall there was little difference between coating order and concentration.

For the mixed 5D4/7D4 substrate, no 6C3 antibody signal was detected above background levels, as expected. 7D4 signal was comparable between coating orders, however increased steadily with increased coating concentration up to 0.5 μg/cm^2 for both coating orders. The signal generated by the 5D4 antibody, however was much higher for glycosaminoglycan coating prior to laminin, and increased with coating concentration.

Finally, for the 6C3 substrate, antibody signal was largely comparable between coating orders, but increased with increasing concentration up to 0.5 μg/cm^2. Other epitopes were not detected including antibody signal from 5D4 and 7D4 (very slight signal was detected above background for 7D4 but was within the range for background signal compared with negative controls).

Overall, the antibody signal of interest increased for each substrate with increasing coating concentrations, with the exception of the 7D4 substrate, and so the highest concentration examined was used for the experiments investigating the effect of GAGs on the differentiation of SEAMs. A concentration of 0.5 μg/cm^2 was used for subsequent experiments due to the highest epitope signal for each respective glycosaminoglycan epitope and the coating order was determined as glycosaminoglycan followed by laminin, due to higher 5D4 antibody signal witnessed in the 5D4/7D4 substrate, with little differences were seen elsewhere. It would also mean the laminin would not be exposed to the high salt ammonium sulphate solution used to immobilise the glycosaminoglycans to the cell culture plate.

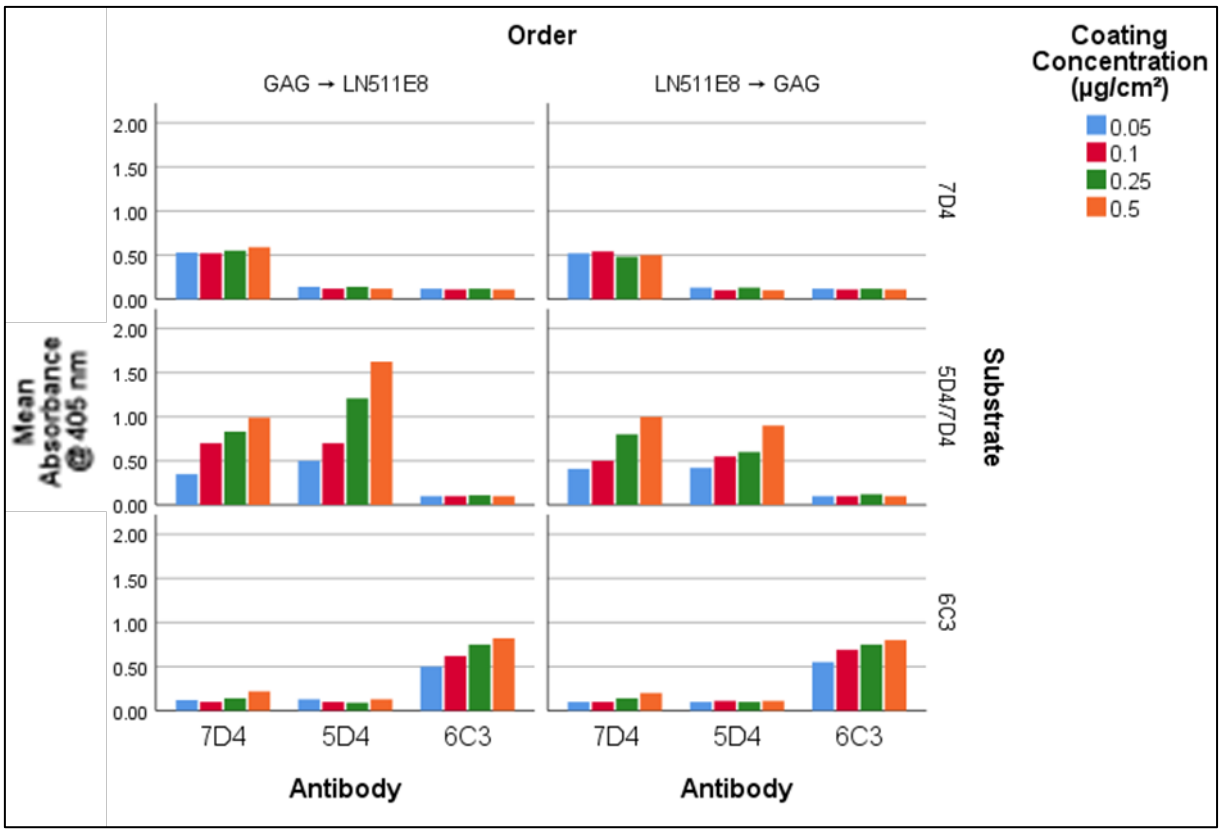

Figure 4.2 ELISA analysis of glycosaminoglycan (GAG) substrate immobilised on iPS cell culture plastic before and after laminin-511E8 (LN511E8) coating, with the order of application identified at the top of the figure. Antibodies used were the CS/DS antibodies, 7D4 and 6C3, and the KS antibody, 5D4. Antibody signal is shown as absorbance, on the left, and the substrate being investigated for each row is shown on the right. Colours correspond to coating concentrations as depicted in the legend on the right hand side. N = 2 from technical repeats.

4.3.2 iPSCs adhere to and retain pluripotency on glycosaminoglycan substrates

Following the establishment of optimal coating conditions to yield the highest glycosaminoglycan signal by ELISA, the same conditions were applied to cell culture plates, which were then seeded with iPS cells. After 5 days in culture, the cells were assessed for the expression of the pluripotency markers SSEA-4 and Tra-1-60 on each of the various substrates, two commonly used cell surface pluripotency markers. The results are shown in **Figure 4.3**.

Importantly, the colony forming efficiency, shape and morphology of the iPS cells did not change on each of the different substrates, and 100% of the colonies on all substrates retained expression of the pluripotency markers described as shown in **Figure 4.3**. The result being that the cells seeded onto glycosaminoglycan and laminin substrates retained pluripotency similar to that seen on laminin alone and so were suitable candidates for further differentiation towards corneal epithelial cell phenotypes. The standard laminin substrate coated iPSCs also retained expression of pluripotency markers, which was useful along with morphological observations that the iPS cell culture was established successfully. The experiment was repeated twice and no colonies negative for either marker were identified in either experiment, with all colonies in the well examined.

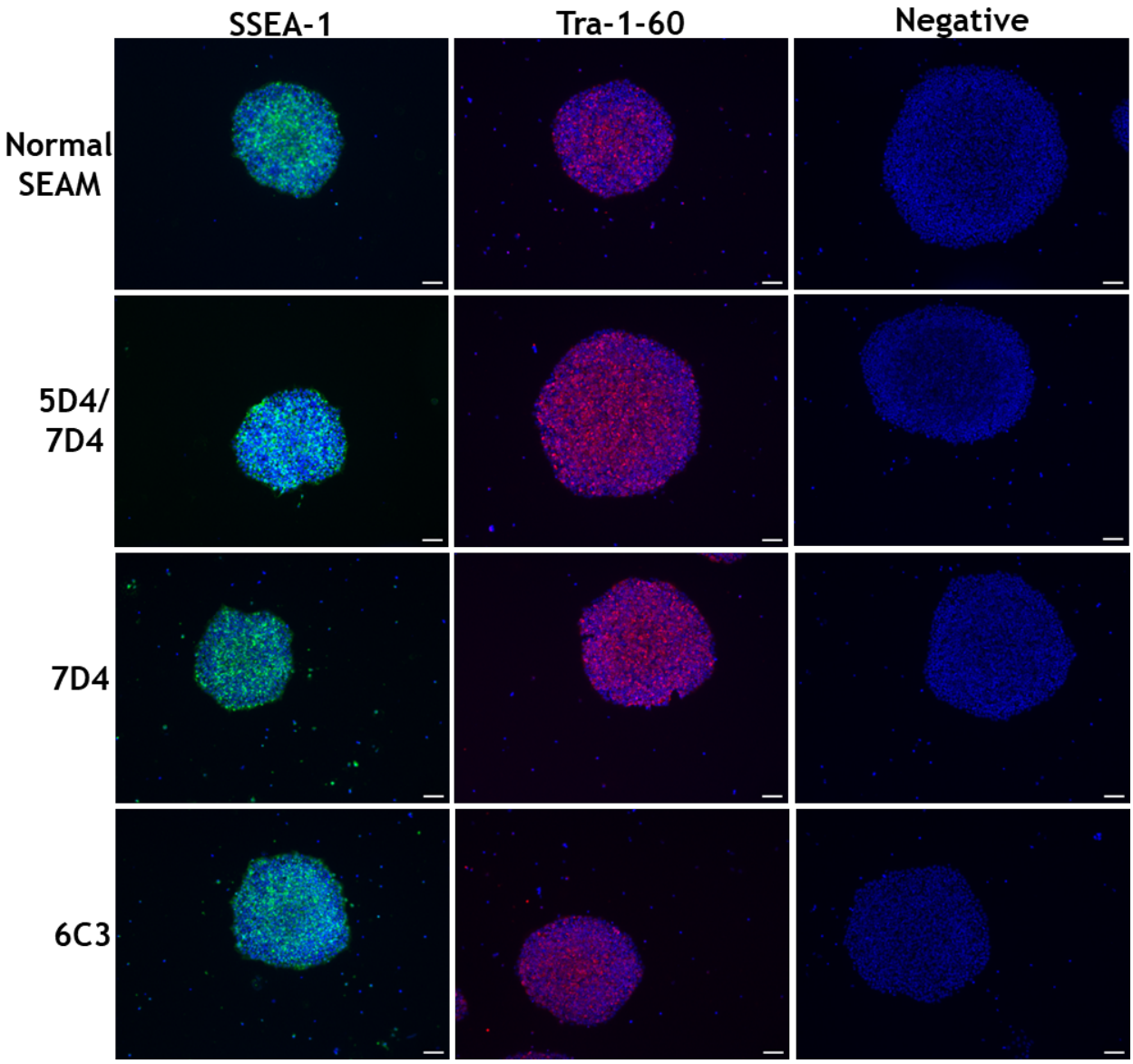

Figure 4.3 Immunohistochemical analysis of the pluripotency markers, SSEA-4 and Tra-1-60 in iPSC colonies on different glycosaminoglycan substrates, with the negative control (primary antibody omission) shown. Representative colonies are shown for each substrate after 5 days of culture. Scale bars represent 100 µm.

4.3.3 Morphological analysis of the differentiation of iPSCs towards corneal epithelial cells on different glycosaminoglycan substrates

Having established a suitable coating protocol, iPSCs were differentiated into SEAMs as described in Section 4.2.4 on each of the different substrates purified in the previous chapter. From the initial cell seeding, to the week 4 timepoint, there were few noticeable differences in colony formation capability, colony shape and morphology. One important difference seen in this study was the ratio of SEAMs generated from each original iPSC colony. In the original study, 60-70% of iPSC colonies developed into SEAMs (Hayashi et al., 2017), however here a much lower percentage was witnessed, between 20 and 30% of colonies forming morphologically accurate SEAMs representing all four zones on SEAMs grown on all substrates, including normal SEAMs on laminin alone. Slight differences in overall morphology of the SEAMs at four weeks were noticeable between normal SEAMs grown on laminin only and those grown on glycosaminoglycan substrates. Representative SEAMs are shown on each of the four substrates at four weeks of differentiation in **Figure 4.4** and discussed in further detail by substrate below.

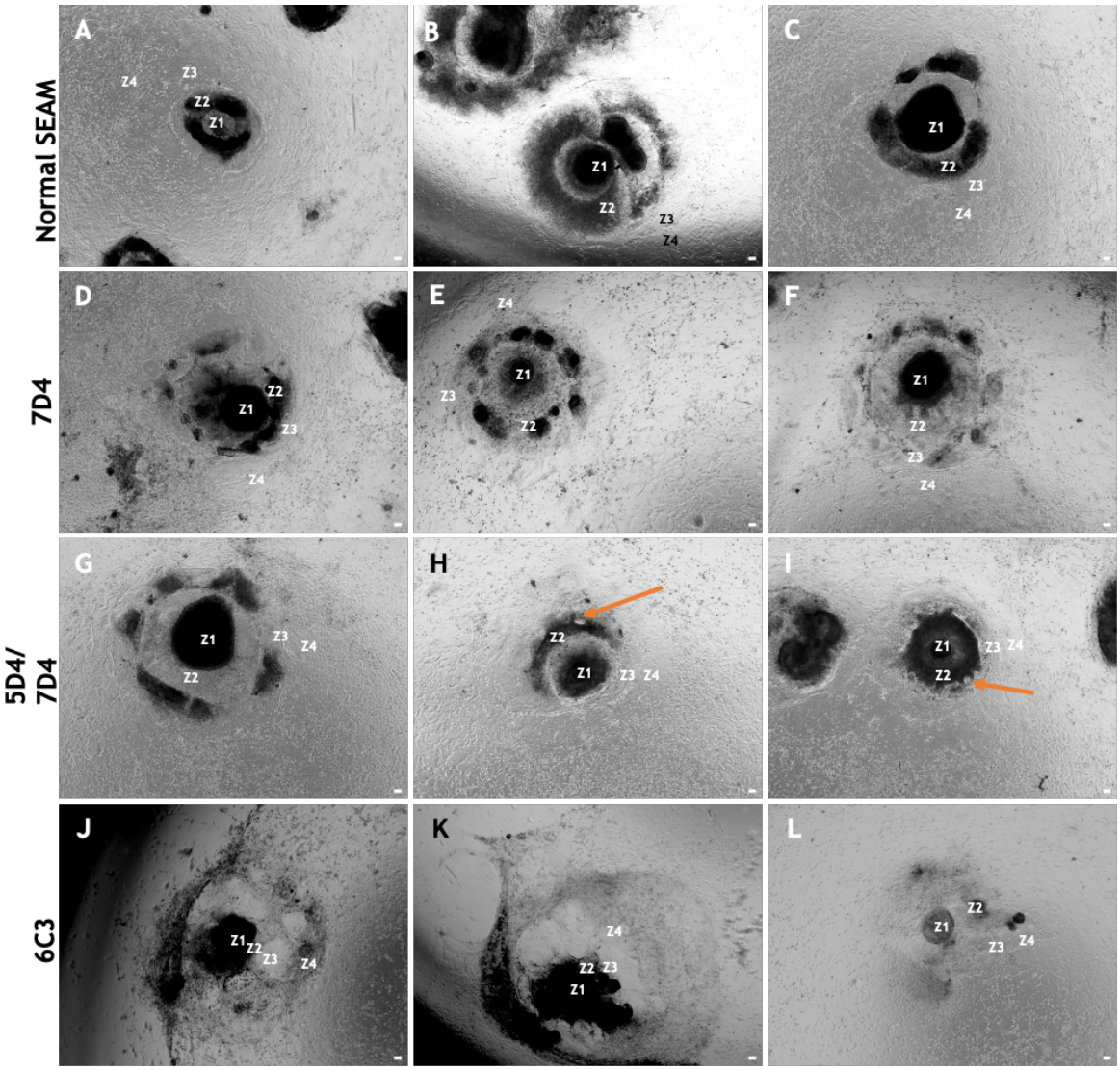

Figure 4.4 Representative SEAM images grown on different substrates at 4 weeks of differentiation. (**A-C**) Representative SEAMs grown on laminin-511E8 substrate alone. (**D-F**) Representative SEAMs grown on the CS/DS substrate enriched in 7D4 epitope and laminin 511E8. (**G-I**) Representative SEAMs grown on the KS and CS/DS substrate enriched in 5D4 and 7D4 epitopes and laminin 511E8, with lens-like bodies identified with an arrow. (**J-L**) Representative SEAMs grown on the CS/DS substrate enriched in 6C3 epitope and laminin 511E8. SEAM zones are identified in each image and scale bars represent 100 μm.

4.3.4 Morphological and immunohistochemical analysis of corneal epithelial markers of SEAMs cultivated normally on laminin 511E8

Immunohistochemical analysis of SEAMs was also performed on each of the substrates of p63, PAX6 and TUBB3 as shown from **Figure 4.5** to **Figure 4.12**. P63 and PAX6 positive cells represent zone 3 corneal epithelial-like cells, whilst p63 and TUBB3 differentiate between corneal epithelial cells and the neuronal centre of the SEAMs representing zone 1 and 2 and also label neuritic outgrowths that spread into the outer zones. Overall morphological differences are inherently difficult to determine, without high throughput imaging, primarily owing to the innate variation of SEAMs during differentiation.

In this study, normal SEAMs seeded onto the laminin 511E8 substrate developed a morphology as has been described previously, by Hayashi *et al*., 2017, as shown in **Figure 4.4A-C**. The four zones were determined morphologically, consisting of a dense neural centre (zone 1), and an almost continuous ring of high optical density neural cells (zone 2). These zones were followed by two monolayer zones, 3 and 4, consisting of mostly densely packed epithelial cells (zone 3), with zone 4 representing other ectoderm anlages of non-ocular origin with a more spread morphology. Immunohistochemical analysis revealed SEAMs developed a neural centre with strong TUBB3 staining, as shown in **Figure 4.6D**, with neuronal outgrowths, representing zone 1 and 2. They also exhibited strong p63/PAX6 signal in zone 3, representing corneal epithelial cells as seen in **Figure 4.5C-E**, consistent with previously published work.

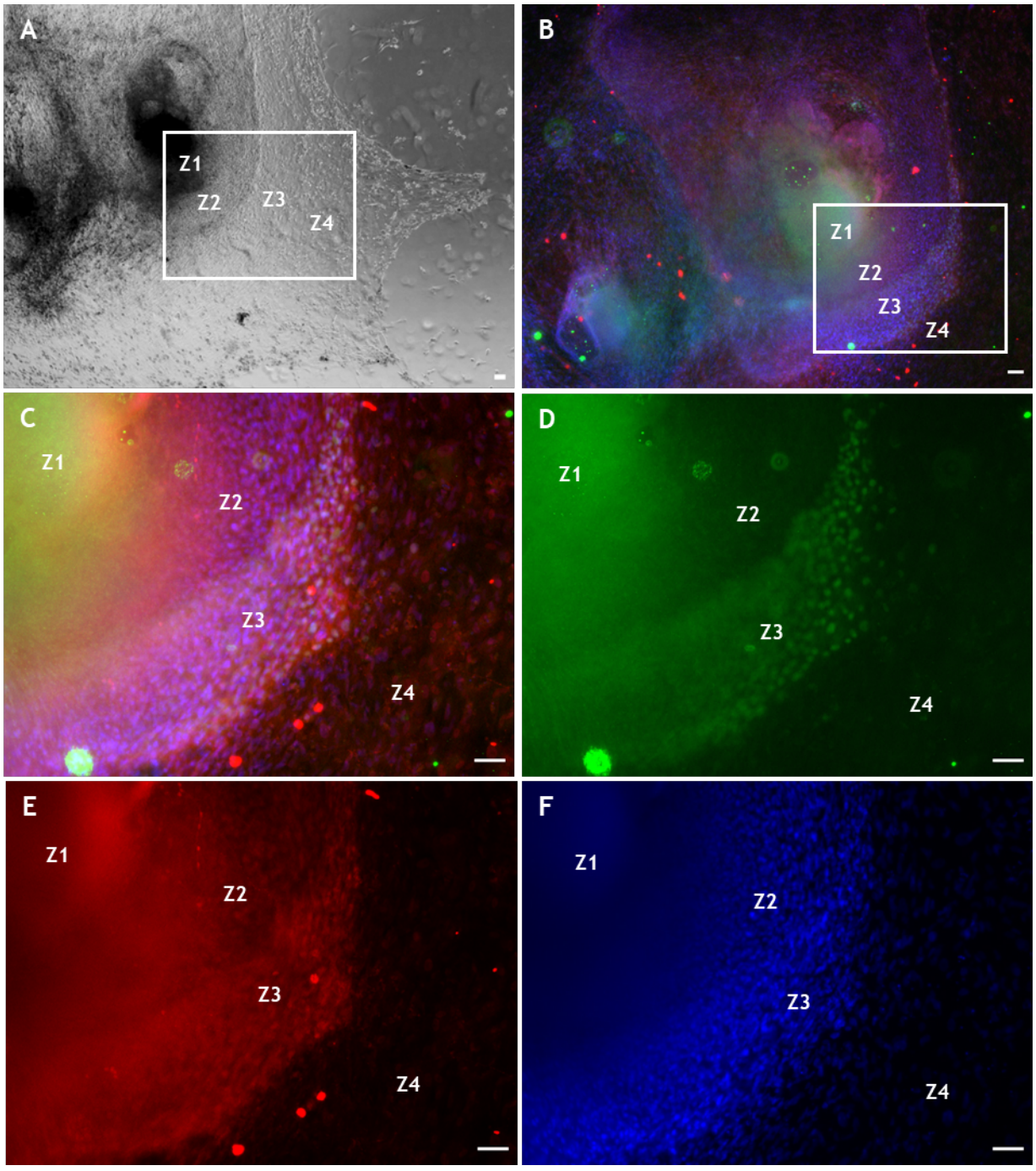

Figure 4.5 Immunohistochemical analysis of the corneal epithelial markers p63 and PAX6 in a normal SEAM after 4 weeks of differentiation. (**A**) Phase contrast image of a SEAM grown on the above substrate. (**B**) Tricolour image of the epithelial marker, p63 (green) and ocular lineage marker, PAX6 (red) and DAPI nuclear stain (blue) of the area represented in A and B. (**C**) Enhanced tricolour image of the area represented in (**A**) and (**B**). (**D**) Single channel image of p63. (**E**) Single channel image of PAX6. (**F**) Single channel image of DAPI. SEAM zones are labelled in each image and scale bars represent 100 μm.

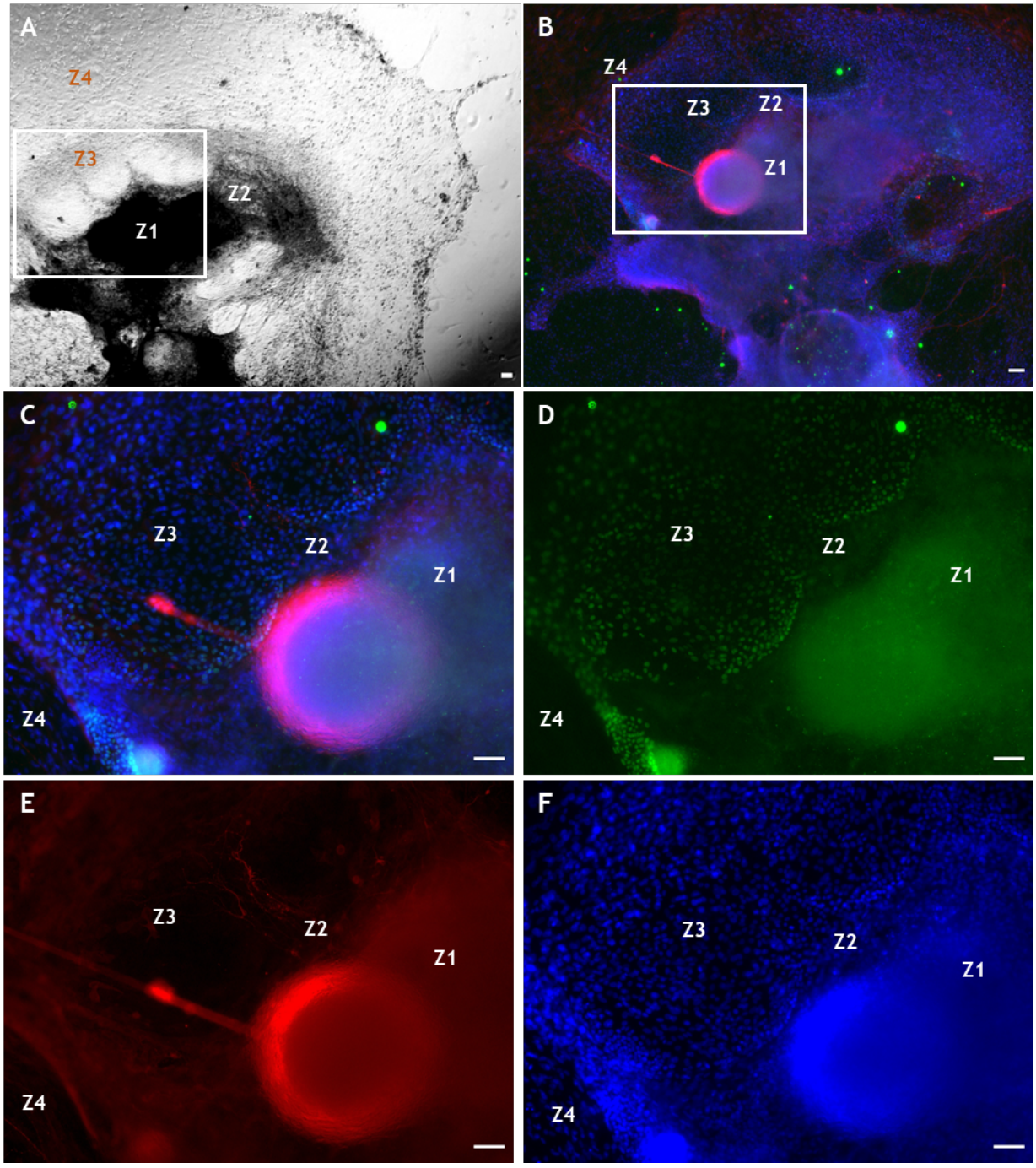

Figure 4.6 Immunohistochemical analysis of the epithelial marker p63 and the neural cell marker, TUBB3 in a normal SEAM after 4 weeks of differentiation. (**A**) Phase contrast image of a SEAM grown on the above substrate. (**B**) Tricolour image of p63 (green) and TUBB3 (red) and DAPI nuclear stain (blue) of the area represented in A and B. (**C**) Enhanced tricolour image of the area represented in (**A**) and (**B**). (**D**) Single channel image of p63. (**E**) Single channel image of TUBB3. (**F**) Single channel image of DAPI. SEAM zones are labelled in each image and scale bars represent 100 µm.

4.3.5 Morphological and immunohistochemical analysis of corneal epithelial markers of SEAMs cultivated on 7D4 substrate

The iPSCs seeded onto laminin and the CS/DS substrate, enriched in the epitope recognised by the 7D4 antibody, developed into SEAMs that appeared morphologically similar to SEAMs grown on the laminin 511E8 substrate alone in **Figure 4.4A-C**. Slight differences were seen in zone 2, based solely on morphology as shown in **Figure 4.4D-F** compared with **A-C**. The high optical density area in zone 2 appeared to not be as continuous and tended to appear more as satellites around the central zone 1, however this was also witnessed in normal SEAMs on occasion and cannot be definitely stated without further quantification. Upon histochemical analysis, again little differences were witnessed in staining patterns , p63/PAX positive cells were witnessed in zone 3 as shown in **Figure 4.7C**. neuronal cells, identified by TUBB3, were also present as shown in **Figure 4.8C, D**. Both of these observations being consistent with normal SEAMs in **Figure 4.5** and **Figure 4.6**.

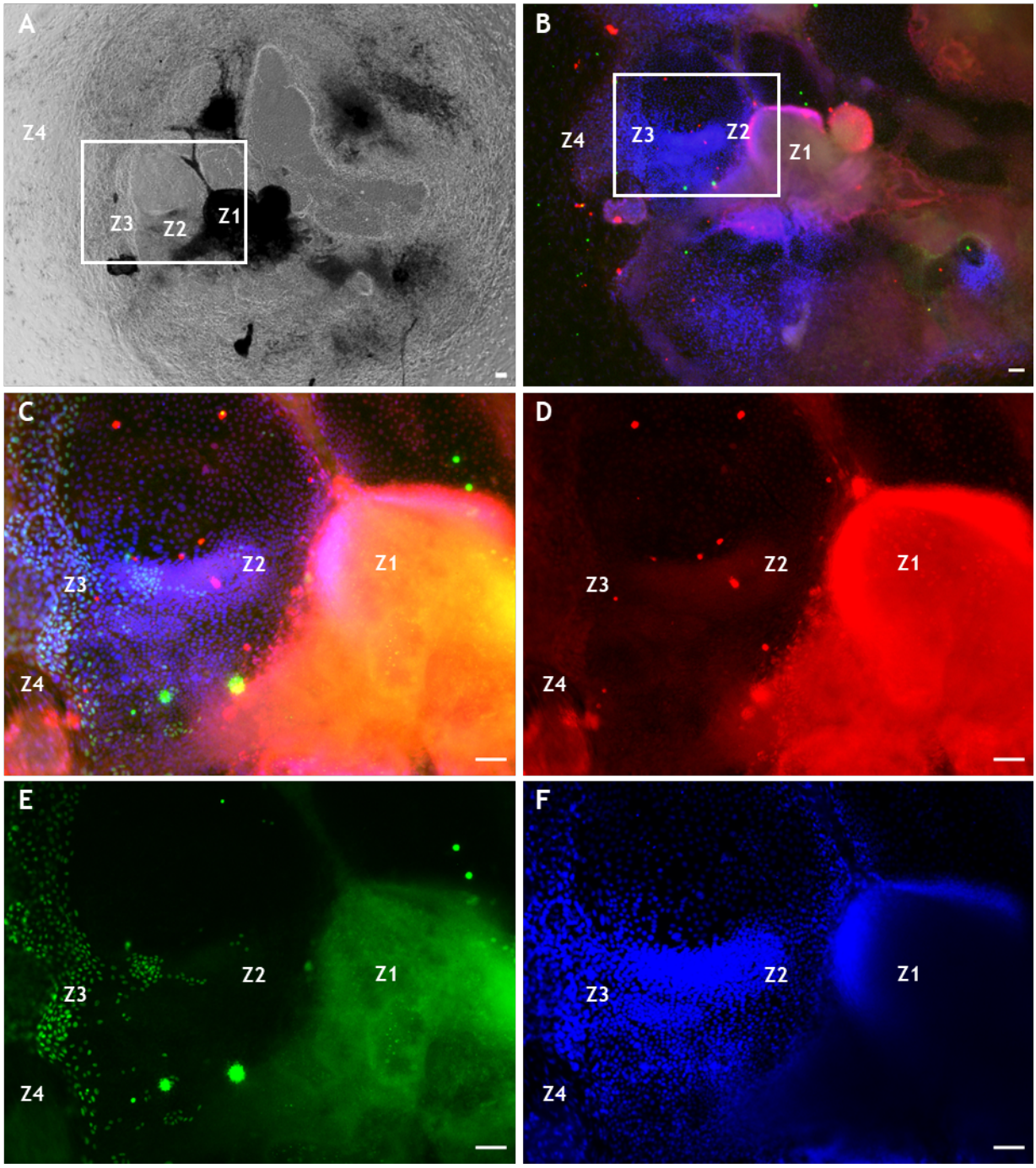

Figure 4.7 Immunohistochemical analysis of the corneal epithelial markers p63 and PAX6 in a SEAM grown on the 7D4 substrate after 4 weeks of differentiation. (**A**) Phase contrast image of a SEAM grown on the above substrate. (**B**) Tricolour image of the epithelial marker, p63 (green) and ocular lineage marker, PAX6 (red) and DAPI nuclear stain (blue) of the area represented in A and B. (**C**) Enhanced tricolour image of the area represented in (**A**) and (**B**). (**D**) Single channel image of PAX6. (**E**) Single channel image of p63. (**F**) Single channel image of DAPI. SEAM zones are labelled in each image and scale bars represent 100 µm.

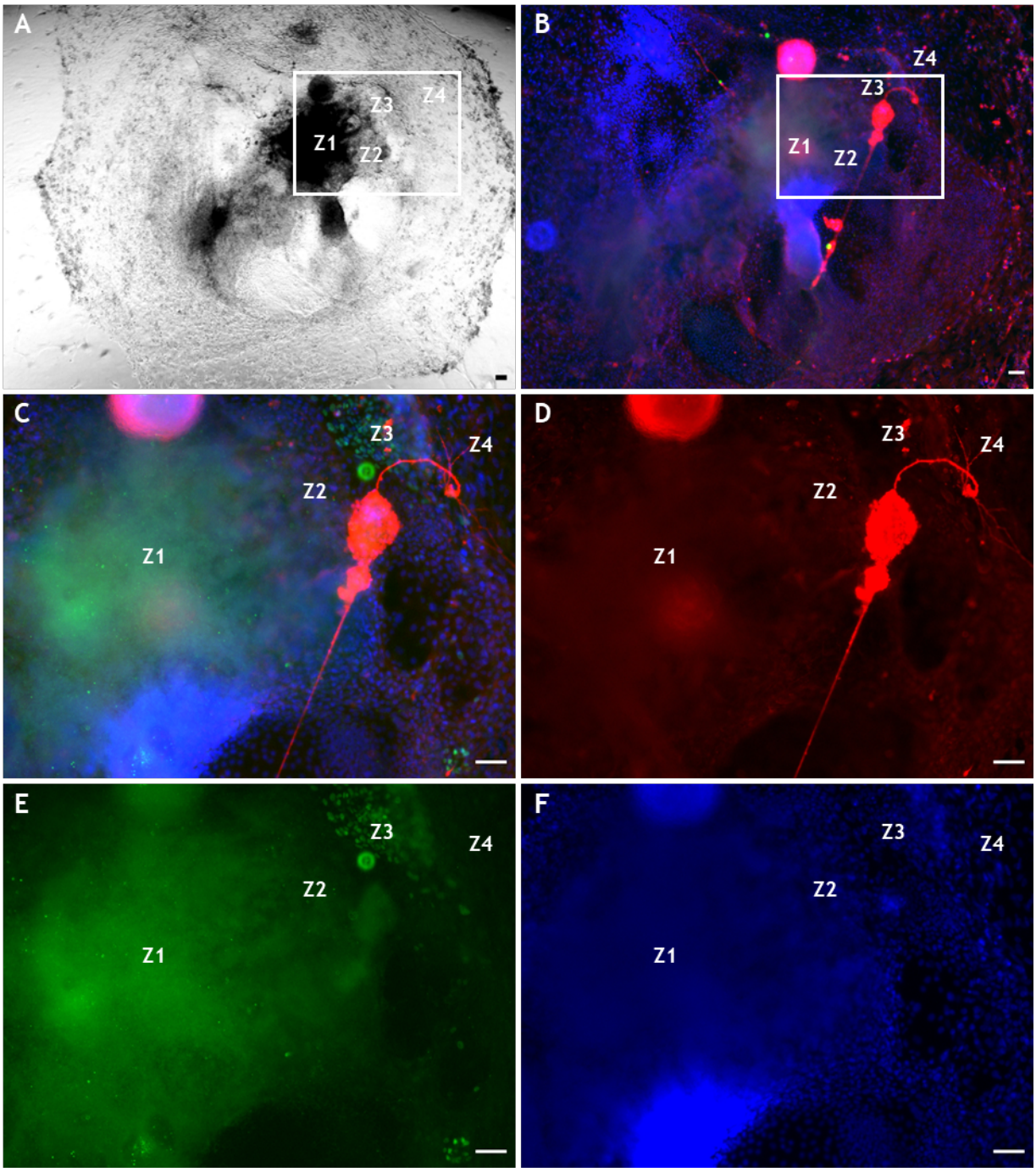

Figure 4.8 Immunohistochemical analysis of the epithelial marker p63 and the neural cell marker, TUBB3 in a SEAM grown on the 7D4 substrate after 4 weeks of differentiation. (**A**) Phase contrast image of a SEAM grown on the above substrate. (**B**) Tricolour image of p63 (green) and TUBB3 (red) and DAPI nuclear stain (blue) of the area represented in A and B. (**C**) Enhanced tricolour image of the area represented in (**A**) and (**B**). (**D**) Single channel image of TUBB3. (**E**) Single channel image of p63. (**F**) Single channel image of DAPI. SEAM zones are labelled in each image and scale bars represent 100 µm.

4.3.6 Morphological and immunohistochemical analysis of corneal epithelial markers of SEAMs cultivated on 5D4/7D4 substrate

For the 5D4/7D4 mixed substrate consisting of CS/DS and KS, the most noticeable difference was the increased presence of lens-like bodies. They are identifiable through morphology as areas with different refractive properties as optically clear round spherules at the border of zones 2 and 3. Whilst present and identified in SEAMs grown on laminin 511E8 alone, in this study they were more abundant and appeared to be present in a greater number of SEAMs grown on 5D4/7D4 substrate and shown in **Figure 4.4** and identified with arrows in **Figure 4.4H** and **I**. The zone 2 also appeared to be slightly smaller in SEAMs grown on this substrates, particularly in **Figure 4.10**A. Immunohistochemically, SEAMs grown on the 5D4/7D4 substrate also exhibited neural centres as labelled by TUBB3 and shown in **Figure 4.10B** and **C** when compared with normal SEAMs in **Figure 4.5** and **Figure 4.6**.. They also had substantial expression of p63/PAX6 positive cells, representing corneal epithelial cells as shown in **Figure 4.9C-E**, similar to, SEAMs grown on laminin alone, but without quantification cannot be stated definitively.

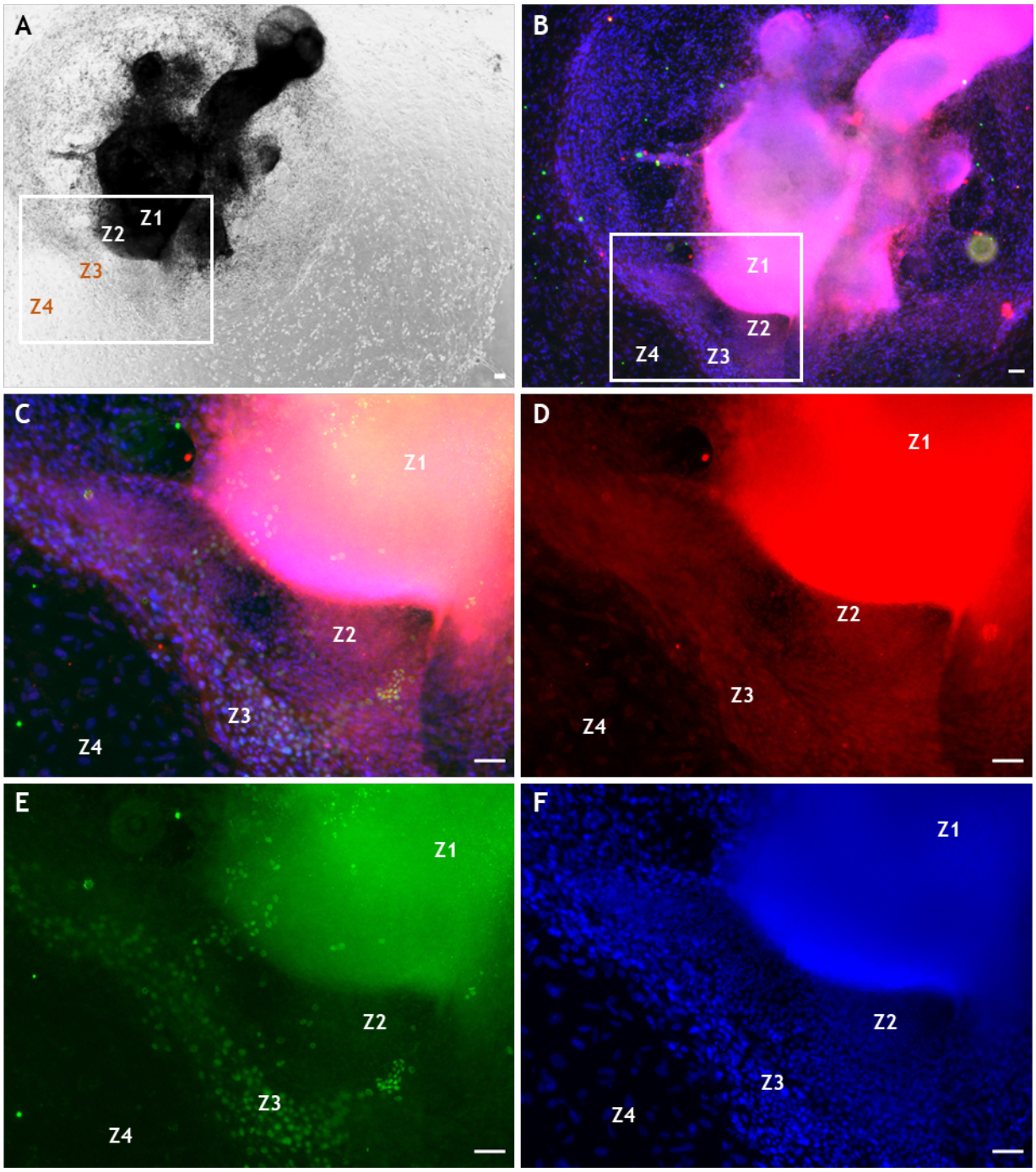

Figure 4.9 Immunohistochemical analysis of the corneal epithelial markers p63 and PAX6 in a SEAM grown on the 5D4/7D4 substrate after 4 weeks of differentiation. (**A**) Phase contrast image of a SEAM grown on the above substrate. (**B**) Tricolour image of the epithelial marker, p63 (green) and ocular lineage marker, PAX6 (red) and DAPI nuclear stain (blue) of the area represented in A and B. (**C**) Enhanced tricolour image of the area represented in (**A**) and (**B**). (**D**) Single channel image of PAX6. (**E**) Single channel image of p63. (**F**) Single channel image of DAPI. SEAM zones are labelled in each image and scale bars represent 100 µm.

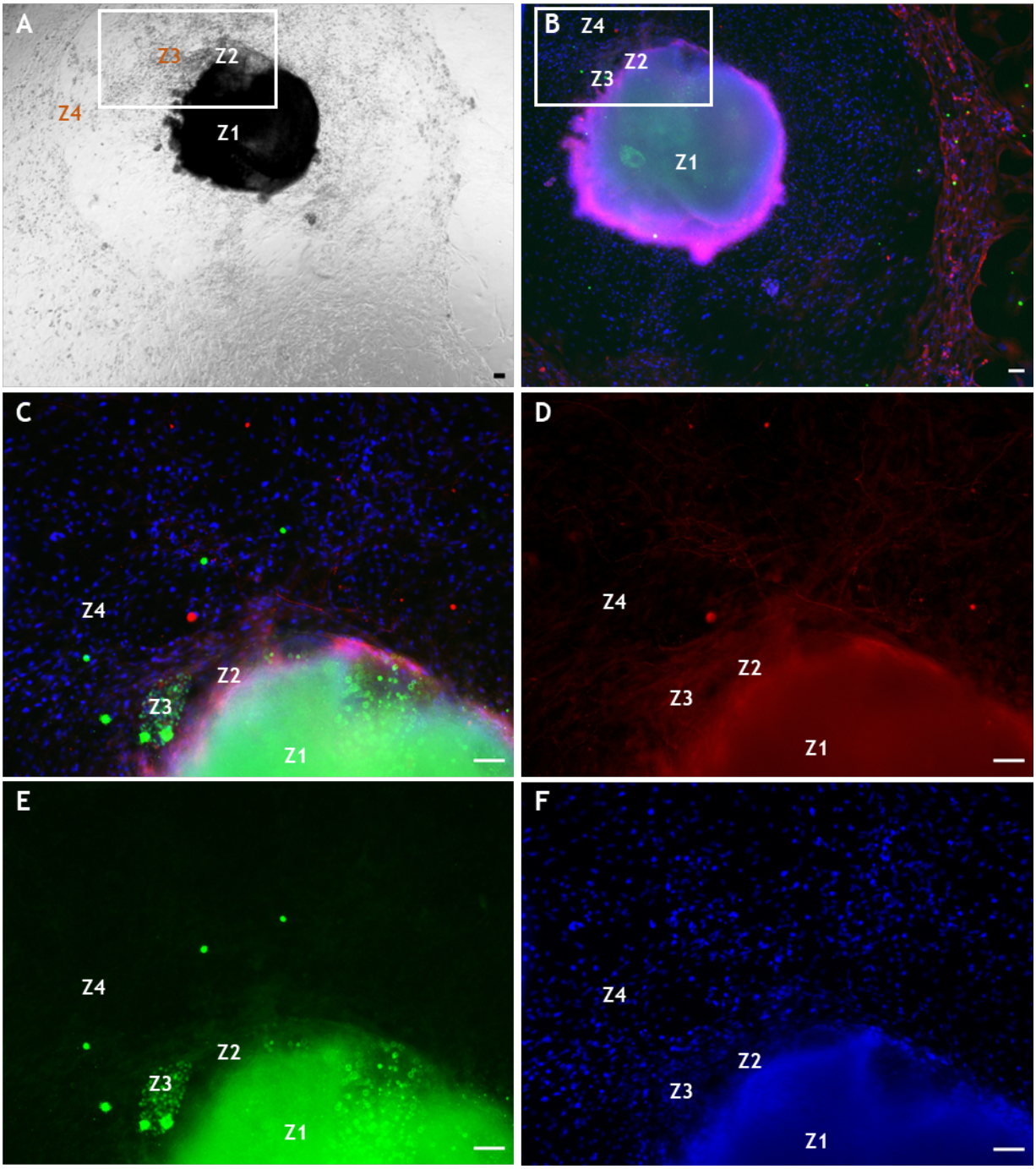

Figure 4.10 Immunohistochemical analysis of the epithelial marker p63 and the neural cell marker, TUBB3 in a SEAM grown on the 5D4/7D4 substrate after 4 weeks of differentiation. (**A**) Phase contrast image of a SEAM grown on the above substrate. (**B**) Tricolour image of p63 (green) and TUBB3 (red) and DAPI nuclear stain (blue) of the area represented in A and B. (**C**) Enhanced tricolour image of the area represented in (**A**) and (**B**). (**D**) Single channel image of TUBB3. (**E**) Single channel image of p63. (**F**) Single channel image of DAPI. SEAM zones are labelled in each image and scale bars represent 100 μm.

4.3.7 Morphological and immunohistochemical analysis of corneal epithelial markers of SEAMs cultivated on 6C3 substrate

Finally, for the 6C3 substrate, morphologically, the SEAMs, again, did not differ substantially from the normal SEAMs morphologically as shown in **Figure 4.4J-L**, but noted in some SEAMs was that zone 1 was smaller and lacked a distinctive high optical density ring in zone 2 as witnessed on other substrates. Zone 4 also appeared larger on this substrate. However, greater differences were witnessed from immunohistochemical examination as shown in **Figure 4.11** and **Figure 4.12** when compared with normal SEAMs as seen in **Figure 4.5** and **Figure 4.6**. There appeared to be a much smaller population of p63/PAX6 positive cells, if any, as shown in **Figure 4.11C** in zone 3. TUBB3 immunolocalisation was also abundant in zones 1 and 2 with substantial neuronal outgrowths present and examples shown in **Figure 4.12**D.

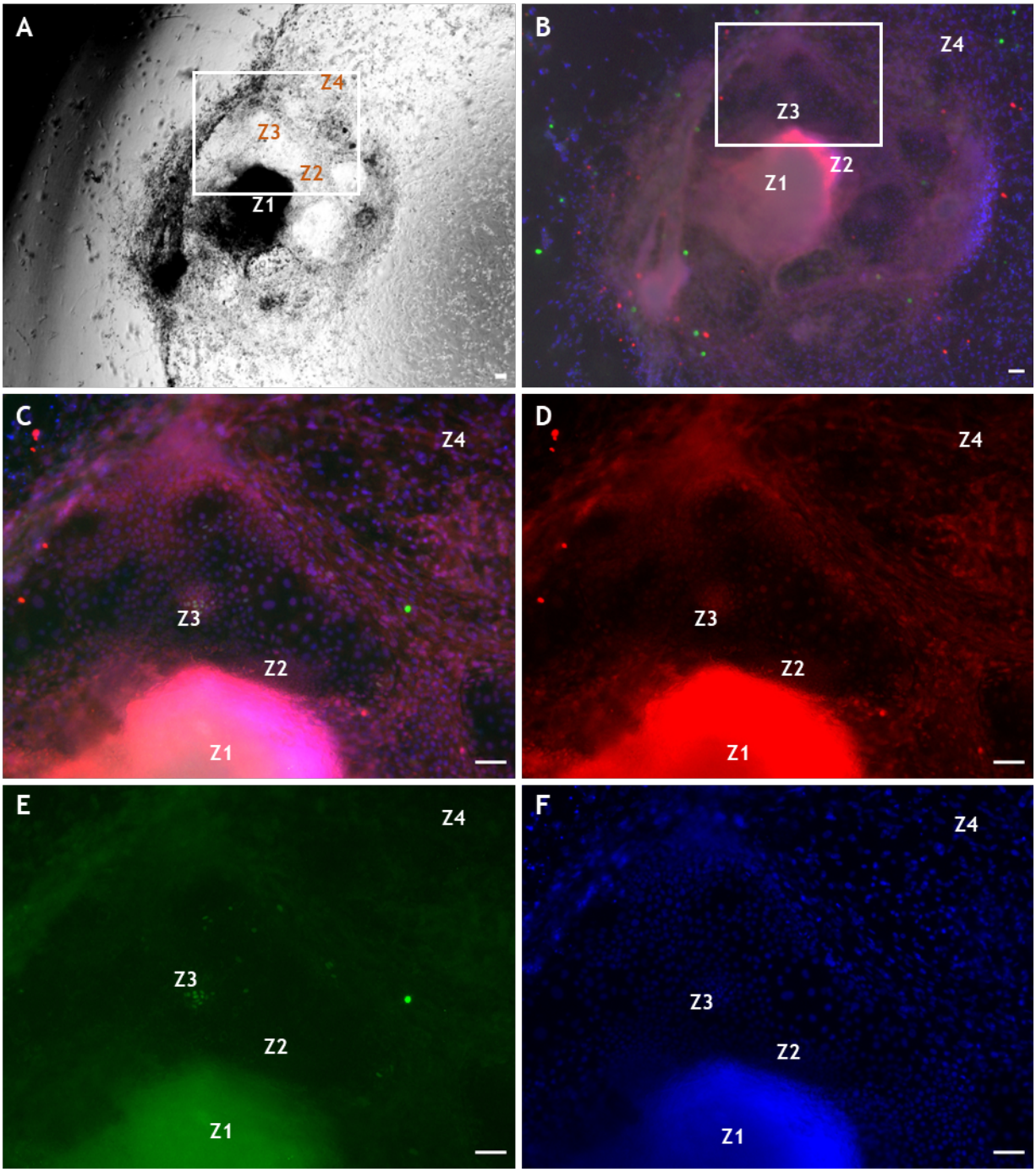

Figure 4.11 Immunohistochemical analysis of the corneal epithelial markers p63 and PAX6 in a SEAM grown on the 6C3 substrate after 4 weeks of differentiation. (**A**) Phase contrast image of a SEAM grown on the above substrate. (**B**) Tricolour image of the epithelial marker, p63 (green) and ocular lineage marker, PAX6 (red) and DAPI nuclear stain (blue) of the area represented in A and B. (**C**) Enhanced tricolour image of the area represented in (**A**) and (**B**). (**D**) Single channel image of PAX6. (**E**) Single channel image of p63. (**F**) Single channel image of DAPI. SEAM zones are labelled in each image and scale bars represent 100 µm.

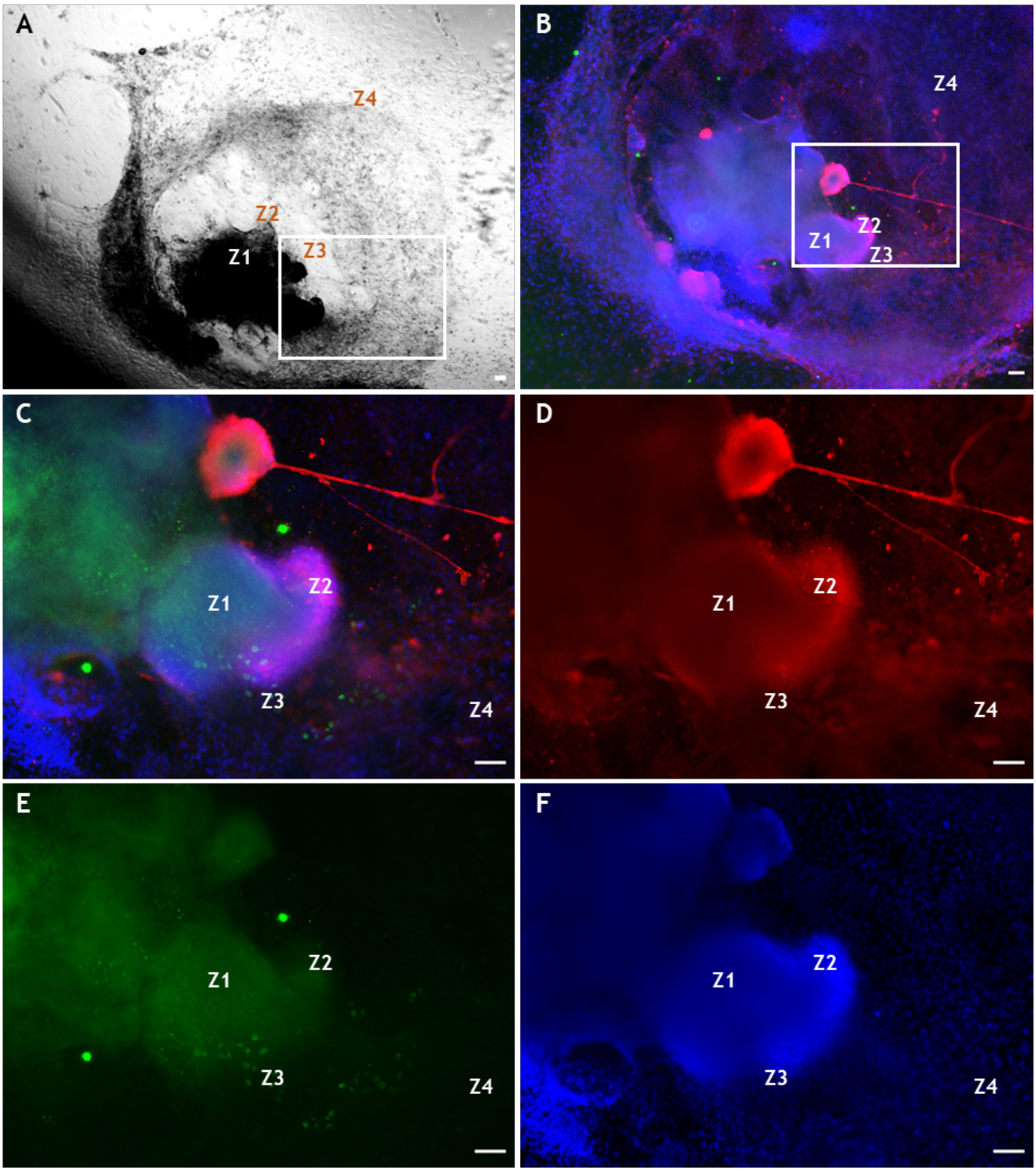

Figure 4.12 Immunohistochemical analysis of the epithelial marker p63 and the neural cell marker, TUBB3 in a SEAM grown on the 6C3 substrate after 4 weeks of differentiation. (**A**) Phase contrast image of a SEAM grown on the above substrate. (**B**) Tricolour image of p63 (green) and TUBB3 (red) and DAPI nuclear stain (blue) of the area represented in A and B. (**C**) Enhanced tricolour image of the area represented in (**A**) and (**B**). (**D**) Single channel image of TUBB3. (**E**) Single channel image of p63. (**F**) Single channel image of DAPI. SEAM zones are labelled in each image and scale bars represent 100 µm.

4.3.8 Gene expression analysis of SEAMs at four and eight weeks of development

The gene expression of various markers was analysed in SEAMs at four weeks (for the 7D4, 5D4/7D4 and 6C3 substrates) and 8 weeks (for the 7D4 and 5D4/7D4 substrates) and represented in **Figure 4.13** and **Figure 4.14** respectively.

4.3.9 E-cadherin

For the epithelial adhesion molecule, E-cadherin (CDH1), only a significant effect was seen on SEAMs grown on the 6C3 substrate. The 6C3 glycosaminoglycan substrate had a significantly higher level of expression of CDH1 than a normal SEAM as seen in **Figure 4.13A,** with expression of CDH1 being increased two-fold ($p = 0.002$). This indicated increased levels of epithelial cells with tight junctions, as present in the corneal epithelial-like cells present in a SEAM. Interestingly after 8 weeks of differentiation, CDH1 was also significantly decreased in the 5D4/7D4 substrate, with approximately half the expression seen compared to the normal SEAM ($p = 0.022$) as seen in **Figure 4.14A**.

4.3.10 PAX6

The key transcription factor for ocular development and gene expression, PAX6, was not significantly different between the samples, however there appeared to an almost two-fold increase in the 6C3 sample, as seen in **Figure 4.13B**. After 8 weeks of differentiation, for the 7D4 and 5D4/7D4 substrates, the expression of PAX6 was significantly reduced by more than half compared to the normal SEAM ($p = 0.000$ for both) as seen in **Figure 4.14B**.

4.3.11 SOX2

The neural cell-specific marker SOX2 appeared to be downregulated in all SEAM samples grown on glycosaminoglycan substrates. However, it was only significantly downregulated on the 6C3 and 7D4 substrates at 4 weeks as seen in **Figure 4.13C** ($p = 0.041$ and 0.002, respectively)**. A**t 8 weeks of differentiation no differences were witnessed as seen in **Figure 4.14C**.

4.3.12 NGFR/p75

Nerve growth factor receptor (NGFR or p75) was also examined in 4 week and 8 week SEAMs and is typically associated with neuronal growth and neural crest formation but possesses many other functions. In this study, it was only significantly downregulated on the 7D4 substrate at 4 weeks of differentiation as seen in **Figure 4.13D** with half the expression witnessed ($p = 0.000$). This observation reversed at 8 weeks of differentiation and increased to an average of over 6-fold increase in expression compared to normal SEAMs ($p = 0.02$) as seen in **Figure 4.14D**.

4.3.13 TUBB3

Another neuronal cell-specific marker, TUBB3, remained relatively stable on all glycosaminoglycan substrates at both 4 and 8 weeks of differentiation, with a slight increase on the 7D4 substrate at 8 weeks of differentiation. However, it was neither significantly up or down-regulated as seen in **Figure 4.13E** and **Figure 4.14E.**

4.3.14 SOX10

Another neural crest marker, SOX10, was significantly upregulated in 6C3, with almost double the expression detected ($p = 0.01$). Conversely the 7D4 and 5D4/7D4 substrates resulted in downregulated expression of SOX10. This was displayed even more so for the 7D4 substrate with nearly a two-fold decrease in expression ($p = 0.000$) as seen in **Figure 4.13F**. However after 8 weeks of differentiation, this early differentiation marker was undetectable in all samples, including normal SEAMs, an interesting finding, given the variability at 4 week SEAMs.

4.3.15 P63

Finally, for the epithelial cell marker, p63, it was significantly downregulated in the 6C3 sample at 4 weeks, with a nearly two-fold decrease ($p = 0.007$) and even more so in the 5D4/7D4 mixed substrate ($p = 0.000$) and was largely similar between 7D4 and normal SEAMs as seen in **Figure 4.13H**. At 8 weeks, there was no significant differences between normal and SEAMs grown on the two glycosaminoglycan substrates analysed for these samples as seen in **Figure 4.14F**.

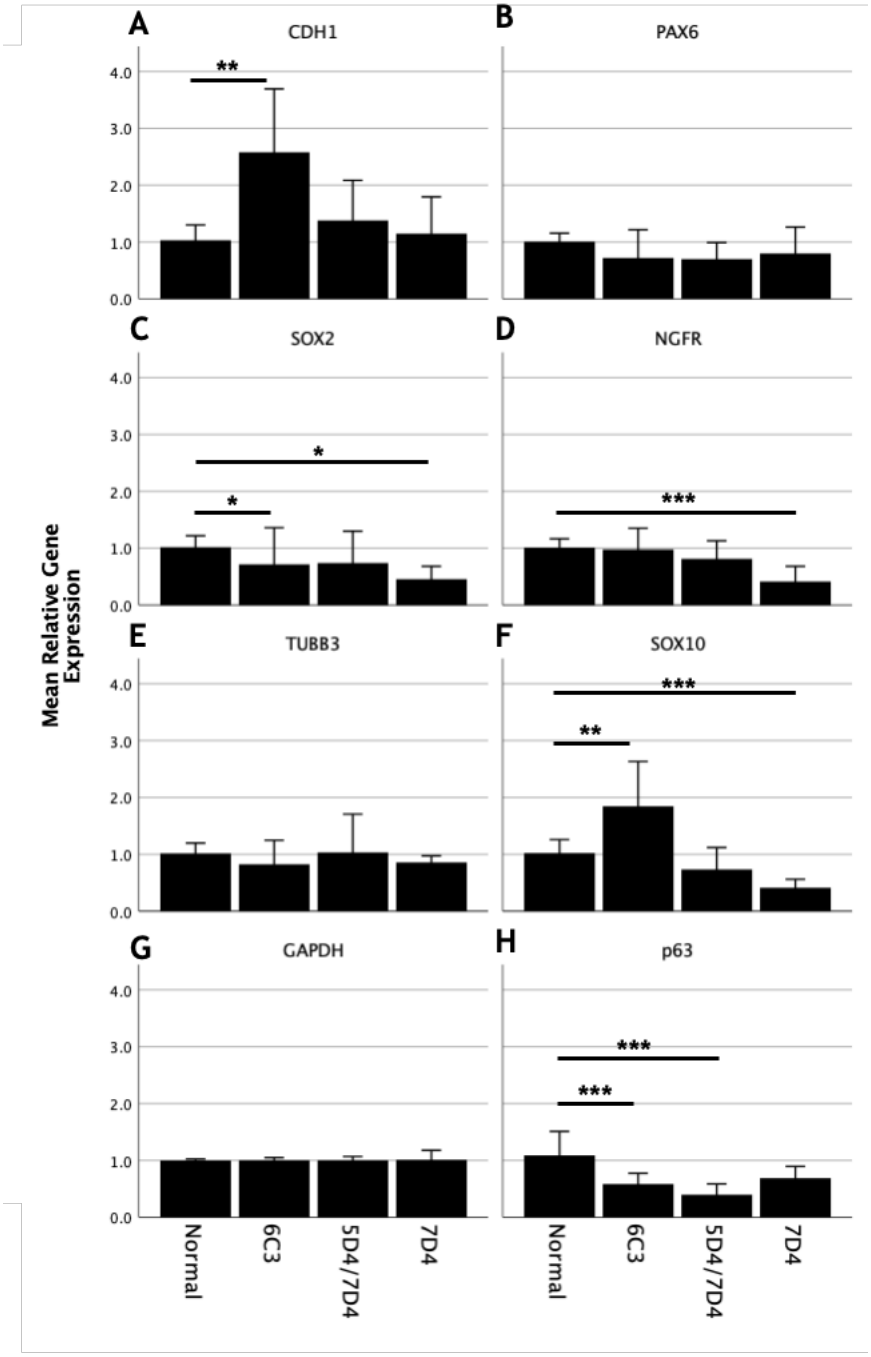

Figure 4.13 Relative gene expression of different ectodermal markers, as described in **Table 4.1**, in 4 week SEAMs on different glycosaminoglycan substrates, normalised to GAPDH. Significant differences are displayed with *, ** and *** representing $p < 0.05$, 0.01, 0.001 respectively (n = 4). Statistics performed were ANOVA, followed by Tukey's post hoc test.

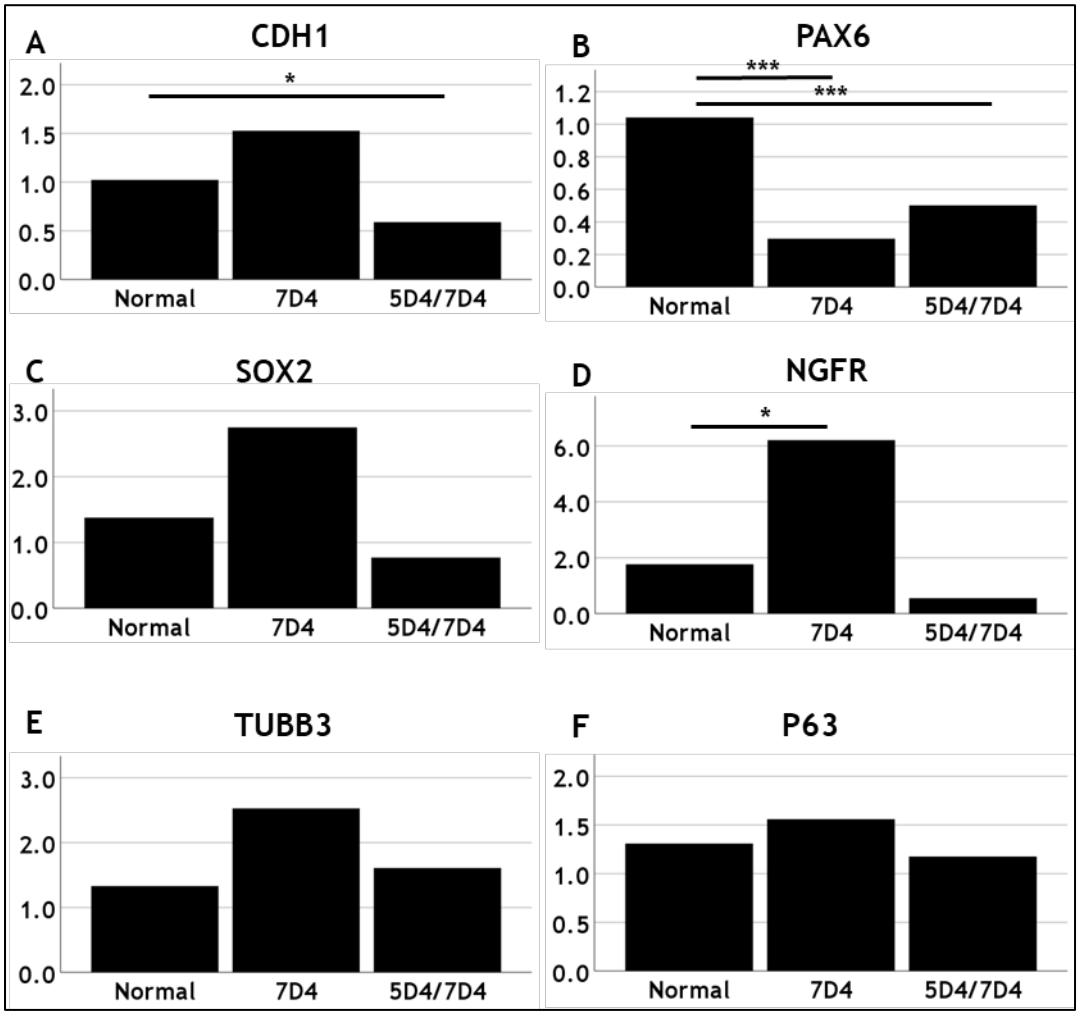

Figure 4.14 Relative gene expression of different ectodermal markers, as described in **Table 4.1**, in 8 week SEAMs on different glycosaminoglycan substrates, normalised to GAPDH. SOX10 was omitted due to lack of expression. Significant differences are displayed with *, ** and *** representing $p < 0.05$, 0.01, 0.001 respectively (n = 2). Statistics performed were ANOVA, followed by Tukey's post hoc test for all samples.

4.4 Discussion

The primary goal for this chapter was to, firstly, develop and optimise the coating conditions used to immobilise glycosaminoglycans in the presence of laminin 511 E8 fragment required for iPS cell adhesion. The immobilisation method used has been previously described and already proved very effective for immobilising glycosaminoglycans onto cell culture surfaces (Hof et al., 2019). There are other examples of combinations of substrates with CS in combination with laminin, but not in the context of naïve iPS cells and their adhesion, nor was the relative amount of CS immobilised verified (Galindo et al., 2018). This chapter describes a method that successfully immobilised glycosaminoglycans with a readily detectable signal, equal or greater to signal generated at the same coating conditions on ELISA plates, after the addition of laminin coating as shown by ELISA as in **Figure 4.2**. Application of glycosaminoglycans at the given concentrations did not appear to interfere with cell adhesion, or colony forming ability, nor did it affect pluripotency as shown by the analysis of the pluripotency markers SSEA-4 and Tra-1-60 As shown in **Figure 4.3**. Whilst acceptable, the presence of glycosaminoglycans was only analysed after 24 hours, and a follow up of up to 10 days for the formation of large colonies prior to SEAM differentiation may be of benefit to assess loss of glycosaminoglycans over the time course. This is further complicated by the unknown interaction between iPS cells and the glycosaminoglycan substrate, and in fact deposition could be increased by the differentiating SEAMs or even degraded. Another prospective experiment would be to create a growth factor gradient using the method described previously (Hof et al., 2019). Owing to the yield of the enriched substrates, small concentrations equivalent to laminin were used, however, if the enrichment method was refined further and a greater yield possible, it would be interesting to use higher concentrations of glycosaminoglycans to determine more significant effects, particularly on naïve iPSCs, however this was outside the scope of this project. In addition, it appeared for some samples, maximum binding capacity was reached, e.g. in the 7D4 substrate as shown in **Figure 4.2**.

Establishment of iPS cell and SEAM culture facilities was performed and normal SEAMs grown, as described previously (Hayashi et al., 2017). They appeared to

differentiate and develop as expected in accordance with original researchers in private communications. One issue, however, was the slightly lower ratio of SEAM generation from each iPSC colony, and iPS cells expanding slightly slower than expected. This may be a result of using a commercial iPSC source, that was previously expanded on a different feeder-free substrate and subsequently adapted to laminin 511 E8 fragment as a substrate. Despite several passages allowing for adaption to the new substrate, the cells passed through a significant bottleneck as only a very small number of iPSC clonal colonies gave rise to the cells used in all of the experiments described. Other supply issues were also obstructive, including the discontinuation of the first cell culture media used, which enabled better expansion similar to that seen in previously described literature. Whilst pluripotency was still confirmed using pluripotency markers, and cell colonies were morphologically undifferentiated, other verification would have been beneficial, for example expression analysis for more pluripotency markers and karyotyping (chromosomal analysis), as described previously (Lund et al., 2012).

In spite of this, SEAMs appeared similar morphologically to those described previously and shown here in **Figure 4.4** (Hayashi et al., 2017, 2016; Shibata et al., 2020, 2018). All zones appeared to be present and immunohistochemical analysis of a marker identifying neuronal cells in zones 1 and 2, TUBB3, was localised to these regions as shown in **Figure 4.6**. Corneal epithelial-like cells were also identified as PAX6/p63 positive cells peripherally to zone 2 in the third, circumferential zone 3 in **Figure 4.5**. Further verification, including gene expression analysis and comparison with samples generated by Hayashi *et al.* would also be of benefit to ensure optimal evaluation of protocol reproduction, and indeed, was the original plan.

After successful reproduction of the SEAM protocol and analysis of glycosaminoglycan coating conditions, SEAMs were then grown on the different substrates. Initially, the CS/DS 7D4-enriched substrate resulted in morphologically and immunohistochemically similar SEAMs to baseline conditions and all zones appeared to be present as shown in **Figure 4.4**, **Figure 4.7** and **Figure 4.8**. There also appeared to be a slight increased presence of zone 2

enhanced optical density areas and extensive TUBB3 expression as identified by immunohistochemistry. The gene expression analysis revealed several significantly decreased neural crest markers in SOX10 and NGFR and neural cell markers were also decreased in SOX2 and TUBB3, an interesting finding and concurrent with inhibitory effects of CS on neuronal growth, given that CS is typically inhibitory in axon and neuronal growth, particularly in injury (Silver and Silver, 2014), however DS may be more highly represented in this enriched substrate, which has much less effect on neuronal migration (Ishii and Maeda, 2008). TUBB3, NGFR and SOX2 were also still elevated at 8 weeks. It is interesting that SOX2, a pluripotency marker in addition to neural transcription factor was still present at 8 weeks, suggesting the presence of undifferentiated cells at this timepoint (Zhang and Cui, 2014). In terms of corneal epithelial-like cells, they appeared to be present in a similar pattern and distribution to normal SEAMs. The key corneal epithelial markers, CDH1, p63 and PAX6 were not up or down regulated relative to normal SEAMs at four weeks of differentiation. The exception to this is the downregulation of PAX6 at eight weeks of differentiation. Overall, these data suggest an decreased induction of cells from neural crest cell anlage and subsequent increaed differentiated neuronal cells compared to normal SEAMs, with comparable levels of p63/PAX6 positive corneal epithelial cells.

Contrarily, the 6C3-enriched substrate appeared to have a slightly potentiating effect on neural crest anlages and further effects on the corneal epithelial-like cells present in the SEAMs. Morphological and immunohistochemical analysis revealed a reduction in the size of zone 2 and an enlarged zone 4 accounting for an increased area of the SEAM as shown in **Figure 4.4**, **Figure 4.11** and **Figure 4.12**. The number of p63/PAX6 positive presumptive corneal epithelial progenitor cells was also visibly reduced and they tended to appear as very small clusters rather than distributed throughout zone 3. Gene expression analysis revealed slightly decreased expression of p63 and PAX6, but significantly increased E-cadherin expression suggesting epithelial cells of non-ocular origin. The neural crest marker, SOX10 was significantly increased, suggesting either decreased differentiation of neural anlages or an overall increase in neural cells present. SOX10 is also important for promoting the survival of neural crest cells

prior to differentiation, and so may be upregulated in the presence of the 6C3-enriched substrate (Mollaaghababa and Pavan, 2003). Zonal analysis of SEAMs using qPCR would be of particularly benefit here for further verification, however the altered morphology of differential SEAMs increases the complexity of dissection, especially in the absence of advanced technical support.

Finally, the mixed substrate consisting of KS and CS/DS, enriched in 5D4 and 7D4 epitopes was, again, similar morphologically to normal SEAMs, with no substantial differences as shown in **Figure 4.4**, **Figure 4.9** and **Figure 4.10**. Slight differences of note were the substantial presence of corneal epithelial-like cells as identified by p63/PAX positivity as shown in **Figure 4.9** and increased occurrence of lens-like cell clusters located on the interface between zone 2 and 3 as in **Figure 4.4H** and **I,** which was an interesting incidental finding. Further analysis of these lens-like cell observations would have been of interest through immunohistochemical and gene expression studies, for example expression of alpha-crystallin, but was outside of the scope of this study, primarily investigating corneal epithelial cells. Interestingly, p63 was downregulated on SEAMs grown on the 5D4/7D4 substrate as shown in **Figure 4.13** and may only be localised in stem cell-like highly expressing cells. Furthermore, PAX6 subsequently was reduced at week 8 of differentiation, as seen in **Figure 4.14**, suggesting perhaps the cells either reached confluence or de- or transdifferentiated as happens when PAX6 expression is lost in epithelial cells (Kitazawa et al., 2017). This finding, coupled with the extensive populations of PAX6/p63 positive cells, suggests this substrate could potentially expediate the expansion of corneal epithelial-like cells at the week 4 timepoint. Further confirmation would be of benefit through the use of flow cytometric analysis to identify the proportion of corneal epithelial cells relative to the size of the SEAM, coupled with zonal analysis of mRNA levels as mentioned above in more samples.

The main limitation of this study is the small sample sizes reported and lack of facilities for whole cell culture plate imaging to track changes in real time. Such facilities are required to analyse many individual SEAMs over a time course to identify incremental changes more accurately. The work described here was

originally planned to be performed with access to a greater range of specialist equipment and technological support, in collaboration with Professor Hayashi and his team in Japan. However, it had to be adapted to be performed separately in Cardiff as a result of the coronavirus pandemic and my inability to travel to Osaka University for my planned placement. Further immunohistochemical and gene expression analysis of SEAMs at different timepoints would also be of benefit, to identify key stages of SEAM development and where developmental changes may occur, as morphologically, few changes were seen before the 4 week timepoint. However, SEAM throughput was hindered somewhat without access to more specialist facilities and due to time restraints.

A final point of note is only the first eight weeks of SEAM differentiation is analysed and described here. In order to generate therapeutic cell sheets of corneal epithelial cell transplantation, further enrichment and purification of cells is required (Hayashi et al., 2017). First cells in zones 1 and 2 are manually removed and remaining cells are maintained for two to seven weeks before being sorted using flow cytometry to isolate corneal epithelial cells and seeded onto cell culture inserts to develop into multi-layered corneal epithelial sheets. This cell sorting step would provide another opportunity to interrogate the development and expansion of corneal epithelial cells and the impact of these glycosaminoglycan substrates by coating prior to cell seeding with SEAM-derived corneal epithelial cells, as again, was originally planned. It would also have been interesting to investigate the matrix produced by iPSC-derived corneal epithelial cells, for example SLRPs and their glycosaminoglycan profiles, to see if they mimic that seen *in vivo*.

Overall, interesting observations were seen immunohistochemically and through gene expression analysis on SEAMs, showing both the potential for this technology and the effect of purified glycosaminoglycan substrates.

4.5 Conclusions

Taken together, small but significant differences were observed between the normal SEAMs and those grown on glycosaminoglycan substrates. From these initial pilot data, the study provides a good starting point for further work, for

example the use of different glycosaminoglycan and proteoglycan substrates and in varying concentrations. Further repeated studies would provide further strength to this statement as well as more exploratory work at different timepoints. In terms of the overall aim of the project, the most promising substrate for further study would be the 5D4/7D4 substrate, immunohistochemically. Further analysis and performing the entire SEAM-based production of corneal epithelial cells including generating mature transplantable cell sheets, would further establish the efficacy of increasing yield or enhanced production of a therapeutic corneal epithelial cell source.

5 Chapter 5: General Discussion

5.1 Summary

The overall aim of this project was to identify and extract proteoglycans and glycosaminoglycans associated with the corneal epithelium and limbal stem cell niche and use them as a substrate addition to improve the generation of corneal epithelial cells from iPS cells through defined means and identify any changes. This was to be achieved through immunohistochemical examination and identification of unique glycosaminoglycan sulphation motifs in the porcine corneal limbus and epithelium, as well as in iPS-derived corneal epithelial cells. Sulphation epitopes of interest, namely those associated with the corneal epithelium and corneal limbus, were extracted from corneal tissue, and enriched using a combination of chemical and affinity purification techniques to produce a sufficient quantity to use for downstream experiments. Finally, these epitopes were applied as a substrate for iPS cells and differentiated using a defined method. Changes in subsequent differentiation cultures, SEAMs, were assessed through morphological, immunohistochemical and gene expression analyses to recognise any changes in corneal epithelial cell development as well as effects on other ocular anlages present in the developing SEAM.

In summary, immunohistochemical analysis of sulphated CS and DS glycosaminoglycan epitopes in the porcine cornea revealed a distinct pattern of sulphation and sulphation epitopes associated with the limbal stem cell niche and corneal epithelial cells both *in vivo* and *in vitro*. The CS/DS sulphation epitope recognised by the 6C3 antibody was identified in the limbal stem cell niche. Associated with the corneal epithelium, both *in vivo* and *in vitro*, the CS/DS sulphation epitope recognised by the 7D4 antibody was identified. Subsequently, these corneal epithelial and limbal stem cell-associated glycosaminoglycan motifs, and their attached proteoglycans, were extracted from porcine corneal tissue and further investigated. Some of the proteoglycan attachments and glycosaminoglycan species present were identified, including the potential identity of the protein cores to which the epitopes detailed above were attached.

Proteoglycan extracts were then further enriched using anion-exchange affinity chromatography for various sulphation epitopes. This was most effective for free glycosaminoglycan chains and subsequent investigations were performed using substrates that appeared to be enriched in free glycosaminoglycan substrates of three types. These were a substrate enriched in the 7D4 CS/DS sulphation epitope from peripheral porcine cornea, a mixed substrate enriched in the KS epitope 5D4 and the CS/DS epitope 7D4 from central porcine cornea and finally a substrate enriched in the 6C3 CS/DS epitope extracted from shark cartilage. The substrates were successfully generated in sufficient quantity and determined to be free of protein and other glycosaminoglycan species. Consequently, these substrates were successfully used in cell culture and a coating method that enabled the co-coating of laminin required for iPS cell adhesion, along with the successfully immobilised glycosaminoglycan substrates, was determined and optimised. Lastly, these substrates were then used to grow iPS cells and subsequently differentiate them into corneal epithelial cells using the SEAMs protocol described previously. The immunohistochemical analysis performed on these SEAMs grown on different substrates suggested that the mixed 5D4/7D4 substrate was enhancing the generation of corneal epithelial cells using this method. Other significant effects were also seen using the 7D4 and 6C3 CS/DS substrates, supporting the use of glycosaminoglycan substrates to meaningfully affect iPSC differentiation.

5.2 General Discussion

Initially, in Chapter 2, immunohistochemical analysis of porcine cornea revealed interesting distributions of CS/DS sulphation patterns, similar to those observed in human and rabbit limbal and corneal epithelial homologues (Yamada et al., 2015). The CS/DS epitopes recognised by the antibodies 7D4 and 6C3 emerged as corneal epithelial-associated markers, with the antibody 6C3 being of particular interest as being closely associated to limbal epithelial stem cells in the basal layer of cells in the corneal limbus.

Despite subsequently being able to extract this epitope from porcine cornea, it remains of particular interest due to its high signal directly subjacent to the limbal epithelial stem cells. The staining pattern was very similar to that seen

with versican in the limbus (Schlötzer-Schrehardt et al., 2007), and appeared as a high molecular weight protein. Similar observations were witnessed in human skin, a tissue type very similar to the cornea, with 6C3 and versican both being present below the epithelial basal stem cells (Sorrell et al., 1990; Zimmermann et al., 1994), as mentioned in Section 3.4.2. If the 6C3 antibody is recognising versican as postulated, this reveals an interesting role of this proteoglycan in maintenance of the stem cell niche. This is supported by other studies, that show versican is highly upregulated in supportive limbal zone cells (including corneal stromal stem cells and resident melanocytes) when compared with basal corneal epithelial stem cells, in which it is undetected (Polisetti et al., 2016). The epitope revealed by 6C3 may recognise a specific isoform of versican that is likely part of an extensive extracellular matrix, consisting of a complex of HA and other extracellular matrix molecules, which are also highly present subjacent to the corneal limbus, forming a glycocalyx around supportive corneal stromal stem cells and melanocytes that maintains the basal epithelial cells in their multipotent and motile state, primed for wound repair (Gesteira et al., 2017; Huang and Tseng, 1991; Ricciardelli et al., 2007). Further investigation is certainly warranted if this model is accurate, as few studies have investigated the specific role of versican in the cornea, which is typically associated with high molecular weight hyaluronan (Gesteira et al., 2017). Other studies have shown versican is highly upregulated after corneal injury, further highlighting its potential role as an enhancement of cell motility as has been witness in other tissues (Mutoji et al., 2021; Ricciardelli et al., 2007). Nevertheless, shown here was the first identification of CS/DS sulphation epitope recognised by the 6C3 antibody being present in the porcine limbus, and potential examination of this CS/DS sulphation motif being present on versican.

The CS/DS sulphation motif recognised by the 7D4 antibody, likely on the SLRP decorin as identified by Western blot, may also play a role in the maintenance of corneal epithelium *in vivo* through its interaction with the basal epithelial cells from the stroma. Interestingly, the epitope recognised by the 7D4 antibody appeared to be present throughout the stroma, similarly to decorin, suggesting it's high likely that, firstly, the epitope recognised by 7D4 is present on this protein core, but also the CS/DS chains of this CS/DS proteoglycan have the

same sulphation patterns present throughout the stroma. Despite decorin's clear role in collagen fibre regulation in the cornea (Zhang et al., 2009), few studies investigate the effect of decorin on corneal epithelium. Decorin null mice also have increased corneal haze following injury and highly increased neovascularisation (Gupta et al., 2022), suggesting a regulatory role beyond simply collagen fibre organisation, but again the effect on corneal epithelium was not investigated further. This warrants further study beyond the effect of the CS/DS glycosaminoglycans, as investigated here using iPS cell model mimicking ocular development.

The 7D4 antibody also recognised a CS/DS epitope present in zone 3 of developing SEAMs, the first such recognition of CS/DS deposition in hiPSC-derived ocular organoids using this model. It is unclear from this study the role of this deposited glycosaminoglycan and, indeed, whether it is present in the matrix deposited by primordial ocular surface cells or present as a cell surface-associated CS/DS proteoglycan. It is possible that it may play a role in growth factor gradient by sequestering growth factors between distinct cell populations present in a SEAM. Recently, microglia-like cells, immunomodulatory cells identified by the marker CD11b, were shown to be present throughout zone 2 and 3 of developing SEAMs and CD11b immunolocalisation bore a striking resemblance to the distribution revealed by 7D4 antibody staining (Shiraki et al., 2022). Co-staining would reveal whether these two molecules were interacting closely and if microglia played a role in the development of ocular surface cells present in zone 3 of a SEAM. A pilot study using elemental mapping, conducted by myself in collaboration with Dr Kalotina Geraki at Diamond Light Source (Oxford, UK), also revealed the presence of small amounts of elemental sulphur as early as 3 weeks in a developing SEAM and showed similar extracellular/pericellular strand-like staining as seen with the 7D4 antibody in immunohistochemistry as shown below in **Figure 5.1**. This method may also reveal further highly sulphated molecules, in addition to sulphated glycosaminoglycans and is extremely sensitive, however was only initially performed on SEAMs at 3 weeks of differentiation as a time-sensitive pilot study.

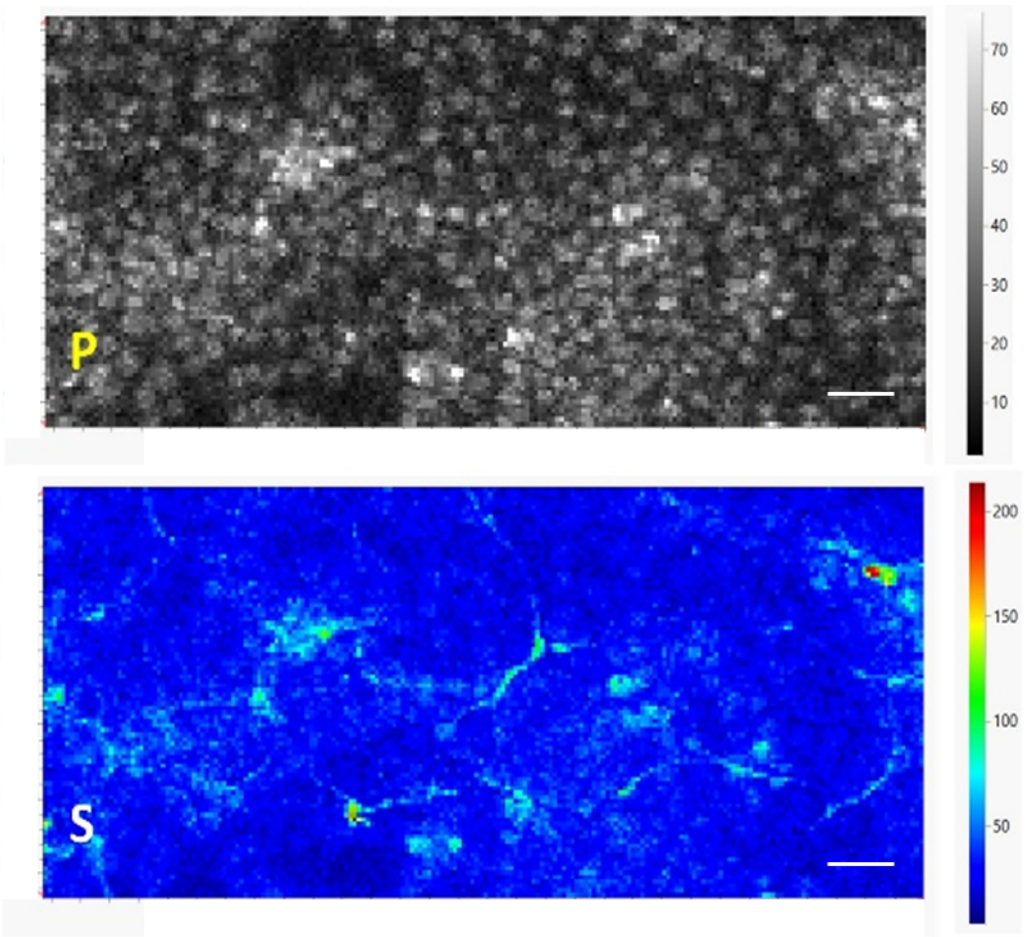

Figure 5.1 Elemental maps of phosphorous (P) (mostly present in the cell nucleus) and sulphur (S) (likely sulphated glycosaminoglycans) in zone 3 of a three week differentiated SEAM. Scale bars represent 50 µm. Elements were identified using synchrotron X-ray fluorescence microscopy as described in (Ugarte et al., 2016).

The CS/DS antibodies used in this study have been used to identify sulphation patterns in a wide range of tissues and have been shown to identify progenitor and stem cells in a wide range of tissues including developing fetal cartilage and adult cartilage (Hayes et al., 2016; Turner et al., 2014), as well as associated with the stem cell niche in skin (Sorrell et al., 1990) and the adult corneal stem cell niche (Ashworth et al., 2021; Yamada et al., 2015). Whilst invaluable in identifying distinct species of CS/DS in a variety of tissues, no attempts have been made to extract and enrich for glycosaminoglycans enriched in these epitopes. The method developed and described here shows enriched populations of these stem cell associated CS/DS can be isolated from porcine cornea and other glycosaminoglycan-rich sources to be used in functional studies. Sulphated glycosaminoglycans differed substantially between central and peripheral

cornea, as shown by their distributions and anion exchange profiles in Chapter 3 and demonstrates the inherent complexity and heterogeneity of sulphated glycosaminoglycans present in the cornea. Discussed in this thesis are only the effects of these distinct sulphation patterns on the development of hiPSC-derived ocular organoids. They may have other significant effects on tissue engineering efforts in many other tissues where they have been identified, for example cartilage and skin generated from PSCs or other multipotent cells and certainly merit further investigation.

Also discovered in this thesis, and in concordance with other researchers, chondroitin sulphate salts from commercial sources contain considerable contaminants (da Cunha et al., 2015; Santos et al., 2017). The CS/DS epitope recognised by the 6C3 antibody gave high signal in ELISA analysis from commercial chondroitin sulphate salts (from whale and shark), but this did not readily separate from the contaminating KS during anion exchange chromatography (data not shown), leading to the use of in-house produced CS/DS from shark cartilage, which was able to separate from contaminating KS and used here as the 6C3 substrate. This highlights the problem of many researchers using commercial chondroitin sulphate preparations for functional cell studies when they contain significant contaminants and demonstrates the need for analysis and purification of commercial glycosaminoglycans prior to use. Ideally, defined, synthetic CS/DS preparations would be used, however there are currently no commercial sources and due to their complicated chemical structure, are very difficult to synthesise beyond small oligosaccharides (Ji et al., 2020). Even when achieved for larger molecules, only one type of sulphation is typically produced along the entire chain (Badri et al., 2021), which does not represent *in vivo* CS/DS chains that are extremely heterogeneous.

Finally, the enriched CS/DS substrates appeared to have significant effects on SEAM generation and significantly affected a wide variety of markers investigated. Immunohistochemical and gross morphological evaluation showed SEAMs grown on the CS/DS substrates extracted from cornea, 7D4 and 5D4/7D4, appeared largely similar to normal SEAMs. The greatest differences observationally were SEAMs grown on the 6C3 substrate, which appeared to have

smaller neural centres and reduced presence of primordial ocular surface cells identified with PAX6/p63 positive staining. Also of interest were the presence of increased numbers of lens-like structures in the SEAMs grown on the 5D4/7D4 substrate. Highly sulphated KS and CS have both been shown to be able to bind many proteins that influence nerve growth cone behaviour in the developing cornea, especially a neurorepellant extracellular matrix component semaphorin 3A expressed by lens cells (Conrad et al., 2010). This interaction may explain the increased observation of lens-like structures on this substrate; however the specific mechanism is unclear. The 7D4 substrate appeared to decrease the expression of the neural markers, SOX2, NGFR and SOX10 in SEAMs grown on this substrate. Contrastingly, SEAMs grown on the 6C3 substrate increased the expression of the neural crest marker SOX10. This difference may be to do with the different ratios of CS and DS, which has been identified previously in the cornea, with central cornea containing higher ratios of DS (for the epitope recognised by 7D4), and peripheral cornea containing higher ratio of CS (for the epitope recognised by 6C3) (Ho et al., 2014). Recently, DS has been shown to accelerate neuronal differentiation in ESCs and neural stem cells, which may accelerate the development of neural crest and subsequently potentiate SEAM generation (Ogura et al., 2021). CS has also been shown to inhibit neural crest cell migration, dependent on the type of CS, which may explain the reduced expression of the neural crest transcription factor SOX10 in SEAMs grown on this substrate (Perris and Johansson, 1990). Fewer differences between normal SEAMs and SEAMs grown on glycosaminoglycan substrates were seen at 8 weeks of differentiation, which may be as a result of extensive matrix remodelling taking place and the effects of exogenous glycosaminoglycan addition were less pertinent, with the exception of slight but significant differences in PAX6 and NGFR expression. Overall, subtle but significant effects of glycosaminoglycan addition were witnessed on SEAMs and further analysis would have been of great benefit to this study but unfortunately was not possible without the availability of key resources as was originally planned.

5.3 Conclusion

In this thesis the aim was to investigate the role of specific CS/DS extracellular matrix molecules on the differentiation of corneal epithelial cells from iPS cells.

Examining CS/DS sulphation pattern distributions in the cornea revealed distinct localisation of specific CS/DS sulphation motifs associated with the corneal epithelium and corneal limbus. Further work revealed the presence of specific patterns in developing corneal epithelial cells derived from iPS cells. These identified glycosaminoglycan species were successfully purified and applied to iPS cells to subsequently differentiate into SEAMs, which are a model of whole eye development. Immunohistochemical and gene expression analysis revealed interesting and significant effects on the development of SEAMs and their propensity to produce early corneal epithelial cells as well as affecting other ocular cell types present in the model. The work described here reveals and furthers the potential for using purified glycosaminoglycans from native tissue in regenerative medicine and developmental studies, as well as interesting insights into the role of CS/DS in the developing cornea and adult corneal homeostasis.

6 References

Ahmad, S., Stewart, R., Yung, S., Kolli, S., Armstrong, L., Stojkovic, M., Figueiredo, F., Lako, M., 2007. Differentiation of human embryonic stem cells into corneal epithelial-like cells by in vitro replication of the corneal epithelial stem cell niche. Stem Cells 25, 1145–1155. https://doi.org/10.1634/stemcells.2006-0516

Allen, B.L., Rapraeger, A.C., 2003. Spatial and temporal expression of heparan sulfate in mouse development regulates FGF and FGF receptor assembly. J Cell Biol 163, 637–648. https://doi.org/10.1083/jcb.200307053

Ashworth, S., Harrington, J., Hammond, G.M., Bains, K.K., Koudouna, E., Hayes, A.J., Ralphs, J.R., Regini, J.W., Young, R.D., Hayashi, R., Nishida, K., Hughes, C.E., Quantock, A.J., 2021. Chondroitin Sulfate as a Potential Modulator of the Stem Cell Niche in Cornea. Front. Cell Dev. Biol. 8. https://doi.org/10.3389/fcell.2020.567358

Atallah, M.R., Palioura, S., Perez, V.L., Amescua, G., 2016. Limbal stem cell transplantation: current perspectives. Clin Ophthalmol 10, 593–602. https://doi.org/10.2147/OPTH.S83676

Badri, A., Williams, A., Awofiranye, A., Datta, P., Xia, K., He, W., Fraser, K., Dordick, J.S., Linhardt, R.J., Koffas, M.A.G., 2021. Complete biosynthesis of a sulfated chondroitin in Escherichia coli. Nat Commun 12, 1389. https://doi.org/10.1038/s41467-021-21692-5

Bains, K.K., Fukuoka, H., Hammond, G.M., Sotozono, C., Quantock, A.J., 2019. Recovering vision in corneal epithelial stem cell deficient eyes. Cont Lens Anterior Eye 42, 350–358. https://doi.org/10.1016/j.clae.2019.04.006

Barbosa, I., Garcia, S., Barbier-Chassefière, V., Caruelle, J.-P., Martelly, I., Papy-García, D., 2003. Improved and simple micro assay for sulfated glycosaminoglycans quantification in biological extracts and its use in skin and muscle tissue studies. Glycobiology 13, 647–653. https://doi.org/10.1093/glycob/cwg082

Bashir, H., Seykora, J.T., Lee, V., 2017. Invisible Shield: Review of the Corneal Epithelium as a Barrier to UV Radiation, Pathogens, and Other Environmental Stimuli. J Ophthalmic Vis Res 12, 305–311. https://doi.org/10.4103/jovr.jovr_114_17

Baylis, O., Figueiredo, F., Henein, C., Lako, M., Ahmad, S., 2011. 13 years of cultured limbal epithelial cell therapy: A review of the outcomes. Journal of Cellular Biochemistry 112, 993–1002. https://doi.org/10.1002/jcb.23028

Bergmanson, J.P.G., Horne, J., Doughty, M.J., Garcia, M., Gondo, M., 2005. Assessment of the Number of Lamellae in the Central Region of the Normal Human Corneal Stroma at the Resolution of the Transmission Electron Microscope. Eye & Contact Lens 31, 281–287. https://doi.org/10.1097/01.ICL.0000165280.94927.0D

Bettelheim, F.A., Plessy, B., 1975. The hydration of proteoglycans of bovine cornea. Biochim Biophys Acta 381, 203–214. https://doi.org/10.1016/0304-4165(75)90202-0

Bi, Y., Ehirchiou, D., Kilts, T.M., Inkson, C.A., Embree, M.C., Sonoyama, W., Li, L., Leet, A.I., Seo, B.-M., Zhang, L., Shi, S., Young, M.F., 2007. Identification of tendon stem/progenitor cells and the role of the

extracellular matrix in their niche. Nature Medicine 13, 1219–1227. https://doi.org/10.1038/nm1630
Biber, J.M., Skeens, H.M., Neff, K.D., Holland, E.J., 2011. The cincinnati procedure: technique and outcomes of combined living-related conjunctival limbal allografts and keratolimbal allografts in severe ocular surface failure. Cornea 30, 765–771. https://doi.org/10.1097/ICO.0b013e318201467c
Bidanset, D.J., Guidry, C., Rosenberg, L.C., Choi, H.U., Timpl, R., Hook, M., 1992. Binding of the proteoglycan decorin to collagen type VI. Journal of Biological Chemistry 267, 5250–5256.
Björck, L., 1988. Protein L. A novel bacterial cell wall protein with affinity for Ig L chains. J Immunol 140, 1194–1197.
Blanco, M., Fraguas, J., Sotelo, C.G., Pérez-Martín, R.I., Vázquez, J.A., 2015. Production of Chondroitin Sulphate from Head, Skeleton and Fins of Scyliorhinus canicula By-Products by Combination of Enzymatic, Chemical Precipitation and Ultrafiltration Methodologies. Mar Drugs 13, 3287–3308. https://doi.org/10.3390/md13063287
Bonanno, J.A., 2012. “Molecular Mechanisms Underlying the Corneal Endothelial Pump.” Exp Eye Res 95, 2–7. https://doi.org/10.1016/j.exer.2011.06.004
Brzeszczynska, J., Samuel, K., Greenhough, S., Ramaesh, K., Dhillon, B., Hay, D.C., Ross, J.A., 2014. Differentiation and molecular profiling of human embryonic stem cell-derived corneal epithelial cells. Int. J. Mol. Med. 33, 1597–1606. https://doi.org/10.3892/ijmm.2014.1714
Buzzega, D., Pederzoli, F., Maccari, F., Aslan, D., Türk, M., Volpi, N., 2010. Comparison of cetylpyridinium chloride and cetyltrimethylammonium bromide extractive procedures for quantification and characterization of human urinary glycosaminoglycans. Clin Chem Lab Med 48, 1133–1139. https://doi.org/10.1515/CCLM.2010.217
Byström, B., Virtanen, I., Rousselle, P., Gullberg, D., Pedrosa-Domellöf, F., 2006. Distribution of Laminins in the Developing Human Eye. Investigative Ophthalmology & Visual Science 47, 777–785. https://doi.org/10.1167/iovs.05-0367
Calonge, M., Pérez, I., Galindo, S., Nieto-Miguel, T., López-Paniagua, M., Fernández, I., Alberca, M., García-Sancho, J., Sánchez, A., Herreras, J.M., 2019. A proof-of-concept clinical trial using mesenchymal stem cells for the treatment of corneal epithelial stem cell deficiency. Transl Res 206, 18–40. https://doi.org/10.1016/j.trsl.2018.11.003
Caterson, B., 2012. Fell-Muir Lecture: Chondroitin sulphate glycosaminoglycans: fun for some and confusion for others. International Journal of Experimental Pathology 93, 1–10. https://doi.org/10.1111/j.1365-2613.2011.00807.x
Caterson, B., Christner, J.E., Baker, J.R., 1983. Identification of a monoclonal antibody that specifically recognizes corneal and skeletal keratan sulfate. Monoclonal antibodies to cartilage proteoglycan. J. Biol. Chem. 258, 8848–8854.
Caterson, B., Melrose, J., 2018. Keratan sulfate, a complex glycosaminoglycan with unique functional capability. Glycobiology 28, 182–206. https://doi.org/10.1093/glycob/cwy003

Chakravarti, S., 2002. Functions of lumican and fibromodulin: Lessons from knockout mice. Glycoconj J 19, 287–293. https://doi.org/10.1023/A:1025348417078

Chakravarti, S., Magnuson, T., Lass, J.H., Jepsen, K.J., LaMantia, C., Carroll, H., 1998. Lumican Regulates Collagen Fibril Assembly: Skin Fragility and Corneal Opacity in the Absence of Lumican. J Cell Biol 141, 1277–1286.

Chen, J., Li, Z., Zhang, L., Ou, S., Wang, Y., He, X., Zou, D., Jia, C., Hu, Q., Yang, S., Li, X., Li, J., Wang, J., Sun, H., Chen, Y., Zhu, Y.-T., Tseng, S.C.G., Liu, Z., Li, W., 2017. Descemet's Membrane Supports Corneal Endothelial Cell Regeneration in Rabbits. Sci Rep 7. https://doi.org/10.1038/s41598-017-07557-2

Chen, S., Birk, D.E., 2013. The regulatory roles of small leucine-rich proteoglycans in extracellular assembly. FEBS J 280, 2120–2137. https://doi.org/10.1111/febs.12136

Chen, S., Mienaltowski, M.J., Birk, D.E., 2015. Regulation of Corneal Stroma Extracellular Matrix Assembly. Exp Eye Res 133, 69–80. https://doi.org/10.1016/j.exer.2014.08.001

Chen, S., Young, M.F., Chakravarti, S., Birk, D.E., 2014. Interclass small leucine-rich repeat proteoglycan interactions regulate collagen fibrillogenesis and corneal stromal assembly. Matrix Biology, Proteoglycan Biology 35, 103–111. https://doi.org/10.1016/j.matbio.2014.01.004

Chen, Z., de Paiva, C.S., Luo, L., Kretzer, F.L., Pflugfelder, S.C., Li, D.-Q., 2004. Characterization of Putative Stem Cell Phenotype in Human Limbal Epithelia. Stem Cells 22, 355–366. https://doi.org/10.1634/stemcells.22-3-355

Conrad, A.H., Zhang, Y., Tasheva, E.S., Conrad, G.W., 2010. Proteomic Analysis of Potential Keratan Sulfate, Chondroitin Sulfate A, and Hyaluronic Acid Molecular Interactions. Invest Ophthalmol Vis Sci 51, 4500–4515. https://doi.org/10.1167/iovs.09-4914

Corpuz, L.M., Funderburgh, J.L., Funderburgh, M.L., Bottomley, G.S., Prakash, S., Conrad, G.W., 1996. Molecular Cloning and Tissue Distribution of Keratocan: BOVINE CORNEAL KERATAN SULFATE PROTEOGLYCAN 37A (*). Journal of Biological Chemistry 271, 9759–9763. https://doi.org/10.1074/jbc.271.16.9759

Cortes, M., Baria, A.T., Schwartz, N.B., 2009. Sulfation of chondroitin sulfate proteoglycans is necessary for proper Indian hedgehog signaling in the developing growth plate. Development 136, 1697–1706. https://doi.org/10.1242/dev.030742

Cotsarelis, G., Cheng, S.Z., Dong, G., Sun, T.T., Lavker, R.M., 1989. Existence of slow-cycling limbal epithelial basal cells that can be preferentially stimulated to proliferate: implications on epithelial stem cells. Cell 57, 201–209. https://doi.org/10.1016/0092-8674(89)90958-6

Coulson-Thomas, Y.M., Coulson-Thomas, V.J., Norton, A.L., Gesteira, T.F., Cavalheiro, R.P., Meneghetti, M.C.Z., Martins, J.R., Dixon, R.A., Nader, H.B., 2015. The Identification of Proteoglycans and Glycosaminoglycans in Archaeological Human Bones and Teeth. PLOS ONE 10, e0131105. https://doi.org/10.1371/journal.pone.0131105

Cvekl, A., Tamm, E.R., 2004. Anterior eye development and ocular mesenchyme: new insights from mouse models and human diseases. BioEssays 26, 374–386. https://doi.org/10.1002/bies.20009

da Cunha, A.L., de Oliveira, L.G., Maia, L.F., de Oliveira, L.F.C., Michelacci, Y.M., de Aguiar, J.A.K., 2015. Pharmaceutical grade chondroitin sulfate: Structural analysis and identification of contaminants in different commercial preparations. Carbohydrate Polymers 134, 300–308. https://doi.org/10.1016/j.carbpol.2015.08.006

Dang, V.T., Mandakhalikar, K.D., Ng, O.-W., Tan, Y.-J., 2013. A simple methodology for conversion of mouse monoclonal antibody to human-mouse chimeric form. Clin Dev Immunol 2013, 716961. https://doi.org/10.1155/2013/716961

DelMonte, D.W., Kim, T., 2011. Anatomy and physiology of the cornea. Journal of Cataract & Refractive Surgery 37, 588–598. https://doi.org/10.1016/j.jcrs.2010.12.037

Di Iorio, E., Barbaro, V., Ruzza, A., Ponzin, D., Pellegrini, G., De Luca, M., 2005. Isoforms of DeltaNp63 and the migration of ocular limbal cells in human corneal regeneration. Proc. Natl. Acad. Sci. U.S.A. 102, 9523–9528. https://doi.org/10.1073/pnas.0503437102

Doane, K.J., Yang, G., Birk, D.E., 1992. Corneal cell-matrix interactions: type VI collagen promotes adhesion and spreading of corneal fibroblasts. Exp Cell Res 200, 490–499. https://doi.org/10.1016/0014-4827(92)90200-r

Dorà, N.J., Hill, R.E., Collinson, J.M., West, J.D., 2015. Lineage tracing in the adult mouse corneal epithelium supports the limbal epithelial stem cell hypothesis with intermittent periods of stem cell quiescence. Stem Cell Res 15, 665–677. https://doi.org/10.1016/j.scr.2015.10.016

Du, Y., Funderburgh, M.L., Mann, M.M., SundarRaj, N., Funderburgh, J.L., 2005. Multipotent Stem Cells in Human Corneal Stroma. Stem Cells 23, 1266–1275. https://doi.org/10.1634/stemcells.2004-0256

Dua, H.S., Azuara-Blanco, A., 2000. Limbal Stem Cells of the Corneal Epithelium. Survey of Ophthalmology 44, 415–425. https://doi.org/10.1016/S0039-6257(00)00109-0

Dua, H.S., Faraj, L.A., Said, D.G., Gray, T., Lowe, J., 2013. Human Corneal Anatomy Redefined: A Novel Pre-Descemet's Layer (Dua's Layer). Ophthalmology 120, 1778–1785. https://doi.org/10.1016/j.ophtha.2013.01.018

Dunlevy, J.R., Rada, J.A.S., 2004. Interaction of Lumican with Aggrecan in the Aging Human Sclera. Investigative Ophthalmology & Visual Science 45, 3849–3856. https://doi.org/10.1167/iovs.04-0496

Dyer, D.P., Salanga, C.L., Volkman, B.F., Kawamura, T., Handel, T.M., 2016. The dependence of chemokine–glycosaminoglycan interactions on chemokine oligomerization. Glycobiology 26, 312–326. https://doi.org/10.1093/glycob/cwv100

Eiraku, M., Takata, N., Ishibashi, H., Kawada, M., Sakakura, E., Okuda, S., Sekiguchi, K., Adachi, T., Sasai, Y., 2011. Self-organizing optic-cup morphogenesis in three-dimensional culture. Nature 472, 51–56. https://doi.org/10.1038/nature09941

Erntell, M., Myhre, E.B., Kronvall, G., 1983. Alternative non-immune F(ab')2-mediated immunoglobulin binding to group C and G streptococci. Scand J Immunol 17, 201–209. https://doi.org/10.1111/j.1365-3083.1983.tb00783.x

Farndale, R.W., Buttle, D.J., Barrett, A.J., 1986. Improved quantitation and discrimination of sulphated glycosaminoglycans by use of

dimethylmethylene blue. Biochimica et Biophysica Acta (BBA) - General Subjects 883, 173–177. https://doi.org/10.1016/0304-4165(86)90306-5
Farndale, R.W., Sayers, C.A., Barrett, A.J., 1982. A direct spectrophotometric microassay for sulfated glycosaminoglycans in cartilage cultures. Connect Tissue Res 9, 247–248. https://doi.org/10.3109/03008208209160269
Ferraro, F., Celso, C.L., Scadden, D., 2010. Adult Stem Cells and Their Niches. Adv Exp Med Biol 695, 155–168. https://doi.org/10.1007/978-1-4419-7037-4_11
Filpula, D., 2007. Antibody engineering and modification technologies. Biomol Eng 24, 201–215. https://doi.org/10.1016/j.bioeng.2007.03.004
Foster, J.W., Wahlin, K., Adams, S.M., Birk, D.E., Zack, D.J., Chakravarti, S., 2017. Cornea organoids from human induced pluripotent stem cells. Scientific Reports 7, 41286. https://doi.org/10.1038/srep41286
Frank, N.Y., Pendse, S.S., Lapchak, P.H., Margaryan, A., Shlain, D., Doeing, C., Sayegh, M.H., Frank, M.H., 2003. Regulation of progenitor cell fusion by ABCB5 P-glycoprotein, a novel human ATP-binding cassette transporter. J. Biol. Chem. 278, 47156–47165. https://doi.org/10.1074/jbc.M308700200
Funderburgh, J.L., Caterson, B., Conrad, G.W., 1987. Distribution of proteoglycans antigenically related to corneal keratan sulfate proteoglycan. J Biol Chem 262, 11634–11640.
Funderburgh, J.L., Conrad, G.W., 1990. Isoforms of corneal keratan sulfate proteoglycan. Journal of Biological Chemistry 265, 8297–8303. https://doi.org/10.1016/S0021-9258(19)39071-4
Funderburgh, J.L., Funderburgh, M.L., Brown, S.J., Vergnes, J.P., Hassell, J.R., Mann, M.M., Conrad, G.W., 1993. Sequence and structural implications of a bovine corneal keratan sulfate proteoglycan core protein. Protein 37B represents bovine lumican and proteins 37A and 25 are unique. Journal of Biological Chemistry 268, 11874–11880. https://doi.org/10.1016/S0021-9258(19)50281-2
Funderburgh, J.L., Hevelone, N.D., Roth, M.R., Funderburgh, M.L., Rodrigues, M.R., Nirankari, V.S., Conrad, G.W., 1998. Decorin and biglycan of normal and pathologic human corneas. Invest. Ophthalmol. Vis. Sci. 39, 1957–1964.
Galindo, L.T., Mundim, M.T.V.V., Pinto, A.S., Chiarantin, G.M.D., Almeida, M.E.S., Lamers, M.L., Horwitz, A.R., Santos, M.F., Porcionatto, M., 2018. Chondroitin Sulfate Impairs Neural Stem Cell Migration Through ROCK Activation. Mol Neurobiol 55, 3185–3195. https://doi.org/10.1007/s12035-017-0565-8
García, B., García-Suárez, O., Merayo-Lloves, J., Alcalde, I., Alfonso, J.F., Cueto, L.F.-V., Meana, Á., Vázquez, F., Quirós, L.M., 2016. Differential Expression of Proteoglycans by Corneal Stromal Cells in Keratoconus. Invest. Ophthalmol. Vis. Sci. 57, 2618–2628. https://doi.org/10.1167/iovs.15-16692
Gealy, E.C., Kerr, B.C., Young, R.D., Tudor, D., Hayes, A.J., Hughes, C.E., Caterson, B., Quantock, A.J., Ralphs, J.R., 2007. Differential expression of the keratan sulphate proteoglycan, keratocan, during chick corneal embryogenesis. Histochem Cell Biol 128, 551–555. https://doi.org/10.1007/s00418-007-0332-4
Gesteira, T.F., Sun, M., Coulson-Thomas, Y.M., Yamaguchi, Y., Yeh, L.-K., Hascall, V., Coulson-Thomas, V.J., 2017. Hyaluronan Rich

Microenvironment in the Limbal Stem Cell Niche Regulates Limbal Stem Cell Differentiation. Investigative Ophthalmology & Visual Science 58, 4407–4421. https://doi.org/10.1167/iovs.17-22326
Gomes, J.A.P., Geraldes Monteiro, B., Melo, G.B., Smith, R.L., Cavenaghi Pereira da Silva, M., Lizier, N.F., Kerkis, A., Cerruti, H., Kerkis, I., 2010. Corneal reconstruction with tissue-engineered cell sheets composed of human immature dental pulp stem cells. Invest Ophthalmol Vis Sci 51, 1408–1414. https://doi.org/10.1167/iovs.09-4029
Gonzalez, G., Sasamoto, Y., Ksander, B.R., Frank, M.H., Frank, N.Y., 2018. Limbal stem cells: identity, developmental origin, and therapeutic potential. Wiley Interdisciplinary Reviews: Developmental Biology 7, e303. https://doi.org/10.1002/wdev.303
Gordon, M.K., Hahn, R.A., 2010. Collagens. Cell Tissue Res 339, 247–257. https://doi.org/10.1007/s00441-009-0844-4
Graw, J., 2010. Eye development. Curr. Top. Dev. Biol. 90, 343–386. https://doi.org/10.1016/S0070-2153(10)90010-0
Gregory, J.D., Cöster, L., Damle, S.P., 1982. Proteoglycans of rabbit corneal stroma. Isolation and partial characterization. Journal of Biological Chemistry 257, 6965–6970. https://doi.org/10.1016/S0021-9258(18)34524-1
Grieve, K., Ghoubay, D., Georgeon, C., Thouvenin, O., Bouheraoua, N., Paques, M., Borderie, V.M., 2015. Three-dimensional structure of the mammalian limbal stem cell niche. Experimental Eye Research 140, 75–84. https://doi.org/10.1016/j.exer.2015.08.003
Gupta, S., Buyank, F., Sinha, N.R., Grant, D.G., Sinha, P.R., Iozzo, R.V., Chaurasia, S.S., Mohan, R.R., 2022. Decorin regulates collagen fibrillogenesis during corneal wound healing in mouse in vivo. Experimental Eye Research 216, 108933. https://doi.org/10.1016/j.exer.2022.108933
Haagdorens, M., Van Acker, S.I., Van Gerwen, V., Ní Dhubhghaill, S., Koppen, C., Tassignon, M.-J., Zakaria, N., 2016. Limbal Stem Cell Deficiency: Current Treatment Options and Emerging Therapies. Stem Cells Int 2016. https://doi.org/10.1155/2016/9798374
Hammond, G.M., 2021. The microanatomy of Bowman's layer in the cornea of the pig: Changes in collagen fibril architecture at the corneoscleral limbus. European Journal of Anatomy 24, 399–406.
Hara, H., Cooper, D.K.C., 2011. Xenotransplantation - The Future of Corneal Transplantation? Cornea 30, 371–378. https://doi.org/10.1097/ICO.0b013e3181f237ef
Hashmani, K., Branch, M.J., Sidney, L.E., Dhillon, P.S., Verma, M., McIntosh, O.D., Hopkinson, A., Dua, H.S., 2013. Characterization of corneal stromal stem cells with the potential for epithelial transdifferentiation. Stem Cell Research & Therapy 4, 75. https://doi.org/10.1186/scrt226
Hay, E.D., 1980. Development of the vertebrate cornea. Int Rev Cytol 63, 263–322. https://doi.org/10.1016/s0074-7696(08)61760-x
Hayashi, R., Ishikawa, Y., Ito, M., Kageyama, T., Takashiba, K., Fujioka, T., Tsujikawa, M., Miyoshi, H., Yamato, M., Nakamura, Y., Nishida, K., 2012. Generation of corneal epithelial cells from induced pluripotent stem cells derived from human dermal fibroblast and corneal limbal epithelium. PLoS ONE 7, e45435. https://doi.org/10.1371/journal.pone.0045435

Hayashi, R., Ishikawa, Y., Katayama, T., Quantock, A.J., Nishida, K., 2018. CD200 facilitates the isolation of corneal epithelial cells derived from human pluripotent stem cells. Scientific Reports 8. https://doi.org/10.1038/s41598-018-34845-2

Hayashi, R., Ishikawa, Y., Katori, R., Sasamoto, Y., Taniwaki, Y., Takayanagi, H., Tsujikawa, M., Sekiguchi, K., Quantock, A.J., Nishida, K., 2017. Coordinated generation of multiple ocular-like cell lineages and fabrication of functional corneal epithelial cell sheets from human iPS cells. Nature Protocols 12, 683–696. https://doi.org/10.1038/nprot.2017.007

Hayashi, R., Ishikawa, Y., Sasamoto, Y., Katori, R., Nomura, N., Ichikawa, T., Araki, S., Soma, T., Kawasaki, S., Sekiguchi, K., Quantock, A.J., Tsujikawa, M., Nishida, K., 2016. Co-ordinated ocular development from human iPS cells and recovery of corneal function. Nature 531, 376–380. https://doi.org/10.1038/nature17000

Hayashi, R., Okubo, T., Kudo, Y., Ishikawa, Y., Imaizumi, T., Suzuki, K., Shibata, S., Katayama, T., Park, S.-J., Young, R.D., Quantock, A.J., Nishida, K., 2022. Generation of 3D lacrimal gland organoids from human pluripotent stem cells. Nature 605, 126–131. https://doi.org/10.1038/s41586-022-04613-4

Hayes, A., Sugahara, K., Farrugia, B., Whitelock, J.M., Caterson, B., Melrose, J., 2018. Biodiversity of CS-proteoglycan sulphation motifs: chemical messenger recognition modules with roles in information transfer, control of cellular behaviour and tissue morphogenesis. Biochemical Journal 475, 587–620. https://doi.org/10.1042/BCJ20170820

Hayes, A.J., Hughes, C.E., Smith, S.M., Caterson, B., Little, C.B., Melrose, J., 2016. The CS Sulfation Motifs 4C3, 7D4, 3B3[−]; and Perlecan Identify Stem Cell Populations and Their Niches, Activated Progenitor Cells and Transitional Areas of Tissue Development in the Fetal Human Elbow. Stem Cells and Development 25, 836–847. https://doi.org/10.1089/scd.2016.0054

Hayes, A.J., Tudor, D., Nowell, M.A., Caterson, B., Hughes, C.E., 2008. Chondroitin Sulfate Sulfation Motifs as Putative Biomarkers for Isolation of Articular Cartilage Progenitor Cells. J Histochem Cytochem 56, 125–138. https://doi.org/10.1369/jhc.7A7320.2007

Ho, L.T.Y., Harris, A.M., Tanioka, H., Yagi, N., Kinoshita, S., Caterson, B., Quantock, A.J., Young, R.D., Meek, K.M., 2014. A comparison of glycosaminoglycan distributions, keratan sulphate sulphation patterns and collagen fibril architecture from central to peripheral regions of the bovine cornea. Matrix Biol 38, 59–68. https://doi.org/10.1016/j.matbio.2014.06.004

Hof, D.J., Versteeg, E.M.M., Lest, C.H.A. van de, Daamen, W.F., Kuppevelt, T.H. van, 2019. A versatile salt-based method to immobilize glycosaminoglycans and create growth factor gradients. Glycoconj J 36, 227–236. https://doi.org/10.1007/s10719-019-09872-4

Holland, E.J., 1996. Epithelial transplantation for the management of severe ocular surface disease. Trans Am Ophthalmol Soc 94, 677–743.

Hongisto, H., Ilmarinen, T., Vattulainen, M., Mikhailova, A., Skottman, H., 2017. Xeno- and feeder-free differentiation of human pluripotent stem cells to two distinct ocular epithelial cell types using simple modifications of one

method. Stem Cell Res Ther 8. https://doi.org/10.1186/s13287-017-0738-4
Huang, A.J., Tseng, S.C., 1991. Corneal epithelial wound healing in the absence of limbal epithelium. Invest Ophthalmol Vis Sci 32, 96–105.
Ihanamäki, T., Pelliniemi, L.J., Vuorio, E., 2004. Collagens and collagen-related matrix components in the human and mouse eye. Progress in Retinal and Eye Research 23, 403–434. https://doi.org/10.1016/j.preteyeres.2004.04.002
Ilari, L., Daya, S.M., 2002. Long-term outcomes of keratolimbal allograft for the treatment of severe ocular surface disorders. Ophthalmology 109, 1278–1284. https://doi.org/10.1016/s0161-6420(02)01081-3
Iozzo, R.V., 1997. The family of the small leucine-rich proteoglycans: key regulators of matrix assembly and cellular growth. Crit Rev Biochem Mol Biol 32, 141–174. https://doi.org/10.3109/10409239709108551
Ishii, M., Maeda, N., 2008. Oversulfated chondroitin sulfate plays critical roles in the neuronal migration in the cerebral cortex. J Biol Chem 283, 32610–32620. https://doi.org/10.1074/jbc.M806331200
Ji, Y., Zhang, S., Qiao, M., Jiao, R., Li, J., Song, P., Zhang, X., Huang, H., 2020. Synthesis of structurally defined chondroitin sulfate: Paving the way to the structure-activity relationship studies. Carbohydrate Polymers 248, 116796. https://doi.org/10.1016/j.carbpol.2020.116796
Kadler, K.E., Hill, A., Canty-Laird, E.G., 2008. Collagen fibrillogenesis: fibronectin, integrins, and minor collagens as organizers and nucleators. Curr. Opin. Cell Biol. 20, 495–501. https://doi.org/10.1016/j.ceb.2008.06.008
Karamanos, N.K., Piperigkou, Z., Theocharis, A.D., Watanabe, H., Franchi, M., Baud, S., Brézillon, S., Götte, M., Passi, A., Vigetti, D., Ricard-Blum, S., Sanderson, R.D., Neill, T., Iozzo, R.V., 2018. Proteoglycan Chemical Diversity Drives Multifunctional Cell Regulation and Therapeutics. Chem. Rev. 118, 9152–9232. https://doi.org/10.1021/acs.chemrev.8b00354
Kawakita, T., Shimmura, S., Higa, K., Espana, E.M., He, H., Shimazaki, J., Tsubota, K., Tseng, S.C.G., 2009. Greater Growth Potential of p63-Positive Epithelial Cell Clusters Maintained in Human Limbal Epithelial Sheets. Invest Ophthalmol Vis Sci 50, 4611–4617. https://doi.org/10.1167/iovs.08-2586
Kenyon, K.R., Tseng, S.C., 1989. Limbal autograft transplantation for ocular surface disorders. Ophthalmology 96, 709–722; discussion 722-723. https://doi.org/10.1016/s0161-6420(89)32833-8
Kerr, B.C., 2005. Keratan sulphate metabolism in connective tissue proteoglycans (phd). Cardiff University.
Kiani, C., Chen, L., Wu, Y.J., Yee, A.J., Yang, B.B., 2002. Structure and function of aggrecan. Cell Research 12, 19–32. https://doi.org/10.1038/sj.cr.7290106
Kitazawa, K., Hikichi, T., Nakamura, T., Sotozono, C., Kinoshita, S., Masui, S., 2017. PAX6 regulates human corneal epithelium cell identity. Experimental Eye Research 154, 30–38. https://doi.org/10.1016/j.exer.2016.11.005
Koike, T., Izumikawa, T., Sato, B., Kitagawa, H., 2014. Identification of Phosphatase That Dephosphorylates Xylose in the Glycosaminoglycan-

Protein Linkage Region of Proteoglycans. J Biol Chem 289, 6695–6708. https://doi.org/10.1074/jbc.M113.520536
Ksander, B.R., Kolovou, P.E., Wilson, B.J., Saab, K.R., Guo, Q., Ma, J., McGuire, S.P., Gregory, M.S., Vincent, W.J.B., Perez, V.L., Cruz-Guilloty, F., Kao, W.W.Y., Call, M.K., Tucker, B.A., Zhan, Q., Murphy, G.F., Lathrop, K.L., Alt, C., Mortensen, L.J., Lin, C.P., Zieske, J.D., Frank, M.H., Frank, N.Y., 2014. ABCB5 is a limbal stem cell gene required for corneal development and repair. Nature 511, 353–357. https://doi.org/10.1038/nature13426
Kureshi, A.K., Dziasko, M., Funderburgh, J.L., Daniels, J.T., 2015. Human corneal stromal stem cells support limbal epithelial cells cultured on RAFT tissue equivalents. Sci Rep 5, 16186. https://doi.org/10.1038/srep16186
Kurpakus, M.A., Maniaci, M.T., Esco, M., 1994. Expression of keratins K12, K4 and K14 during development of ocular surface epithelium. Curr Eye Res 13, 805–814. https://doi.org/10.3109/02713689409025135
Kwitko, S., Marinho, D., Barcaro, S., Bocaccio, F., Rymer, S., Fernandes, S., Neumann, J., 1995. Allograft conjunctival transplantation for bilateral ocular surface disorders. Ophthalmology 102, 1020–1025. https://doi.org/10.1016/s0161-6420(95)30918-9
LaBarge, M.A., Nelson, C.M., Villadsen, R., Fridriksdottir, A., Ruth, J.R., Stampfer, M.R., Petersen, O.W., Bissell, M.J., 2009. Human mammary progenitor cell fate decisions are products of interactions with combinatorial microenvironments. Integrative Biology 1, 70–79. https://doi.org/10.1039/b816472j
Lai, J.-Y., 2013. Corneal Stromal Cell Growth on Gelatin/Chondroitin Sulfate Scaffolds Modified at Different NHS/EDC Molar Ratios. International Journal of Molecular Sciences 14, 2036–2055. https://doi.org/10.3390/ijms14012036
Lai, J.-Y., Li, Y.-T., Cho, C.-H., Yu, T.-C., 2012. Nanoscale modification of porous gelatin scaffolds with chondroitin sulfate for corneal stromal tissue engineering. Int J Nanomedicine 7, 1101–1114. https://doi.org/10.2147/IJN.S28753
Lakowski, J., Gonzalez-Cordero, A., West, E.L., Han, Y.-T., Welby, E., Naeem, A., Blackford, S.J.I., Bainbridge, J.W.B., Pearson, R.A., Ali, R.R., Sowden, J.C., 2015. Transplantation of Photoreceptor Precursors Isolated via a Cell Surface Biomarker Panel From Embryonic Stem Cell-Derived Self-Forming Retina. Stem Cells 33, 2469–2482. https://doi.org/10.1002/stem.2051
Lakowski, J., Welby, E., Budinger, D., Di Marco, F., Di Foggia, V., Bainbridge, J.W.B., Wallace, K., Gamm, D.M., Ali, R.R., Sowden, J.C., 2018. Isolation of Human Photoreceptor Precursors via a Cell Surface Marker Panel from Stem Cell-Derived Retinal Organoids and Fetal Retinae. Stem Cells 36, 709–722. https://doi.org/10.1002/stem.2775
Lavker, R.M., Sun, T.-T., 2000. Epidermal stem cells: Properties, markers, and location. Proceedings of the National Academy of Sciences 97, 13473–13475. https://doi.org/10.1073/pnas.250380097
Lee, H.S., Osuga, D.T., Nashef, A.S., Ahmed, A.I., Whitaker, J.R., Feeney, R.E., 1977. Effects of alkali on glycoproteins. .beta.-Elimination and nucleophilic addition reactions of substituted threonyl residues of antifreeze glycoprotein. J. Agric. Food Chem. 25, 1153–1158. https://doi.org/10.1021/jf60213a057

Lehrer, M.S., Sun, T.T., Lavker, R.M., 1998. Strategies of epithelial repair: modulation of stem cell and transit amplifying cell proliferation. Journal of Cell Science 111, 2867–2875. https://doi.org/10.1242/jcs.111.19.2867
Leonard, D.W., Meek, K.M., 1997. Refractive indices of the collagen fibrils and extrafibrillar material of the corneal stroma. Biophys J 72, 1382–1387. https://doi.org/10.1016/S0006-3495(97)78784-8
Levis, H.J., Daniels, J.T., 2016. Recreating the Human Limbal Epithelial Stem Cell Niche with Bioengineered Limbal Crypts. Current Eye Research 41, 1153–1160. https://doi.org/10.3109/02713683.2015.1095932
Li, D.-Q., Kim, S., Li, J.-M., Gao, Q., Choi, J., Bian, F., Hu, J., Zhang, Y., Li, J., Lu, R., Li, Y., Pflugfelder, S.C., Miao, H., Chen, R., 2021. Single-cell transcriptomics identifies limbal stem cell population and cell types mapping its differentiation trajectory in limbal basal epithelium of human cornea. Ocul Surf 20, 20–32. https://doi.org/10.1016/j.jtos.2020.12.004
Li, S., Cui, Z., Gu, J., Wang, Y., Tang, S., Chen, J., 2021. Effect of porcine corneal stromal extract on keratocytes from SMILE-derived lenticules. Journal of Cellular and Molecular Medicine 25, 1207–1220. https://doi.org/10.1111/jcmm.16189
Liang, L., Sheha, H., Li, J., Tseng, S.C.G., 2009. Limbal stem cell transplantation: new progresses and challenges. Eye (Lond) 23, 1946–1953. https://doi.org/10.1038/eye.2008.379
Linhardt, R.J., Liu, J., 2012. Synthetic heparin. Curr Opin Pharmacol 12, 217–219. https://doi.org/10.1016/j.coph.2011.12.002
Livak, K.J., Schmittgen, T.D., 2001. Analysis of relative gene expression data using real-time quantitative PCR and the 2(-Delta Delta C(T)) Method. Methods 25, 402–408. https://doi.org/10.1006/meth.2001.1262
Lund, R.J., Nikula, T., Rahkonen, N., Närvä, E., Baker, D., Harrison, N., Andrews, P., Otonkoski, T., Lahesmaa, R., 2012. High-throughput karyotyping of human pluripotent stem cells. Stem Cell Res 9, 192–195. https://doi.org/10.1016/j.scr.2012.06.008
Ly, M., Laremore, T.N., Linhardt, R.J., 2010. Proteoglycomics: Recent Progress and Future Challenges. OMICS 14, 389–399. https://doi.org/10.1089/omi.2009.0123
Maccari, F., Volpi, N., 2002. Glycosaminoglycan blotting on nitrocellulose membranes treated with cetylpyridinium chloride after agarose-gel electrophoretic separation. Electrophoresis 23, 3270–3277. https://doi.org/10.1002/1522-2683(200210)23:19<3270::AID-ELPS3270>3.0.CO;2-I
McKee, H.D., Irion, L.C.D., Carley, F.M., Jhanji, V., Brahma, A.K., 2011. Residual corneal stroma in big-bubble deep anterior lamellar keratoplasty: a histological study in eye-bank corneas. British Journal of Ophthalmology 95, 1463–1465. https://doi.org/10.1136/bjophthalmol-2011-300360
Meek, K.M., 2009. Corneal collagen—its role in maintaining corneal shape and transparency. Biophys Rev 1, 83–93. https://doi.org/10.1007/s12551-009-0011-x
Mellough, C.B., Collin, J., Khazim, M., White, K., Sernagor, E., Steel, D.H.W., Lako, M., 2015. IGF-1 Signaling Plays an Important Role in the Formation of Three-Dimensional Laminated Neural Retina and Other Ocular

Structures From Human Embryonic Stem Cells. Stem Cells 33, 2416–2430. https://doi.org/10.1002/stem.2023
Melrose, J., Fuller, E.S., Roughley, P.J., Smith, M.M., Kerr, B., Hughes, C.E., Caterson, B., Little, C.B., 2008. Fragmentation of decorin, biglycan, lumican and keratocan is elevated in degenerate human meniscus, knee and hip articular cartilages compared with age-matched macroscopically normal and control tissues. Arthritis Res Ther 10, R79. https://doi.org/10.1186/ar2453
Merril, C.R., Harrington, M., Alley, V., 1984. A photodevelopment silver stain for the rapid visualization of proteins separated on polyacrylamide gels. ELECTROPHORESIS 5, 289–297. https://doi.org/10.1002/elps.1150050509
Meyer, J.S., Shearer, R.L., Capowski, E.E., Wright, L.S., Wallace, K.A., McMillan, E.L., Zhang, S.-C., Gamm, D.M., 2009. Modeling early retinal development with human embryonic and induced pluripotent stem cells. Proc Natl Acad Sci U S A 106, 16698–16703. https://doi.org/10.1073/pnas.0905245106
Mikhailova, A., Ilmarinen, T., Ratnayake, A., Petrovski, G., Uusitalo, H., Skottman, H., Rafat, M., 2016. Human pluripotent stem cell-derived limbal epithelial stem cells on bioengineered matrices for corneal reconstruction. Exp Eye Res 146, 26–34. https://doi.org/10.1016/j.exer.2015.11.021
Miyazaki, T., Futaki, S., Suemori, H., Taniguchi, Y., Yamada, M., Kawasaki, M., Hayashi, M., Kumagai, H., Nakatsuji, N., Sekiguchi, K., Kawase, E., 2012. Laminin E8 fragments support efficient adhesion and expansion of dissociated human pluripotent stem cells. Nat Commun 3, 1236. https://doi.org/10.1038/ncomms2231
Moffatt, P., Geng, Y., Lamplugh, L., Nanci, A., Roughley, P., 2017. Absence of the dermatan sulfate chain of decorin does not affect mouse development. Journal of Negative Results in BioMedicine 16. https://doi.org/10.1186/s12952-017-0074-3
Mollaaghababa, R., Pavan, W.J., 2003. The importance of having your SOX on: role of SOX10 in the development of neural crest-derived melanocytes and glia. Oncogene 22, 3024–3034. https://doi.org/10.1038/sj.onc.1206442
Mukhey, D., Phillips, J.B., Daniels, J.T., Kureshi, A.K., 2018. Controlling human corneal stromal stem cell contraction to mediate rapid cell and matrix organization of real architecture for 3-dimensional tissue equivalents. Acta Biomaterialia 67, 229–237. https://doi.org/10.1016/j.actbio.2017.11.047
Mutoji, K.N., Sun, M., Elliott, G., Moreno, I.Y., Hughes, C., Gesteira, T.F., Coulson-Thomas, V.J., 2021. Extracellular Matrix Deposition and Remodeling after Corneal Alkali Burn in Mice. Int J Mol Sci 22, 5708. https://doi.org/10.3390/ijms22115708
Myhre, E.B., Erntell, M., 1985. A non-immune interaction between the light chain of human immunoglobulin and a surface component of a Peptococcus magnus strain. Mol Immunol 22, 879–885. https://doi.org/10.1016/0161-5890(85)90073-2
Nakamura, T., Inatomi, T., Sotozono, C., Amemiya, T., Kanamura, N., Kinoshita, S., 2004. Transplantation of cultivated autologous oral mucosal epithelial cells in patients with severe ocular surface disorders. Br J Ophthalmol 88, 1280–1284. https://doi.org/10.1136/bjo.2003.038497

Nakano, T., Ando, S., Takata, N., Kawada, M., Muguruma, K., Sekiguchi, K., Saito, K., Yonemura, S., Eiraku, M., Sasai, Y., 2012. Self-Formation of Optic Cups and Storable Stratified Neural Retina from Human ESCs. Cell Stem Cell 10, 771–785. https://doi.org/10.1016/j.stem.2012.05.009
Nakazawa, K., Newsome, D.A., Nilsson, B., Hascall, V.C., Hassell, J.R., 1983. Purification of keratan sulfate proteoglycan from monkey cornea. J Biol Chem 258, 6051–6055.
Natunen, S., Satomaa, T., Pitkänen, V., Salo, H., Mikkola, M., Natunen, J., Otonkoski, T., Valmu, L., 2011. The binding specificity of the marker antibodies Tra-1-60 and Tra-1-81 reveals a novel pluripotency-associated type 1 lactosamine epitope. Glycobiology 21, 1125–1130. https://doi.org/10.1093/glycob/cwq209
Nilsson, B., De Luca, S., Lohmander, S., Hascall, V.C., 1982. Structures of N-linked and O-linked oligosaccharides on proteoglycan monomer isolated from the Swarm rat chondrosarcoma. J Biol Chem 257, 10920–10927.
Nishida, K., Yamato, M., Hayashida, Y., Watanabe, K., Yamamoto, K., Adachi, E., Nagai, S., Kikuchi, A., Maeda, N., Watanabe, H., Okano, T., Tano, Y., 2004. Corneal Reconstruction with Tissue-Engineered Cell Sheets Composed of Autologous Oral Mucosal Epithelium. New England Journal of Medicine 351, 1187–1196. https://doi.org/10.1056/NEJMoa040455
Nishina, S., Kohsaka, S., Yamaguchi, Y., Handa, H., Kawakami, A., Fujisawa, H., Azuma, N., 1999. PAX6 expression in the developing human eye. Br J Ophthalmol 83, 723–727.
Ogura, C., Hirano, K., Mizumoto, S., Yamada, S., Nishihara, S., 2021. Dermatan sulphate promotes neuronal differentiation in mouse and human stem cells. J Biochem 169, 55–64. https://doi.org/10.1093/jb/mvaa087
Osmond, M., Bernier, S.M., Pantcheva, M.B., Krebs, M.D., 2017. Collagen and collagen-chondroitin sulfate scaffolds with uniaxially aligned pores for the biomimetic, three dimensional culture of trabecular meshwork cells. Biotechnol. Bioeng. 114, 915–923. https://doi.org/10.1002/bit.26206
Pacella, E., Pacella, F., De Paolis, G., Parisella, F.R., Turchetti, P., Anello, G., Cavallotti, C., 2015. Glycosaminoglycans in the Human Cornea: Age-Related Changes. Ophthalmol Eye Dis 7, 1–5. https://doi.org/10.4137/OED.S17204
Pellegrini, G., Golisano, O., Paterna, P., Lambiase, A., Bonini, S., Rama, P., De Luca, M., 1999. Location and Clonal Analysis of Stem Cells and Their Differentiated Progeny in the Human Ocular Surface. J Cell Biol 145, 769–782.
Pellegrini, G., Lambiase, A., Macaluso, C., Pocobelli, A., Deng, S., Cavallini, G.M., Esteki, R., Rama, P., 2016. From discovery to approval of an advanced therapy medicinal product-containing stem cells, in the EU. Regen Med 11, 407–420. https://doi.org/10.2217/rme-2015-0051
Pellegrini, G., Traverso, C.E., Franzi, A.T., Zingirian, M., Cancedda, R., Luca, M.D., 1997. Long-term restoration of damaged corneal surfaces with autologous cultivated corneal epithelium. The Lancet 349, 990–993. https://doi.org/10.1016/S0140-6736(96)11188-0
Perris, R., Johansson, S., 1990. Inhibition of neural crest cell migration by aggregating chondroitin sulfate proteoglycans is mediated by their hyaluronan-binding region. Developmental Biology 137, 1–12. https://doi.org/10.1016/0012-1606(90)90002-Z

Polisetti, N., Roschinski, B., Schlötzer-Schrehardt, U., Maier, P., Schlunck, G., Reinhard, T., 2021a. A Decellularized Human Limbal Scaffold for Limbal Stem Cell Niche Reconstruction. Int J Mol Sci 22, 10067. https://doi.org/10.3390/ijms221810067

Polisetti, N., Schmid, A., Schlötzer-Schrehardt, U., Maier, P., Lang, S.J., Steinberg, T., Schlunck, G., Reinhard, T., 2021b. A decellularized human corneal scaffold for anterior corneal surface reconstruction. Sci Rep 11, 2992. https://doi.org/10.1038/s41598-021-82678-3

Polisetti, N., Zenkel, M., Menzel-Severing, J., Kruse, F.E., Schlötzer-Schrehardt, U., 2016. Cell Adhesion Molecules and Stem Cell-Niche-Interactions in the Limbal Stem Cell Niche. STEM CELLS 34, 203–219. https://doi.org/10.1002/stem.2191

Poole, C.A., Brookes, N.H., Clover, G.M., 1993. Keratocyte networks visualised in the living cornea using vital dyes. Journal of Cell Science 106, 685–691.

Prydz, K., 2015. Determinants of Glycosaminoglycan (GAG) Structure. Biomolecules 5, 2003–2022. https://doi.org/10.3390/biom5032003

Prydz, K., Dalen, K.T., 2000. Synthesis and sorting of proteoglycans. J Cell Sci 113, 193–205.

Purushothaman, A., Sugahara, K., Faissner, A., 2012. Chondroitin Sulfate "Wobble Motifs" Modulate Maintenance and Differentiation of Neural Stem Cells and Their Progeny. J Biol Chem 287, 2935–2942. https://doi.org/10.1074/jbc.R111.298430

Rada, Jody A., Cornuet, P.K., Hassell, J.R., 1993. Regulation of Corneal Collagen Fibrillogenesis In Vitro by Corneal Proteoglycan (Lumican and Decorin) Core Proteins. Experimental Eye Research 56, 635–648. https://doi.org/10.1006/exer.1993.1081

Radner, W., Zehetmayer, M., Aufreiter, R., Mallinger, R., 1998. Interlacing and cross-angle distribution of collagen lamellae in the human cornea. Cornea 17, 537–543.

Rama, P., Matuska, S., Paganoni, G., Spinelli, A., De Luca, M., Pellegrini, G., 2010. Limbal Stem-Cell Therapy and Long-Term Corneal Regeneration. New England Journal of Medicine 363, 147–155. https://doi.org/10.1056/NEJMoa0905955

Reichman, S., Terray, A., Slembrouck, A., Nanteau, C., Orieux, G., Habeler, W., Nandrot, E.F., Sahel, J.-A., Monville, C., Goureau, O., 2014. From confluent human iPS cells to self-forming neural retina and retinal pigmented epithelium. Proc. Natl. Acad. Sci. U.S.A. 111, 8518–8523. https://doi.org/10.1073/pnas.1324212111

Ricard-Blum, S., 2011. The Collagen Family. Cold Spring Harb Perspect Biol 3. https://doi.org/10.1101/cshperspect.a004978

Ricciardelli, C., Russell, D.L., Ween, M.P., Mayne, K., Suwiwat, S., Byers, S., Marshall, V.R., Tilley, W.D., Horsfall, D.J., 2007. Formation of hyaluronan- and versican-rich pericellular matrix by prostate cancer cells promotes cell motility. J Biol Chem 282, 10814–10825. https://doi.org/10.1074/jbc.M606991200

Roch, A., Giger, S., Girotra, M., Campos, V., Vannini, N., Naveiras, O., Gobaa, S., Lutolf, M.P., 2017. Single-cell analyses identify bioengineered niches for enhanced maintenance of hematopoietic stem cells. Nat Commun 8. https://doi.org/10.1038/s41467-017-00291-3

Rodriguez, E., Roland, S.K., Plaas, A., Roughley, P.J., 2006. The Glycosaminoglycan Attachment Regions of Human Aggrecan *. Journal of Biological Chemistry 281, 18444–18450. https://doi.org/10.1074/jbc.M512531200
Romano, A.C., Espana, E.M., Yoo, S.H., Budak, M.T., Wolosin, J.M., Tseng, S.C.G., 2003. Different cell sizes in human limbal and central corneal basal epithelia measured by confocal microscopy and flow cytometry. Invest. Ophthalmol. Vis. Sci. 44, 5125–5129.
Roughley, P.J., White, R.J., Magny, M.C., Liu, J., Pearce, R.H., Mort, J.S., 1993. Non-proteoglycan forms of biglycan increase with age in human articular cartilage. Biochem J 295, 421–426.
Rüfer, F., Schröder, A., Erb, C., 2005. White-to-white Corneal Diameter: Normal Values in Healthy Humans Obtained With the Orbscan Ii Topography System. Cornea 24, 259–261. https://doi.org/10.1097/01.ico.0000148312.01805.53
Säämänen, A.M., Tammi, M., 1984. Determination of unsaturated glycosaminoglycan disaccharides by spectrophotometry on thin-layer chromatographic plates. Anal Biochem 140, 354–359. https://doi.org/10.1016/0003-2697(84)90177-5
Saika, S., Shiraishi, A., Liu, C.Y., Funderburgh, J.L., Kao, C.W., Converse, R.L., Kao, W.W., 2000. Role of lumican in the corneal epithelium during wound healing. J Biol Chem 275, 2607–2612. https://doi.org/10.1074/jbc.275.4.2607
Sangwan, V.S., Basu, S., MacNeil, S., Balasubramanian, D., 2012. Simple limbal epithelial transplantation (SLET): a novel surgical technique for the treatment of unilateral limbal stem cell deficiency. British Journal of Ophthalmology 96, 931–934. https://doi.org/10.1136/bjophthalmol-2011-301164
Santos, G.R.C., Piquet, A.A., Glauser, B.F., Tovar, A.M.F., Pereira, M.S., Vilanova, E., Mourão, P.A.S., 2017. Systematic Analysis of Pharmaceutical Preparations of Chondroitin Sulfate Combined with Glucosamine. Pharmaceuticals 10, 38. https://doi.org/10.3390/ph10020038
Schatton, T., Murphy, G.F., Frank, N.Y., Yamaura, K., Waaga-Gasser, A.M., Gasser, M., Zhan, Q., Jordan, S., Duncan, L.M., Weishaupt, C., Fuhlbrigge, R.C., Kupper, T.S., Sayegh, M.H., Frank, M.H., 2008. Identification of cells initiating human melanomas. Nature 451, 345–349. https://doi.org/10.1038/nature06489
Schlötzer-Schrehardt, U., Dietrich, T., Saito, K., Sorokin, L., Sasaki, T., Paulsson, M., Kruse, F.E., 2007. Characterization of extracellular matrix components in the limbal epithelial stem cell compartment. Experimental Eye Research 85, 845–860. https://doi.org/10.1016/j.exer.2007.08.020
Shalom-Feuerstein, R., Serror, L., De La Forest Divonne, S., Petit, I., Aberdam, E., Camargo, L., Damour, O., Vigouroux, C., Solomon, A., Gaggioli, C., Itskovitz-Eldor, J., Ahmad, S., Aberdam, D., 2012. Pluripotent stem cell model reveals essential roles for miR-450b-5p and miR-184 in embryonic corneal lineage specification. Stem Cells 30, 898–909. https://doi.org/10.1002/stem.1068
Shanbhag, S.S., Patel, C.N., Goyal, R., Donthineni, P.R., Singh, V., Basu, S., 2019. Simple limbal epithelial transplantation (SLET): Review of indications, surgical technique, mechanism, outcomes, limitations, and

impact. Indian J Ophthalmol 67, 1265–1277. https://doi.org/10.4103/ijo.IJO_117_19
Sharifi, R., Yang, Y., Adibnia, Y., Dohlman, C.H., Chodosh, J., Gonzalez-Andrades, M., 2019. Finding an Optimal Corneal Xenograft Using Comparative Analysis of Corneal Matrix Proteins Across Species. Scientific Reports 9, 1876. https://doi.org/10.1038/s41598-018-38342-4
Sheng, W., Wang, G., Wang, Y., Liang, J., Wen, J., Zheng, P.-S., Wu, Y., Lee, V., Slingerland, J., Dumont, D., Yang, B.B., 2005. The Roles of Versican V1 and V2 Isoforms in Cell Proliferation and Apoptosis. Mol Biol Cell 16, 1330–1340. https://doi.org/10.1091/mbc.E04-04-0295
Shibata, S., Hayashi, R., Kudo, Y., Okubo, T., Imaizumi, T., Katayama, T., Ishikawa, Y., Kobayashi, Y., Toga, J., Taniguchi, Y., Honma, Y., Sekiguchi, K., Nishida, K., 2020. Cell-Type-Specific Adhesiveness and Proliferation Propensity on Laminin Isoforms Enable Purification of iPSC-Derived Corneal Epithelium. Stem Cell Reports 14, 663–676. https://doi.org/10.1016/j.stemcr.2020.02.008
Shibata, S., Hayashi, R., Okubo, T., Kudo, Y., Katayama, T., Ishikawa, Y., Toga, J., Yagi, E., Honma, Y., Quantock, A.J., Sekiguchi, K., Nishida, K., 2018. Selective Laminin-Directed Differentiation of Human Induced Pluripotent Stem Cells into Distinct Ocular Lineages. Cell Reports 25, 1668–1679.e5. https://doi.org/10.1016/j.celrep.2018.10.032
Shiraki, N., Maruyama, K., Hayashi, R., Oguchi, A., Murakawa, Y., Katayama, T., Takigawa, T., Sakimoto, S., Quantock, A.J., Tsujikawa, M., Nishida, K., 2022. PAX6-positive microglia evolve locally in hiPSC-derived ocular organoids. Stem Cell Reports 17, 221–230. https://doi.org/10.1016/j.stemcr.2021.12.009
Shortt, A.J., Secker, G.A., Munro, P.M., Khaw, P.T., Tuft, S.J., Daniels, J.T., 2007. Characterization of the Limbal Epithelial Stem Cell Niche: Novel Imaging Techniques Permit In Vivo Observation and Targeted Biopsy of Limbal Epithelial Stem Cells. Stem Cells 25, 1402–1409. https://doi.org/10.1634/stemcells.2006-0580
Silver, D.J., Silver, J., 2014. Contributions of Chondroitin Sulfate Proteoglycans to Neurodevelopment, Injury, and Cancer. Curr Opin Neurobiol 0, 171–178. https://doi.org/10.1016/j.conb.2014.03.016
Sorrell, J.M., Carrino, D.A., Caplan, A.I., 1993. Structural Domains in Chondroitin Sulfate Identified by Anti-Chondroitin Sulfate Monoclonal Antibodies. Immunosequencing of Chondroitin Sulfates. Matrix 13, 351–361. https://doi.org/10.1016/S0934-8832(11)80040-5
Sorrell, J.M., Mahmoodian, F., Schafer, I.A., Davis, B., Caterson, B., 1990. Identification of monoclonal antibodies that recognize novel epitopes in native chondroitin/dermatan sulfate glycosaminoglycan chains: their use in mapping functionally distinct domains of human skin. J Histochem Cytochem. 38, 393–402. https://doi.org/10.1177/38.3.1689338
Susaimanickam, P.J., Maddileti, S., Pulimamidi, V.K., Boyinpally, S.R., Naik, R.R., Naik, M.N., Reddy, G.B., Sangwan, V.S., Mariappan, I., 2017. Generating minicorneal organoids from human induced pluripotent stem cells. Development 144, 2338–2351. https://doi.org/10.1242/dev.143040
Takahashi, K., Tanabe, K., Ohnuki, M., Narita, M., Ichisaka, T., Tomoda, K., Yamanaka, S., 2007. Induction of Pluripotent Stem Cells from Adult

Human Fibroblasts by Defined Factors. Cell 131, 861–872. https://doi.org/10.1016/j.cell.2007.11.019
Takahashi, T., Cho, H.I., Kublin, C.L., Cintron, C., 1993. Keratan sulfate and dermatan sulfate proteoglycans associate with type VI collagen in fetal rabbit cornea. J Histochem Cytochem 41, 1447–1457. https://doi.org/10.1177/41.10.8245404
Teye, K., Hashimoto, K., Numata, S., Ohta, K., Haftek, M., Hashimoto, T., 2017. Multimerization is required for antigen binding activity of an engineered IgM/IgG chimeric antibody recognizing a skin-related antigen. Sci Rep 7, 8212. https://doi.org/10.1038/s41598-017-08294-2
Thomson, J.A., Itskovitz-Eldor, J., Shapiro, S.S., Waknitz, M.A., Swiergiel, J.J., Marshall, V.S., Jones, J.M., 1998. Embryonic stem cell lines derived from human blastocysts. Science 282, 1145–1147.
Turner, S., Balain, B., Caterson, B., Morgan, C., Roberts, S., 2014. Viability, growth kinetics and stem cell markers of single and clustered cells in human intervertebral discs: implications for regenerative therapies. Eur Spine J 23, 2462–2472. https://doi.org/10.1007/s00586-014-3500-y
Ugarte, M., Geraki, K., Jeffery, G., 2016. Iron accumulates in the primate choroid of the eye with aging as revealed with synchrotron X-ray fluorescence microscopy. Metallomics 8, 1071–1080. https://doi.org/10.1039/C6MT00125D
van der Meer, J.-Y., Kellenbach, E., van den Bos, L.J., 2017. From Farm to Pharma: An Overview of Industrial Heparin Manufacturing Methods. Molecules 22, 1025. https://doi.org/10.3390/molecules22061025
Varki, A., Cummings, R.D., Esko, J.D., Stanley, P., Hart, G.W., Aebi, M., Darvill, A.G., Kinoshita, T., Packer, N.H., Prestegard, J.H., Schnaar, R.L., Seeberger, P.H. (Eds.), 2015. Essentials of Glycobiology, 3rd ed. Cold Spring Harbor Laboratory Press, Cold Spring Harbor (NY).
Vázquez, J.A., Fraguas, J., Novoa-Carvallal, R., Reis, R.L., Antelo, L.T., Pérez-Martín, R.I., Valcarcel, J., 2018. Isolation and Chemical Characterization of Chondroitin Sulfate from Cartilage By-Products of Blackmouth Catshark (Galeus melastomus). Mar Drugs 16, 344. https://doi.org/10.3390/md16100344
Vernardis, S.I., Terzoudis, K., Panoskaltsis, N., Mantalaris, A., 2017. Human embryonic and induced pluripotent stem cells maintain phenotype but alter their metabolism after exposure to ROCK inhibitor. Sci Rep 7, 42138. https://doi.org/10.1038/srep42138
Volpi, N., Maccari, F., 2015. Glycosaminoglycan Blotting and Detection After Electrophoresis Separation, in: Kurien, B.T., Scofield, R.H. (Eds.), Western Blotting: Methods and Protocols, Methods in Molecular Biology. Springer, New York, NY, pp. 119–127. https://doi.org/10.1007/978-1-4939-2694-7_16
Watanabe, K., Nishida, K., Yamato, M., Umemoto, T., Sumide, T., Yamamoto, K., Maeda, N., Watanabe, H., Okano, T., Tano, Y., 2004. Human limbal epithelium contains side population cells expressing the ATP-binding cassette transporter ABCG2. FEBS Lett. 565, 6–10. https://doi.org/10.1016/j.febslet.2004.03.064
Wen, J., Xiao, J., Rahdar, M., Choudhury, B.P., Cui, J., Taylor, G.S., Esko, J.D., Dixon, J.E., 2014. Xylose phosphorylation functions as a molecular switch

to regulate proteoglycan biosynthesis. Proc Natl Acad Sci U S A 111, 15723–15728. https://doi.org/10.1073/pnas.1417993111
Wight, T.N., Kang, I., Evanko, S.P., Harten, I.A., Chang, M.Y., Pearce, O.M.T., Allen, C.E., Frevert, C.W., 2020. Versican—A Critical Extracellular Matrix Regulator of Immunity and Inflammation. Frontiers in Immunology 11.
Wilson, S.E.M.D., Hong, J.-W.M.D., 2000. Bowman's Layer Structure and Function: Critical or Dispensable to Corneal Function? A Hypothesis. Cornea 19, 417–420.
Wollensak, J., Buddecke, E., 1990. Biochemical studies on human corneal proteoglycans--a comparison of normal and keratoconic eyes. Graefes Arch Clin Exp Ophthalmol 228, 517–523. https://doi.org/10.1007/BF00918483
Wright, A.J., Andrews, P.W., 2009. Surface marker antigens in the characterization of human embryonic stem cells. Stem Cell Res 3, 3–11. https://doi.org/10.1016/j.scr.2009.04.001
Yamada, K., Young, R.D., Lewis, P.N., Shinomiya, K., Meek, K.M., Kinoshita, S., Caterson, B., Quantock, A.J., 2015. Mesenchymal–epithelial cell interactions and proteoglycan matrix composition in the presumptive stem cell niche of the rabbit corneal limbus. Mol Vis 21, 1328–1339.
Yoon, J.J., Ismail, S., Sherwin, T., 2014. Limbal stem cells: Central concepts of corneal epithelial homeostasis. World J Stem Cells 6, 391–403. https://doi.org/10.4252/wjsc.v6.i4.391
Zhang, C., Du, L., Sun, P., Shen, L., Zhu, J., Pang, K., Wu, X., 2017. Construction of tissue-engineered full-thickness cornea substitute using limbal epithelial cell-like and corneal endothelial cell-like cells derived from human embryonic stem cells. Biomaterials 124, 180–194. https://doi.org/10.1016/j.biomaterials.2017.02.003
Zhang, G., Chen, S., Goldoni, S., Calder, B.W., Simpson, H.C., Owens, R.T., McQuillan, D.J., Young, M.F., Iozzo, R.V., Birk, D.E., 2009. Genetic Evidence for the Coordinated Regulation of Collagen Fibrillogenesis in the Cornea by Decorin and Biglycan. J Biol Chem 284, 8888–8897. https://doi.org/10.1074/jbc.M806590200
Zhang, S., Cui, W., 2014. Sox2, a key factor in the regulation of pluripotency and neural differentiation. World J Stem Cells 6, 305–311. https://doi.org/10.4252/wjsc.v6.i3.305
Zhong, X., Gutierrez, C., Xue, T., Hampton, C., Vergara, M.N., Cao, L.-H., Peters, A., Park, T.S., Zambidis, E.T., Meyer, J.S., Gamm, D.M., Yau, K.-W., Canto-Soler, M.V., 2014. Generation of three-dimensional retinal tissue with functional photoreceptors from human iPSCs. Nat Commun 5, 4047. https://doi.org/10.1038/ncomms5047
Zimmermann, D.R., Dours-Zimmermann, M.T., Schubert, M., Bruckner-Tuderman, L., 1994. Versican is expressed in the proliferating zone in the epidermis and in association with the elastic network of the dermis. J Cell Biol 124, 817–825. https://doi.org/10.1083/jcb.124.5.817

7 Appendix

7.1 Negative Control Images of SEAMs from Chapters 2 and 4

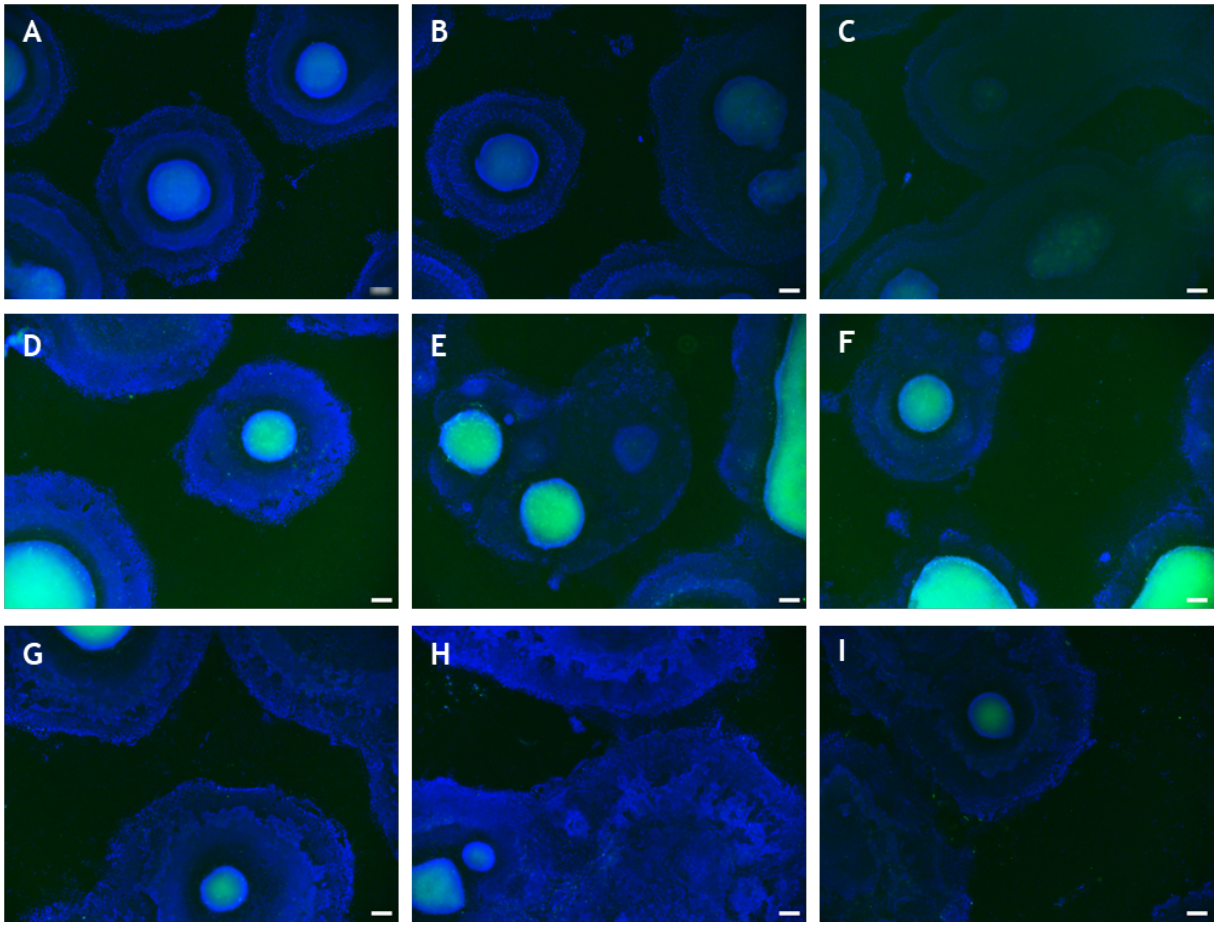

Figure 7.1 Negative control images of SEAMs presented in **Figure 2.4**, **Figure 2.5**, **Figure 2.6**, **Figure 2.7** and **Figure 2.11** with primary antibody omission. (**A-C**) SEAMs at 4 weeks of differentiation at the seeding densities of 300 (**A**), 600 (**B**) and 900 (**C**). (**D-F**) SEAMs at 5 weeks of differentiation at seeding densities of 300 (**D**), 600 (**E**) and 900 (**F**). (**G-I**) SEAMs at 6 weeks of differentiation at seeding densities of 300 (**G**), 600 (**H**) and 900 (**I**). Scale bars represent 100 µm.

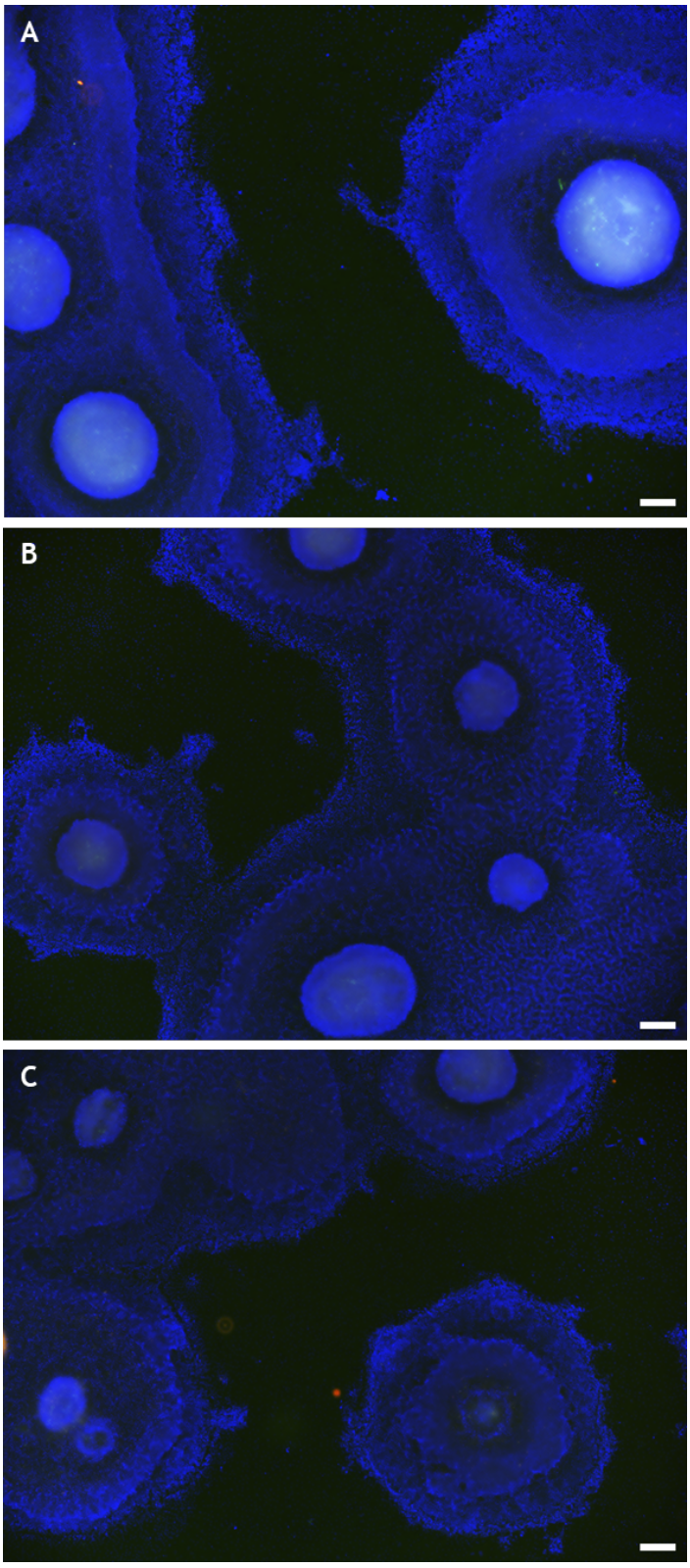

Figure 7.2 Negative control images of primary antibody omission of week four SEAMs for co-localisation studies depicted in **Figure 2.8**, **Figure 2.9** and **Figure 2.10**. Negative control image for at 300 (**A**), 600 (**B**) and 900 (**C**) seeding densities. Scale bars represent 100 µm.

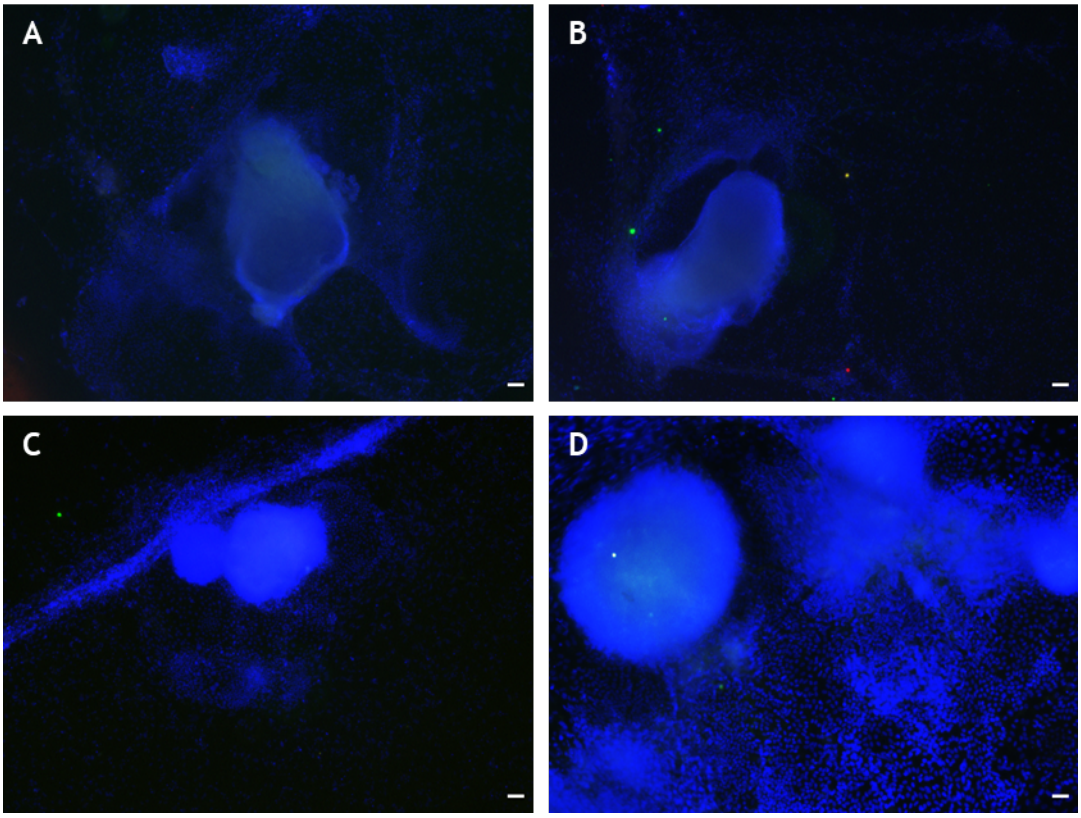

Figure 7.3 Negative control images of SEAMs grown on glycosaminoglycan substrates depicted in **Figures 4.5-4.12.** Negative control image for SEAMs grown on normal (**A**), 7D4 (**B**), 5D4/7D4 (**C**) and 6C3 (**D**) substrates. Scale bars represent 100 μm.

7.2 Publications and Conference Presentations

7.2.1 Publications

- Ashworth S, Harrington J, Hammond GM, Bains KK, Koudouna E, Hayes AJ, Ralphs JR, Regini JW, Young RD, Hayashi R, Nishida K, Hughes CE, Quantock AJ. Chondroitin Sulfate as a Potential Modulator of the Stem Cell Niche in Cornea. Front Cell Dev Biol. 2021 Jan 12;8:567358. doi: 10.3389/fcell.2020.567358. PMID: 33511110; PMCID: PMC7835413.

7.2.2 Conference presentations

- Oral and poster presentation with the title: Identifying Chondroitin Sulfate Substrates for the Cultivation of iPSC-derived Corneal Epithelium at Proteoglycans 2019 – October 2019, Kanazawa, Japan. Received Young Investigator Award.
- Oral and poster presentation with the title: Investigating Chondroitin Sulfate Substrates for the Cultivation of iPSC-derived Corneal Epithelium at Gordon Research Seminar and Conference: Cornea and Ocular Surface Biology – February 2020, Barga, Italy. Received Presenter's Travel Award

frontiers in Cell and Developmental Biology

PERSPECTIVE
published: 12 January 2021
doi: 10.3389/fcell.2020.567358

Chondroitin Sulfate as a Potential Modulator of the Stem Cell Niche in Cornea

Sean Ashworth[1,2], Jodie Harrington[1,3], Greg M. Hammond[1], Kiranjit K. Bains[1], Elena Koudouna[1], Anthony J. Hayes[2], James R. Ralphs[2], Justyn W. Regini[1], Robert D. Young[1], Ryuhei Hayashi[3,4], Kohji Nishida[4], Clare E. Hughes[2] and Andrew J. Quantock[1]*

[1] Structural Biophysics Group, School of Optometry and Vision Sciences, College of Biomedical and Life Sciences, Cardiff University, Cardiff, United Kingdom, [2] School of Biosciences, College of Biomedical and Life Sciences, Cardiff University, Cardiff, United Kingdom, [3] Department of Stem Cells and Applied Medicine, Osaka University Graduate School of Medicine, Osaka, Japan, [4] Department of Ophthalmology, Osaka University Graduate School of Medicine, Osaka, Japan

OPEN ACCESS

Edited by:
Jeremy Turnbull,
University of Liverpool,
United Kingdom

Reviewed by:
Andreas Faissner,
Ruhr University Bochum, Germany
Shuji Mizumoto,
Meijo University, Japan

***Correspondence:**
Clare E. Hughes
HughesCE1@cf.ac.uk

Specialty section:
This article was submitted to Signaling, a section of the journal Frontiers in Cell and Developmental Biology

Received: 29 May 2020
Accepted: 07 December 2020
Published: 12 January 2021

Citation:
Ashworth S, Harrington J, Hammond GM, Bains KK, Koudouna E, Hayes AJ, Ralphs JR, Regini JW, Young RD, Hayashi R, Nishida K, Hughes CE and Quantock AJ (2021) Chondroitin Sulfate as a Potential Modulator of the Stem Cell Niche in Cornea. Front. Cell Dev. Biol. 8:567358. doi: 10.3389/fcell.2020.567358

Chondroitin sulfate (CS) is an important component of the extracellular matrix in multiple biological tissues. In cornea, the CS glycosaminoglycan (GAG) exists in hybrid form, whereby some of the repeating disaccharides are dermatan sulfate (DS). These CS/DS GAGs in cornea, through their presence on the proteoglycans, decorin and biglycan, help control collagen fibrillogenesis and organization. CS also acts as a regulatory ligand for a spectrum of signaling molecules, including morphogens, cytokines, chemokines, and enzymes during corneal growth and development. There is a growing body of evidence that precise expression of CS or CS/DS with specific sulfation motifs helps define the local extracellular compartment that contributes to maintenance of the stem cell phenotype. Indeed, recent evidence shows that CS sulfation motifs recognized by antibodies 4C3, 7D4, and 3B3 identify stem cell populations and their niches, along with activated progenitor cells and transitional areas of tissue development in the fetal human elbow. Various sulfation motifs identified by some CS antibodies are also specifically located in the limbal region at the edge of the mature cornea, which is widely accepted to represent the corneal epithelial stem cell niche. Emerging data also implicate developmental changes in the distribution of CS during corneal morphogenesis. This article will reflect upon the potential roles of CS and CS/DS in maintenance of the stem cell niche in cornea, and will contemplate the possible involvement of CS in the generation of eye-like tissues from human iPS (induced pluripotent stem) cells.

Keywords: cornea, chondroitin sulfate, proteoglycan, glycosaminoglycan, stem cell niche, human iPS cells

INTRODUCTION

Proteoglycans form key components of the extracellular matrix, typically consisting of a protein core with one or more covalently attached glycosaminoglycan (GAG) chains. These molecules play vital roles in cell-cell signaling, tissue homeostasis and wound healing. Chondroitin sulfate/dermatan sulfate (CS/DS) and certain sulfation motifs of these GAG species are present in the stem cell niche in various tissues (Hayes et al., 2008, 2016; Caterson, 2012; Melrose et al., 2012),

and reportedly influence progenitor and stem cell function in composite tissue scaffolds (Farrugia et al., 2018). The importance of CS/DS as a structural extracellular matrix component in the cornea is fairly well-established (Lewis et al., 2010; Chen and Birk, 2011; Parfitt et al., 2011; Chen et al., 2014, 2015), but its potential role in the maintenance and development of the stem cell niche in cornea has been little studied until recently.

The cornea is the transparent tissue at the front of the eye. In humans, it is ∼0.5 mm thick and 11–12 mm in diameter, wherein it merges with the white sclera of the eye at an anatomical region known as the limbus. The bulk of the cornea is composed of a collagen-rich extracellular matrix – the corneal stroma – that contains ∼250 stacked and interwoven sheets or lamellae, made up of uniformly thin (∼30 nm diameter), and regularly-spaced, hybrid type I/V collagen fibrils. CS/DS and keratan sulfate (KS) proteoglycans associate with collagen fibrils to maintain the characteristic collagen architecture essential for transparency of the corneal stroma (Kao et al., 2006; Hassell and Birk, 2010; Lewis et al., 2010; Quantock et al., 2010; Meek and Knupp, 2015). The anterior-most region of the corneal stroma in most species is a thin, acellular, disorganized meshwork of collagen fibrils called Bowman's layer, which is integral at its distal limit with a basement membrane that supports the corneal epithelium. An intact and properly stratified corneal epithelium is vital for clear vision. Throughout life, superficial corneal epithelial cells are constantly shed into the tear film, a loss that is counteracted by replenishment by a population of corneal epithelial stem cells at the limbus (Kinoshita et al., 2001).

THE CORNEAL LIMBAL STEM CELL NICHE

The concept of a limbal stem cell niche (**Figure 1**) was first proposed almost 50 years ago, as a regenerative source of epithelial cells migrating centrally from a distinct, pigmented region of the peripheral cornea (Davanger and Evensen, 1971). Further work revealed a distinct side-population of slow-cycling cells within the basal layer of corneal limbal epithelium, which appeared to be responsible for centripetal migration of epithelium and the restoration of the corneal surface in wound healing (Cotsarelis et al., 1989; Dua and Forrester, 1990). These cells were subsequently distinguished by virtue of their small size, characteristically high nucleus to cytoplasmic ratio, and expression of various stem cell markers such as ABCG2 or p63 and its various isoforms (Romano et al., 2003; Watanabe et al., 2004; Di Iorio et al., 2005; Kawakita et al., 2009). Further markers include ABCB5, which is essential for limbal epithelial stem cell maintenance and development; cells isolated using this marker are able to restore the cornea in limbal epithelial stem cell-deficient mouse models (Ksander et al., 2014). A 3D structural analysis has further elucidated the architecture of the limbal stem cell niche, revealing the presence of limbal crypts circumferentially around the eye, interspaced alongside distal invaginations of stromal extracellular matrix, termed the palisades of Vogt (Grieve et al., 2015). The identification of limbal epithelial stem cells has galvanized the study of these cells for therapeutic purposes to treat various corneal epithelial diseases (Pellegrini et al., 1997; Bains et al., 2019; Le et al., 2020).

Damage or loss of resident corneal epithelial stem cells, either through disease or injury, can lead to a limbal stem cell deficiency that ultimately results in corneal blindness, necessitating corneal surgery to restore vision. Transplantation is one treatment option for late-stage corneal pathology, however, this carries the risk of tissue rejection. Moreover, there is a distinct lack of donor tissue, with only one cornea available for every 70 required for transplantation worldwide (Gain et al., 2016). For this reason, other therapies have been investigated, including *ex vivo* expanded limbal epithelial stem cell transplantation (autograft or allograft), and the generation of an epithelial multilayer derived from oral mucosal epithelium (Oie and Nishida, 2016; Bains et al., 2019), or induced pluripotent stem cells (Hayashi et al., 2016, 2017). Whilst these pioneering technologies have shown great clinical promise, they could be further optimized by careful manipulation of culture conditions for these regenerative cells, as well as through their selection. A further potential avenue of exploration from a tissue engineering standpoint might be recreating an extracellular matrix microenvironment of the limbal stem cell niche seeded with isolated corneal limbal epithelial stem cells or induced pluripotent stem (iPS) cell derived-corneal epithelial cells.

The limbal region of the cornea also harbors a population of mesenchymal stem cells, termed corneal stromal stem cells, in the extracellular matrix subjacent to the corneal epithelial stem cell niche (Du et al., 2005). Electron microscopy has provided evidence for direct connections between corneal epithelial and stromal cells at the limbus that traverse the epithelial basement membrane (Higa et al., 2013; Dziasko et al., 2014; Yamada et al., 2015). This, along with the results of studies of the behavior of limbal epithelial and stromal cells in culture, has led to the notion of a multicellular limbal niche complex at the edge of the cornea involving both epithelial and stromal cells (Hertsenberg and Funderburgh, 2015; Dziasko and Daniels, 2016; Funderburgh et al., 2016). Work with bovine cells from the corneal stroma in culture has shown that ^{35}S-labeled CS/DS, when measured by sensitivity to chondroitinase ABC, is increased 3–3.5-fold in activated fibroblasts and myofibroblasts compared with quiescent keratocytes (Funderburgh et al., 2003). To the best of our knowledge, however, the association between corneal stromal stem cells and CS has not been directly investigated. Nevertheless, it is noteworthy that the peripheral human cornea and limbus, where corneal stromal stem cells reside, contain less acidic GAG than the central cornea, primarily because KS levels are decreased (Borcherding et al., 1975). This work also indicated that chondroitin was replaced by CS at the limbus and that DS was present at detectable levels. More recently, immunohistochemistry was conducted to probe the composition of the bovine corneal stroma in which monoclonal antibody 2B6 was utilized after (i) chondroitinase ABC treatment to identify CS and DS, (ii) chondroitinase ACII treatment to identify CS, and (iii) chondroitinase B treatment to identify DS (Ho et al., 2014). This revealed that DS was present throughout the corneal stroma and into the sclera, with CS detected toward the outer periphery of the cornea and the limbus.

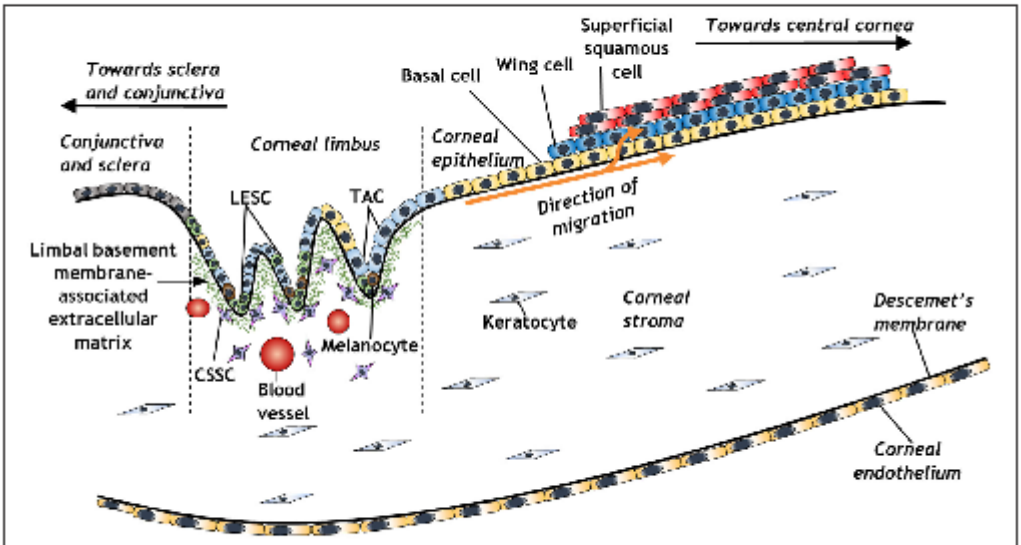

FIGURE 1 | Schematic representation of the corneal limbal stem cell niche and some of its constituent elements (LESC, limbal epithelial stem cell; CSSC, corneal stromal stem cell; TAC, transient amplifying cell).

Investigations enabling us to accurately recreate the microenvironment of the limbal stem cell niche would be of great scientific value, not only in terms of understanding the biological functions of different components of this environment, but also because of the potential in regenerative medicine. To this end, various attempts have been made to elucidate the extracellular matrix molecules and cell-cell interactions that are important for the maintenance of the corneal limbal stem cell niche. Indeed, the corneal limbus has a distinct extracellular matrix profile compared to the central cornea and conjunctiva (Schlötzer-Schrehardt et al., 2007; Mei et al., 2012). CS, amongst other matrix molecules such as laminin isoforms and tenascin-C, are enriched at the corneal limbus where they co-localize with putative stem and progenitor cells in the basal limbal epithelium (Schlötzer-Schrehardt et al., 2007). The importance of tenascin-C in several stem cell niches has been well-documented, particularly within neural and hematopoietic environments (Seiffert et al., 1998; Garcion et al., 2001; Chiquet-Ehrismann et al., 2014). Tenascin-C, as mentioned, has been identified in the corneal limbal stem cell niche (Maseruka et al., 2000), and its spatial and temporal expression during development and wound healing, aligned to its presence in the adult limbus (Maseruka et al., 1997; Ljubimov et al., 1998; Ding et al., 2008) advocate a potential role in the self-renewal and differentiation of stem cells. It is likely that this can be achieved by providing a favorable stem cell microenvironment via interactions with other extracellular matrix components such as fibronectin (Hunt et al., 2012; Singh and Schwarzbauer, 2012) and CS, with an association between tenascin and CS having been reported in experimental models of neural repair (Gates et al., 1996).

CHONDROITIN SULFATE/DERMATAN SULFATE STRUCTURE AND ANTIBODIES

CS and CS/DS GAG structures are typically heterogeneous and polydisperse from molecule to molecule. The disaccharide repeat unit of CS consists of a (hex)uronic acid (glucuronic) and a hexosamine (galactosamine, typically N-acetylated), whilst in DS disaccharides the D-glucuronic acid residue is converted to αL-iduronic acid, yielding DS. Linkage of these CS disaccharide units occurs through ß3-linkage (GlcAß3GalNAc), whilst DS is through ∂3 -linkage (IdoA∂3GalNAc) (Caterson, 2012). CS/DS heterogeneity is further generated through sulfation of hydroxyl groups at positions 2, 4 and C6 on the sugar molecules, giving rise to great structural diversity (Sugahara et al., 2003; Hayes et al., 2018). Indeed, recent estimates from Persson et al. (2020) suggest, with a chain of 50 CS/DS disaccharides, an estimated 16^{50} theoretical variants arise from sixteen possible disaccharide variants. Such structural diversity is believed to be responsible for the ability of CS/DS to interact with a range of growth factors, morphogens, cytokines and chemokines, to potentially help regulate cell proliferation, cell differentiation, and tissue development (Nandini and Sugahara, 2006; Caterson, 2012; Purushothaman et al., 2012; Hayes et al., 2018; Karamanos et al.,

2018). In a number of tissues, cornea included, CS exists as a co-polymer with DS forming CS/DS hybrid GAGs (Habuchi et al., 1973; Inoue and Iwasaki, 1976). An ability to recognize different sulfation patterns on CS or CS/DS is useful for the study of structurally diverse CS/DS isoforms within a tissue, and a range of monoclonal antibodies have been developed to help with this endeavor (Sorrell et al., 1990). For example, antibodies 6C3, 4C3, 7D4, and 3B3 (Caterson et al., 1985), can recognize distinct, native (i.e. non-chondroitinase-digested) and non-native (i.e., chondroitinase-digested) epitopes on CS/DS chains.

Some examples of these antibodies and the location of their respective CS/DS binding sites are shown in **Figure 2** along with a simplified structure of a typical CS/DS hybrid chain, the location of the binding site having been deciphered by sequential enzymatic digestion. Other CS antibodies developed in our lab include 4D3 and 3B5, which also recognize a specific pattern of carbon sulfation on sequential sugar molecules within a polysaccharide chain (Sorrell et al., 1990). Whilst the exact epitope for some of these antibodies remains to be elucidated, other studies of D-type CS antibodies (which bind sites of sulfation on carbon-2 of the glucuronic acid and carbon-6 of the *N*-acetylgalactosamine sugar) have indicated they require at least an hexasaccharide (in the case of 473HD), or octasaccharide (in the case of CS-56 and MO-225), to bind and recognize a specific tetrasaccharide within the chain (Ito et al., 2005). Whilst useful, it is important to note that the flanking regions of the recognized tetrasaccharide can affect antibody affinity and *in vivo* growth factor binding. This results in overlapping oligosaccharide binding regions, termed "wobble motifs," further increasing the complexity of epitope definition and discussed in more detail elsewhere (Caterson, 2012; Purushothaman et al., 2012).

Immunohistochemical investigations using these and other antibodies have disclosed that a number of stem cell niches exhibit specific or preferential sulfation patterns. For example, in human skin, the 6C3 epitope is located just below the basal lamina of the epidermis, adjacent to resident epidermal stem cells (Sorrell et al., 1990). This is of particular interest, given the similarities between epidermal stem cells and limbal epithelial stem cells, which both form a stratified epithelium that expresses the p63 stem cell marker (Pellegrini et al., 2001). Also, of note, is the finding that epidermal stem cells can convert into corneal epithelial-like cells when placed in corneal tissue (Gao et al., 2007). CS GAGs are also present in primordial stem cell populations in fetal tissue, such as hair bulbs and perichondrium (Hayes et al., 2016), allowing us to hypothesize a potential role for CS in maintenance of the corneal limbal stem cell niche.

CHONDROITIN SULFATE IN THE CORNEAL LIMBAL STEM CELL NICHE

Whilst much work has focused on the role of CS in the corneal stroma, less attention has been paid to a potential role for CS in the stem cell niche of the corneal limbus. The main CS proteoglycans present in cornea are decorin and biglycan, which are expressed widely throughout the corneal stroma, with biglycan levels decreasing toward maturity. CS in the cornea helps define stromal architecture, and decorin and biglycan null mice have significantly disrupted collagen ultrastructure (Zhang et al., 2009). Similar effects are seen in biglycan/lumican null mice, which display significant corneal opacity compared to mice with single proteoglycan knockouts (Chen et al., 2014).

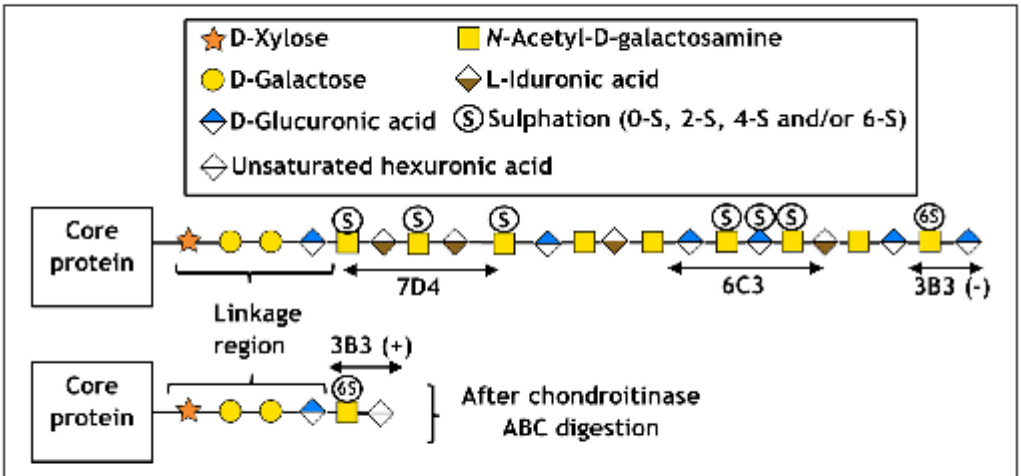

FIGURE 2 | Schematic of CS/DS following the symbol nomenclature for the graphical representation of glycans (Varki et al., 2015), including the approximate location of epitopes for antibodies 7D4, 6C3, and 3B3. Respectively, (+) and (–) indicate with and without chondroitinase ABC digestion.

In terms of overall GAG distribution, the cornea is primarily constituted of KS GAG (both high and low sulfated forms), with CS/DS hybrid GAGs also present in slightly lower quantities, and with CS located preferentially toward the limbus (Ho et al., 2014). Heparan sulfate has also been shown to play a role in maintenance of the corneal epithelium, as its absence results in reduced corneal epithelial wound repair and improper stratification of epithelial cells (Coulson-Thomas et al., 2015).

In order to determine in more detail the specific pattern of CS distribution within the cornea, previous work by our group used the aforementioned panel of CS antibodies to map CS/DS in rabbit corneas (Yamada et al., 2015). The rabbit eye, however, differs in its microanatomy to that of human cornea and lacks a series of limbal epithelial crypts that are located circumferentially around the limbus and which form the palisades of Vogt. Limbal crypts are essentially downward focal projections of epithelial cells into the underlying extracellular matrix and run around the periphery of the cornea. The porcine limbus is believed to have a series of epithelial crypts, which is somewhat analogous to that of the human cornea. However, the positioning of the crypts around the limbal circumference of the pig eye is debated (Notara et al., 2011; Grieve et al., 2015), and new evidence about their size, shape and circumferential extent is adding to this debate (Hammond et al., unpublished results). Porcine corneas are closer in size to human corneas with a similar anatomical structure (Sanchez et al., 2011) and protein composition (Sharifi et al., 2019), thus their obvious value for corneal research. Both porcine and human corneas have a Bowman's layer – a thin, acellular layer of the distal corneal stroma immediately subjacent to the corneal epithelial basement membrane – as demonstrated by recent high-resolution investigations (Hammond et al., 2020). Bowman's layer is often missing in many other species commonly used for corneal research (Hayashi et al., 2002), identifying the pig as a reasonable animal model.

Native CS sulfation motifs identified by the antibodies 7D4 and 6C3 were detected in the porcine cornea (**Figures 3A,C**), specifically at the limbus in the case of 6C3 (**Figure 3C**), as was observed in the presumptive stem cell niche in rabbit cornea (Yamada et al., 2015). 3B3, an antibody recognizing non-native, chondroitinase ABC-digested stubs without digestion of a terminal disaccharide of the CS chain (6-*O*-sulfated *N*-acetylgalactosamine adjacent to the terminal glucuronate), also appeared to label CS structures surrounding the limbal niche (**Figure 3F**). The 6C3 CS epitope also localized in close proximity to putative limbal epithelial stem cells, as identified by two markers, ABCB5 and keratin 19 (**Figures 3G,H**). Although these are preliminary data, such co-localization of an extracellular matrix component and putative stem cell identifiers is an interesting discovery, which invites speculation as to a causal link in terms of the potential for the matrix to define a milieu that favorably sustains stem cell expression. With this in mind and as alluded to earlier, we also note that mesenchymal stem cells have been identified in the corneal stroma, subjacent to the basement membrane at the limbus, and are hypothesized to be supportive of the resident limbal epithelial stem cells (Du et al., 2005; Pinnamaneni and Funderburgh, 2012; Funderburgh et al., 2016). We speculate whether the 6C3 antibody might recognize cell surface-associated CS on corneal stromal stem cells or sub-epithelial stromal melanocytes that, when present within the epithelium, have been shown to be supportive of the limbal epithelial stem cell population (Dziasko et al., 2015). Ongoing studies will serve to better characterize CS in the limbal environment and aim to clarify its involvement as a potential modulator of the stem cell niche.

CHONDROITIN SULFATE AND REGENERATIVE MEDICINE

In recent years, CS has been highlighted as essential for the functional integrity of pluripotent and multipotent stem cells, and as an important factor in the maintenance of pluripotency and differentiation propensity. For example, when CS is depleted through genetic knockout or removed by enzymatic digestion, mouse embryonic stem cells become arrested in a pluripotent state and are unable to differentiate. The addition of exogenous CS, however, recovers the differentiation propensity thus pointing to an influential role for CS in pluripotent stem cell biology (Izumikawa et al., 2014). Accordingly, CS has considerable relevance to both embryological development and stem cell biology and has been shown to be implicated in the differentiation and proliferation of multipotent stem cells from a range of tissues. Many of these studies focus on neural-derived tissue and have indicated that the removal of CS through enzymatic degradation, typically using chondroitinase ABC, can have a marked effect on neural progenitor/stem cell proliferation, differentiation and migration. The mechanism is believed to be mediated by fibroblast growth factor-2 (FGF-2) and epidermal growth factor (EGF) (Sirko et al., 2007, 2010; Gu et al., 2009). Removal of CS can also cause spontaneous differentiation of oligodendrocyte precursor cells (Karus et al., 2016), whilst the disruption of CS/DS in mesenchymal stem cells has been shown to influence osteogenic differentiation (Manton et al., 2007). Owing to the localization of specific CS motifs in corneal limbal stroma, we speculate that these molecules could potentially facilitate maintenance of corneal limbal epithelial stem cells and/or potentiate their differentiation from iPS cells *in vitro*. Various researchers have developed differentiation protocols for generating corneal epithelium from both pluripotent and multipotent stem cells. Initial attempts involved recreating the limbal niche using collagen IV and limbal fibroblast-conditioned medium to differentiate pluripotent stem cells toward a corneal epithelial phenotype. However, the cells generated were not very robust and differed from native corneal epithelium (Ahmad et al., 2007).

Other studies using pluripotent stem cells generated improved corneal epithelial-like cells that displayed corneal epithelial markers (K3/K12 and Pax-6), and showed how the regulation of *PAX6* is critical for *in vitro* differentiation (Hayashi et al., 2012; Shalom-Feuerstein et al., 2012; Brzeszczynska et al., 2014). Whilst promising, these studies failed to take into account the elaborate nature of whole eye development with the

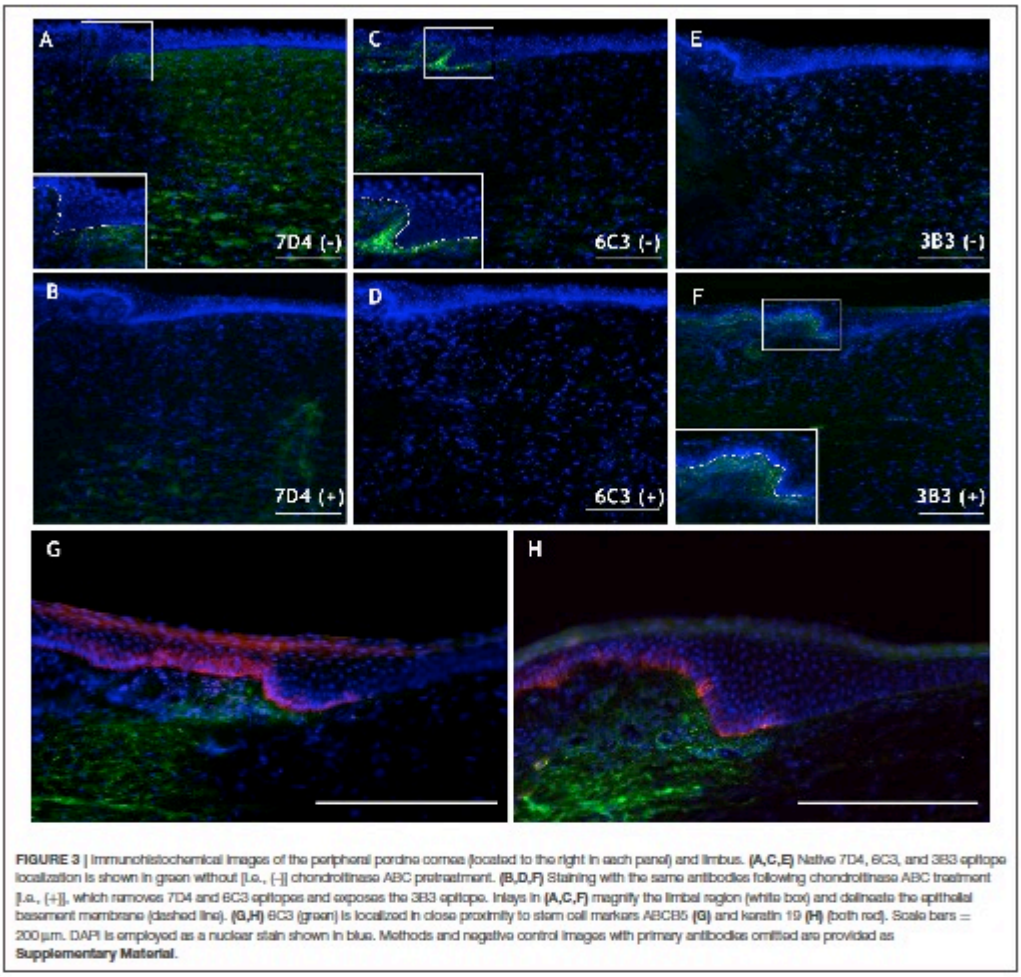

FIGURE 3 | Immunohistochemical images of the peripheral porcine cornea (located to the right in each panel) and limbus. **(A,C,E)** Native 7D4, 6C3, and 3B3 epitope localization is shown in green without [i.e., [–]] chondroitinase ABC pretreatment. **(B,D,F)** Staining with the same antibodies following chondroitinase ABC treatment [i.e., [+]], which removes 7D4 and 6C3 epitopes and exposes the 3B3 epitope. Inlays in **(A,C,F)** magnify the limbal region (white box) and delineate the epithelial basement membrane (dashed line). **(G,H)** 6C3 (green) is localized in close proximity to stem cell markers ABCB5 **(G)** and keratin 19 **(H)** (both red). Scale bars = 200 μm. DAPI is employed as a nuclear stain shown in blue. Methods and negative control images with primary antibodies omitted are provided as **Supplementary Material**.

plethora of spatial and temporal developmental cues that occur between distinct cell types. One recently-developed method demonstrated that human iPS cells can give rise to self-forming ectodermal autonomous multi-zones (SEAMs), representing concentric zones of cells of distinct ocular lineages, including cells that resemble those of the corneal epithelium (Hayashi et al., 2016, 2017; **Supplementary Video**). In the original discovery of SEAM formation (Hayashi et al., 2016), which was modified by other researchers (Li et al., 2019), the cellular zones represented neuronal lineages (innermost zone 1), retina-like and neural crest-like cells (zone 2, more peripherally), ocular surface ectoderm-like cells (zone 3, more peripherally still), and finally non-ocular surface epithelial-like cells in the outermost zone 4. Lens-like cells appeared at the borders of SEAM zones 2 and 3.

Further work involving manipulation within the substrate of laminin, another extracellular matrix molecule present in basement membrane of the corneal limbus, showed that different isoforms differentially influence the differentiation propensity of corneal epithelial cells derived from human iPS cells (Shibata et al., 2018). Laminin can also influence cell phenotype based upon the selective adhesiveness of the

cells toward various substrates (Shibata et al., 2020). We also note, in relation to the eye, that both CS and laminin are temporally and spatially expressed during optic nerve regeneration in fish (Battisti et al., 1992), and more recently have been applied in the expansion of corneal endothelial cells for potential transplantation (Kennedy et al., 2019). In addition, CS and laminin are suggested to have counteractive roles in precursor cell differentiation, due to regulation of the β1-integrin signaling pathway (Sun et al., 2017), which highlights potential impacting interactions (indirect and/or direct) between these ECM molecules. As mentioned, laminin influences SEAM development, and some recent preliminary data indicate that CS, too, is likely involved in the differentiation of human iPS cells in a developing SEAM as it is increasingly deposited from weeks 4–6 (**Figure 4**). Specifically, the CS moiety revealed by 7D4 was detected in SEAM zones 3, outward to zone 4 (**Figures 4A–C**). Furthermore, CS is ubiquitously deposited into the surrounding matrix by week 6 (**Figure 4D**). Thus, facilitating deposition or exogenous supply of CS, could potentially be used to modulate differentiation of human iPS cells in SEAMs.

Whilst the application of CS to bioengineered scaffolds and its use to promote cell differentiation is not new, there are few investigations into defined species of CS and their influence on stem cell differentiation in the context of the corneal epithelium. Also, seldom considered is the fact that commercially prepared CS can often contain significant impurities, for example KS (Santos et al., 2017). Essentially, there has been relatively little detailed exploration into possible modulatory roles for CS, or indeed other GAGs, within the corneal limbal stem cell niche, but emerging knowledge will provide an enhanced understanding of the influence of CS upon the behavior of

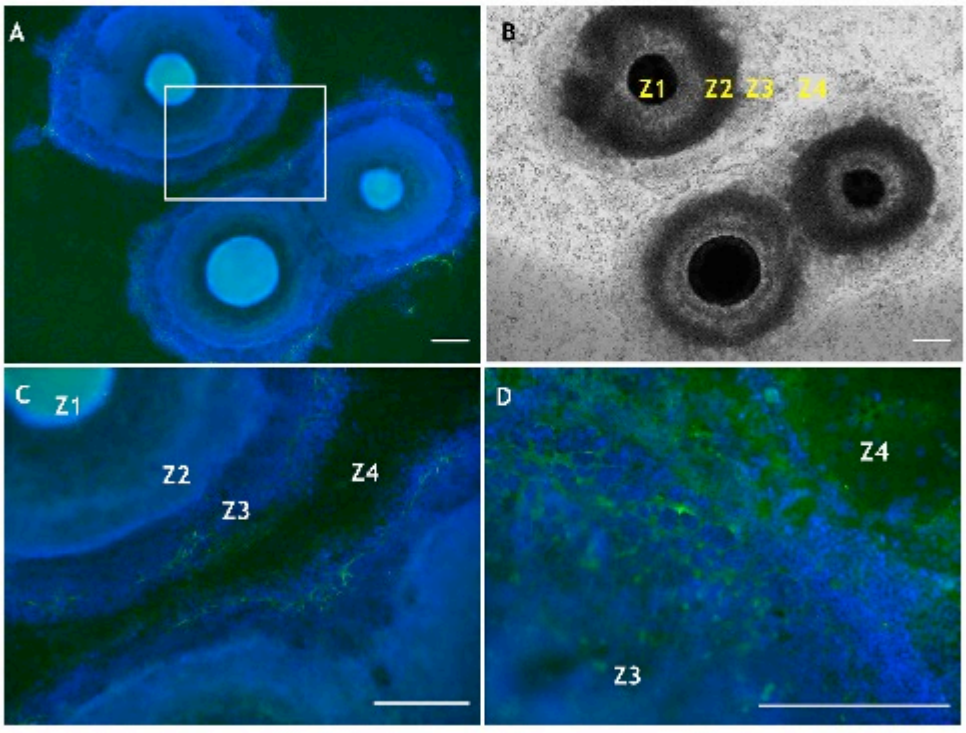

FIGURE 4 | Localization of CS using antibody 7D4 within developing SEAM cultures at weeks 4 and 6 of differentiation. **(A)** Wide-field view of three SEAM colonies at week 4 of differentiation, two of which are beginning to merge (7D4 is shown in green and nuclear Hoechst-334 staining in blue). **(B)** Bright-field image of a SEAM at week 4 of differentiation with each zone (Z) indicated. **(C)** Higher magnification view of CS immunolocalisation in a selected region in **(A)**. **(D)** High magnification of a SEAM at week 6 of differentiation indicating a widespread deposition of CS. Scale bars = 100 μm. Methods and negative control images with primary antibodies omitted are provided as **Supplementary Material**.

human stem cells and their potential involvement in corneal regenerative medicine.

DATA AVAILABILITY STATEMENT

The original contributions presented in the study are included in the article/**Supplementary Materials**, further inquiries can be directed to the corresponding author/s.

AUTHOR CONTRIBUTIONS

AQ, SA, and CH planned the article. SA composed **Figures 1**, **2**. GH and SA obtained the data presented in **Figure 3**. JH, SA, and RH obtained the data presented in **Figure 4**. AQ, JRe, JRa, CH, RH, and KN obtained funding. All authors contributed to the writing of the article.

FUNDING

The research described in this article was funded by BBSRC Responsive Mode Project Grant BB/P017843/1 (to AQ, JRe, and JRa), BBSRC International Partnering Award BB/R021244/1 (to AQ and KN), and Ph.D. studentships for SA and GH from Fight-for-Sight (5069/5070 to AQ and CH) and the BBSRC (South West Biosciences Doctoral Training Partnership, Grant reference BB/M009122/1 to AQ), respectively.

SUPPLEMENTARY MATERIAL

The Supplementary Material for this article can be found online at: https://www.frontiersin.org/articles/10.3389/fcell.2020.567358/full#supplementary-material

REFERENCES

Ahmad, S., Stewart, R., Yung, S., Kolli, S., Armstrong, L., Stojkovic, M., et al. (2007). Differentiation of human embryonic stem cells into corneal epithelial-like cells by *in vitro* replication of the corneal epithelial stem cell niche. *Stem Cells* 25, 1145–1155. doi: 10.1634/stemcells.2006-0516

Bains, K. K., Fukuoka, H., Hammond, G. M., Sotozono, C., and Quantock, A. J. (2019). Recovering vision in corneal epithelial stem cell deficient eyes. *Cont. Lens Anterior Eye* 42, 350–358. doi: 10.1016/j.clae.2019.04.006

Battisti, W. P., Shinar, Y., Schwartz, M., Levitt, P., and Murray, M. (1992). Temporal and spatial patterns of expression of laminin, chondroitin sulphate proteoglycan and HNK-1 immunoreactivity during regeneration in the goldfish optic nerve. *J. Neurocytol.* 21, 557–573. doi: 10.1002/cne.903540211

Borcherding, M. S., Blacik, L. J., Sittig, R. A., Bizzell, J. W., Breen, M., and Weinstein, H. G. (1975). Proteoglycans and collagen fibre organization in human corneoscleral tissue. *Exp. Eye Res.* 21, 59–70. doi: 10.1016/0014-4835(75)90057-3

Brzeszczynska, J., Samuel, K., Greenhough, S., Ramaesh, K., Dhillon, B., Hay, D. C., et al. (2014). Differentiation and molecular profiling of human embryonic stem cell-derived corneal epithelial cells. *Int. J. Mol. Med.* 33, 1597–1606. doi: 10.3892/ijmm.2014.1714

Caterson, B. (2012). Fell-muir lecture: chondroitin sulphate glycosaminoglycans: fun for some and confusion for others. *Int. J. Exp. Pathol.* 93, 1–10. doi: 10.1111/j.1365-2613.2011.00807.x

Caterson, B., Christner, J. E., Baker, J. R., and Couchman, J. R. (1985). Production and characterization of monoclonal antibodies directed against connective tissue proteoglycans. *Fed. Proc.* 44, 386–393.

Chen, S., and Birk, D. E. (2011). Focus on molecules: decorin. *Exp. Eye Res.* 92, 444–445. doi: 10.1016/j.exer.2010.05.008

Chen, S., Mienaltowski, M. J., and Birk, D. E. (2015). Regulation of corneal stroma extracellular matrix assembly. *Exp. Eye Res.* 133, 69–80. doi: 10.1016/j.exer.2014.08.001

Chen, S., Young, M. F., Chakravarti, S., and Birk, D. E. (2014). Interclass small leucine-rich repeat proteoglycan interactions regulate collagen fibrillogenesis and corneal stromal assembly. *Matrix Biol.* 35, 103–111. doi: 10.1016/j.matbio.2014.01.004

Chiquet-Ehrismann, R., Orend, G., Chiquet, M., Tucker, R. P., and Midwood, K. S. (2014). Tenascins in stem cell niches. *Matrix Biol.* 37, 112–123. doi: 10.1016/j.matbio.2014.01.007

Cotsarelis, G., Cheng, S. Z., Dong, G., Sun, T. T., and Lavker, R. M. (1989). Existence of slow-cycling limbal epithelial basal cells that can be preferentially stimulated to proliferate: implications on epithelial stem cells. *Cell* 57, 201–209. doi: 10.1016/0092-8674(89)90958-6

Coulson-Thomas, V. J., Chang, S.-H., Yeh, L.-K., Coulson-Thomas, Y. M., Yamaguchi, Y., Esko, J., et al. (2015). Loss of corneal epithelial heparan sulfate leads to corneal degeneration and impaired wound healing. *Invest. Ophthalmol. Vis. Sci.* 56, 3004–3014. doi: 10.1167/iovs.14-15341

Davanger, M., and Evensen, A. (1971). Role of the pericorneal papillary structure in renewal of corneal epithelium. *Nature* 229, 560–561. doi: 10.1038/229560a0

Di Iorio, E., Barbaro, V., Ruzza, A., Ponzin, D., Pellegrini, G., and De Luca, M. (2005). Isoforms of DeltaNp63 and the migration of ocular limbal cells in human corneal regeneration. *Proc. Natl. Acad. Sci. U.S.A.* 102, 9523–9528. doi: 10.1073/pnas.0503437102

Ding, Z., Dong, J., Liu, J., and Deng, S. X. (2008). Preferential gene expression in the limbus of the vervet monkey. *Mol Vis.* 14, 2031–2041.

Du, Y., Funderburgh, M. L., Mann, M. M., SundarRaj, N., and Funderburgh, J. L. (2005). Multipotent stem cells in human corneal stroma. *Stem Cells* 23, 1266–1275. doi: 10.1634/stemcells.2004-0256

Dua, H. S., and Forrester, J. V. (1990). The corneoscleral limbus in human corneal epithelial wound healing. *Am. J. Ophthalmol.* 110, 646–656. doi: 10.1016/s0002-9394(14)77062-x

Dziasko, M. A., Armer, H. E., Levis, H. J., Shortt, A. J., Tuft, S., and Daniels, J. T. (2014). Localisation of epithelial cells capable of holoclone formation *in vitro* and direct interaction with stromal cells in the native human limbal crypt. *PLoS ONE* 9:e94283. doi: 10.1371/journal.pone.0094283

Dziasko, M. A., and Daniels, J. T. (2016). Anatomical features and cell-cell interactions in the human limbal epithelial stem cell niche. *Ocul. Surf.* 14, 322–330. doi: 10.1016/j.jtos.2016.04.002

Dziasko, M. A., Tuft, S. J., and Daniels, J. T. (2015). Limbal melanocytes support limbal epithelial stem cells in 2D and 3D microenvironments. *Exp. Eye Res.* 138, 70–79. doi: 10.1016/j.exer.2015.06.026

Farrugia, B. L., Lord, M. S., Whitelock, J. M., and Melrose, J. (2018). Harnessing chondroitin sulphate in composite scaffolds to direct progenitor and stem cell function for tissue repair. *Biomater. Sci.* 6, 947–957. doi: 10.1039/C7BM01158J

Funderburgh, J. L., Funderburgh, M. L., and Du, Y. (2016). Stem cells in the limbal stroma. *Ocul. Surf.* 14, 113–120. doi: 10.1016/j.jtos.2015.12.006

Funderburgh, J. L., Mann, M. M., and Funderburgh, M. L. (2003). Keratocyte phenotype mediates proteoglycan structure: a role for fibroblasts in corneal fibrosis. *J. Biol. Chem.* 278, 45629–45637. doi: 10.1074/jbc.M303292200

Gain, P., Jullienne, R., He, Z., Aldossary, M., Acquart, S., Cognasse, F., et al. (2016). Global survey of corneal transplantation and eye banking. *JAMA Ophthalmol.* 134, 167–173. doi: 10.1001/jamaophthalmol.2015.4776

Gao, N., Wang, Z., Huang, B., Ge, J., Lu, R., Zhang, K., et al. (2007). Putative epidermal stem cell convert into corneal epithelium-like cell under corneal tissue *in vitro*. *Sci. China C Life Sci.* 50, 101–110. doi: 10.1007/s11427-007-0006-4

Garcion, E., Faissner, A., and ffrench-Constant, C. (2001). Knockout mice reveal a contribution of the extracellular matrix molecule tenascin-C to neural precursor proliferation and migration. *Development* 128, 2485–2496. Available online at: https://dev.biologists.org/content/128/13/2485

Gates, M. A., Fillmore, H., and Steindler, D. A. (1996). Chondroitin sulfate proteoglycan and tenascin in the wounded adult mouse neostriatum *in vitro*: dopamine neuron attachment and process outgrowth. *J. Neurosci.* 16, 8005–8018. doi: 10.1523/JNEUROSCI.16-24-08005.1996

Grieve, K., Ghoubay, D., Georgeon, C., Thouvenin, O., Bouheraoua, N., Paques, M., et al. (2015). Three-dimensional structure of the mammalian limbal stem cell niche. *Exp. Eye Res.* 140, 75–84. doi: 10.1016/j.exer.2015.08.003

Gu, W. L., Fu, S. L., Wang, Y. X., Li, Y., Lu, H. Z., Xu, X. M., et al. (2009). Chondroitin sulfate proteoglycans regulate the growth, differentiation and migration of multipotent neural precursor cells through the integrin signaling pathway. *BMC Neurosci.* 10:128. doi: 10.1186/1471-2202-10-128

Habuchi, H., Yamagata, T., Iwata, H., and Suzuki, S. (1973). The occurrence of a wide variety of dermatan sulfate-chondroitin sulfate copolymers in fibrous cartilage. *J. Biol. Chem.* 248, 6019–6028.

Hammond, G. M., Young, R. D., Muir, D. D., and Quantock, A. J. (2020). The microanatomy of Bowman's layer in the cornea of the pig: changes in collagen fibril structure at the corneoscleral limbus. *Eur. J. Anat.* 24, 399–406. Available online at: http://www.eurjanat.com/web/paper.php?id=200195gh

Hassell, J. R., and Birk, D. E. (2010). The molecular basis of corneal transparency. *Exp. Eye Res.* 91, 326–335. doi: 10.1016/j.exer.2010.06.021

Hayashi, R., Ishikawa, Y., Ito, M., Kageyama, T., Takashiba, K., Fujioka, T., et al. (2012). Generation of corneal epithelial cells from induced pluripotent stem cells derived from human dermal fibroblast and corneal limbal epithelium. *PLoS ONE* 7:e45435. doi: 10.1371/journal.pone.0045435

Hayashi, R., Ishikawa, Y., Katori, R., Sasamoto, Y., Taniwaki, Y., Takayanagi, H., et al. (2017). Coordinated generation of multiple ocular-like cell lineages and fabrication of functional corneal epithelial cell sheets from human iPS cells. *Nat. Protoc.* 12, 683–696. doi: 10.1038/nprot.2017.007

Hayashi, R., Ishikawa, Y., Sasamoto, Y., Katori, R., Nomura, N., Ichikawa, T., et al. (2016). Co-ordinated ocular development from human iPS cells and recovery of corneal function. *Nature* 531, 376–380. doi: 10.1038/nature17000

Hayashi, S., Osawa, T., and Tohyama, K. (2002). Comparative observations on corneas, with special reference to Bowman's layer and Descemet's membrane in mammals and amphibians. *J. Morphol.* 254, 247–258. doi: 10.1002/jmor.10030

Hayes, A., Sugahara, K., Farrugia, B., Whitelock, J. M., Caterson, B., and Melrose, J. (2018). Biodiversity of CS–proteoglycan sulphation motifs: chemical messenger recognition modules with roles in information transfer, control of cellular behaviour and tissue morphogenesis. *Biochem. J.* 475, 587–620. doi: 10.1042/BCJ20170820

Hayes, A. J., Hughes, C. E., Smith, S. M., Caterson, B., Little, C. B., and Melrose, J. (2016). The CS sulfation motifs 4C3, 7D4, 3B3[–]; and perlecan identify stem cell populations and their niches, activated progenitor cells and transitional areas of tissue development in the fetal human elbow. *Stem Cells Dev.* 25, 836–847. doi: 10.1089/scd.2016.0054

Hayes, A. J., Tudor, D., Nowell, M. A., Caterson, B., and Hughes, C. E. (2008). Chondroitin sulfate sulfation motifs as putative biomarkers for isolation of articular cartilage progenitor cells. *J. Histochem. Cytochem.* 56, 125–138. doi: 10.1369/jhc.7A7320.2007

Hertsenberg, A. J., and Funderburgh, J. L. (2015). Stem cells in the cornea. *Prog. Mol. Biol. Transl. Sci.* 134, 25–41. doi: 10.1016/bs.pmbts.2015.04.002

Higa, K., Kato, N., Yoshida, S., Ogawa, Y., Shimazaki, J., Tsubota, K., et al. (2013). Aquaporin 1-positive stromal niche-like cells directly interact with N-cadherin-positive clusters in the basal limbal epithelium. *Stem Cell Res.* 10, 147–155. doi: 10.1016/j.scr.2012.11.001

Ho, L. T. Y., Harris, A. M., Tanioka, H., Yagi, N., Kinoshita, S., Caterson, B., et al. (2014). A comparison of glycosaminoglycan distributions, keratan sulphate sulphation patterns and collagen fibril architecture from central to peripheral regions of the bovine cornea. *Matrix Biol.* 38, 59–68. doi: 10.1016/j.matbio.2014.06.004

Hunt, G. C., Singh, P., and Schwarzbauer, J. E. (2012). Endogenous production of fibronectin is required for self-renewal of cultured mouse embryonic stem cells. *Exp. Cell Res.* 318, 1820–1831. doi: 10.1016/j.yexcr.2012.06.009

Inoue, S., and Iwasaki, M. (1976). Dermatan sulfate-chondroitin sulfate copolymers from umbilical cord isolation and characterization. *J. Biochem.* 80, 513–524. doi: 10.1093/oxfordjournals.jbchem.a131306

Ito, Y., Hikino, M., Yajima, Y., Mikami, T., Sirko, S., von Holst, A., et al. (2005). Structural characterization of the epitopes of the monoclonal antibodies 473HD, CS-56, and MO-225 specific for chondroitin sulfate D-type using the oligosaccharide library. *Glycobiology* 15, 593–603. doi: 10.1093/glycob/cwi036

Izumikawa, T., Sato, B., and Kitagawa, H. (2014). Chondroitin sulfate is indispensable for pluripotency and differentiation of mouse embryonic stem cells. *Sci. Rep.* 4:3701. doi: 10.1038/srep03701

Kao, W. W., Funderburgh, J. L., Xia, Y., Liu, C. Y., and Conrad, G. W. (2006). Focus on molecules: lumican. *Exp. Eye Res.* 82, 3–4. doi: 10.1016/j.exer.2005.08.012

Karamanos, N. K., Piperigkou, Z., Theocharis, A. D., Watanabe, H., Franchi, M., Baud, S., et al. (2018). Proteoglycan chemical diversity drives multifunctional cell regulation and therapeutics. *Chem. Rev.* 118, 9152–9232. doi: 10.1021/acs.chemrev.8b00354

Karus, M., Ulc, A., Ehrlich, M., Czopka, T., Hennen, E., Fischer, J., et al. (2016). Regulation of oligodendrocyte precursor maintenance by chondroitin sulphate glycosaminoglycans. *Glia* 64, 270–286. doi: 10.1002/glia.22928

Kawakita, T., Shimmura, S., Higa, K., Espana, E. M., He, H., Shimazaki, J., et al. (2009). Greater growth potential of p63-positive epithelial cell clusters maintained in human limbal epithelial sheets. *Invest. Ophthalmol. Vis. Sci.* 50, 4611–4617. doi: 10.1167/iovs.08-2586

Kennedy, S., Lace, R., Carserides, C., Gallagher, A. G., Wellings, D. A., Williams, R. L., et al. (2019). Poly-ε-lysine based hydrogels as synthetic substrates for the expansion of corneal endothelial cells for transplantation. *J. Mater. Sci. Mater. Med.* 30:102. doi: 10.1007/s10856-019-6303-1

Kinoshita, S., Adachi, W., Sotozono, C., Nishida, K., Yokoi, N., Quantock, A. J., et al. (2001). Characteristics of the human ocular surface epithelium. *Prog. Retin. Eye Res.* 20, 639–673. doi: 10.1016/s1350-9462(01)00007-6

Ksander, B. R., Kolovou, P. E., Wilson, B. J., Saab, K. R., Guo, Q., Ma, J., et al. (2014). ABCB5 is a limbal stem cell gene required for corneal development and repair. *Nature* 511, 353–357. doi: 10.1038/nature13426

Le, Q., Chauhan, T., Yung, M., Tseng, C. H., and Deng, S. X. (2020). Outcomes of limbal stem cell transplant: a meta-analysis. *JAMA Ophthalmol.* 138, 660–670. doi: 10.1001/jamaophthalmol.2020.1120

Lewis, P. N., Pinali, C., Young, R. D., Meek, K. M., Quantock, A. J., and Knupp, C. (2010). Structural interactions between collagen and proteoglycans are elucidated by three-dimensional electron tomography of bovine cornea. *Structure* 18, 239–245. doi: 10.1016/j.str.2009.11.013

Li, Z., Duan, H., Li, W., Hu, X., Jia, Y., Zhao, C., et al. (2019). Rapid differentiation of multi-zone ocular cells from human induced pluripotent stem cells and generation of corneal epithelial and endothelial cells. *Stem Cells Dev.* 28, 454–463. doi: 10.1089/scd.2018.0176

Ljubimov, A. V., Saghizadeh, M., Spirin, K. S., Mecham, R. P., Sakai, L. Y., and Kenney, M. C. (1998). Increased expression of fibrillin-1 in human corneas with bullous keratopathy. *Cornea* 17, 309–314.

Manton, K. J., Leong, D. F. M., Cool, S. M., and Nurcombe, V. (2007). Disruption of heparan and chondroitin sulfate signaling enhances mesenchymal stem cell-derived osteogenic differentiation via bone morphogenetic protein signaling pathways'. *Stem Cells* 25, 2845–2854. doi: 10.1634/stemcells.2007-0065

Maseruka, H., Bonshek, R. E., and Tullo, A. B. (1997). Tenascin-C expression in normal, inflamed, and scarred human corneas. *Br. J. Ophthalmol.* 81, 677–682. doi: 10.1136/bjo.81.8.677

Maseruka, H., Ridgway, A., Tullo, A., and Bonshek, R. (2000). Developmental changes in patterns of expression of tenascin-C variants in the human cornea. *Invest. Ophthalmol. Vis. Sci.* 41, 4101–4107. Available online at: https://iovs.arvojournals.org/article.aspx?articleid=2162675

Meek, K. M., and Knupp, C. (2015). Corneal structure and transparency. *Prog. Retin. Eye Res.* 49, 1–16. doi: 10.1016/j.preteyeres.2015.07.001

Mei, H., Gonzalez, S., and Deng, S. X. (2012). Extracellular matrix is an important component of limbal stem cell niche. *J. Funct. Biomater.* 3, 879–894. doi: 10.3390/jfb3040879

Melrose, J., Isaacs, M. D., Smith, S. M., Hughes, C. E., Little, C. B., Caterson, B., et al. (2012). Chondroitin sulphate and heparan sulphate sulphation motifs and their proteoglycans are involved in articular cartilage formation during human foetal knee joint development. *Histochem. Cell Biol.* 138, 461–475. doi: 10.1007/s00418-012-0968-6

Nandini, C. D., and Sugahara, K. (2006). Role of the sulfation pattern of chondroitin sulfate in its biological activities and in the binding of growth factors. *Adv. Pharmacol.* 53, 253–279. doi: 10.1016/S1054-3589(05)53012-6

Notara, M., Schrader, S., and Daniels, J. T. (2011). The porcine limbal epithelial stem cell niche as a new model for the study of transplanted tissue-engineered human limbal epithelial cells. *Tissue Eng. Part A* 17, 741–750. doi: 10.1089/ten.TEA.2010.0343

Ote, Y., and Nishida, K. (2016). Corneal regenerative medicine. *Regen. Ther.* 5, 40–45. doi: 10.1016/j.reth.2016.06.002

Parfitt, G. J., Pinali, C., Akama, T. O., Young, R. D., Nishida, K., Quantock, A. J., et al. (2011). Electron tomography reveals multiple self-association of chondroitin sulphate/dermatan sulphate proteoglycans in Chst5-null mouse corneas. *J. Struct. Biol.* 174, 536–541. doi: 10.1016/j.jsb.2011.03.015

Pellegrini, G., Dellambra, E., Golisano, O., Martinelli, E., Fantozzi, I., Bondanza, S., et al. (2001). P63 identifies keratinocyte stem cells. *Proc. Natl. Acad. Sci. U.S.A.* 98, 3156–3161. doi: 10.1073/pnas.061032098

Pellegrini, G., Traverso, C. E., Franzi, A. T., Zingirian, M., Cancedda, R., and De Luca, M. (1997). Long-term restoration of damaged corneal surfaces with autologous cultivated corneal epithelium. *Lancet* 349, 990–993. doi: 10.1016/S0140-6736(96)11188-0

Persson, A., Voronisov, E., Larson, G., and Nilsson, J. (2020). Glycosaminoglycan domain mapping of cellular chondroitin/dermatan sulfates. *Sci. Rep.* 10:3506. doi: 10.1038/s41598-020-60526-0

Pinnamaneni, N., and Funderburgh, J. L. (2012). Concise review: stem cells in the corneal stroma. *Stem Cells* 30, 1059–1063. doi: 10.1002/stem.1100

Purushothaman, A., Sugahara, K., and Faissner, A. (2012). Chondroitin sulfate "wobble motifs" modulate maintenance and differentiation of neural stem cells and their progeny. *J. Biol. Chem.* 287, 2935–2942. doi: 10.1074/jbc.R111.298430

Quantock, A. J., Young, R. D., and Akama, T. O. (2010). Structural and biochemical aspects of keratan sulphate in the cornea. *Cell. Mol. Life Sci.* 67, 891–906. doi: 10.1007/s00018-009-0228-7

Romano, A. C., Espana, E. M., Yoo, S. H., Budak, M. T., Wolosin, J. M., and Tseng, S. C. G. (2003). Different cell sizes in human limbal and central corneal basal epithelia measured by confocal microscopy and flow cytometry. *Invest. Ophthalmol. Vis. Sci.* 44, 5125–5129. doi: 10.1167/iovs.03-0628

Sanchez, I., Martin, R., Ussa, F., and Fernandez-Bueno, I. (2011). The parameters of the porcine eyeball. *Graefes Arch. Clin. Exp. Ophthalmol.* 249, 475–482. doi: 10.1007/s00417-011-1617-9

Santos, G. R. C., Piquet, A. A., Glauser, B. F., Tovar, A. M. F., Pereira, M. S., Vilanova, E., et al. (2017). Systematic analysis of pharmaceutical preparations of chondroitin sulfate combined with glucosamine. *Pharmaceuticals* 10:38. doi: 10.3390/ph10020038

Schlötzer-Schrehardt, U., Dietrich, T., Saito, K., Sorokin, L., Sasaki, T., Paulsson, M., et al. (2007). Characterization of extracellular matrix components in the limbal epithelial stem cell compartment. *Exp. Eye Res.* 85, 845–860. doi: 10.1016/j.exer.2007.08.020

Setifert, M., Beck, S. C., Schermutzki, F., Müller, C. A., Erickson, H. P., and Klein, G. (1998). Mitogenic and adhesive effects of tenascin-C on human hematopoietic cells are mediated by various functional domains. *Matrix Biol.* 17, 47–63. doi: 10.1016/s0945-053x(98)90124-x

Shalom-Feuerstein, R., Serror, L., De La Forest Divonne, S., Petit, I., Aberdam, E., Camargo, L., et al. (2012). Pluripotent stem cell model reveals essential roles for miR-450b-5p and miR-184 in embryonic corneal lineage specification. *Stem Cells* 30, 898–909. doi: 10.1002/stem.1068

Shartifi, R., Yang, Y., Adibnia, Y., Dohlman, C. H., Chodosh, J., and Gonzalez-Andrades, M. (2019). Finding an optimal corneal xenograft using comparative analysis of corneal matrix proteins across species. *Sci. Rep.* 9:1876. doi: 10.1038/s41598-018-38342-4

Shibata, S., Hayashi, R., Kudo, Y., Okubo, T., Imaizumi, T., Katayama, T., et al. (2020). Cell-type-specific adhesiveness and proliferation propensity on laminin isoforms enable purification of tPSC-derived corneal epithelium. *Stem Cell Rep.* 14, 663–676. doi: 10.1016/j.stemcr.2020.02.008

Shibata, S., Hayashi, R., Okubo, T., Kudo, Y., Katayama, T., Ishikawa, Y., et al. (2018). Selective laminin-directed differentiation of human induced pluripotent stem cells into distinct ocular lineages. *Cell Rep.* 25, 1668–1679. doi: 10.1016/j.celrep.2018.10.032

Singh, P., and Schwarzbauer, J. E. (2012). Fibronectin and stem cell differentiation - lessons from chondrogenesis. *J. Cell Sci.* 125, 3703–3712. doi: 10.1242/jcs.095786

Sirko, S., von Holst, A., Weber, A., Wizenmann, A., Theocharidis, U., Götz, M., et al. (2010). Chondroitin sulfates are required for fibroblast growth factor-2-dependent proliferation and maintenance in neural stem cells and for epidermal growth factor-dependent migration of their progeny. *Stem Cells* 28, 775–787. doi: 10.1002/stem.309

Sirko, S., von Holst, A., Wizenmann, A., Götz, M., and Faissner, A. (2007). Chondroitin sulfate glycosaminoglycans control proliferation, radial glia cell differentiation and neurogenesis in neural stem/progenitor cells. *Development* 134, 2727–2738. doi: 10.1242/dev.02871

Sorrell, J. M., Mahmoodian, F., Schafer, I. A., Davis, B., and Caterson, B. (1990). Identification of monoclonal antibodies that recognize novel epitopes in native chondroitin/dermatan sulfate glycosaminoglycan chains: their use in mapping functionally distinct domains of human skin. *J. Histochem. Cytochem.* 38, 393–402. doi: 10.1177/38.3.1689338

Sugahara, K., Mikami, T., Uyama, T., Mizuguchi, S., Nomura, K., and Kitagawa, H. (2003). Recent advances in the structural biology of chondroitin sulfate and dermatan sulfate. *Curr. Opin. Struct. Biol.* 13, 612–620. doi: 10.1016/j.sbi.2003.09.011

Sun, Y., Deng, Y., Xiao, M., Hu, L., Li, Z., and Chen, C. (2017). Chondroitin sulfate proteoglycans inhibit the migration and differentiation of oligodendrocyte precursor cells and its counteractive interaction with laminin. *Int. J. Mol. Med.* 40, 1657–1668. doi: 10.3892/ijmm.2017.3153

Varki, A., Cummings, R. D., Aebi, M., Packer, N. H., Seeberger, P. H., Esko, J. D., et al. (2015). Symbol nomenclature for graphical representations of glycans. *Glycobiology* 25, 1323–1324. doi: 10.1093/glycob/cwv091

Watanabe, K., Nishida, K., Yamato, M., Umemoto, T., Sumide, T., Yamamoto, K., et al. (2004). Human limbal epithelium contains side population cells expressing the ATP-binding cassette transporter ABCG2. *FEBS Lett.* 565, 6–10. doi: 10.1016/j.febslet.2004.03.064

Yamada, K., Young, R. D., Lewis, P. N., Shinomiya, K., Meek, K. M., Kinoshita, S., et al. (2015). Mesenchymal–epithelial cell interactions and proteoglycan matrix composition in the presumptive stem cell niche of the rabbit corneal limbus. *Mol. Vis.* 21, 1328–1339.

Zhang, G., Chen, S., Goldoni, S., Calder, B. W., Simpson, H. C., Owens, R. T., et al. (2009). Genetic evidence for the coordinated regulation of collagen fibrillogenesis in the cornea by decorin and biglycan. *J. Biol. Chem.* 284, 8888–8897. doi: 10.1074/jbc.M806590200

Conflict of Interest: The authors declare that the research was conducted in the absence of any commercial or financial relationships that could be construed as a potential conflict of interest.